THE PIEZOCONE

IN LIGHTLY OVER CONSOLIDATED CLAY

Thesis submitted for the Degree
of Doctor of Philosophy

Zedi M Nyirenda

St Catherine's College
Oxford

ACKNOWLEDGEMENTS

I wish to express my sincere thanks to all who helped to bring about the completion of this research programme.

Special thanks are due to Dr. Gilliane C. Sills for the discussions and the thoughtful suggestions which have been invaluable during the course of this research programme. Her advice and comments made during the preparation of this thesis were also very much valued and greatly appreciated.

During the course of the research programme, there were many times when Technician help was a necessity. For these times, I would like to thank the Technicians of the Oxford University Soil Mechanics Group who were always handy and helpful. In particular, I would like to thank Mr. Robert Sawala, Mr. Christopher Waddup, Mrs. Gillian Jenkins and lastly but not least, Mr. Ron Morton for their assistance in the laboratory.

The work presented in this thesis was sponsored by S.E.R.C. in the first three years and I am grateful to them for supporting Dr.Sills' proposal for the research. I am also thankful to the Dawson Trust, members of St. Clement's Church and my brother William, for their support during the final year of the programme.

During the preparation of the Figures for the thesis, Mrs. Sonia Copper's help and advice were greatly appreciated.

A very special thanks to Joanna, whose love, support, encouragement and understanding have been a source of motivation throughout the programme.

ABSTRACT

The Piezocone in Lightly Over Consolidated Clay

Zedi Mesheck Nyirenda
St Catherine's College, University of Oxford

A thesis submitted for the Degree of Doctor of Philosophy
Michaelmas Term, 1989

A laboratory experimental programme was carried out to investigate the behaviour of the piezocone in lightly over consolidated clay. The clay samples were prepared from reconstituted kaolin. The powdered form of this clay was mixed with water to form a slurry at a moisture content of approximately 120% under vacuum. The clay slurry was consolidated and then allowed to swell in chambers which were well instrumented.

Penetration tests were carried out with two sizes of piezocones. The smaller piezocone had a cross sectional area of 1 cm^2 with pore pressure measurement at the cone shoulder. The larger piezocone with a cross sectional area of 5 cm^2 had pore pressure measurements at four locations.

In addition to penetration testing, further information on the strength and consolidation characteristics of the test chamber samples was obtained from shear vane, restricted flow consolidation, flow pump permeabilty and consolidated undrained triaxial tests.

The horizontal effective stress and the vertical stress ratio were found to influence the generated excess pore pressure at all four different locations on the piezocone shaft and the net tip resistance. This led to the establishment of direct correlations for the tip resistance factor Q with the coefficient for lateral earth pressure at rest K_0 and the vertical effective stress ratio (OCR). Direct correlations for the excess pore pressure ratio at all four measuring positions with K_0 and OCR were also established.

Several methods of estimating over consolidation ratio were examined. One of the factors examined was B_q which was found to correlate poorly with OCR before tending asymptotically to a value of approximately 0.4. Other examples of factors which showed promising results as estimators of OCR were B_{mi}, the excess pore pressure ratio, and Q, the tip resistance factor.

The excess pore pressures well behind the cone shoulder, which are partly generated by the shear stress in the area, showed promising correlations with the undrained shear strength. However, because correlations with pore pressure on the piezocone are dependent upon the position of the filter element, the particular results from this series may only be used for piezocones whose filter elements are at equivalent positions.

The undrained strength ratio was also correlated with the tip resistance factor Q and the result was very promising for future interpretation of piezocone data.

Table of contents

LIST OF FIGURES

LIST OF PLATES

LIST OF TABLES

1 THE PIEZOCONE: A LITERATURE REVIEW

1.1 Introduction

The cone penetrometer is an apparatus used to determine soil parameters by measuring the soil resistance to penetration at the tip, and the local side friction resistance. It consists of a series of cylindrical rods with a terminal body, the penetrometer tip, in which the tip resistance and local side friction sensors are located.

Tip resistance or end bearing is developed at the structurally isolated conical front end piece of the terminal body. Local side friction is mobilised on the friction sleeve, which is situated above the cone tip. Specifications of a typical probe, as recommended by the International Symposium for Soil Mechanics and Foundation Engineering (1977), consist of a cone angle of 60° with a 10 cm^2 cross-section area at the cone base and a surface roughness of 1 μm.

The piezocone is a cone penetrometer which incorporates the measurement of pore water pressure generated in the soil during penetration. The position of the filter, or porous element, and indeed the whole geometry of the piezocone has not yet been standardised because it is "still under development" (De Beer et al, 1988). Filter element positions on some piezocones are shown in Figure 1.1.

Cone penetration tests (and piezocone tests), are performed in order to obtain data on one or more of the following subjects:

a) the stratigraphy of soil layers, and their homogeneity over the site,
b) soil identification,
c) the depth to firm layers, the location of cavities, voids and other discontinuities in

the soil,

d) mechanical and consolidation characteristics of the soil,

e) the driveability and bearing capacity of piles in the soil under investigation.

This thesis will concentrate on the mechanical and consolidation characteristics of the soil from piezocone data. Therefore this subject will be dealt with in detail later, but for completeness the other subjects will be discussed briefly below.

1.1.1 Stratigraphy and soil identification

Stratigraphy and soil identification have been combined together in this section because one leads to the other. Before the development of the piezocone from the cone penetrometer, stratigraphic information was obtained from the variation of tip resistance with depth coupled with the friction ratio. With the advent of the piezocone, the pore water pressure during penetration gives more accurate stratigraphical data for the ground being investigated (Milligan, 1987). The aim of a stratigraphic study for a site would be to investigate the homogeneity of the site by comparing the responses, both tip resistance and pore water pressure at each depth, at all the soundings on the site. These will give an indication of the depth to, and the thicknesses of, various strata.

In general, excess pore pressure during penetration will be higher in normally consolidated clays; will get smaller with increasing over consolidation ratio; and will be virtually non existent in sands. Tip resistance, on the contrary, will be much higher in sands than in clays. As an example, Figure 1.2 shows a result of one sounding reported by Zuidberg et al, (1982). The figure presents the pore water pressure, sleeve friction, cone or tip resistance, the friction ratio which is the ratio of the sleeve friction to the tip resistance expressed as a percentage, and the borehole log for the site. The borehole log gives the changes in soil strata which the tip resistance and pore pressure profiles predict. From the tip resistance profile it can be seen that the change in soil strata corresponds with changes in the profile which occur near the following depths in meters; 1.5, 4, 11, 16 and 28. These changes are

an indication of strata changes. From the pore pressure profile it is possible to distinguish between the response at, say, 3 m and 15 m where in the tip resistance profile they appear to be the same material. Also it is possible to tell from pore pressure profile that the material at depth 10 m, for example, is the same as that at 24 m because the pore water pressure response is the same. In this case the tip resistance helps to distinguish between loose and dense sand. The borehole log in this figure confirms the accuracy of the combination of pore pressure and tip resistance in soil identification.

In the discussion above it has been shown that piezocone data can be used to identify different soil strata and to that effect several soil classifying charts have been published. The earlier ones rely on empirical relationships between the friction ratio (f_r) and the tip resistance (q_c). This type of chart was published by Schmertmann (1969) and Robertson and Campanella (1984). Other charts used empirical relationships between the tip resistance, q_c , and the excess pore pressure. Jones and Rust (1982) produced a chart that related excess pore pressure at the shoulder to the effective tip resistance, i.e. $(q_c - \sigma_{v0})$ while Senneset and Janbu (1984) produced one which related the tip resistance, q_t , to the pore pressure factor, B_q . Wroth (1988) argued that well conditioned relationships such as $(q_t - \sigma_{v0})$ should be used instead of q_t in charts for identification of soil type. This argument supports the chart produced by Jones and Rust (1982) and that by Robertson (1988) who produced a chart which uses empirical relationships of non dimensional parameters to arrive at the soil type classification. The charts, by Robertson (1988) are reproduced in Figure 1.3.

1.1.2 Bearing capacity of piles

The piezocone penetrates the soil as a miniature pile. Therefore the tip resistance and the skin friction can together be expected to relate to the ultimate bearing capacity of a larger diameter pile. In the Netherlands, where cone penetration was first developed, pile bearing capacity has long been based on cone penetration data.

The standard pile bearing capacity equations hold, but the estimation of the end bearing and the skin friction from piezocone data is what forms the bulk of the differences in the various methods that are used in practice.

$$Q_{ult} = Q_b + Q_s \qquad [1.1]$$

where Q_b is the end bearing,

Q_s is the skin friction.

Several writers, such as Begemann (1963), Sanglerat (1972), Brenner and Panichpatananon (1982), Broug (1982) and Bustamante and Gianeselli (1982), have contributed to the debate. For end bearing, a form of averaging the tip resistance before and after the final depth of the pile and over varying distances is used. As an example, the method described by Sanglerat (1972) involves taking a weighted average of the tip resistance over a depth of 11.75D, of which 3.75D is below the pile toe (D is the pile diameter). The averaging is done in the following way:

$$q_b = \overline{q}_t(\text{above}) + \overline{q}_t(\text{below}) \qquad [1.2]$$

where $\overline{q}_t(\text{above})$ is the average tip resistance over a depth of 8D above the largest section of the base of the pile,

$\overline{q}_t(\text{below})$ is the average tip resistance below the point of the pile tip over a depth of at least 3.5D.

The averaging of tip resistance above the largest section of the base of the pile is a straight forward arithmetical average. Below the pile tip, it is important to to take into account the possibility of a punch type of failure. Therefore this average is weighted towards the lowest tip resistance in the following manner:

$$\overline{q}_t(\text{below}) = \frac{(q_1 + q_2 + \ldots + q_n) + nq_n}{2n} \qquad [1.3]$$

$q_1, q_2, \ldots q_n$ are tip resistance values at regular intervals within the minimum 3.5D depth below the pile tip. The last value q_n is the lowest tip resistance over the same depth. By including the lowest value n number of times more, the average is weighted towards the lower tip resistance and thereby avoids pile over-designing.

There is built-in empiricism in the method above and as such the method is more of a guideline which may need to be adapted to fit the prevailing situation. For example, when the tip resistance continually increases below the depth of the pile tip, the averaging below the pile tip may need to be modified.

On the other hand, Bustamante and Gianeselli (1982) report a method which considers a straight arithmetical average, after rounding off the peaks and troughs, over 3.0 pile diameters equally divided above and below the pile toe. In this method a penetrometer bearing capacity factor, k_c , derived from full scale loading tests, is used to arrive at the ultimate or limiting end bearing capacity:

$$Q_b = q_{ta} \times k_c \times \frac{\pi D^2}{4} \qquad [1.4]$$

where q_{ta} is the equivalent tip resistance at the level of the pile point,

k_c is the penetrometer bearing capacity,

D is the pile diameter.

The penetrometer bearing capacity, k_c, depends on whether the pile in question is driven or bored, the magnitude of the tip resistance and the type of soil in which the pile is being installed. k_c ranges from 0.2, in weathered chalk, to 0.55, in compact to stiff clay or compact silt. This method has a built-in factor of safety since it does not utilise the total available ultimate bearing capacity. To illustrate this method, Figure 1.4 shows an artificial tip resistance profile on which the peaks are truncated to smoothen the profile. The smoothing of the profile is made to pass closer to valleys than to peaks of the raw profile as a weighting towards the smaller values of tip resistance. In the Figure, the profile represents the stage after the initial smoothing of raw data. The averages between the smoothed valleys and peaks, in the region between +a and -a of the pile toe, is the line q'_{ta} and the equivalent tip resistance is the average of the values which are between 0.7 and 1.3 times q'_{ta} over the same region. The different values of k_c suggested by Bustamante and Gianeselli, (1982) are also presented in Figure 1.4.

The skin friction mobilised by a pile depends upon its average adhesion with the soil:

$$q_s = \alpha s_u \qquad [1.5]$$

where α is the adhesion factor,

s_u is the undrained shear strength,

q_s is the ultimate unit skin friction.

However, the determination of a suitable value of the adhesion factor can be a problem as it not only depends upon the consistency of the soil but also upon whether the pile is to be bored or driven. Tomlinson (1969) suggested that for driven piles, this factor (α) is greater than unity for very soft clays with undrained shear strengths of less than 50 kPa but falls off rapidly with increasing shear strength to a limit value of about 0.4, as shown in Figure 1.5. For bored piles Skempton (1966) suggested an (α) factor of 0.45.

Among the semi empirical and empirical methods of determining q_s are the methods proposed by Vijayvergiya and Focht (1972) and Bustamante and Gianeselli (1982). The former is only useful for the design of driven piles while the latter uses the tip resistance factored by the coefficient of skin friction to arrive at q_s . The coefficient, derived from full scale tests, depends on the soil type, the pile production and pile placement method.

The skin friction measured during many cone penetrometer and piezocone tests provides a continuous indication of the mobilised skin friction which can be used directly in the calculation of the total skin friction resistance. Whatever the method of determining q_s, the total skin friction resistance would be calculated as follows:

$$Q_s = \sum_{1}^{i} Q_{si} = \sum_{1}^{i} q_{si} \times \pi D l_i \qquad [1.6]$$

where q_{si} is the ultimate unit skin friction at the level of layer i (kPa),

l_i is the thickness of the layer i (m).

1.1.3 Voids and firmer layers

In some cases, such as where old mining works are suspected, the cone penetration data is used only to identify depths to the beginning and end of voids. If this is the only reason for the site investigation, the piezocone may not be used and the cone penetrometer soundings

would need to be much closer to reduce the likelihood of missing the void.

The ability of the cone penetrometer or piezocone to identify firmer layers can be used to check the progress of compaction of soils on reclaimed land and to determine depths to firmer layers, including depth to bed-rock.

1.2 Pore Pressure Measurement

As early as 1974 there were arguments about the differences in q_c using the electric cone in drained and undrained conditions. In discussion, Schmertmann (1974) concluded that tests which produced positive pore pressure around the electric cone would ordinarily increase or reduce q_c if fully drained and fully undrained conditions prevailed respectively. So the need for pore pressure measurement was already recognised, albeit for a different reason.

In 1975, Torstensson, and Wissa et al reported the development of their pore pressure measuring probes. Wissa et al (1975) used their probe to determine the rapid changes in excess pore pressures under different loading conditions, including wave action in submarine soils. Torstensson (1975) reported the use of pore pressure measurements made with the new probe to determine soil stratigraphy, shear strength and time deformation characteristics. The literature reflects continuing developments in research from Richards et al (1975), Parez et al (1976), Baligh et al (1980) and Sugawara and Chikaraishi (1982). In 1981, Tumay et al published results of a study of the wear of the cone tip penetration testing. These results showed that the maximum wear, and consequently the maximum shear resistance occurred towards the middle of the cone tip. This implies that maximum pore pressure would be generated in this region.

This was an important result in as far as the measurement of maximum excess pore pressure on the piezocone was concerned because the larger measured pressures would have enabled more accurate determination of soil stratigraphy. However, some authors still preferred

measurement of pore ressure at other positions on the piezocone. Consequently, in the develpment of soil profiling charts, both Jones and Rust (1982) and Senneset and Janbu (1984) used the excess pore pressure measured at the cone shoulder as mentioned earlier.

Zuidberg et al (1982) addressed the problem of the effect of the generated pore water pressure on the measured tip resistance (q_c). They discovered that if the piezocone was subject to a uniform water pressure in a chamber then the tip resistance measured was less than the applied water pressure. They concluded that the difference was due to the fact that the pore pressure acting on unequal end areas behind the cone shoulder had a resultant force acting against the soil, thereby reducing the measured tip resistance (Figure 1.6).

$$q_t = q_c + \alpha U \qquad [1.7]$$

where q_c is measured tip resistance,

U is measured pore pressure,

α is the correction factor.

Zuidberg et al (1982) preferred pore pressure measurement on the cone face, where it was maximum, to that on the shoulder. At the time, soil profiling was the main use of the pore pressure measurement made on the piezocone. Maximum pore pressure on the cone face undoubtedly improved the resolution in soil profiling and was, therefore economically, a better choice.

It was not long before the importance of correcting q_c for q_t became recognised (Jamiolkowski et al 1985, Robertson et al 1986, May 1987), but the question of universally agreed locations for pore pressure measurements is yet to be resolved in the piezocone testing industry.

1.2.1 Locations for pore pressure measurement

Filters or porous elements for pore pressure measurement can be located anywhere on the piezocone from the cone tip to the cone shaft. The choice of a particular position will depend on the intended use of the pore pressure result obtained. In the discussion earlier it was shown why, for soil profiling, the maximum generated pore pressure should be measured. For this reason, many early and some modern piezocone manufacturers have placed the porous element at or near the tip (e.g. the McClelland piezocone) although it is now known that this is not in fact the position for maximum induced pore pressure. Others, such as Fugro, placed their porous element near the top of the cone face. There are those for whom measuring the maximum pore pressure was not the main aim but who still use the results for soil profiling. This group of manufacturers, which include Delft, have placed the porous element at the shoulder.

Analytical results by Baligh and Levadoux (1980) and Teh (1987) on the distribution of excess pore pressure along the piezocone and the field and laboratory results of Tumay et al (1981) discussed earlier has provided a greater insight into the optimum positions for measuring excess pore pressure.

Therefore, for maximum pore water pressure response, the cone face near the cone shoulder is the best location for the pore pressure element. This is the region of high pore pressures, but the pressure gradient along the face is also very high. This means that cone face pore pressure results from different piezocones will not be directly comparable if they are measured from different locations on the face. As an example, cone face pore pressure from a McClelland piezocone may not be comparable with a cone face measurement from a Fugro piezocone, even though the pore pressure locations may be separated by less than 10 mm. Therefore, it is important to standardise the exact position on the cone face where pore pressure measurements can be made.

Robertson (1988) has reported that pore pressure measurement on the cone face has become important for the purposes of soil profiling while Sully et al (1988) reported the importance of this measurement for the estimation of over consolidation ratios and shear strength. These points will be discussed further in Chapter 7 of this thesis.

However, where tip resistance is required for analysis other than soil profiling, the pore pressure generated at, or near, the discontinuity which allows for tip resistance measurement to be independent of the other parameters on the piezocone, (normally the cone shoulder) ought to be measured. The correction of the measured tip resistance q_c (see Equation 1.7) must be made using the pore pressure measured at the shoulder. The use of pore pressures measured at other locations, which are then factored to represent the pore pressure at the shoulder, is not an accurate method since the factors used, such as the ratio between the cone shoulder to the cone face pore pressure, β, may be soil type or stress history dependent (Sills et al 1988b).

The interpretation of pore pressure measurements at the shoulder, as at the cone face, has the difficulty of being in an area of high pressure gradient. The actual position of the porous element in this area is as sensitive as that on the cone face. Therefore, standardisation of this position would also enable the direct comparison of measured excess pore pressures at this position between different piezocones.

Other points about measuring pore water pressure at the shoulder reported by Robertson (1988), with the author's comments, are as follows:

(a) Stratigraphic detailing of non dilatant soils using excess pore pressure at this position is still very good because the pore pressure remains quite high in comparison with that on the cone face. In dilatant or heavily over consolidated stiff clays, negative pore pressures at the cone shoulder have been reported by

Bond, 1989 and Powell, 1988. Therefore it would be better to use excess pore pressure measured at the cone face, which is always positive, in soil stratigraphy for this type of soil.

(b) Pore water pressure dissipation is predominantly in the horizontal direction, because of the high localised pressure gradients in the horizontal direction; therefore the data provides a good estimate of the horizontal coefficient of consolidation.

(c) The filter element at this position receives some protection from abrasion when penetrating through layers of granular material. Chen and Bassett (1988) support this view.

The locations discussed so far are for those piezocones where only one pore pressure measurement is made. Most research piezocones have more than one pore pressure location. Sugawara and Chikaraishi (1982), Sully et al (1988), and May (1987) all report piezocones with multiple pore pressure measurements. So far only the pore pressures at the face and shoulder have had uses, other than for dissipation analysis, reported in literature. Other uses of the pore pressures measured above the shoulder will be reported later in this thesis.

1.3 Filters Used in Piezocone Tests

The way in which the transducer responds to pressure necessitates a flow of fluid, however small, to account for the displaced volume on the transducer face. In order to get as quick a response as the transducer can provide during penetration, this flow must be minimised to the pressure transducer requirement only. This entails two requirements for the filter element. Firstly, the filter must be rigidly designed to allow free pore fluid flow and preventing it from flexing, which would increase the required flow. Secondly, the filter itself must not contain or entrain any fluid that would compress and increase the required

flow. The second requirement leads on to operational requirements of filter elements and must be extended to include the fluid channels which lead to the pressure transducer. This calls for the filter and the channels to be de-aired and fully saturated with an incompressible fluid throughout the duration of the test.

Apart from the requirement of full saturation and permeability, the selection of filters also depends upon the type of soil being tested. While porous stone filters with a pore diameter of 2 μm have been recommended for cohesive soils (Smits, 1982), they would not be suitable for non-cohesive soils and stiff over consolidated clays. This is due to abrasion of the stone which subsequently causes clogging of the filter (Jamiolkowski et al, 1985). In this particular case, a filter made from a non-abrasive material (such as stainless steel or sintered bronze) could be used. More recently, plastic filter elements are being used extensively.

There is still more scope for research on the effects of the dimensions or the compressibility of filters on the measured pore pressure, since very little has been done in this field. Campanella et al (1988) present the results of a comparison between a 2.5 mm and 5 mm filter and concluded that the sluggish response of the 2.5 mm filter after encountering negative pressures was due to partial pore blockage. Whilst the result was inconclusive, it pointed to the difficulty of piezocone soundings on sites where cavitation may be encountered. The difference in the amount of available fluid for cavitation may have favoured the larger filter in the case above. In the case of compressibility, and in the absence of elaborate research results, it may be speculated that very compressible filters will tend to reduce the pore diameters when they flex under high pressure gradients. When the pore diameter is reduced enough, this would cause a constriction in the flow which might in turn cause either a delayed transducer response, due to reduced flow over the filter, or an increase in the measured pressure due to increased velocity of flow at the constriction in the filter.

1.3.1 Saturation of filters for pore pressure measurements

Transducers for pore pressure measurement are designed to respond to changes in water pressure in the soil without being in direct contact with the soil. Only the saturation fluid and pore water are in contact, as discussed above. The pore pressure measurement depends on the incompressibility of the fluid between the transducer and the soil to transmit the pressure. Therefore, there should be no compressible fluid in the passage between the filters and the transducer. To achieve this, various researchers have used different methods, some of which are reviewed below:

(a) Campanella et al (1983) suggest saturation by using glycerine and designing the sensing cavity to be as small as practical, especially avoiding unnecessary corners that may trap air. Glycerine is miscible with water, yet it develops a high air entry tension preventing loss of saturation during penetration through soils above the water table.

(b) Almeida and Parry (1985), using Druck's PDCR 81 for a pore pressure transducer, allowed a 'very small gap' between the back of the filter and the transducer, and the whole system was de-aired under vacuum and saturated in water.

(c) For low temperature work, the small volume of saturating fluid leading to the transducer will be susceptible to freezing. Therefore, a fluid with a low freezing point is required. Wissa et al (1982) filled the probe with alcohol and successfully measured pore pressures at an ambient temperature of $-34°C$.

Campanella et al (1983) reported the paradox of the need to saturate the probe before penetration and the impossibility of checking that full saturation has been achieved. In fact, not all those who have taken steps to saturate the probe have reported methods of checking full saturation.

One way to check whether or not the piezocone is fully saturated is to apply a known pressure to it when immersed in de-aired saturation fluid in a chamber. Then the time the piezocone takes to read the same pressure is noted. This time should be as close to the response time of the particular transducer as will be acceptable. A more detailed description of this procedure follows later in the thesis. It is acknowledged that although it is necessary at the very least to perform the above check, it is still not sufficient because the saturation fluid is able to flow more freely in the fluid filled chamber than the water would in the field.

1.4 Excess Pore Water Pressure Dissipation

In addition to correcting the measured tip resistance and aiding in soil identification, pore water pressure measurements, taken from the moment the piezocone is stopped until the excess pore pressures have dissipated, also provide a basis for estimates of the coefficient of consolidation using either of the following consolidation theories:

a) The Terzahi-Rendulic uncoupled theory in which it is assumed that the total stress remains constant everywhere so that strains are caused only by the change in pore water pressure.

b) Biot's coupled consolidation theory in which the full interaction between the soil skeleton and pore pressure is taken into account throughout the consolidation process.

Of the two theories, Biot's coupled theory is refined, more complex and mathematically correct than the uncoupled theory (Battaglio et al, 1981), but is in some ways more restricting because the soil has to behave elastically. However, many researchers have found the uncoupled theory satisfactory for the penetration situation because its predictions are similar to those of the coupled theory (Randolph and Wroth, 1979; Randolph et al, 1979; Battaglio et al, 1981; and Davies and Poulos, 1970). Baligh and Levadoux (1980) also looked at the difference between the theories with respect to the dissipation of pore water

pressure from the piezocone and found that there was little difference between the two solutions. Therefore the uncoupled solution has been used to analyse dissipation data in this programme.

Solutions for analysing dissipation data from the piezocone have been provided by Torstensson (1978), Baligh and Levadoux (1980) and Teh (1987), to mention a few. The last two used the strain path method to obtain the initial pore water pressure distribution, while Torstensson used the spherical and cylindrical cavity expansion method. One advantage of the strain path method is its ability to predict strain reversals around the piezocone. This enables accurate predictions of stresses around the piezocone to be made. While the strain path method satisfies compatibility conditions, it does not satisfy equilibrium conditions. However, in practice, it is reported to predict tip resistance and pore water pressures satisfactorily (Baligh and Levadoux 1980). Teh (1987) used an iterating technique to produce results which satisfy equilibrium equations more closely. Therefore Baligh and Levadoux's (1980) and Teh's (1987) solutions, which are solutions of the uncoupled theory, have been used in analysing dissipation data for the present tests.

Baligh and Levadoux's solutions were developed with soil properties of the Boston blue clay and should therefore be used for soils with similar properties. Most notably, the rigidity indices should be similar to those at the site where the properties of the Boston blue clay were obtained (Baligh and Levadoux, 1980). The normalised pore water pressure dissipation was plotted against the non dimensional time factor described below. Their solutions for the pore water pressure dissipation at the cone face, the cone shoulder and ten times the piezocone radius up the shaft from the tip, are given in Figure 1.7:

$$T = \frac{c_v t}{R^2} \qquad [1.8]$$

where c_v is the vertical coefficient of consolidation,

t is the time from start of dissipation,

R is the shaft radius of the piezocone.

Teh (1987) was concerned about the normalising parameter R in the time factor which does not represent the drainage path, as in one dimensional consolidation, nor the zone of pore water pressure influence around the piezocone, the plastic radius (R_p). He therefore suggested normalising with the root of the rigidity index, $\sqrt{I_r}$, which is an approximation of the plastic radius (R_p). The re-defined time factor T^* is shown below in Equation 1.9. The resulting dissipation curves for rigidity indices between 75 and 500 can be seen to be in a very narrow band for all the four pore pressure positions, as shown in Figure 1.8. The solutions from Figure 1.8 have been put together in Figure 1.9 because the differences between this range of rigidity indices are not significant at each of the locations chosen.

$$T^* = \frac{c_v t}{\sqrt{I_r} R^2} \qquad [1.9]$$

where I_r is the rigidity index, (G/s_u).

In both solutions, it is important to specify the correct initial pore water pressure distribution because the results of the dissipation analysis depend upon it (Baligh and Levadoux, 1980; Teh, 1987; Sills et al, 1988a). In Teh's solution, in addition, the rigidity index must be known. In practice, this means that tests such as the pressuremeter test, from which this parameter can be obtained, ought to be carried out on the same site. However, it also means increased costs which, on small projects, may prove difficult to overcome.

Pore pressures generated during penetration are localised near the penetrating instrument. It would be expected, therefore, that there will be high pressure gradients between this localised high pore pressure area around the piezocone and the surrounding soil, ie generally

in the horizontal direction. If natural permeabilities in clays were considered, the mode of deposition of natural clays makes the horizontal permeability higher than the vertical one, thus making the preferred dispersion of a localised water source in the horizontal direction. It follows then, that the coefficient of consolidation so estimated from dissipation tests after penetration is the horizontal coefficient of consolidation c_h .

However, it should be mentioned that an initial increase of pore pressure is very noticeable in the early stages of dissipation from locations well behind the shoulder. This is an indication of upward flow of pore water due to high pressure gradients. This initial increase of pore pressure has been reported by May (1987), Sills et al (1988a) and Lutenegger and Kabir (1988) to mention a few. As this local vertical pressure gradient gets smaller, the upward flow of water decreases to a point where it is not possible to see its influence on the dissipation process.

1.4.1 Problems with dissipation tests

Dissipation analyses have both theoretical and practical problems to overcome. Among the theoretical problems are:

a) The uncertainties of initial excess pore pressure distribution around the cone which arise from the two dimensional nature of the theoretical idealisation of the cone penetration process.

b) The anisotropy and non-linearity of soil behaviour, and the unknown coupling between total stresses and pore pressures during consolidation.

There are practical problems which are encountered during the analysis of field data. Among these are:

a) Current theoretical solutions describe excess pore pressure dissipation at specific positions on the piezocone which do not necessarily correspond to the locations of

the filter element on most piezocones. Therefore, unless the two positions correspond, the consolidation coefficient thus obtained can only be described as an estimate.

b) The sufficient degree of consolidation, and hence the acceptable time for the test, which will give workable properties and yet make the test economical in practice.

c) The acceptable level of data fitting between field and theoretical data. The usual method of fitting one value cannot be recommended because of the difficulties in the theoretical solutions. Methods which utilise the full range of available data should be encouraged, such as those suggested by Battaglio et al (1981) and Thomas (1986).

1.5 Stress History from Piezocone Data

The stress history of a clay deposit has been related to the pore pressure parameter B_q .

$$B_q = \frac{\Delta U}{q_t - \sigma_{v_0}} \qquad [1.10]$$

This parameter has been likened to Henkel's pore pressure parameter A which is a function of over consolidation ratio (OCR) (Wroth 1984).

$$A = \frac{\Delta U - \Delta\sigma_{oct}}{\Delta\tau_{oct}} = f(OCR) \qquad [1.11]$$

Experience with B_q has shown that it decreases as OCR increases (Wroth, 1984; Coutts, 1986). The trend is not linear and shows a considerable scatter of data. Sugawara (1988) postulated that the scatter of the data when relating B_q with OCR is due to the fines content

of the clays involved. However, Mayne and Bachus (1988) have shown that B_q does not have a unique relationship with OCR. They showed, using cylindrical cavity expansion theory, that B_q depends upon the N_{kt} factor which Teh and Houlsby (1988) have shown to depend on the rigidity index, and is not a function of OCR. Therefore it is not surprising that writers, such as Konrad and Law (1987), have expressed reservations in the usefulness of B_q as an indicator of OCR.

Another parameter suggested by Mayne (1986), Wroth (1988), Powell et al (1988) and Sugawara (1988) is the tip resistance factor Q:

$$Q = \frac{q_t - \sigma_{v_0}}{\sigma'_v} = f(OCR) \qquad [1.12]$$

The relationship with OCR and Q would be better understood when Q is seen in the form below:

$$Q = \frac{q_t - \sigma_{v_0}}{\sigma'_v} = N_{kt}\frac{s_u}{\sigma'_v} = f(OCR) \qquad [1.13]$$

From Equation 1.13, the relationship between Q and OCR may be better seen since (s_u/σ'_v) is known to correlate with OCR. This parameter is further discussed later in the thesis.

May (1987) postulated that the ratio of the pore pressure measured at the shoulder to that at the face (β) was a function of the over consolidation ratio:

$$\beta = \frac{U_{shld}}{U_{face}} \qquad [1.14]$$

Sills et al (1988b) reported results which showed that this might be the case. Their results, reproduced in Figure 1.10, show a clear trend of reducing β with increasing over consolidation ratio. There is further discussion about this factor later on in the thesis where more laboratory results will be included.

Sully et al (1988), also using the pore pressure at the face and shoulder, found that the Pore Pressure Difference (PPD), normalised by the hydrostatic pressure (U_0) was a function of the over consolidation ratio:

$$PPD = \frac{U_{face} - U_{shld}}{U_0} \qquad [1.15]$$

where U_0 is the hydrostatic pressure.

Wroth (1988) stipulated the need to express all variables for correlation purposes in non dimensional terms so that scaling laws of continuum mechanics may be taken advantage of. While the above correlation is expressed in non dimensional terms, the selection of hydrostatic pressure, i.e. what is essentially a total stress, as the normalising parameter for the pore pressure difference puts the whole correlation into question. Houlsby (1988) described this type of normalising as "incorrect", and the author is of the same opinion.

1.6 Shear Strength from Piezocone Data

The estimation of shear strength from piezocone data stems from the bearing capacity type of relationship.

$$q_t = N_{kt} s_u + \sigma_{v_0} \qquad [1.16]$$

This relationship depends upon the accurate determination of N_{kt}. May (1987) has done an extensive review of the historical development of the understanding of the parameters which govern N_{kt} . Field observations have also shown that N_{kt} is site dependent and varies between 6 and 25 (Mayne and Bachus, 1988). This large variation has made it very difficult to make realistic estimates of shear strengths from piezocone data.

Rigden et al (1982) postulated that the evaluation of N_{kt} required the knowledge of the horizontal stress and the elastic moduli. This was confirmed by Teh (1987) who showed that N_{kt} was a function of the rigidity index, the cone roughness, shaft roughness and the horizontal stress as expressed below.

$$N_{kt} = N_s\left(1.25 + \frac{I_r}{2000}\right) + 2.4a_f - 0.2\alpha_s - 1.8\Delta \qquad [1.17]$$

where N_s is $\frac{4}{3}(1 + \ln I_r)$

α_f is $(\sqrt{3}\,\tau_f)/2s_u$, the cone roughness factor,

α_s is $(\sqrt{3}\,\tau_s)/2s_u$, the shaft roughness factor,

Δ is $(\sigma_{v_0} - \sigma_{h_0})/2s_u$

Teh (1987) has shown the importance of the rigidity index among the factors that influence N_{kt} since it appears on its own and in the N_s term. The rigidity index is, however, the most elusive value to estimate with any reliability. Generally, this value decreases with increase in OCR as observed by Wroth and Houlsby (1985) but it can be affected by the sensitivity of the clay, as reported by D'Appolonia et al (1971) and is also strain level dependent. Although attempts have been made to correlate plasticity index with rigidity index by

Keaveny and Mitchell (1986), it is best to measure it on every site under investigation. This would require other reliable in situ testing equipment to be used. In this case pressuremeter testing would be the only contender.

The cone and shaft roughness factors are instrument dependent and likely to be constant for a particular piezocone over a period of time. However, at best, these can only be estimates. The Δ term also requires pressuremeter test results and a knowledge of the undrained shear strength. This appears to be a contradiction, since N_{kt} is used to estimate shear strength. However, Teh (1987) has shown that N_{kt} is a complex factor. In the author's opinion, these results serve to show the need for calibration chamber correlations which was one of the objectives of the research.

Other methods of estimating shear strength from piezocone data have focussed on the relationship of the undrained shear strength ratio (s_u/σ'_v) with OCR. Mayne (1988) reported correlations of OCR with (s_u/σ'_v) for shear strength by various methods. Becker et al (1987) reported correlations between the field vane and over consolidation ratio. This type of direct correlation would be useful for piezocone results because it would provide an efficient but reliable method of estimating the undrained shear strength of the particular deposit or strata. The over consolidation ratio can be estimated using the tip resistance factor and an estimate of the undrained shear strength ratio obtained from the figure. This is discussed further later in the thesis.

Rad and Lunne (1988) reported some direct correlation between tip resistance and excess pore water pressure results with the undrained shear strength (s_u). Unfortunately they did not normalise their correlation so their results cannot be compared directly with those from other sites or instruments. On the other hand, the authors provided the raw data for anyone interested to use. The more data that can be accumulated, the better future advancement of the interpretation of piezocone results.

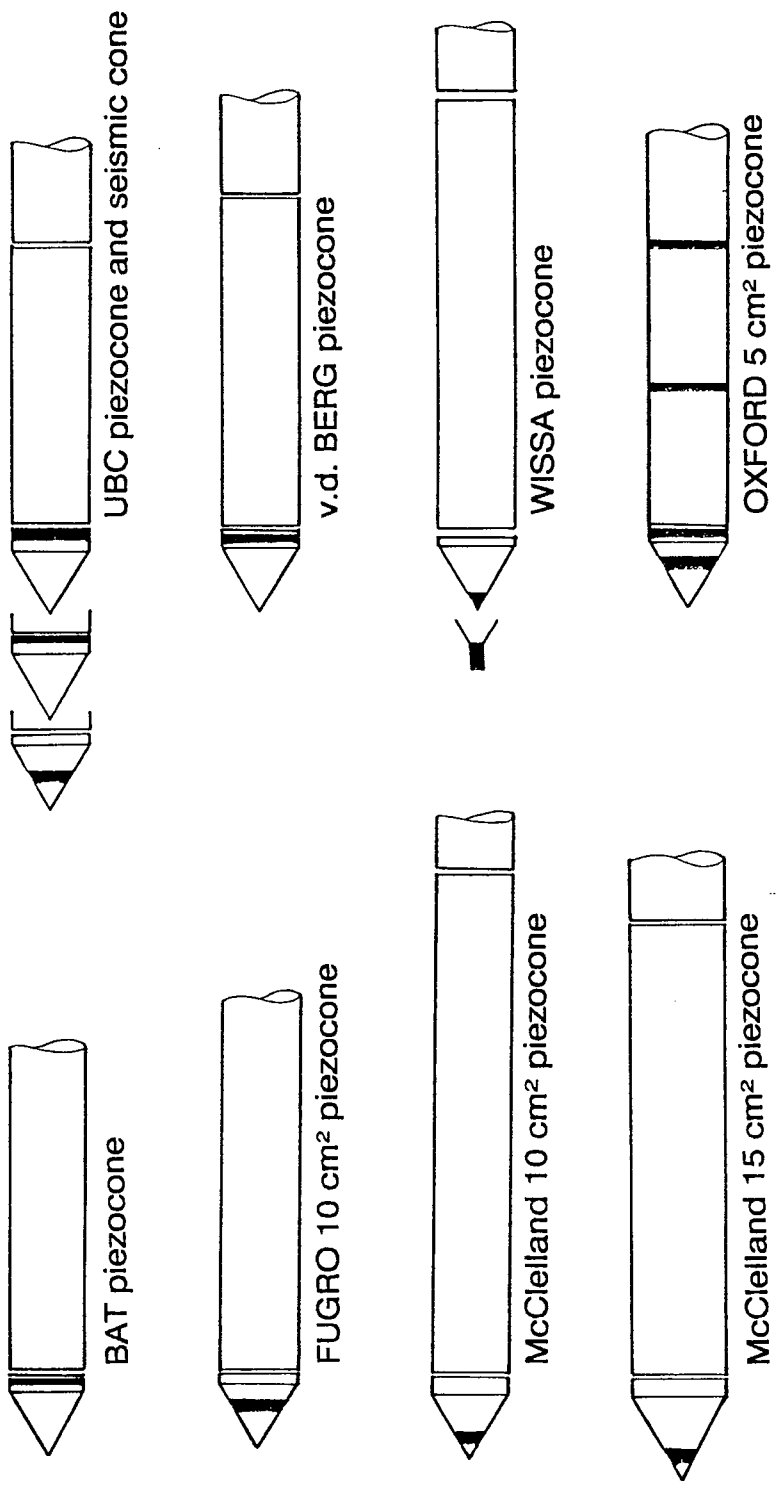

Figure 1.1 A selection of piezocones currently in use in industry and research (Lunne et al, 1986).

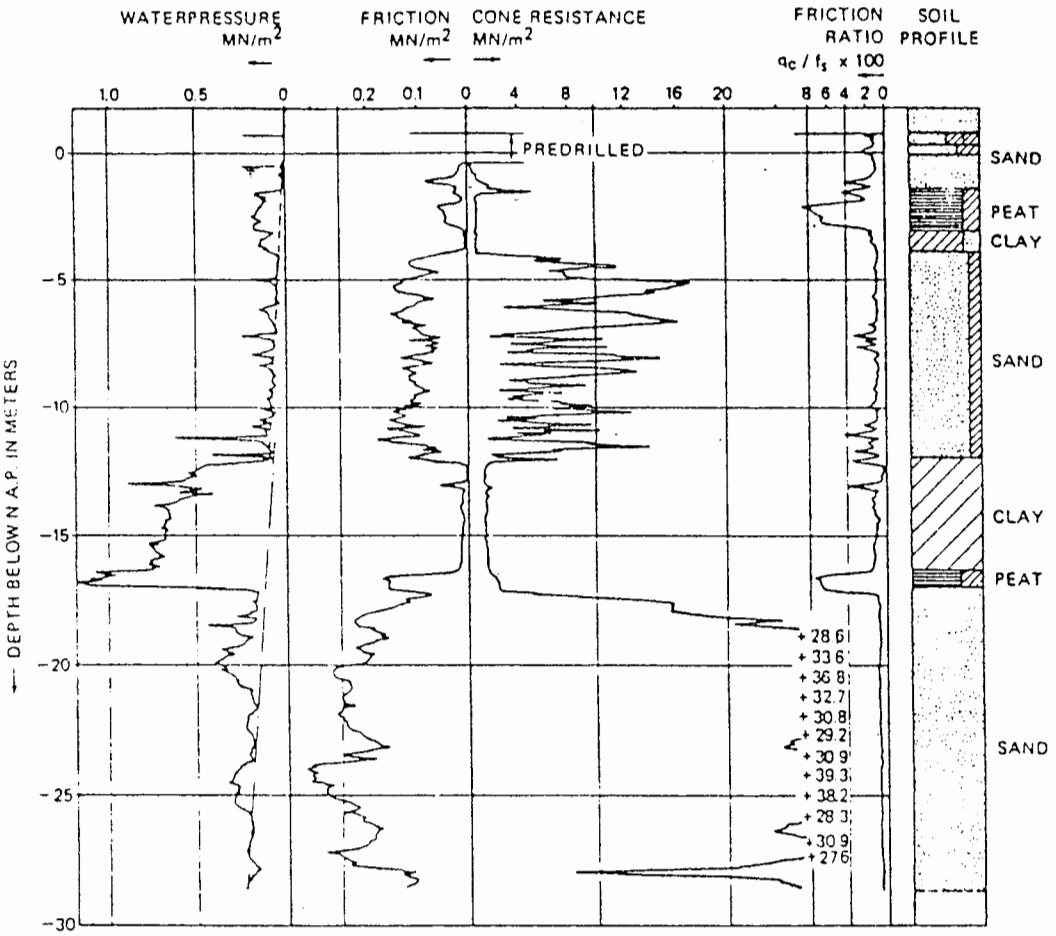

Figure 1.2 Results of an onshore piezocone test (Zuidberg.et al, 1982).

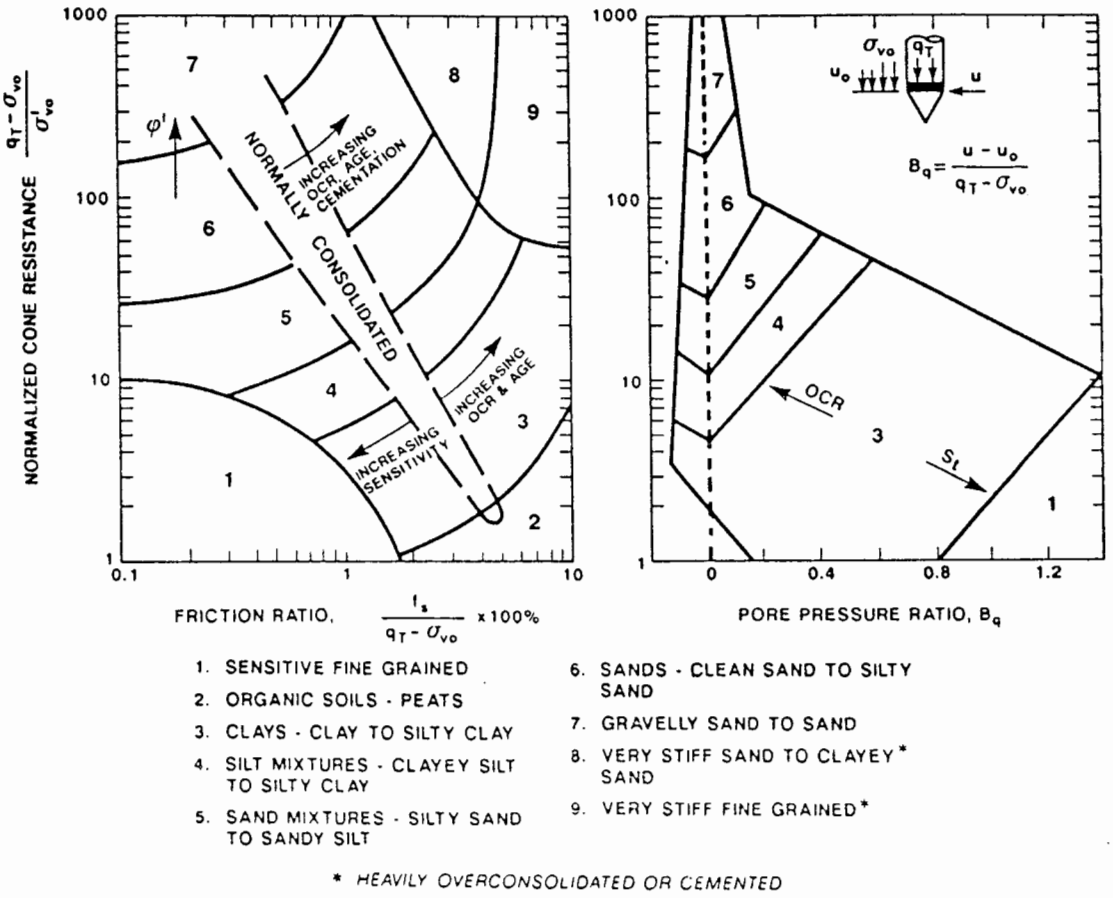

Figure 1.3 A soil classification chart using non-dimensional variables (Robertson, 1988).

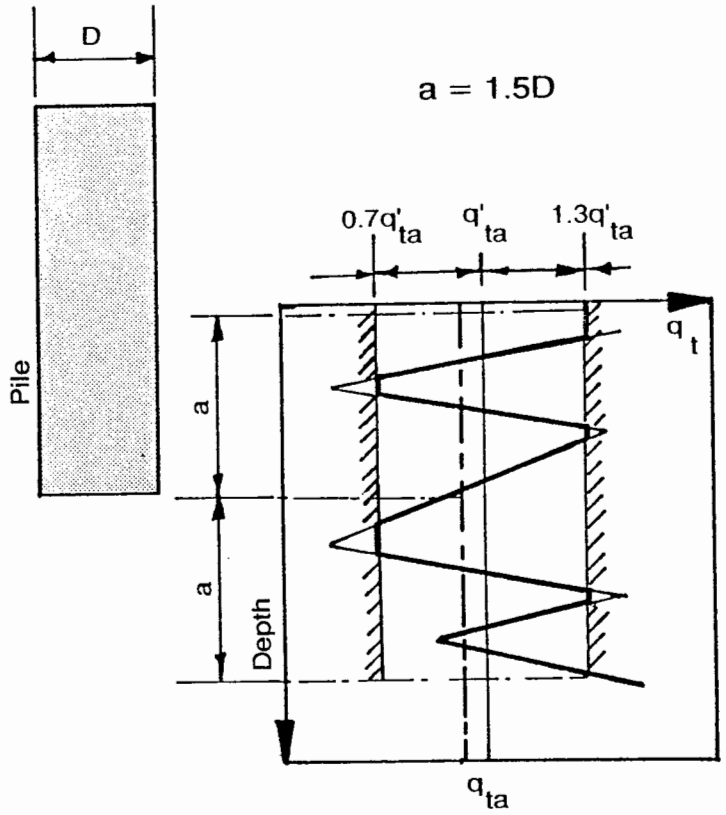

Nature of soil	q_c (MPa)	Factors k_c	
		Bored	Driven
Soft clay and mud	<<1	0.4	0.5
Moderately compact clay	1-5	0.35	0.45
silt and loose sand	≤5	0.4	0.5
Compact to stiff clay and silt	>5	0.45	0.55
Soft chalk	≤5	0.2	0.3
Moderately compact sand and gravel	5-12	0.4	0.5
Wethered to fragmented chalk	>5	0.2	0.4
Compact to very compact sand and gravel	12	0.3	0.4

Figure 1.4 Bustamente and Gianeselli (1982) method of pile design.

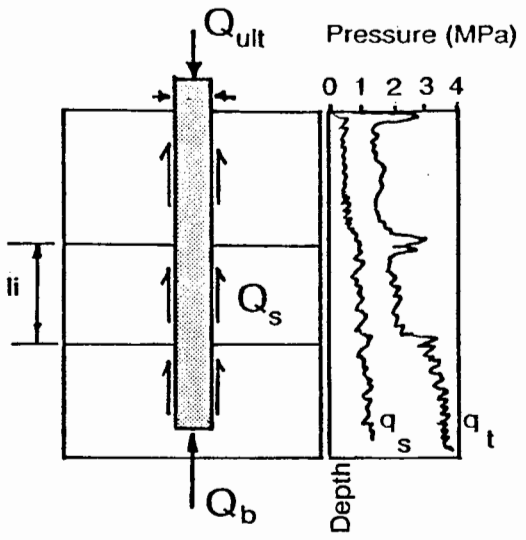

Figure 1.5a The determination of skin friction (Bustamente and Gianeselli, 1982).

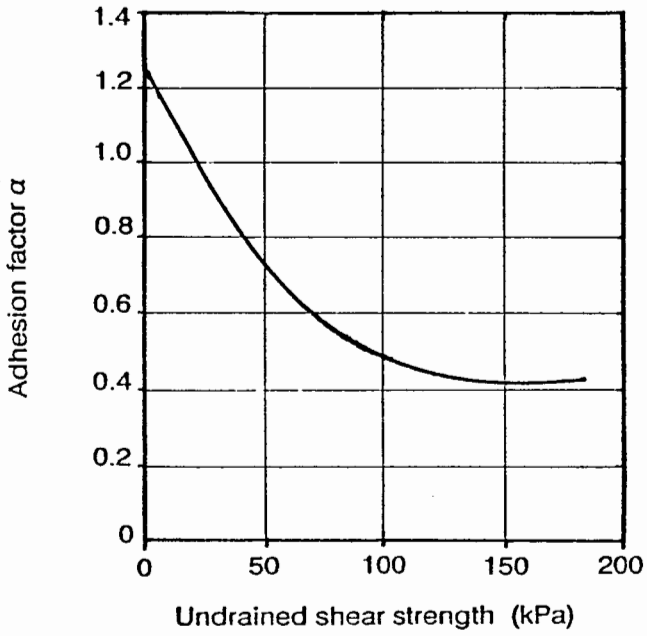

Figure 1.5b Tomlinson (1969) adhesion factor.

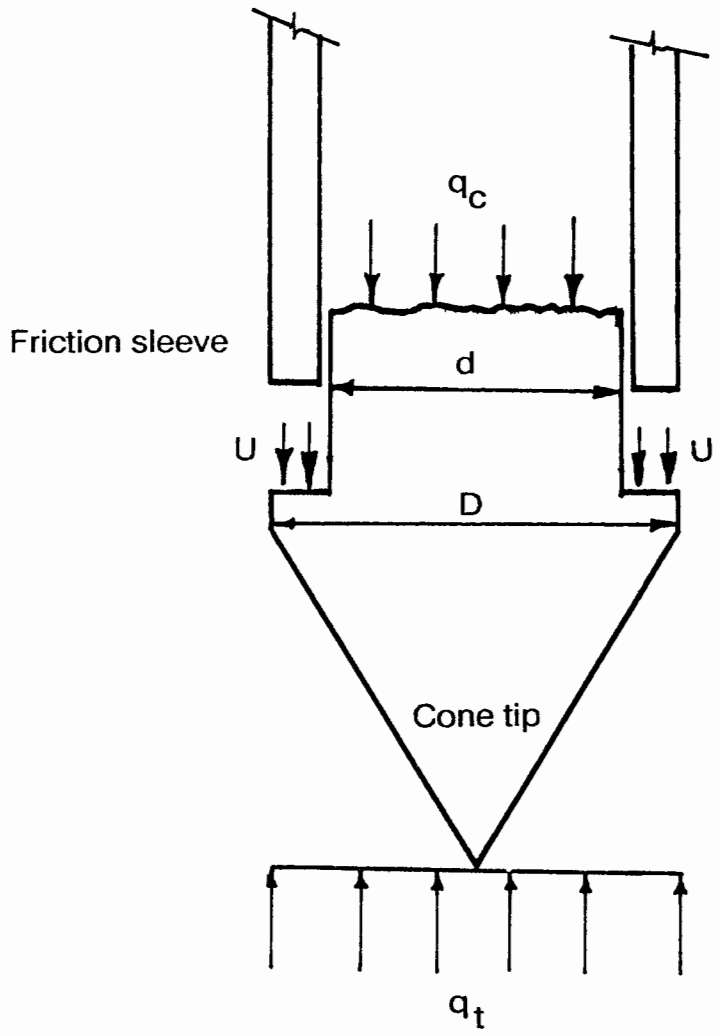

$$a = \left(\frac{d}{D}\right)^2$$

$$\alpha = (1 - a)$$

$$q_t = q_c + \alpha U$$

Figure 1.6 The correction for tip resistance q_t

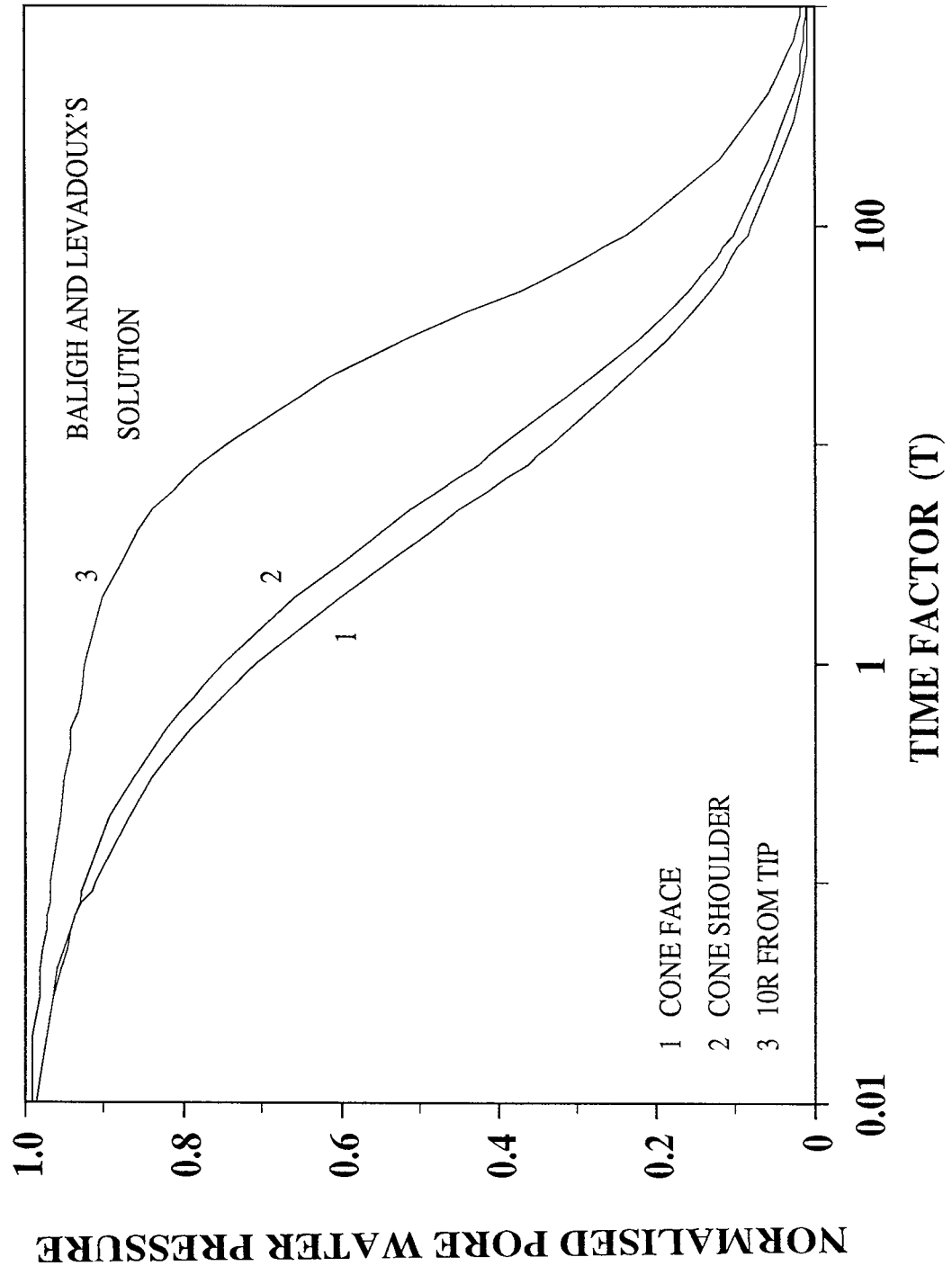

Figure 1.7 Baligh and Levadoux (1980) excess pore pressure dissipation curves for the 60° cone.

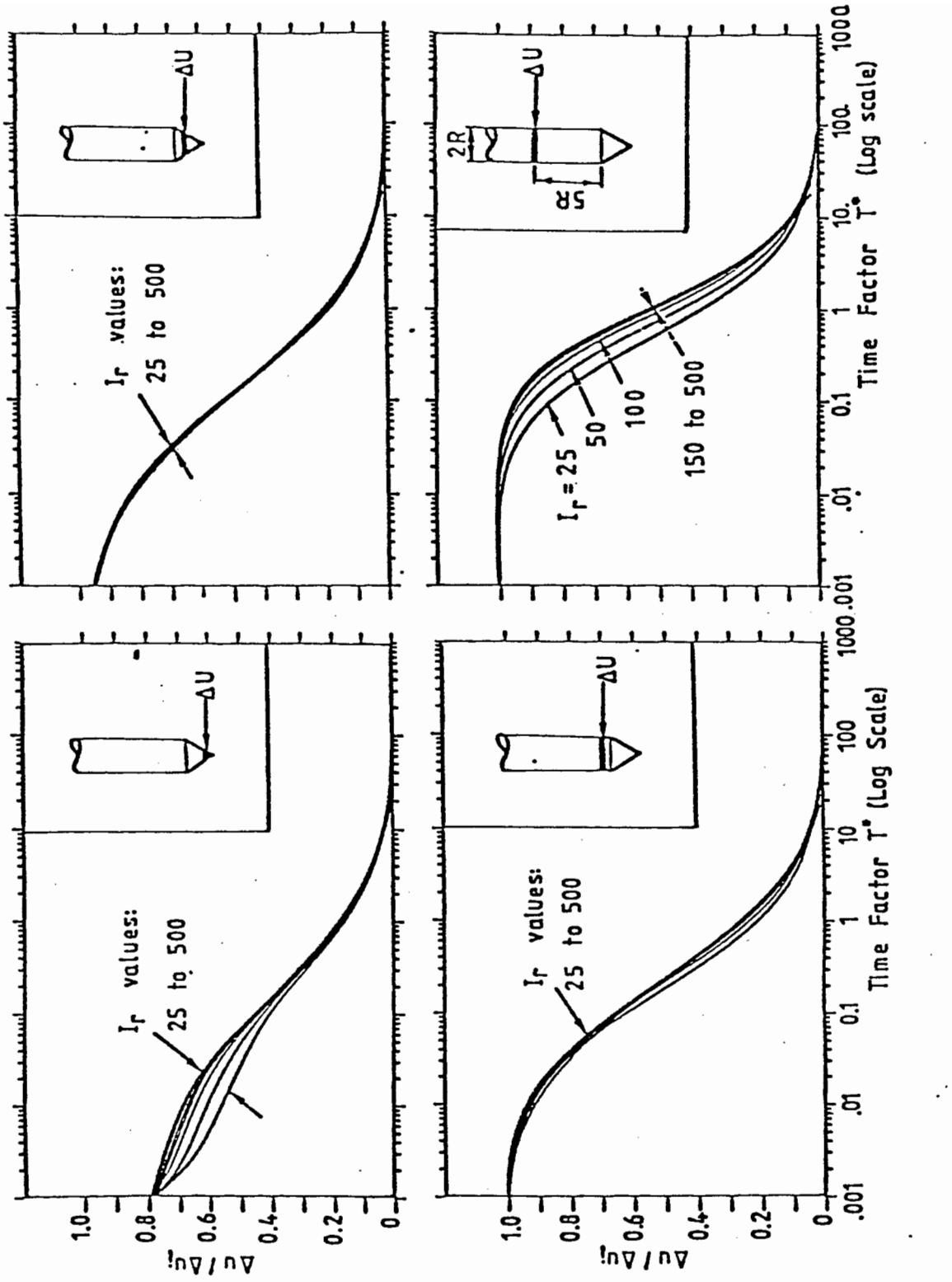

Figure 1.8 Influence of rigidity index on the solution of the uncoupled consolidation theory (Teh, 1987).

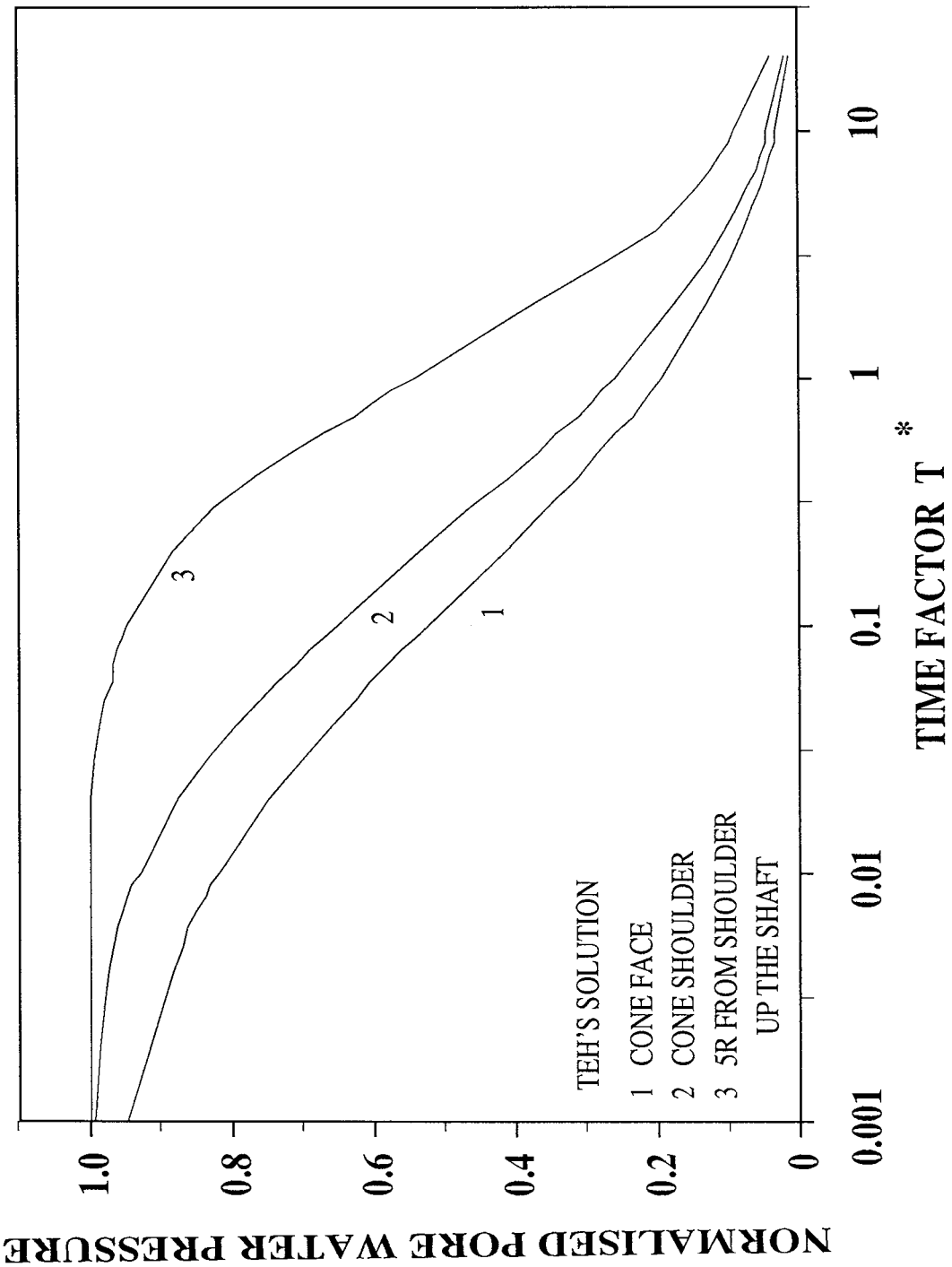

Figure 1.9 Teh (1987) excess pore pressure dissipation curves for the 60° piezocone.

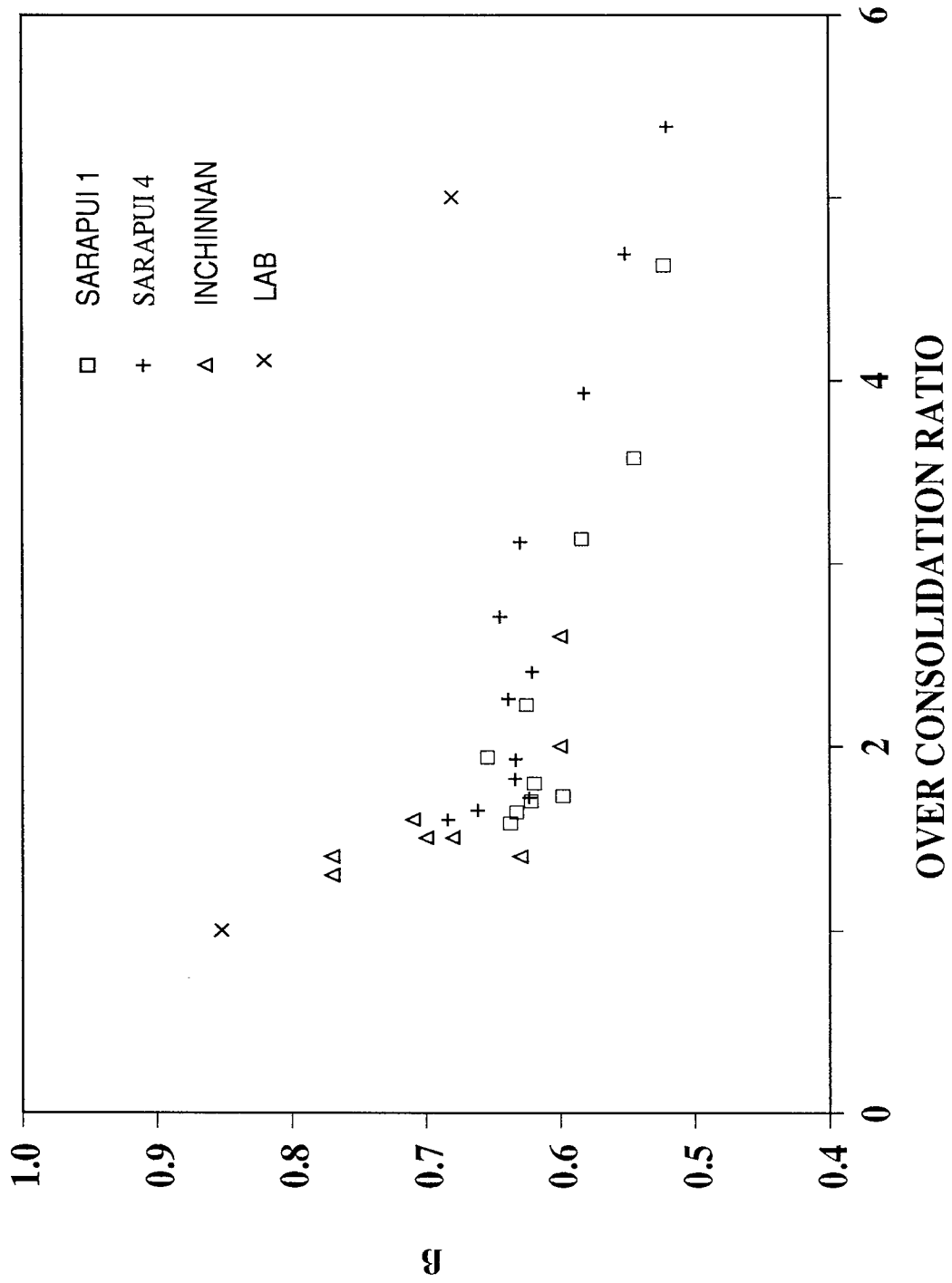

Figure 1.10 β values from field and laboratory data (Sills et al, 1988).

2 THE PIEZOCONE IN LIGHTLY OVER CONSOLIDATED CLAY

In order to continue the laboratory study of the piezocone started by Dr R.E. May on normally consolidated clay, a study programme to extend the work to lightly over consolidated clays was set up. It involved the use of some of the equipment used in the earlier work but with the scope to develop new equipment where necessary.

2.1 Terms of Reference

The terms of reference of this programme were as follows:

> To study the behaviour of the piezocone in lightly over consolidated clay (kaolin). The kaolin samples were to be prepared under careful laboratory conditions, so that as much as possible could be known about their properties before penetration testing.

2.1.1 Objectives of the research programme

The umbrella objective was to calibrate the behaviour of the piezocone in lightly over consolidated clay. This included the study of the following:

a) Tip resistance response,

b) Pore pressure response at four locations on the 5 cm^2 and one location (shoulder) on the 1 cm^2 piezocones respectively,

c) The influencing factors for tip resistance and other measured parameters on the piezocone, thereby identifying sound correlations which can be used to estimate soil parameters such as over consolidation ratio (OCR) and shear strength.

In order to achieve the above, a subsidiary objective was to prepare samples which were as uniform as could be achieved under the prevailing laboratory conditions.

2.1.2 Over consolidation.

Over consolidation of soils in the field is caused by factors such as erosion, the rise and fall of the water table, ageing, chemical decomposition or a combination of these. Erosion and the fluctuations of the water table are mechanisms which each produce mechanical over consolidation because it is effectively a load - unload cycle. In the laboratory, it is not easy and perhaps not possible to simulate over consolidation by chemical decomposition or ageing but mechanical over consolidation may be simulated easily. This is achieved by consolidating at a predetermined pressure and when consolidation is complete, allowing the soil to swell as the pressure is reduced to a value that will give the required over consolidation ratio.

'Lightly over consolidated' was taken to mean over consolidation ratios of up to about 10. These were to be achieved from pre-consolidation pressures divided into two ranges. The first is the lower range for consolidation pressures between 450 kPa and 650 kPa whilst the second is the higher range between 700 kPa and 900 kPa.

2.2 Laboratory Penetration Testing

Most of the results that have been reviewed in the previous chapter were field results. Whilst the tests were undoubtedly of high quality, there were some limitations in the estimation of parameters such as the over consolidation ratio. This shadow of doubt makes the need for laboratory tests where conditions are controlled appealing.

In the laboratory, controlled conditions would result in the preparation of homogeneous samples leading to more uniform soil parameters which would form a firmer basis for correlations which may arise subsequently. Mechanical over consolidation can be accurately controlled and horizontal stresses and shear strengths may be measured accurately. However, there will be problems which laboratory conditions impose and which must be fully appreciated. These problems include the following:

a) Boundary effects and the maintenance of suitable stresses and displacement conditions.

b) Constitution of the sample and the time taken to achieve the desired sample quality.

c) Possible scale effects due to confinement and piezocone size.

These will now be discussed individually below.

2.2.1 Boundary effects

In the field the soil exists in an initial state of stress established by its loading history, extending to considerable distances without constraint. In the laboratory, in contrast, the soil is confined in some sort of cell, tank or sample chamber.

It is generally possible to reproduce a realistic stress condition for the initial state by making assumptions such as the applicability of K_0 conditions. However, if additional localised stresses are applied, as in the driving of an instrument or the application of a foundation load, then these assumptions do not apply and the laboratory soil is subject to constraints that do not exist in the field. Therefore, the quality of the experimental results will largely depend on these differences between field and laboratory (Sills, 1987).

During operation in the field, the effects of driving a piezocone into a clay soil can be identified as follows:

a) The soil displaced by the piezocone will be accommodated by heave and lateral movement.

b) The soil will undergo changes both in total and effective stress in response to the loading.

c) The clay is constrained around the piezocone by the rigid geometry.

d) Any effects of the penetration will have disappeared an infinite distance away (in practice, measurable effects will dissipate much closer than infinity).

In the laboratory, however, if the piezocone is driven into a consolidated sample of clay, the boundary conditions will impose effects of their own. Some comments about different types of boundary are presented below with a summary of the advantages and disadvantages in Table 2.1.

a) Stress controlled boundaries allow displacements to occur. However, the value chosen for the stress is usually the initial stress state, and therefore the change of stress that would occur in the field is not able to occur at the boundary.

b) Displacement controlled boundaries allow changes in stress within the soil to occur, but the boundary displacement is not generally equal to the field movements.

Therefore, laboratory experiments would need to compromise between the field condition and the constraints of laboratory chambers in which the clay samples to be tested are prepared.

Table 2.1 Control on Boundary (Side Walls) of Chamber

Stress control		**Displacement control** (Zero displacement)	
Advantages	Disadvantages	Advantages	Disadvantages
Lateral displacement of soil possible.	Not easily able to produce K_0 conditions for initial stress state. Generally more difficult to produce, especially if initial consolidation stage is required.	Comparatively simple to produce.	Soil is forced to heave with no lateral displacement

During penetration testing in laboratory prepared samples, the bottom face is generally of a zero displacement condition, since a stress controlled boundary would influence the driving force and complicate the analysis of results. The top surface, on the other hand, can be any of the following listed below.

a) Zero stress, achieved by exposing the surface to the atmosphere.

b) Constant stress, achieved by a flexible boundary (usually a rubber membrane) with controlled air or fluid pressure above it.

c) Uniform unspecified displacement, achieved by applying a rigid boundary, free to move in the vertical direction only, with controlled air or fluid pressure above it.

The advantages and disadvantages of each of the conditions above are presented in Table 2.2.

Table 2.2 Top Surface Stress Conditions.

Conditions	Advantages	Disadvantages
Zero stress	Simple	Unrealistic since consolidation stresses have been removed, causing immediate and time-dependent reductions in strength.
Constant stress	Heave can occur	In the field, local stress concentrations would develop near the piezocone during penetration. These cannot be simulated.
Zero displacement	Simple in itself	Lateral displacement must take place; hence requires use of stress-controlled side walls, which are not easy to produce.
Constant displacement	Heave can occur	In the field, vertical displacement would be highest near piezocone and lower further away. This cannot be simulated.

With all boundaries, the further they are away they are from the piezocone the better, ie the larger the chamber for testing the better.

2.3 Sample Constitution

It has been said above that the larger the testing chamber the better, which also means that the larger the sample is, the smaller the boundary effects will be. This has the following consequences:

a) It takes a long time to mix the clay, with potential difficulty in obtaining a uniform sample.

b) It takes a long time to consolidate the sample to the required initial stresses. Consolidation times can be minimised by draining from both top and bottom faces of the sample. Further reduction in consolidation time may be realised by enabling radial drainage, but when the consolidation pressure is either from the top or bottom, radial drainage would allow the soil nearest to the side walls to consolidate rapidly and form a cylindrical crust (assuming a cylindrical chamber) which would act like a hollow pillar. The consolidation pressure will then not get to the soil nearer to the centre because it would be supported by the already consolidated soil at the edges of the sample. Therefore the sample would not be uniformly consolidated (Nageswaran and Houlsby, 1982).

2.4 Scale Effects

The effects of the boundary can also be reduced by using small scale piezocones. The possibility of a scale effect on some or all of the experimental results must be appreciated. This point will be discussed later in the thesis.

3 TESTING EQUIPMENT

This chapter will describe the equipment used in the test programme, including the modifications that had to be carried out to existing equipment.

3.1 Laboratory Scale Piezocones

The piezocones used in the test programme were scaled-down versions of the Fugro 10 cm^2 piezocone. These were the 5 cm^2 and 1 cm^2 piezocones, a half and one tenth of the Fugro piezocone cross-section area respectively.

3.1.1 5 cm^2 piezocone

This piezocone was specially designed to measure pore water pressure at four positions as follows, and as illustrated in Figure 3.1.

a) On the cone face,

b) On the cone shoulder,

c) Mid sleeve,

d) At the top of the sleeve.

With the current debate on the optimum position of the filter, this work will provide some guidance as to the preferred position. This piezocone incorporates a 100 cm^2 friction sleeve. Plate 3.1 shows the two piezocones described here.

The instrumentation of the 5 cm^2 piezocone consists of two load cells and four pressure transducers. Load cells measure the end bearing and the total force (end bearing plus skin friction). Both cells have temperature compensated full bridges of orthogonal strain gauges equally spaced around the circumference. Their load capacity is 10 kN with a signal output of 0.45 mV/V at full load. Although the strain gauges are temperature compensated, experiments showed that input voltages of greater than 3 V DC generated enough heat to cause drift in the output. Therefore, the excitation voltage was maintained at 3 V DC. This

small excitation voltage, coupled with the fact that only about 5% of the end bearing capacity could be mobilised in the laboratory tests, meant that outputs of no more than 0.01 mV could be produced in the current experiments. This called for greater care in the signal conditioning process described later in this chapter.

The four pressure transducers, used to measure pore water pressure during penetration, are the Kyowa PS-10KB subminiature pressure sensors whose rated output is 0.93 mV/V with a working pressure capacity of 1000 kN/m^2. The manufacturer's recommended excitation voltage is 3 volts, which allowed all transducers on the piezocone to be powered at the same voltage. Each of the subminiature transducers is placed in a recess in the piezocone behind a Vyon filter element. Filters serve as rigid interfaces between the saturating fluid on the transducer face and the pore water in the soil.

3.1.2 1 cm^2 piezocone

This piezocone was designed to have interchangeable tips to measure pore water pressure at the cone face or at the cone shoulder. The small size of this piezocone made it difficult to incorporate either the skin friction or multiple location pore pressure measurements.

The instrumentation is similar to that of the 5 cm^2 piezocone described above, except that there is only one load cell and one subminiature pressure transducer. Therefore only the end bearing and one pore water pressure measurement, either at the face or the shoulder pore water pressure, can be made in each test.

3.1.3 Rate of penetration

Despite the reduced size of the laboratory piezocones, a comparison between the tip resistance responses from the 5 cm^2 and 10 cm^2 piezocones, driven at the same rate on the same site, showed no significant difference (Henderson, 1987; May, 1987).

May (1987) reported that a tenfold increase in the rate of penetration produced a 15% increase in tip resistance response, a fact supported by research at the Building Research Establishment (Powell 1989). However, part of the 15% increase reported is likely to have been due to soil variability because the two could not be separated. This means that the rate effect alone may be much less than 15%.

Therefore the rate of penetration for both sizes of laboratory piezocones was set at the standard 20 mm/s

3.1.4 Piezocone calibration.

The two sizes of piezocone used in the programme have tip load capacities well in excess of the maximum load conditions encountered in the laboratory; therefore it was important to calibrate the load cells within the range expected in the laboratory. All the transducers and load cells on the piezocone were calibrated before each series of tests.

3.1.4.1 Load cell calibration

The load cells in both piezocones were calibrated in a specially adapted loading frame, which also served as a shear vane reaction frame. The adaptation of the centrally and vertically aligned frame was such that the piezocone could be placed in the frame with a 500N Schlumberger D95 load transducer at the tip. The design also incorporated structural pins at the top and tip of the piezocone to eliminate any loading due to bending. The load transducer was periodically calibrated with dead weights, but using the same power supply, and its calibration did not change over the period of the test programme.

3.1.4.2 Piezocone saturation and calibration system

Plate 3.2 shows the saturation chamber which also serves as a calibration chamber for pore pressure transducers on the piezocone, and for quantifying the effects of pore water pressure on the measured tip resistance. The main feature of the system is the facility to de-air the

piezocone and fill the space left by the air with de-aired saturating fluid. This two stage process can be repeated as many times as necessary until a satisfactory saturation is achieved without at any time introducing air in the saturation chamber.

In the present programme, the saturating fluid used is glycerol. This is a viscous liquid yet it develops high air entry tension. Due to its viscosity, glycerol flows very slowly, allowing a fully saturated filter and the space between the filter and the pressure transducer some time before beginning to lose saturation.

The initial process was to de-air the filters and the glycerol separately. Therefore, referring to Plate 3.2, with all the taps except B and F closed, a high vacuum was applied for at least one hour, depending on the amount of air in the glycerol. At first the glycerol turns milky but becomes clearer as air is withdrawn. Using the glycerol as an indicator, when all the air has been drawn out, the vacuum and the calibration chamber are isolated by closing taps D and F. The reservoir is opened to the atmosphere before opening tap A which allows the de-aired glycerol to be drawn into the calibration chamber. When the chamber is full, it is also opened to the atmosphere, thereby allowing the glycerol to be drawn into the filter pores vacated by the air. After another hour, the process is reversed to draw the glycerol back into the reservoir, and the whole process is repeated before checking saturation.

Full saturation can be checked in two ways. The first is by monitoring the responses of the pore pressure transducer and the chamber transducer on a chart recorder at its highest chart speed. The responses should be identical. This is a quick way of finding out whether something is wrong, but is obviously not very rigorous since the response record is also dependent upon the chart and pen speeds. A more accurate method is to monitor both transducer responses on a dual channel oscilloscope and check their response times. Both methods were used in this programme.

If saturation is not satisfactory, the chamber is depressurised and isolated. A vacuum is then applied to the reservoir and the glycerol allowed to flow back into it from the chamber. When the level of glycerol is below that of the lowest filter on the piezocone, the vacuum is re-applied to the chamber and the cycle repeated.

3.1.5 The α factor

The importance of correcting the measured tip resistance to take account of the water pressure acting in the groove between the tip and the friction sleeve was first reported by Zuidberg et al (1982) and is now generally accepted. The corrected tip resistance q_t is given by:

$$q_t = q_c + \alpha U \qquad [3.3]$$

where U is the pore pressure in the groove (normally taken to be the pressure measured at the shoulder of the piezocone because it is close to the value at the groove),

α is the correction factor.

When α is calculated from geometry:

$$\alpha = (1 - a) \qquad [3.4]$$

$$a = \frac{(d^2)}{(D^2)} \qquad [3.5]$$

where d is the inner diameter of the groove,

D is the diameter of the piezocone.

The other method of calculating α is by calibration. In this programme the calibration chamber described earlier was used. The piezocone, with fully saturated filters, is subjected

to uniform pressure in a chamber filled with de-aired glycerol. The tip load cell response to the uniform pressure is lower than the applied pressure. The correction factor (1-a) is the value needed to make them equal. In this programme, this calibration was done before the start of every test series and two results were observed:

a) The calibration value of α was lower than that obtained by geometry. This is demonstrated in the table below.

Table 3.1 Comparison of α factors

Piezocone	**α factor**	
	by geometry	**by calibration**
5 cm^2	0.46	0.43
1 cm^2	0.47	0.45

b) It was found, after essential maintenance work was carried out on the piezocones, that the α by calibration changed even though the geometrical value remained constant. This problem was encountered with both piezocones. In the 1 cm^2 piezocone the change in α occurred after a new tip was introduced and, in the 5 cm^2 piezocone, after it was dismantled for maintenance and O-ring replacement. This finding emphasises the importance of calibration before every test. The α factors changed from 0.38 to 0.45, and 0.33 to 0.43 in the 1 cm^2 and 5 cm^2 respectively. However, although the values changed, they were still less than those calculated from geometry.

This difference may be explained by considering the action of water in the groove. Figure 3.2 shows a typical arrangement for a seal between the cone tip and the rest of the piezocone body. The pressure of the water in the groove acts downwards on to the back of the tip,

providing a downward force. However, the pressure acting upwards on the O-ring seal transmits an upward shear force on the stem of the probe. This therefore reduces the net downward force. The geometric calculation does not take this fact into account.

It is essential, therefore, to obtain α by calibration because the geometric calculation can overestimate the factor by up to 50% (Nyirenda and Sills, 1988). [It should be noted that this reference contains a printing error: the α factor quoted as 0.83 should read 0.33].

3.2 Test Chambers

The design and development of the test chambers was undertaken by Dr R.E. May and Mr N. Baker and is described in May (1987). Table 3.2 gives the dimensions of the three chambers used in this programme. However, modifications were necessary in order to adapt the test chambers to the requirements of this study programme.

Table 3.2 Consolidation chamber dimensions (mm)

	Chamber		
	A	**B**	**C**
Shell height	1012	1012	1850
Shell internal diameter	581	581	1001
Piston height	195	195	320
Maximum initial sample depth	780	780	1495
Depth of pore pressure and total stress ports below shell rim:			
Port 1	135	135	210
Port 2	225	225	410
Port 3	315	315	610
Weight of kaolin required (kg)	125	125	625

3.2.1 Test chamber modifications

The original design of the total stress transducers on the piston allowed for one transducer at the centre of the piston. This set-up would not help to study the chamber/soil interaction discussed by May (1987) because it provides no information on the distribution of the stress on the piston. Therefore, in order to attempt to quantify the effect of side friction, two extra total stress transducers were installed on the piston. One was placed half way along the radius of the piston and the other 40 mm from the chamber wall, this being the closest position possible (Figure 3.3). These transducers also help to assess the homogeneity of the lightly over consolidated clay sample at the time of the test (see Chapter 6).

Other modifications to the tanks were made to improve the sealing of the flexible stress controlled boundary. These were as follows:

a) The port membrane joint, which caused many problems during the trial test, needed to be strengthened. The final detail (Figure 3.4) fared well and the ports did not give any further problems.

b) The contact area between the membrane clamping rings needed to be increased because the original contact area had been reduced by cleaning with emery paper. This involved making and welding new rings with a larger contact area to the top plate and machining it so that the two rings coincided when clamped together.

These two modifications, together with the change of membrane to a 1.5 mm thick shot blasterers rubber, enabled the tests to proceed without leakages at the stress controlled boundary.

3.2.2 Diameter ratios

In order to reduce the chamber boundary effects on the tip resistance, it is important that the boundaries be as far away from the point of penetration as is economical. Suitable

diameters of test chambers will therefore depend upon the acceptable level of interference from the boundary on the results. One way to arrive at this is to examine the distribution of radial stresses due to the expansion of a cylindrical cavity in an infinite medium whose diameter is equal to that of the piezocone. Sagaseta (1984) produced a solution (shown in Figure 3.5) which considers a soil to be linear elastic-plastic with a Von Mises yield criterion. Anisotropic initial stresses were incorporated together with shear forces on the cavity wall.

The input parameters to Sagaseta's analysis were as follows:

Rigidity Index (Ir) of 100 and 250

Initial stress ratio $(\sigma_{v_0} - \sigma_{h_0})/(2s_u) = 0.5$

Adhesion factor $\alpha = \sigma_z/s_u, \alpha = 0.3$

This is a lower bound solution and is largely influenced by the rigidity index which, in the test programme, was unlikely to be higher than 200. Using this lower bound solution as a base, it can be said that a diameter ratio that would give no boundary effects would not be economically attainable in the laboratory. Therefore a compromise ratio is needed. Houlsby (1986) suggested a ratio of 30 for chamber tests which, according to Figure 3.5, is equivalent to a radial stress ratio of 10%. The diameter ratios of the chambers used in this programme are given below in Table 3.3 and it can be seen that at the centre port the diameter ratios are 40 and 89 in the large chamber (1 m diameter) for the 5 cm^2 and 1 cm^2 piezocone, respectively, and 53 for the 1 cm^2 piezocone in the small chamber (0.58 m diameter). In Figure 3.5, these are equivalent to radial stress ratios of less than 5%, which would be generally acceptable for an experimental programme.

The side ports, however, cannot be analysed in the same way as the centre port. While the distance to the nearest boundary is less than that of the centre port, they have a much longer distance to the opposite boundary. Clearly, one way to quantify the boundary effects at the side ports is by comparison with the centre port.

Table 3.3 Diameter ratios and distance from nearest boundaries

Piezocone	Diameter ratio (from the centre port)		Distance to nearest boundary (diameters from side port)	
	1 m diameter	0.580 m diameter	1 m diameter	0.580 m diameter
5 cm^2	39.5		10	
1 cm^2	89.3	53.4	22.3	13.4

3.2.3 Test chamber and piezocone instrumentation

The test chamber was instrumented and manually monitored during the consolidation and swelling stages. During the penetration and dissipation stages, the piezocone instrumentation was added and automatic data logging was used. The instrumentation during sample preparation will be discussed here, followed by the additional instrumentation required during penetration and dissipation testing. Figure 3.6 shows the instrumentation of the 1 m diameter test chamber together with that for the 5 cm^2 piezocone. The instrumentation of the 0.58 m diameter test chamber is similar to that shown, except that there is only one radial stress transducer and the 1 cm^2 piezocone used has fewer measured parameters (see Section 3.1).

Details of the piston displacement transducer, and the Druck PDCR 10 and 22 transducers used in this programme have been given by May (1987). The three pore water pressure transducers embedded into the soil are Gaeltec type 3EA/a. Strain gauges in these half

bridge transducers are made from chromium cermet which has electrical properties similar to steel but has a gauge factor of up to ten times greater, thus providing greater sensitivity of measurement.

These pressure transducers were found to be susceptible to an ingress of water through the seal at the back. The author was able to suggest to the manufacturers an improvement to the design, namely that the sealant be changed to a glass compound which did not dissolve in water. This modification has since been implemented.

The front of the 3EA/a pressure transducer is threaded to allow a perspex cap with a porous stone face to be fitted. A gap of approximately 2 mm is left between the porous stone and the sensor to be filled with the saturating fluid. The pressure transducer is powered by an alternating current to prevent the sensor from being etched. To do this, a driver is used to convert 10 volts DC to 5 volts AC. In the same driver box is the passive resistor which completes the bridge for the transducer.

The power supply to all pressure transducers is provided by a custom-made unit. There are sixteen possible channels, each capable of providing 5, 10 and 12 volts DC, depending on the wiring of the six pin DIN plug. This arrangement solved the earthing problems encountered when the three voltages were powered from separate power supply units.

During the penetration and dissipation stages of the tests the piezocone instrumentation is added. This includes up to two load cells, up to four pore water pressure transducers and a linear displacement transducer. The load cells and pore water pressure transducers on the piezocone are described in Section 3.1. The linear displacement transducer is a Celesco type PT101 with a linearity and hysteresis of 0.01%.

3.3 Penetration System

The penetration system employed in the programme was developed around a 1.8° stepper motor. The choice of the size of the motor was based on the calculated thrust, assuming a tip load of 1.0 kN and a maximum shear load of 6.25 kN. Figure 3.7 illustrates the main components of the penetration rig while Plate 3.3 shows the assembled rig with the driver for the stepper motor. The main features of the system are described below:

a) A 1.8°, three stack, size 42, stepper motor capable of providing 6.2 Nm at 2000 pulses/s and powered by a bipolar chopper driver at 12 Amps/phase. The driver incorporates a multi-turn potentiometer with dial mechanism for speed control; a four decade thumbwheel switch for setting travel distance; forward/reverse and zero/index switches, all mounted on the front panel. For switching on/off only, the driver is remote controlled to enable synchronisation with the switching on of the data acquisition system.

b) A 5 mm pitch, 20 mm diameter ball screw mounted on a linear bearing to facilitate smooth guided linear motion and to take the moment due to the eccentricity of the connection of the piezocone to the ball screw. The ball screw is connected to the motor through a flexible coupling which enables the efficient transfer of torque to the lead screw, even with a misalignment between the motor and the lead screw. The load is transferred via thrust bearings at both ends of the lead screw to the reaction frame which is bolted to the top plate of the chamber.

The driving system, as designed, is capable of pushing the piezocone at varying speeds up to 50 mm/s and has a facility to lock at one speed.

3.4 Data Acquisition and Electrical Noise

The data logger (Analogue Express) used in the data acquisition system in this programme of research was fully described by May (1987), but it is important to reiterate that it is a 12 bit resolution machine with a possible 16 channels which are recorded simultaneously. This is achieved by the use of a sample and hold facility on each channel. However, due to electrical noise and other hardware problems, a considerable number of changes were made to the system. The level of electrical noise in the system, as recorded by the data logger, was approximately ± 50 mV, which was unacceptable for the following reasons:

a) The maximum output from the piezocones was approximately 250 mV. This meant that up to 20% of the output could be attributed to noise and, because of its random nature, could not be properly accounted for.

b) The most affected outputs were those from the piezocone, most notably the tip and total resistance outputs, which made it even more important to find a method of reducing the noise to manageable levels.

The reasons for noise were threefold. In the first place, there was the 10 m cable between the piezocone and the amplifier which was unshielded, unearthed and carrying signals in microvolts. This acted as an antenna, as did all the long cables, and induced voltages in the signal lines. Therefore the cable had to be shielded, shortened and earthed. The amplifiers were brought to within 2 m of the piezocone, thereby reducing the length of cable over which noise pick-up occurred; and the amplification increased five times to 5000, so that any noise picked up between the amplifiers and the data logger in the shielded and earthed cable would be insignificant.

Secondly, many cables were not earthed and those that were tended to form earth loops, which caused more problems. Therefore all the cables were re-made to provide the necessary shielding and earthing, taking great care to avoid earth loops. The final layout is shown in Figure 3.8.

The interaction between the data logger and the computer (Commodore 64) caused a lot of interference because of lack of synchronisation. The computer was therefore replaced by an Opus III. This meant rewriting all data logging software, but provided an opportunity to incorporate the following improvements:

a) The addition of the facility to record the times at which the readings were taken. This is very useful in determining the penetration depth since the rate can be set accurately. This is of particular importance in this programme because of the electrical noise problem which badly affected the displacement transducer.

b) The facility to store data on to disk while the test is taking place. This is a safeguard against power failure which was missing in the previous software.

The logging program, A2D.EXE, was written to record data at specified intervals laid down in an experiment plan. The plan consists of two columns of numbers. The first one is the scan rates or interval between readings in seconds, and the second one gives the times, from the beginning of the test, when the corresponding scan rate stops and the next starts. The times in this column are entered on the basis of the 24 hour clock. Hours, minutes, and seconds are separated by a colon (:). Table 3.4 shows an example of an experiment plan; in this case, one which was used in Z10A series of tests.

Table 3.4 An example of an experiment plan.

#TESTING PLAN FOR Z10 SERIES

0.05	25
0.10	45
0.5	60
1.0	80
2.0	2:00
4.0	3:00
15.0	6:00
30.0	12:00
60.0	30:00
240.0	1:00:00
540.0	2:30:00
900.0	3:30:00

3.5 Shear Vane Apparatus

Plate 3.4 shows the motorised shear vane system which can be converted into a loading or reaction frame for calibrating the load cells of the piezocones. The latter use requires an extra frame bolted to the base and a separate, recently calibrated, load cell. The motorised shear vane was developed in order to eliminate operator dependency on the results from hand operated shear vane tests. Included in the development is the casing around the extension rod which eliminates the skin friction on the rods from measured shear strengths, and a universal joint at the top of the rod to ensure uniaxial rotation of the vane. The only piece of equipment from the original vane apparatus (May 1987) was the 19.05 mm (or 0.75 inches) vane itself. The main features of the system are therefore as follows:

a) The torque transducer, comprising a full bridge torque strain gauge configuration made from Welwyn Strain Measurement strain gauge type EA-XX-067TV-350 with a pattern width of 2.92 mm, bonded onto a 5 mm diameter mild steel hollow tube with a wall thickness of 1.5 mm. The transducer is fixed to the top end of the shear vane rod (Plate 3.5 shows a close up of the shear vane where the torque transducer can be seen more clearly). It is calibrated against known applied torque and the standard BS 1377 (1975) relationship repeated below is used to find the relevant undrained shear strength.

$$T = 0.5\pi D^2 H\left[1 + \frac{D}{3H}\right] s_{uv} \qquad [3.5]$$

where T is the applied torque,

D is the vane blade diameter,

H is the vane blade height,

s_{uv} is the undrained shear strength.

The dimensions of the vane used in this programme are diameter 19.05 mm, and height 28.7 mm. In which case:

$$s_{uv} = 50.05T \quad \text{kPa} \qquad [3.6]$$

where H and D are measured in metres and T in kNm.

b) A single phase single speed motor capable of transmitting 5 Nm at a speed of 2.42 rpm. The speed was reduced by a worm-wheel gear with a reduction ratio of 81:1 giving a steady rotation speed of 10.8° per minute. This is still a fast enough speed for undrained conditions to hold, and it falls within the limits set in BS 1377 (1975).

3.6 Restricted Flow Consolidation and Permeability Apparatus

All consolidation tests were carried out in restricted flow apparatus (Sills et al, 1986) instead of the conventional oedometer, because of the shorter time taken to carry out each test. Pore water pressure (both on the drained and undrained face) and the total stress during consolidation are monitored together with the displacement. This allows a stress-strain relationship of the sample to be established for any point during consolidation.

The addition of the flow pump apparatus and a differential pressure transducer converts the system into the flow pump permeability apparatus (Oslen, 1984). This dual purpose apparatus was useful in that it enabled the consolidation test to be stopped at the appropriate effective stress level in order to carry out permeability tests on the same sample.

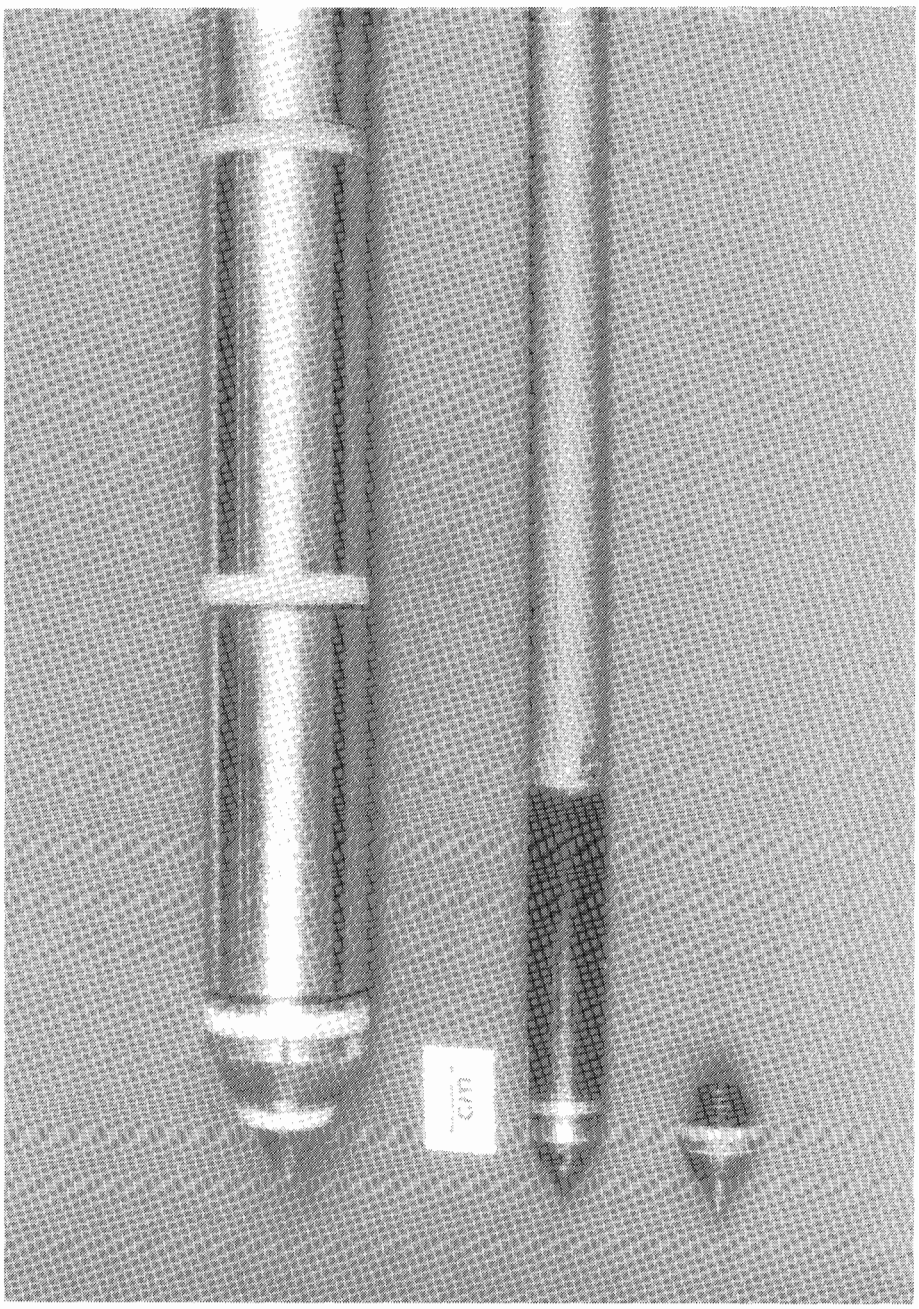

Plate 3.1 The two piezocones used in this programme. The 5 cm^2 piezocone with pore pressure measurements at four locations and the 1 cm^2 piezocone with interchangeable tips.

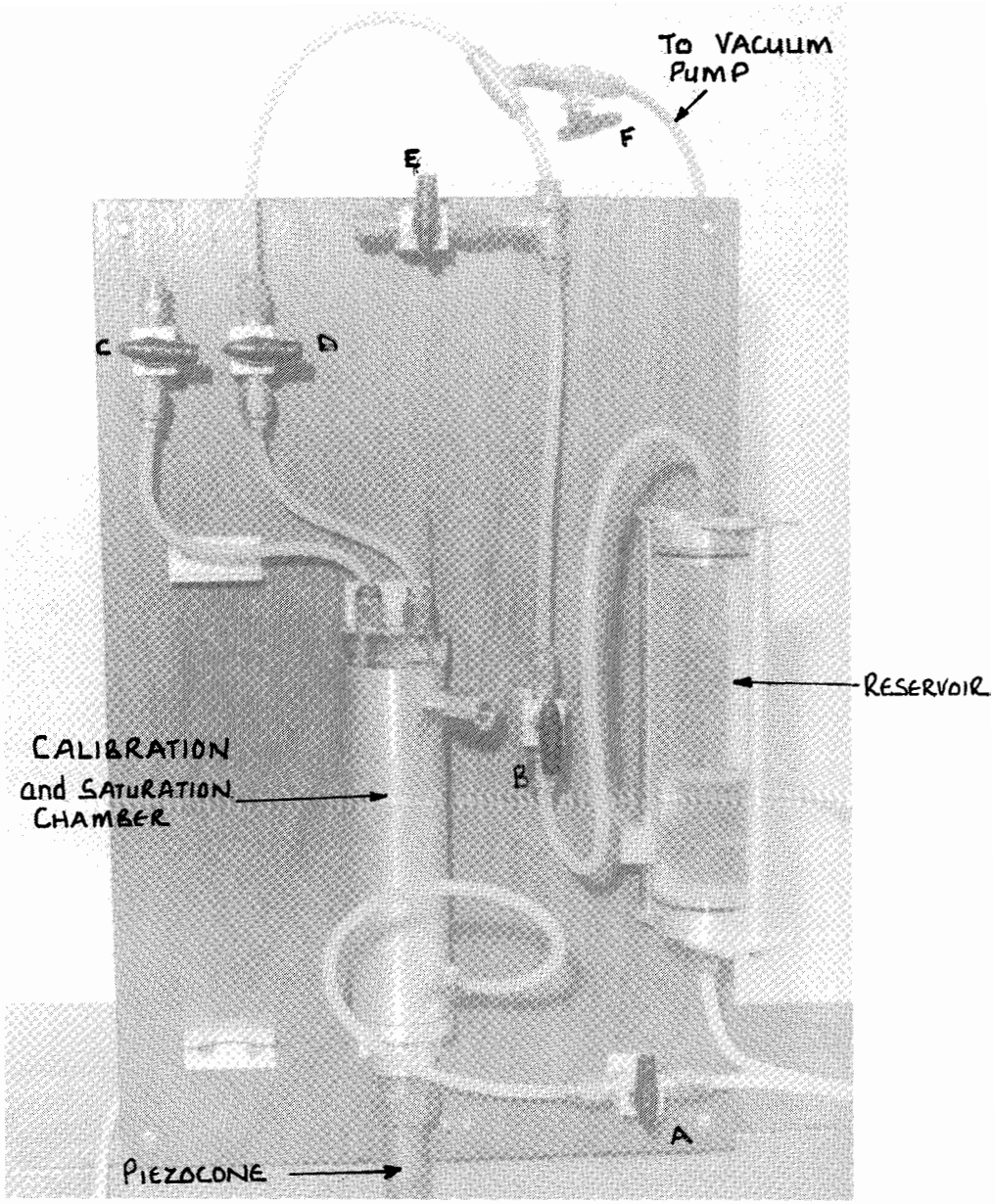

Plate 3.2 The saturation and calibration chamber for pore pressure transducers on the piezocone.

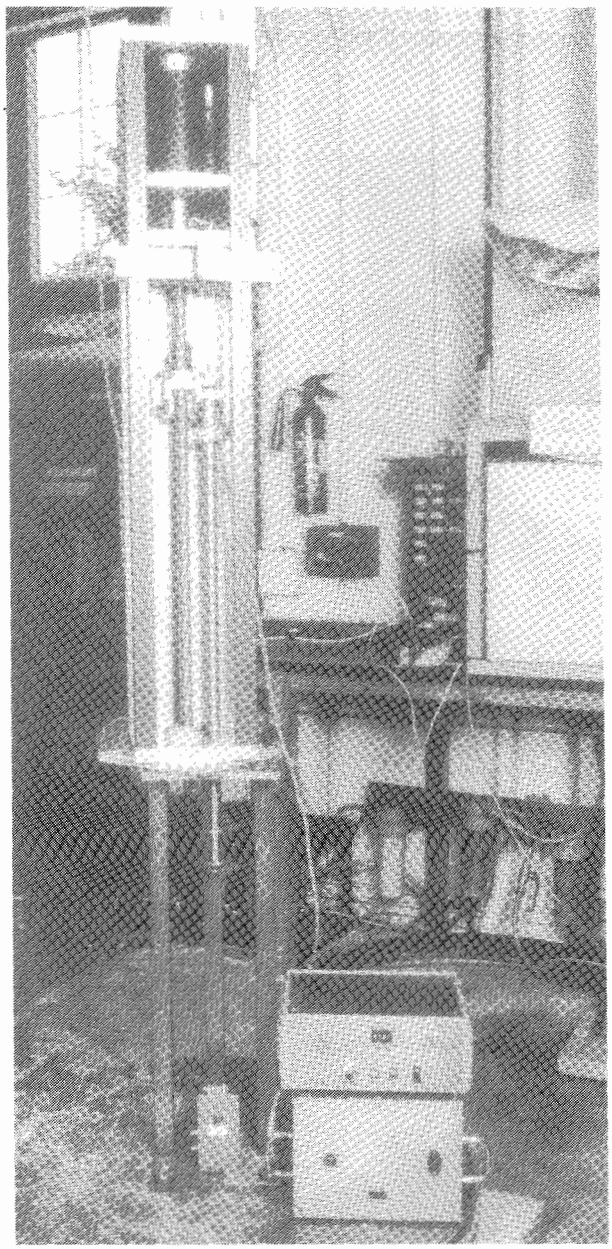

Plate 3.3 The stepper motor driven penetration system.

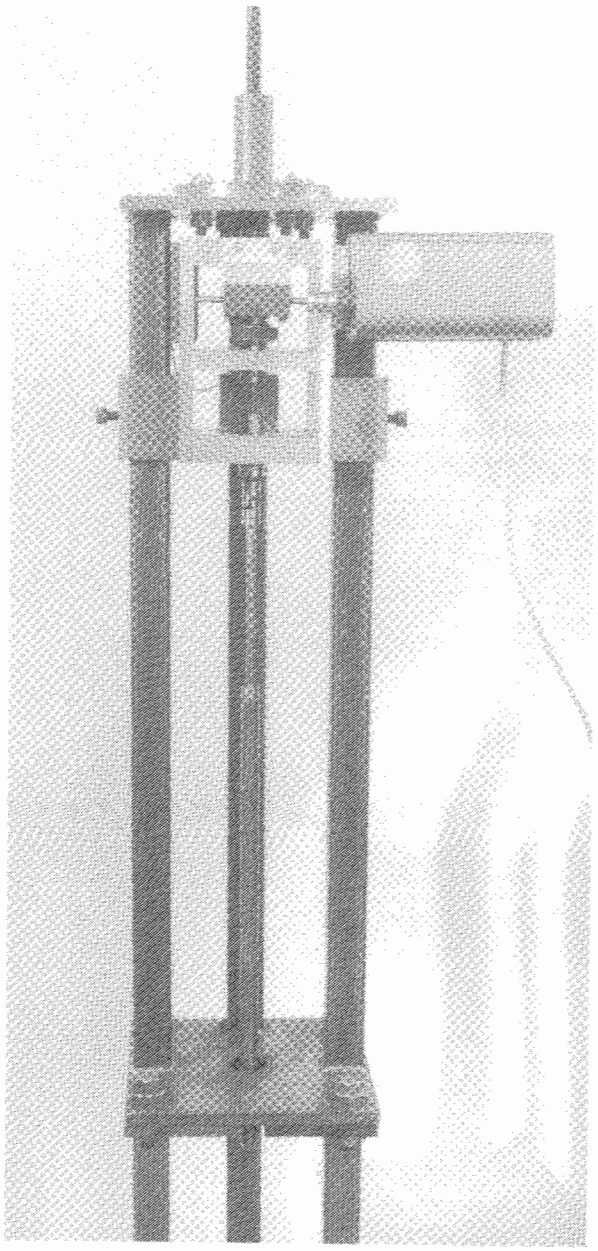

Plate 3.4 The motorised shear vane.

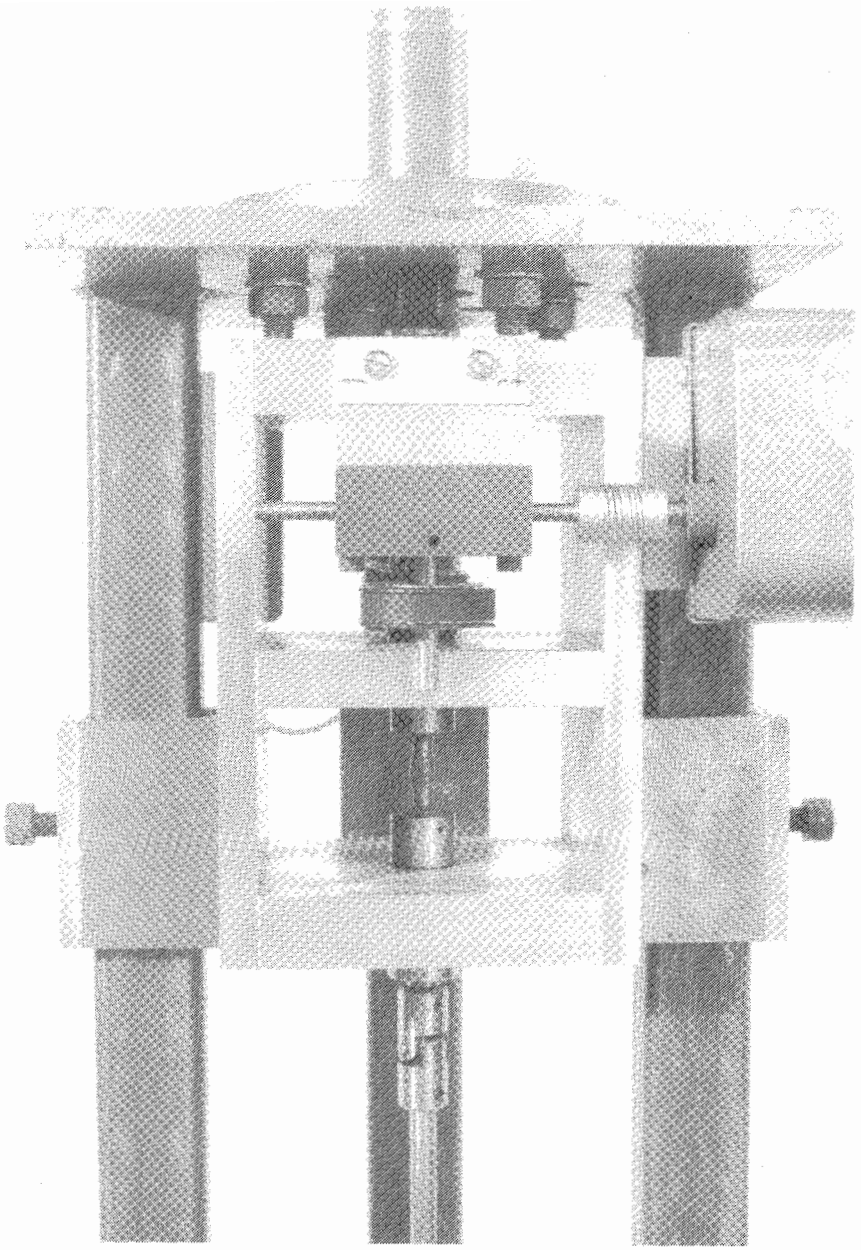

Plate 3.5 A close up of the motorised shear vane showing the universal joint, the torque transducer and the driving mechanism.

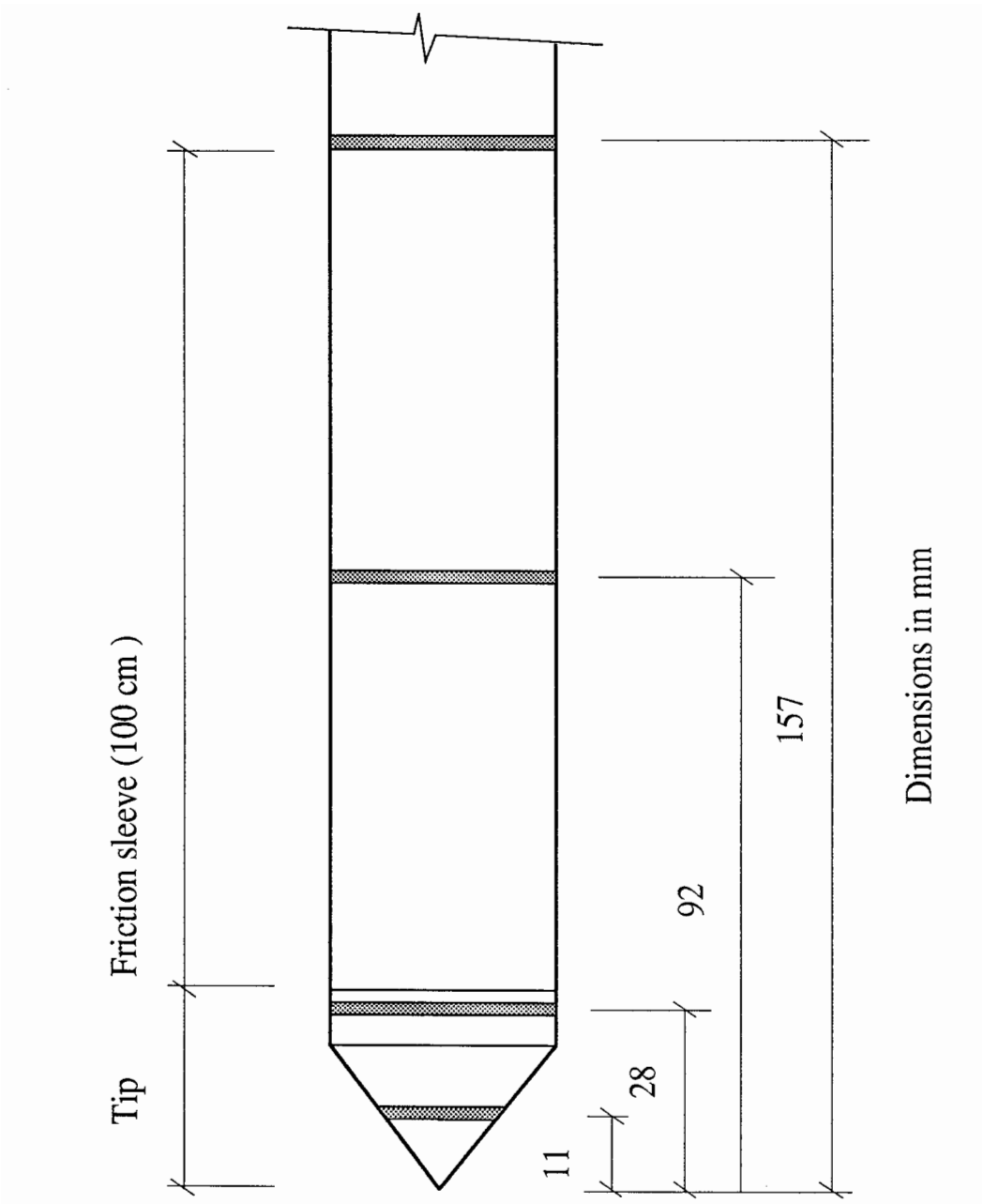

Figure 3.1 Diagrammatical representation of the Oxford piezocone.

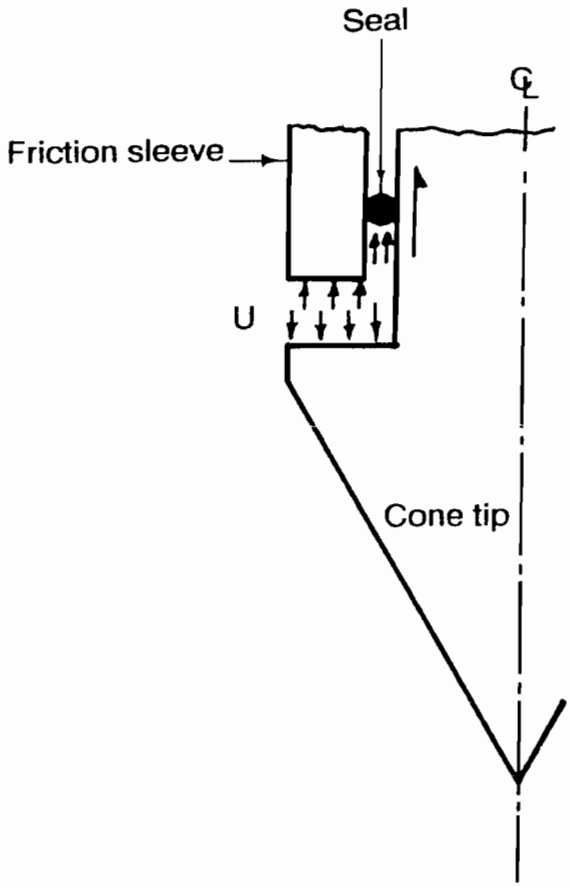

Figure 3.2 Typical seal arrangement between cone tip and the piezocone body.

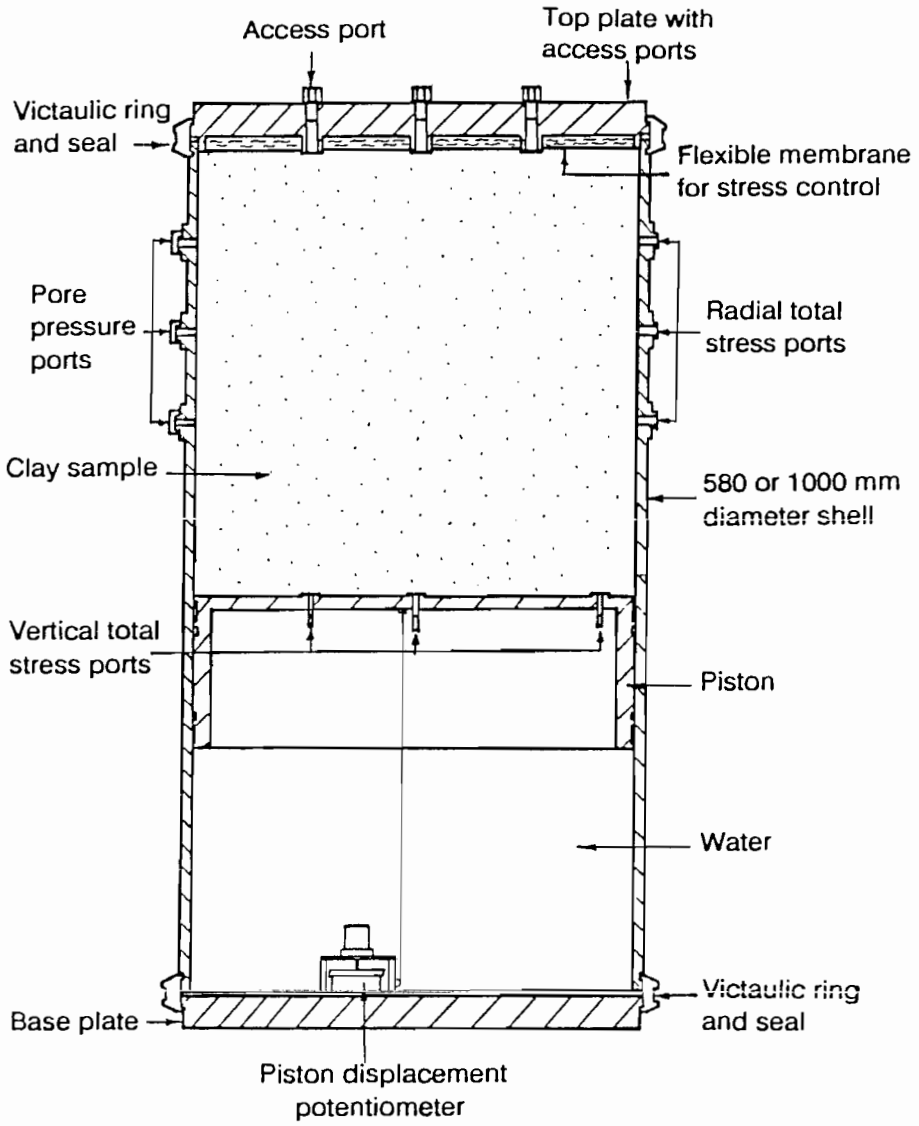

Figure 3.3 Some details of the consolidation chamber.

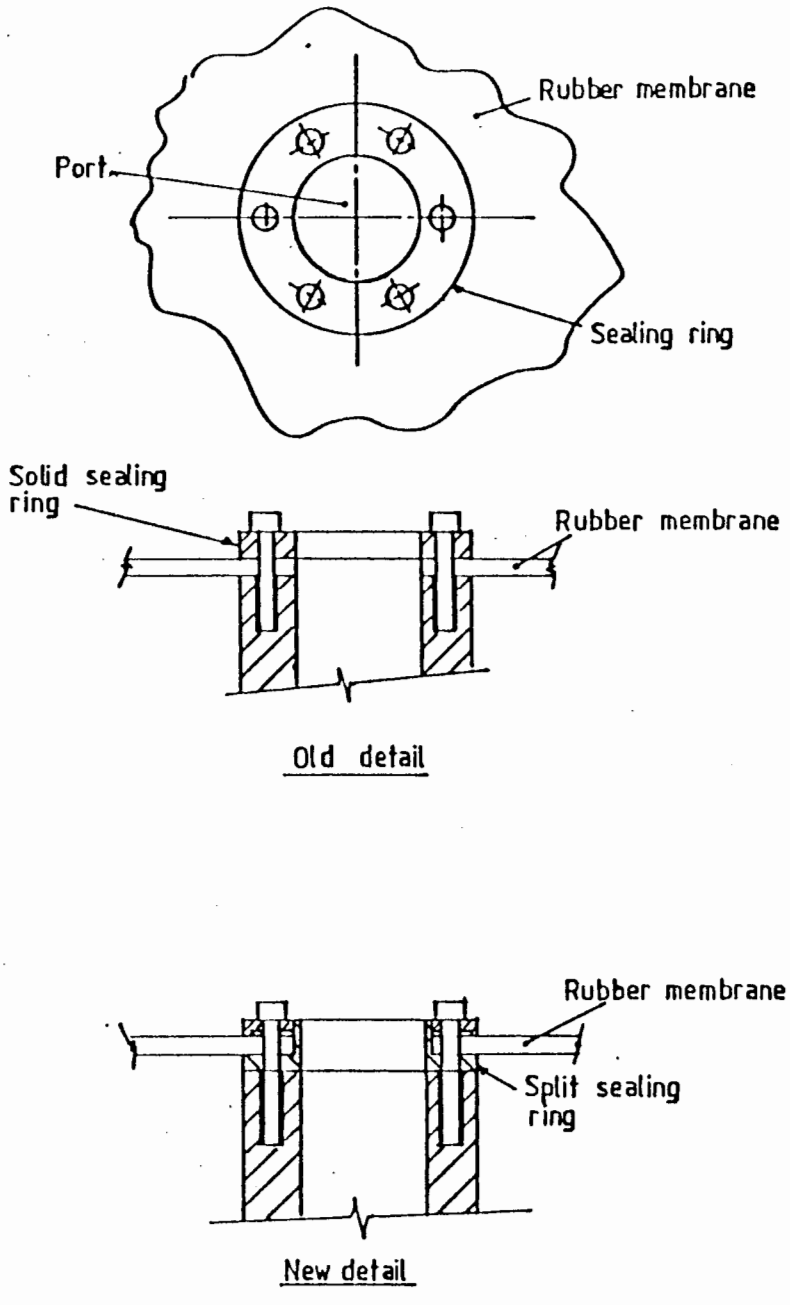

Figure 3.4 Details of the old and new access port.

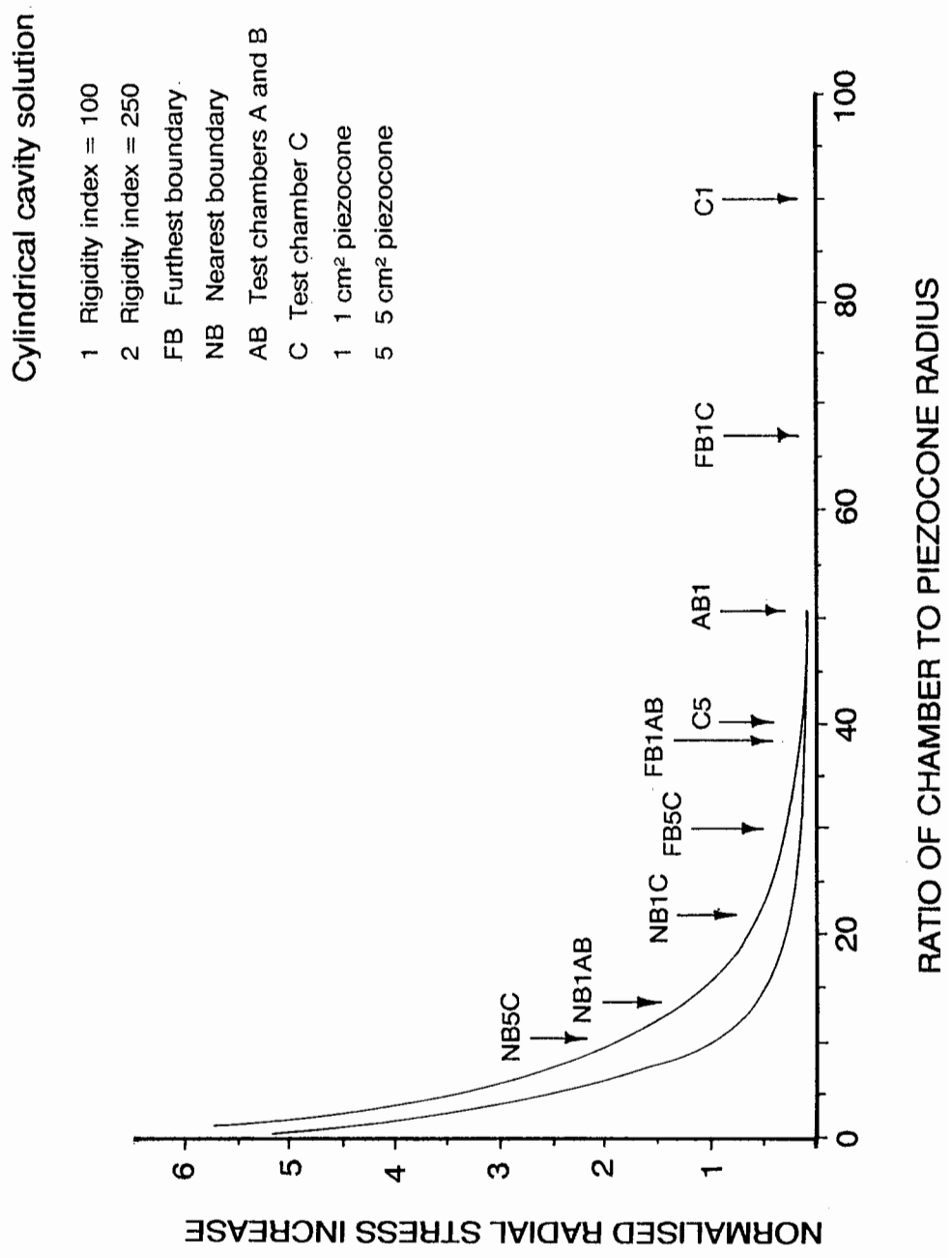

Figure 3.5 Normalised radial stress distribution marking positions of the diameter ratios and distances to the nearest and furthermost boundaries for the two sizes of piezocone in the two sizes of test chamber. (Adapted from May 1987).

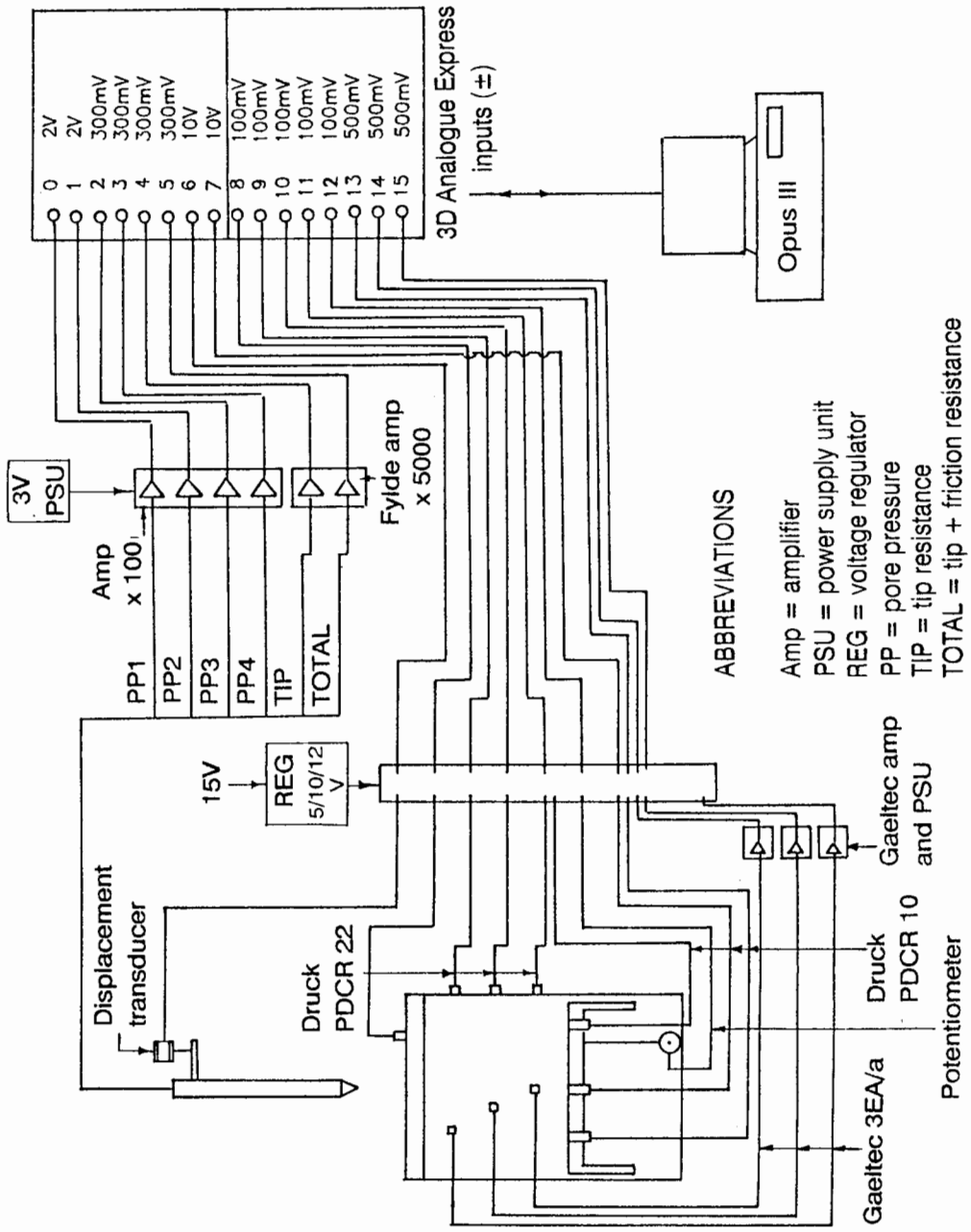

Figure 3.6 Instrumentation diagram for consolidation chambers and the piezocone.

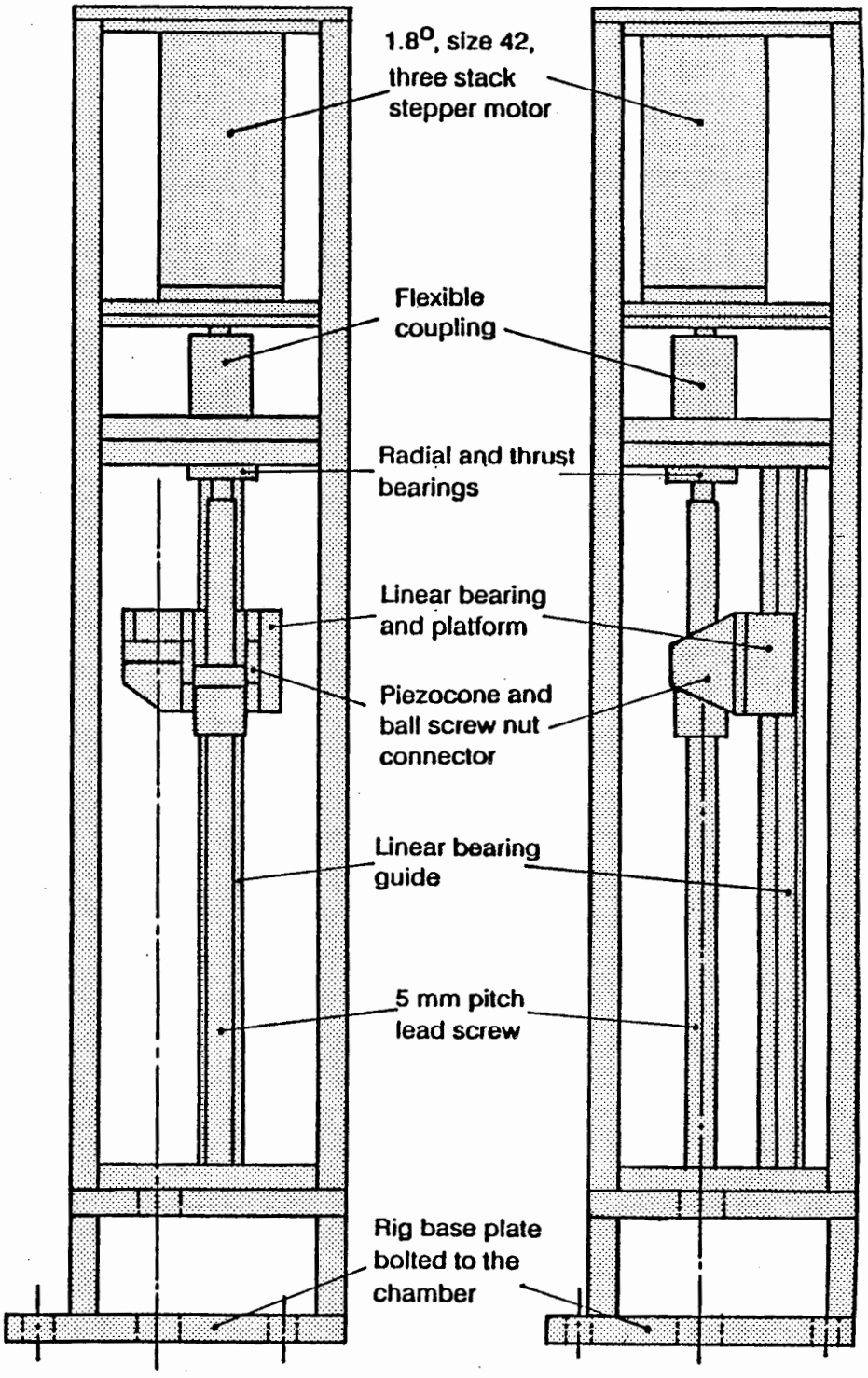

Figure 3.7 Schematic drawing of the stepper motor driven penetration rig. (Not to scale).

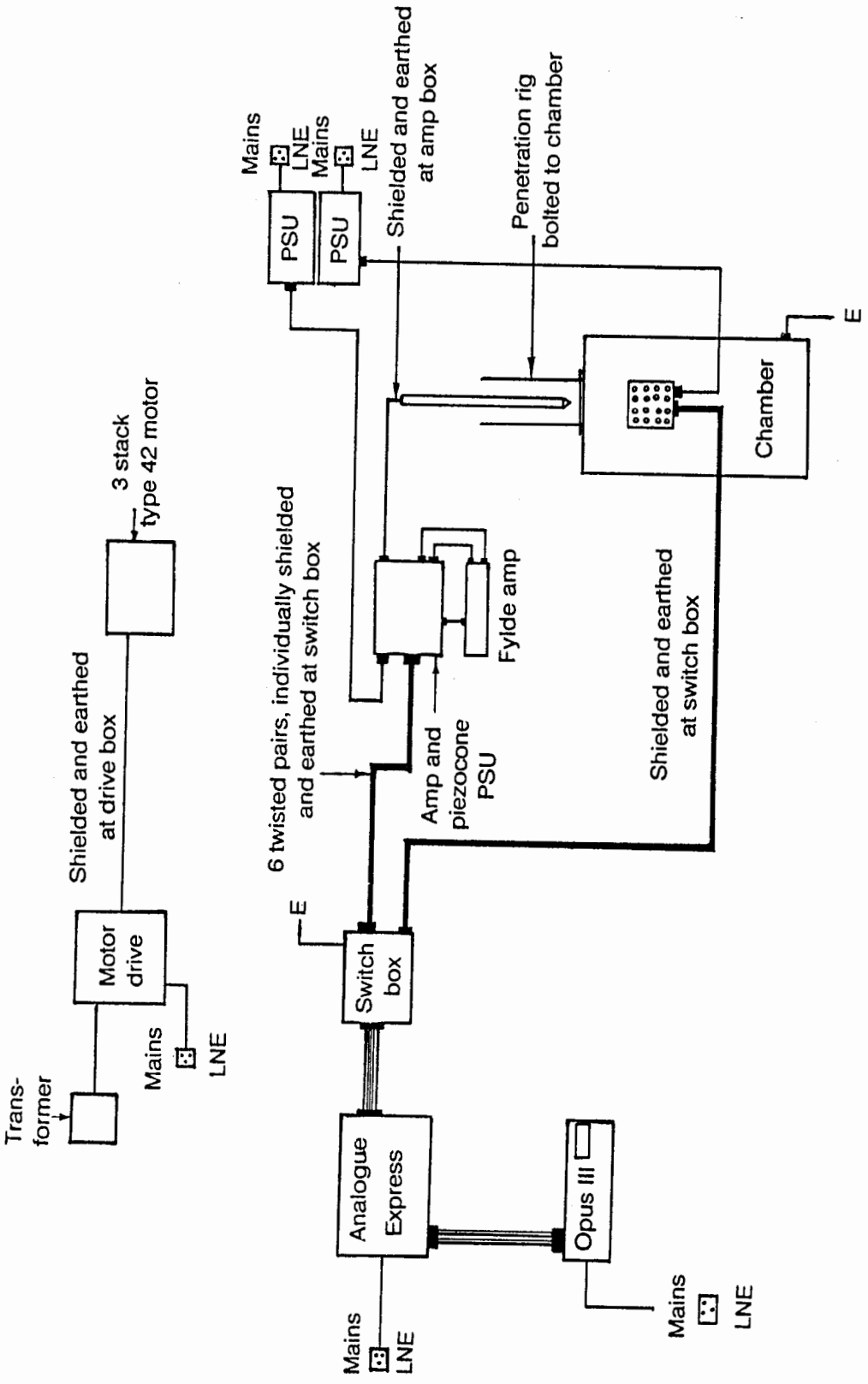

Figure 3.8 Schematic details of the wiring diagram.

4 SAMPLE PREPARATION

Sample preparation encompasses all the procedures that take place before the penetration tests can start. This includes the preparation of the consolidation chambers themselves to receive speswhite kaolin slurry; ensuring that the consolidation pressure system was functioning properly before consolidation could start; the consolidation process itself, which in this programme involved loading and unloading; and finally the preparation of the stress controlled pressure system for the top plate. Sample preparation took a minimum of seven weeks or four weeks in the 1 m or 0.580 m diameter chambers respectively.

4.1 Initial Chamber Preparation

Before the mixing of speswhite kaolin can start, it is important to ensure that the chamber to be filled is prepared. To do so, all transducers on the piston must be calibrated, fitted in place and their initial readings recorded. Drainage lines should be checked for blockages or leakages by flushing water through them. Both top and bottom drainage lines empty into a stand pipe, as shown in Figure 4.1, thus ensuring that there is a hydrostatic pressure difference across the sample at all times. The inside of the cylindrical shell must be well greased using water pump grease which remains lubricant over long periods.

The sealing quad rings and the low friction, fabric reinforced, plastic bearing rings should be well greased and in place before the shell is lowered over the piston and clamped to the base plate with a Victaulic ring and seal arrangement. The underside of the piston should be filled with water and properly de-aired and a water saturated Vyon filter carefully positioned so that the three total stress transducers fit into the correct holes without being damaged.

Horizontal total stress transducers could be installed and initial readings taken at this stage but this operation could also be carried out in between mixes.

4.2 Speswhite Kaolin Mixing

The clay used in the programme is powdered speswhite kaolin with the following specifications:

Liquid limit	66%
Plastic limit	31%
Clay content	80%
Fine silt	18%
Medium silt	2%
Specific gravity	2.64

The Plasticity Index of 35% makes this reconstituted clay of medium plasticity. In order to ensure little or no macro fractures in the freshly mixed clay, and for the purpose of pumping the slurry into the chambers, the water content in the mix was about twice the liquid limit. Also, in order to avoid excessive air entraining, the mixing was carried out under vacuum.

The procedure involved weighing 2.5 bags (approximately 62.5 kg) of speswhite kaolin and working out the appropriate amount of water for a moisture content of 120%. Approximately two thirds of the water was first poured into the mixer followed by the dry speswhite kaolin powder. The remaining water was then added and worked into the powdered clay until it had all sunk under the water. The mixer was then closed and clamped before switching on. When the mixer had been running for about five minutes and all the clay powder had been mixed with the water, the vacuum was turned on, thus preventing the clay powder being sucked into the vacuum pump. The mixer was allowed to run for approximately two hours; a time arrived at from experience by other workers (Love, 1984; Fannin, 1986; May, 1987).

After the mixing was finished the slurry should look and feel smooth when squeezed between fingers. A compressed air driven pump was used to tremie the mixed slurry into the chambers. Two mixes were required for the small chamber and ten for the large chamber or, in terms of time, one and three 12 hour working days respectively.

4.3 Top Plate Preparation

The preparation for this stage is similar to that of the piston. Firstly, drainage lines were flushed through to ensure that there were no blockages. Then the space behind the flexible rubber membrane was filled with dyed water which would indicate any leak in the drainage lines.

This is a stress controlled boundary and it is important that there should be no pockets of air behind the rubber membrane. Therefore a simple, but effective, technique was employed every time the dye had to be poured in. A template with polystyrene backing was clamped to the underside of the top plate. This made the rubber membrane level with the base of the ports. The whole system was then tilted at approximately 30° with one of the two openings into the fluid chamber at the top. The dyed water was then introduced into the bottom opening until it began to flow out at the top opening. The whole system was then further tilted backwards and forwards until no more air was seen to come out.

At this point a pressure transducer was fitted as close to one opening as possible, to measure the pressure of the dyed water in the membrane. It was necessary to place this pressure transducer immediately above the top plate because of the possible loss of pressure along the 8 mm Enot tubing, owing to expansion or flexing under fluid pressure. Both taps, top and bottom, were then closed before righting the plate and unclamping the template. Finally a 1.5 mm Vyon filter, cut to fit the membrane, was fitted and secured round the ports before the top plate was lifted into place and clamped to the cylinder with a Victaulic ring and seal arrangement.

The four outer penetration ports were plugged during consolidation but the centre port was fitted with a further total stress transducer such that it was flush with the membrane and in direct contact with the soil. The plugs were also designed to fit flush with the membrane. When all of this was finished, the top plate drainage could then be completed by connecting 8 mm Enot tubing to the drainage ports and letting them drain into a stand pipe made of clear perspex (see Figure 4.1).

4.4 The Consolidation Stage

Madan's Uni-Cub Airhydropumps provided the required pressure for consolidation. The Uni-Cub is an air driven pump which consists of a hydraulic ram driven by two differential air pressure pistons, one of which (the return piston) is at a constant pressure. Reciprocation is achieved by a change-over shuttle which directs air to and from the drive piston. Inlet and outlet non-return valves in the hydraulic cylinder allow the displacement of the reciprocating hydraulic ram to produce a pumping action.

To maintain a near constant consolidation pressure, there must be a trade-off between the pressure required to drive the pump, and the amount of water allowed to bleed back to the reservoir through the non-return release valves. In the test programme, fluctuation due to pump action was reduced to less than 20 kPa, which was less than 5% of the total consolidation pressure.

Consolidation pressure was applied in three steps, the first two being applied through Uni-Cub pumps. At the end of the second stage, the pressure was only 80% of the final consolidation pressure. This allowed for the embedding of pore water pressure transducers into the sample. Gaeltec type 3EA/a pressure transducers, fitted with glycerol-saturated filters, were embedded into the soil at varying distances from the centre of the chamber. The method of embedding was by auguring a hole into the sample to the required depth via the soil pore water pressure port. Then, using a tool specially designed for the purpose, the

transducer was gently pushed down the pre-drilled hole until it was in contact with the soil. The transducer cable was then carefully positioned in a specially prepared rubber bung and the pore pressure port sealed.

The application of consolidation pressure was then transferred either to an Oxygen Free Nitrogen (OFN) bottle, or to the on-line compressed air system, via an air-water interface before the third step increased the pressure to its final value. The final compression of the sample due to this last loading stage was enough to close the augured holes so that they did not form horizontal drainage conduits during penetration testing. Consolidation was assumed complete when the pore pressure transducers showed a hydrostatic distribution of pore pressure through the sample.

4.5 Swelling Stage

Since the programme involved studying the behaviour of the piezocone in lightly over consolidated clay, the ultimate stage in sample preparation was unloading to the required testing pressure, depending upon the chosen over consolidation ratio. The main concern during this swelling stage was the effect of high suction on the sample which might cause cavitation if all the load was removed at once. Cavitation in saturated soils is a phenomenon which comes about when pore water (or indeed any pore fluid) cannot withstand negative pressures imposed on it by the sudden removal of confining pressure, and it vaporises. This would cause loss of shear strength due to the voids that would be created by the vaporising fluid (Bishop et al, 1975; Mair, 1979). Free water would vaporise at about one atmosphere but, in clay soils, higher suctions are sustainable due to ionic attraction between water and soil molecules.

However there will be a threshold pressure at which the water in saturated clay soils will vaporise. Bishop et al (1975) investigated cavitation of kaolin in a set of isotropically, normally consolidated, triaxial tests over the confining pressure range of 860-6900 kPa and found that there was no significant reduction in shear strength due to removal of confining

pressures below about 1400 kPa. Mair (1979), however, showed that at lower confining pressures than suggested by Bishop et al, there was still a loss of strength due to cavitation. He also concluded that susceptibility to cavitation increased with increasing void ratio and that the phenomenon propagates from free boundaries. Therefore the bulk strength of large specimens was less affected.

The circumstances under which these conclusions were made were different to the ones faced in this programme. In both cases, samples were tested immediately after removal of confining pressure and no sample swelling was allowed. In this programme, sample swelling was allowed under a constant head of water and the confining pressures were not reduced to zero. Sample testing was also only carried out after the generated suction pressures had dissipated. Therefore, whilst cavitation reduced shear strength immediately, the effect of swelling on the cavitated soil is not known.

However, in view of these findings, it was necessary to take precautions against cavitation, and two methods were used in the programme. Where the final consolidation pressure was provided by an OFN bottle, unloading to the testing pressure was achieved by a gradual, but continuous, loss of pressure on the air side of the air-water interface. This was equivalent to a slow leak in the system and reduced the consolidation pressure very slowly, generating a maximum suction pressure of approximately 60 kPa.

Where the final consolidation pressure was provided by the laboratory on-line compressed air supply, it was found to be more convenient to unload in small steps and allow generated suction pressures to dissipate at each step. Steps of 50 kPa were used in this programme.

When the consolidation pressure had been reduced to the final testing pressure, the top plate was then prepared for its stress control function during the penetration testing stage. To achieve this, the pressure in the membrane was transferred to, and controlled from, an air-water interface. The pressure in the interface was supplied by the on-line compressed air system and controlled by a Norgren bleeding type pressure regulator.

The water pressure under the piston was locked in place by turning off taps on inlet pipes. The latter action assumes that water will not compress but does not account for possible air pockets under the piston due to dissolved air under pressure coming out of solution as the pressure is reduced. However, because of the removal of air under the piston during chamber preparation, the closing of the taps provided adequate clamping of the piston because no piston displacement was recorded during penetration. This final stage was completed when the pore water pressure in the sample had dissipated, usually taking up to five days.

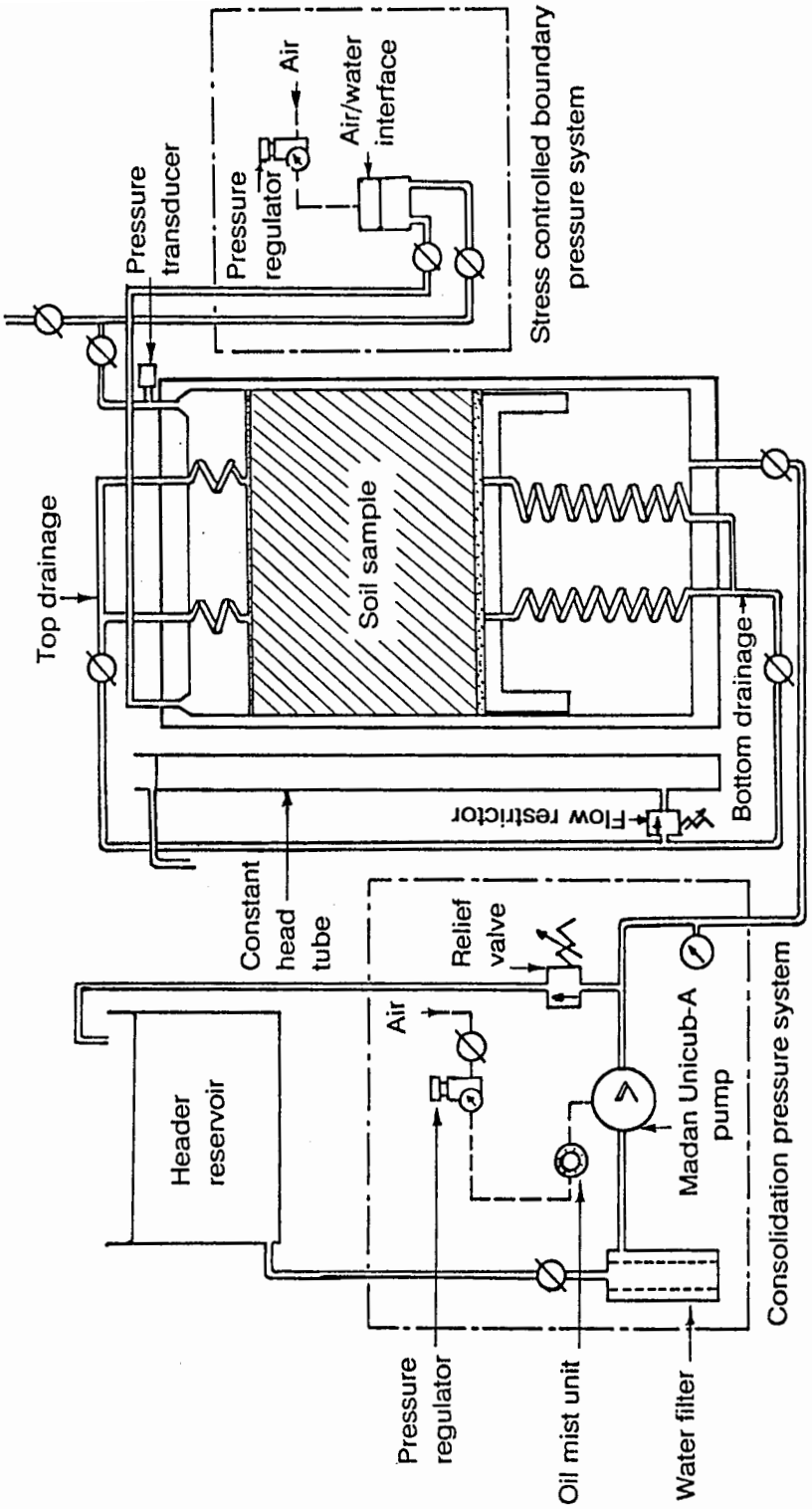

Figure 4.1 Schematic drawing of consolidation chamber pressure systems

5 TESTING PROCEDURE AND DATA ACQUISITION

This chapter describes the tests on the prepared sample in the chamber and those carried out on sub-samples. Penetration tests were carried out in four of the five ports and shear vane tests in the remaining one. The sample was then sub-sampled for triaxial, restricted flow and permeability tests.

5.1 Penetration Testing Procedure

The penetration testing procedure included the saturation of the piezocone (and calibration for the first test of the series), the preparation of the data acquisition and the penetration systems.

The saturation procedure described in Chapter 3 commenced up to eight hours before the start of penetration to allow several cycles to be achieved. Where calibration of the piezocone was necessary, the saturation procedure was started the day before the penetration tests.

While the piezocone filters were saturating, the inputs from the piezocone and the chamber were connected to the correct data logger (Analogue Express) channels. In order to check the wiring, and the transducer responses, a Basic program, Zed.bas, was run. This program was designed to interrogate the data logger in the same way as the main logging program, A2D.exe, but the output is sent to the screen. Dummy tests were sometimes carried out at this juncture by applying pressure to the calibration chamber where the piezocone was saturating.

When saturation of the piezocone filters was complete, the preparation of the testing rig was begun. The plug in the port to be tested was removed and the testing rig hoisted into position and secured to the top plate. The stepper motor driver was then connected, together with the remote control switch, which was also connected to the data logger.

At this point, the piezocone was removed from the saturation chamber and secured to the piezocone connector on the testing rig. It was then lowered slowly, using a 2 mm distance setting on the stepper motor drive, until the tip of the piezocone rested at the top of the soil sample (see Plate 5.1). The travel distance was set at the drive box, after zeroing the previous setting, and the logging program A2D.exe was initiated manually to take five calibration readings. A remotely controlled switch then triggered the synchronised start of penetration and data logging.

When penetration was complete (see Plate 5.2) the test continued into the dissipation stage. The penetration test took 14 seconds and 29 seconds in the 0.58 m and 1 m diameter chambers respectively. Total test times, including dissipation, were set for three and four hours respectively.

5.2 Post Penetration Testing

In situ testing would be of little value if the results did not relate to the soil parameters required for the design of structures in the ground. Therefore, the calibration of an in situ instrument would be incomplete if its results did not relate to strength and deformation parameters of the particular soil in which it is being calibrated. It was for this reason that shear strength and consolidation tests were carried out.

5.2.1 Moisture Content.

It is very important to take moisture content samples as quickly as practically possible after extracting the sample. However, samples were taken from three radii and three depths, involving considerable delay between each level during the removal of the intervening soil.

For example, in the 1 m diameter chamber sampling times between the levels could be as long as five hours. Delays were also caused by the need to sub-sample for triaxial and consolidation tests. Consequently, a variation in the results of moisture content could be expected as a result of moisture evaporation and migration within the sample.

5.2.2 Shear strength testing.

The shear strength of a soil is one parameter which is sought after in most soil investigations, and yet it is also one which is not unique for any particular soil because it depends on such factors as the mean effective stress and the type of test used in determining the parameter (Wroth 1984).

It has also been pointed out by Kirkpatrick and Khan (1984), Hight (1985), and May (1987) that sub-sampling for triaxial or other laboratory testing causes loss of strength of the soil being tested. The loss of strength is due to the relaxation of confining stresses. In view of this factor it was necessary to find the shear strength of the clay sample in the chamber with the stresses which existed during penetration.

However, shear strengths from sub samples were also needed because standard practice is to use shear strengths obtained from triaxial samples. In this case, isotropically consolidated undrained compression tests were carried out on at least three samples from each test series.

5.2.2.1 Shear vane testing

In order to find the shear strength of the clay sample with the confining stresses still acting on it, a pilcon vane was used with a 300 mm and 600 mm extension rod in the 0.58 m and 1.0 m diameter chambers, respectively.

However, it was soon found that, for a relatively homogeneous soil sample, the variation of vane shear strength with depth was not satisfactory because of the skin friction along the extension rods. Another reason for dissatisfaction with the Pilcon vane was the operator-dependency of the results; turning the vane by hand creates difficulties in

maintaining a consistent shear rate from one test to another. Therefore, to standardise the shear rate and to remove the soil-extension rod interaction, a motorised shear vane with a torque transducer and sleeved extension rod was developed (see Chapter 3). Figures 5.1 and 5.2 show typical results of shear strength with depth before and after the improvement to the shear vane apparatus.

After the final penetration test, the shear vane rig was mounted over the fifth port and shear strength tests carried out at 50 mm intervals of depth. After shear vane testing was completed the tank was dismantled and the clay sample extruded and sub-sampled for triaxial testing and consolidation testing.

5.2.2.2 Triaxial compression testing

Sub-sampling for triaxial testing was carried out with thin walled brass tubes whose area ratio was 12 %. To aid penetration, both the inner and outer surfaces of the tubes were sprayed with silicon oil. For each test series, four sub-samples were taken from the central region of the sample. These were waxed and kept in an incubator until required for testing.

5.2.3 Consolidation and permeability tests

Consolidation tests on sub-samples were carried out in the restricted flow testing apparatus. Since the water flow during dissipation in the chamber is predominantly in the horizontal direction (Campanella et al, 1986; Teh, 1987) these consolidation tests were made on samples orientated at 90° to the direction of penetration. In this way, the horizontal coefficient of volume change m_h was obtained.

Permeability tests were also carried out on the same samples and in the same apparatus using the flow pump method. Flow pump apparatus was attached to the restricted flow consolidation apparatus as described earlier. The coefficient of consolidation was then obtained from the following;

$$c_h = \frac{k_h}{\gamma_w m_h} \qquad [5.1]$$

where k_h is the horizontal coefficient of permeability,

m_h is the horizontal coefficient of volume change.

5.3 Testing Summary

Table 5.1 gives the sequence of chamber tests carried out, with summaries of events which took place during sample preparation and testing periods. Difficulties in the early part of the programme are evident, notably the failure of the top membrane for vertical stress control, and the malfunction of the automatic data acquisition system. Further details relating to the test series are given below.

5.3.1 Membrane failure

It was, perhaps, fortuitous that all cases of membrane failure requiring interruption of the loading process took place in the earlier stages, making it possible to unload, repair and reload to a higher consolidation pressure and thereby override the effect of unloading. This took place during the preparation of test series Z1C, Z2B and Z3A. During the preparation of sample Z1C and Z4C, leaks developed after the final consolidation pressure had been applied and the sample pore pressures were nearly dissipated. Fortunately these leaks were so slow that it was possible to incorporate them in the swelling processes.

By test series Z4C, the top plates of the two small tanks had been modified to give a larger contact area between the rings that clamp the membranes together. The result of the modifications was that there were no more leaks or membrane failures in the remaining part of the programme.

5.3.2 Automatic data logging

The Analogue Express malfunctioned during two test series, when at least one data set was lost in each test. The problem was found to be the synchronisation between the Commodore 64 and that of the data logger. A change of computer to an IBM-compatible Opus III solved the timing problem but caused delays whilst new software was written and hardware purchased. The advantages of the new system were discused in an earlier section.

5.3.3 Test series Z1C

Test Z1C was carried out with the 1 cm^2 instead of the 5 cm^2 piezocone because the latter was delayed back from Fugro (Holland) where it had been sent for necessary repairs. This meant that the diameter ratio for the test at the centre port was 88.5, a distance of 44.25 piezocone diameters to the nearest boundary. At the side ports, the distance to the nearest boundary was reduced to 22.12 piezocone diameters. Therefore, penetration tests in this series were much less affected by the rigid boundaries. This was borne out by the change in horizontal stress during penetration, which averaged 23 kPa or 5% of the original horizontal effective stress. Further discussion on data quality is presented in the next Chapter.

5.3.4 Test series Z4C

Events which took place during test series Z4C are worth mentioning because they showed some results which would otherwise not have been recorded. During penetration testing, the top surface was stress controlled. This was done, as explained in Chapter 3, through an air/water interface. When this device functions properly, the displaced fluid from the membrane is accommodated in the interface container, thus maintaining a constant pressure in the membrane.

In test Z41C, the volume displaced was much greater than that allowed for in the container. As a result, the fluid overflowed, but since the overflow was smaller than the displaced outflow, pressure built up in the membrane. Larger volumes for displaced fluid were

allowed for in subsequent tests. During penetration test Z42C, the compressed air inlet tap to the pressure regulator was closed momentarily by mistake. As would be expected, this led to a drop in the total stress in the membrane. However, as Figure 5.3 demonstrates, the surge of the fluid back into the membrane caused the pressure to overshoot the equilibrium pressure. The recovery to equilibrium pressure, as shown by Z43C, was very slow. Tip resistance results from this series did not seem to be affected by this and are further discussed later in the thesis.

5.3.5 Flow restrictors

Flow restrictors, in the form of needle valves, were incorporated in the drainage lines of the consolidating samples from series Z5C onwards. These allowed a controlled flow of water from the samples as they consolidated. The point of zero pore water pressure was moved from the sample surface to the flow restrictor. This provided a smaller pressure gradient between the centre of the sample and its drained surfaces. The effect of this was to reduce the creation of a diversely changing permeability regime between the drained surface, where it would be smaller, and the centre of the sample, where it would be larger in comparison. The flow restrictor thus helped to reduce, if not eliminate, the formation of crusts at the two drained boundaries. This process, therefore, increased the homogeneity of the samples during consolidation.

Table 5.1A Summary of tests and other events

Test series	Chamber	Piezocone	Remarks
Z1C	C	004 [1 cm^2] Filter location *cone face* -Z11C and Z12C *cone shoulder* -Z13C and Z14C	1. Membrane broke twice in early stages of consolidation. (Sec. 5.3.1) 2. Data logger malfunction leading to loss of Z11C data. (Sec. 5.3.2) 3. 001 [5 cm^2] piezocone under going necessary repair to the load cells. (Sec. 5.3.3)
Z2B	B	004 [1 cm^2] Filter location *cone shoulder*	1. Membrane broke twice in early stages of consolidation. (Sec. 5.3.1) 2. No vertical stress control during penetration test Z21B
Z3A	A	004 [1 cm^2] Filter location *cone shoulder*	1. Membrane broke twice in early stages of consolidation. (Sec. 5.3.1) 2. Total failure of automatic data logging system. A chart recorder was used instead. (Sec. 5.3.2)
Z4C	C	001 [5 cm^2] Filter location *cone face* *cone shoulder* *mid sleeve* *top sleeve*	1. New logging system 2. Volume displacement in stress controlled boundary constrained. (Sec 5.3.4)
Z5B	B	004 [1 cm^2] Filter location *cone shoulder*	1. Top plate modified to stop membrane breakages. 2 Flow restrictor incorporated. (Sec 5.3.5) 3. Tests Z51B and Z52B failed.
Z6A	A	004 [1 cm^2] Filter location *cone shoulder*	Flow restrictor incorporated

Table 5.1B Summary of tests and other events (continued).

Test series	Chamber	Piezocone	Remarks
Z7C	C	001 [5 cm^2] Filter location *cone face* *cone shoulder* *mid sleeve* *top sleeve*	Flow restrictor incorporated
Z8B	B	004 [1 cm^2] Filter location *cone shoulder*	Flow restrictor incorporated
Z9C	C	001 [5 cm^2] Filter location *cone face* *cone shoulder* *mid sleeve* *top sleeve*	Flow restrictor incorporated
Z10A	A	004 [1 cm^2] Filter location *cone shoulder*	Flow restrictor incorporated
Z11B	B	004 [1 cm^2] Filter location *cone shoulder*	Flow restrictor incorporated
Z12C	C	001 [5 cm^2] Filter location *cone face* *cone shoulder* *mid sleeve* *top sleeve*	Flow restrictor incorporated

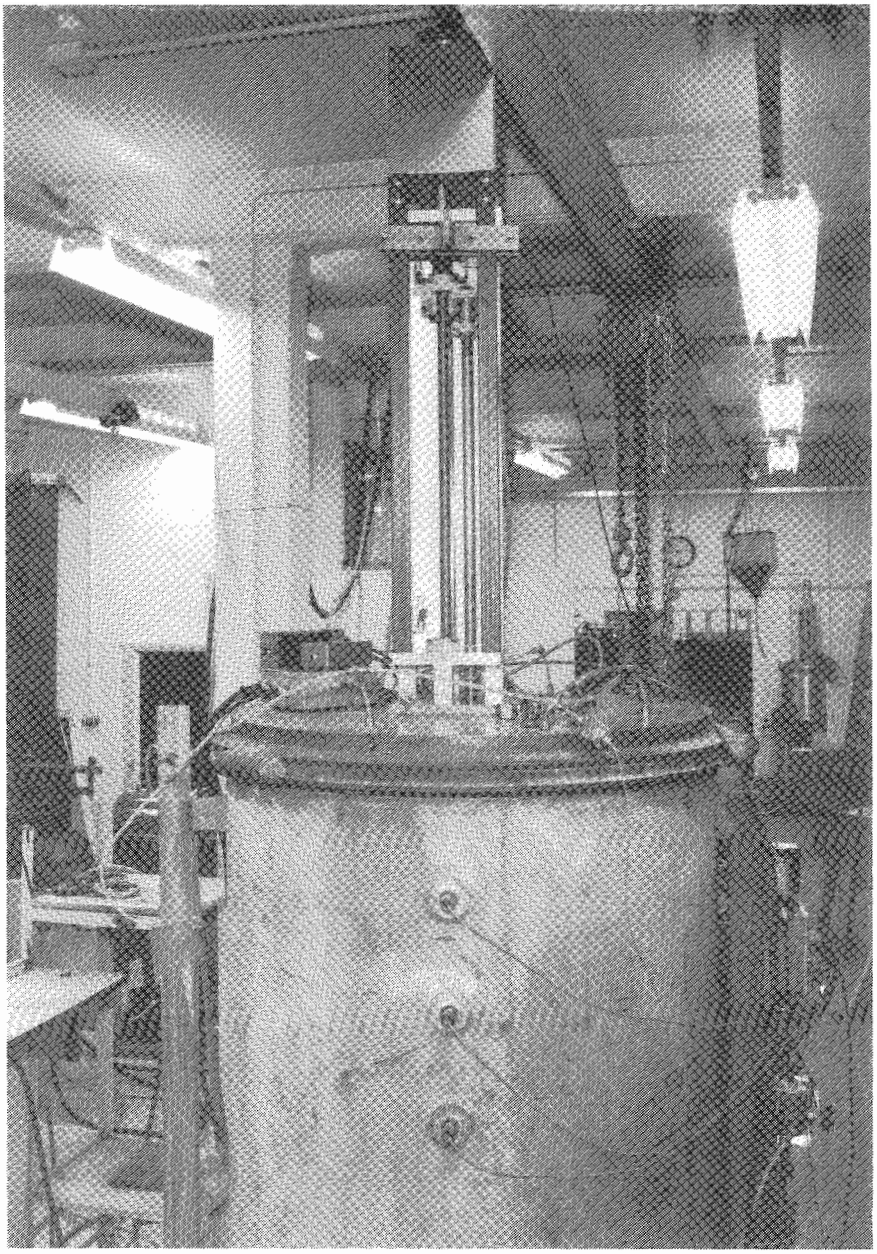

Plate 5.1 The driving system with piezocone ready for a penetration test in the 1 m diameter testing chamber.

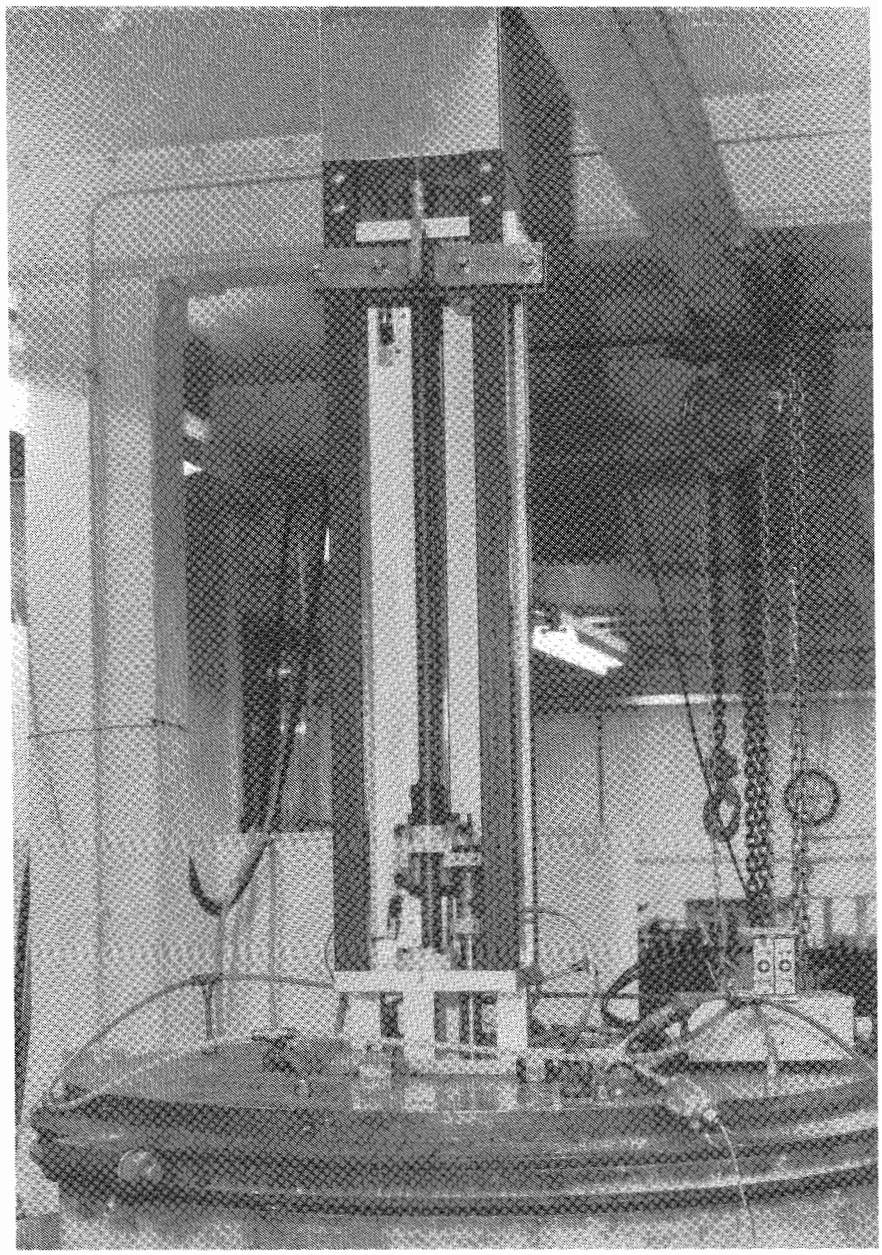

Plate 5.2 The driving system showing the piezocone during dissipation at the end of a penetration test in the 1 m diameter testing chamber.

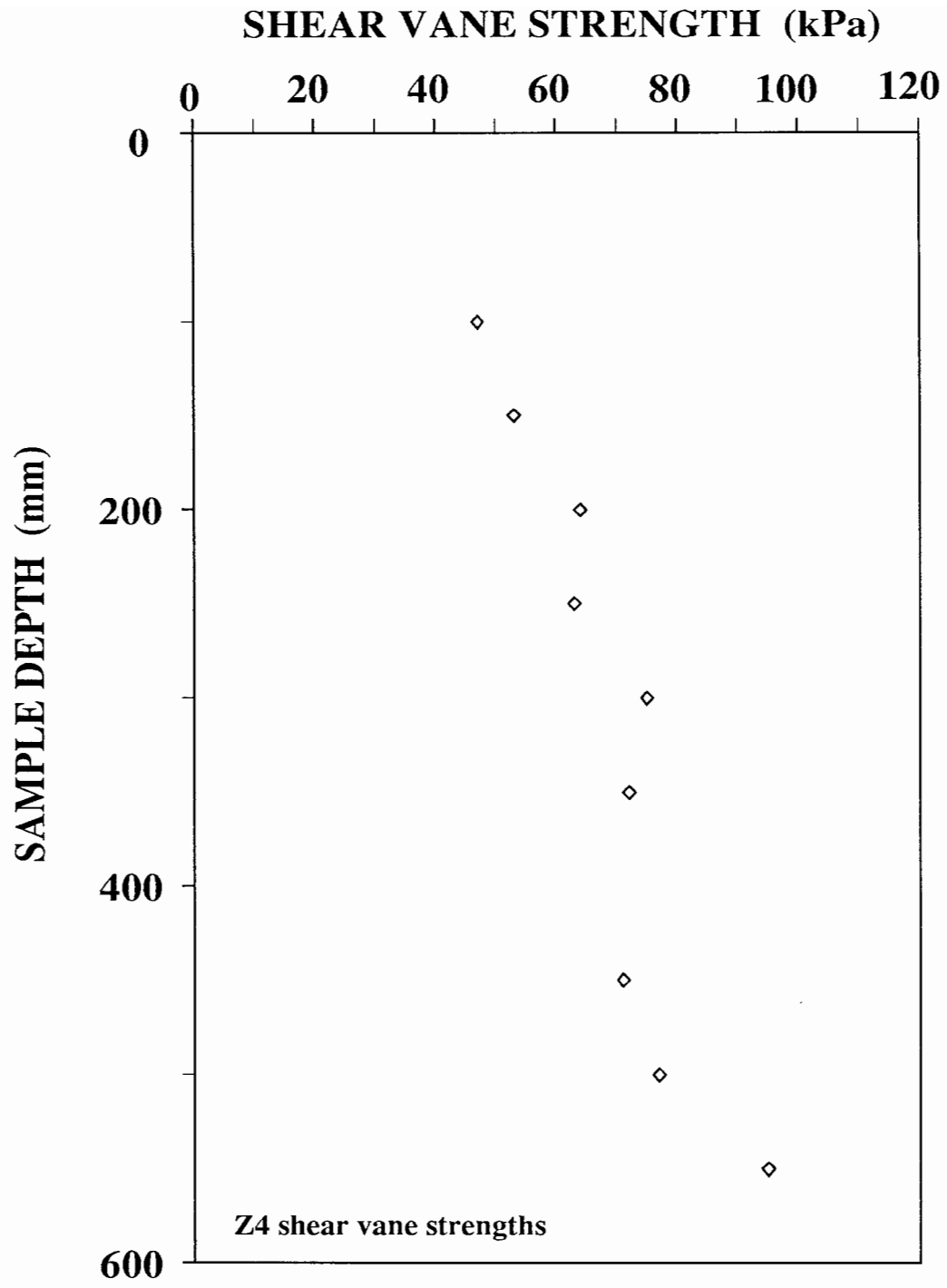

Figure 5.1 Vane shear strength with depth using a motorised shear vane (The extension rod was not encased).

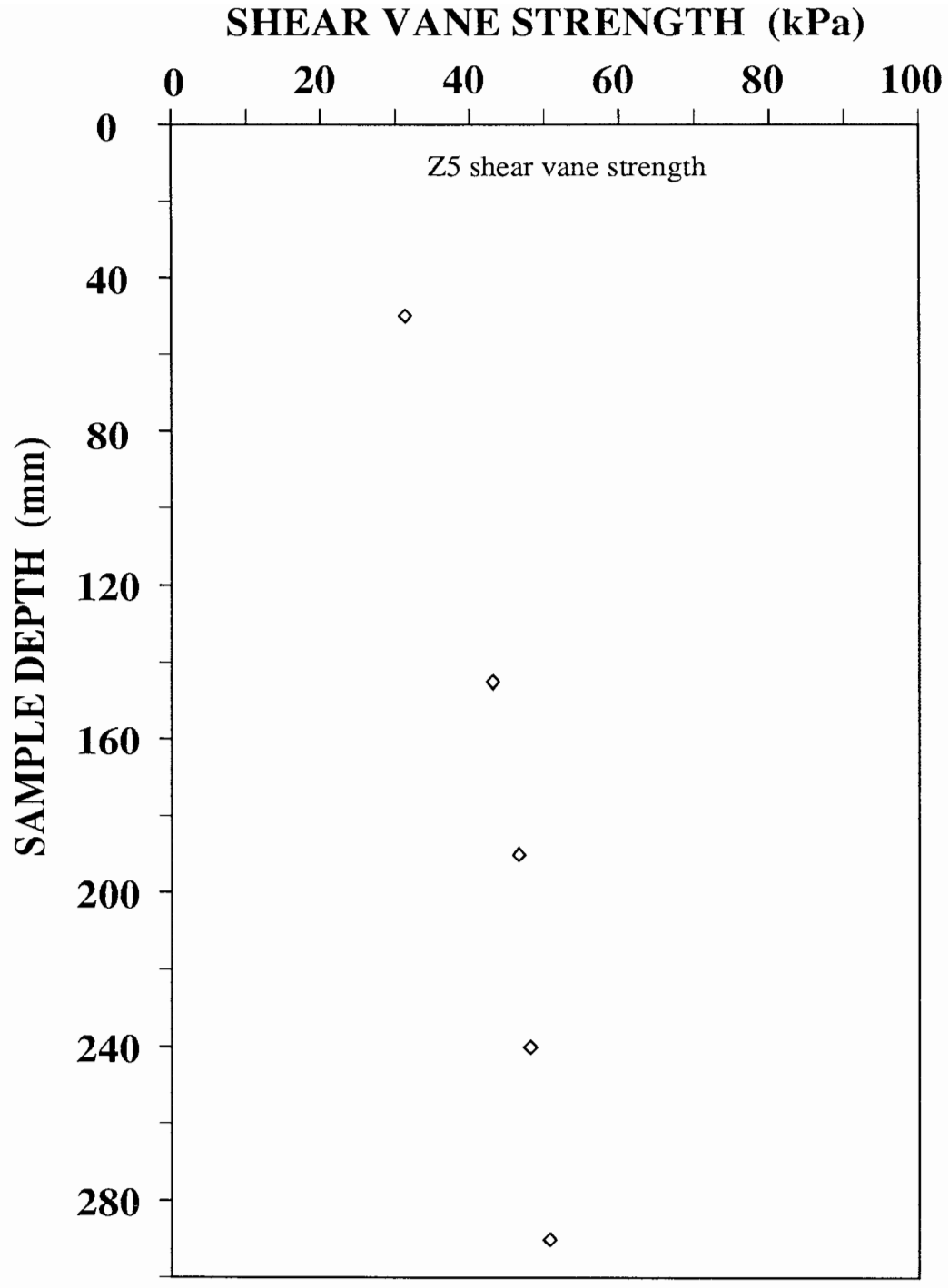

Figure 5.2 Vane shear strength with depth on Z5 sample using a motorised shear vane with the rod enclosed in an external tube.

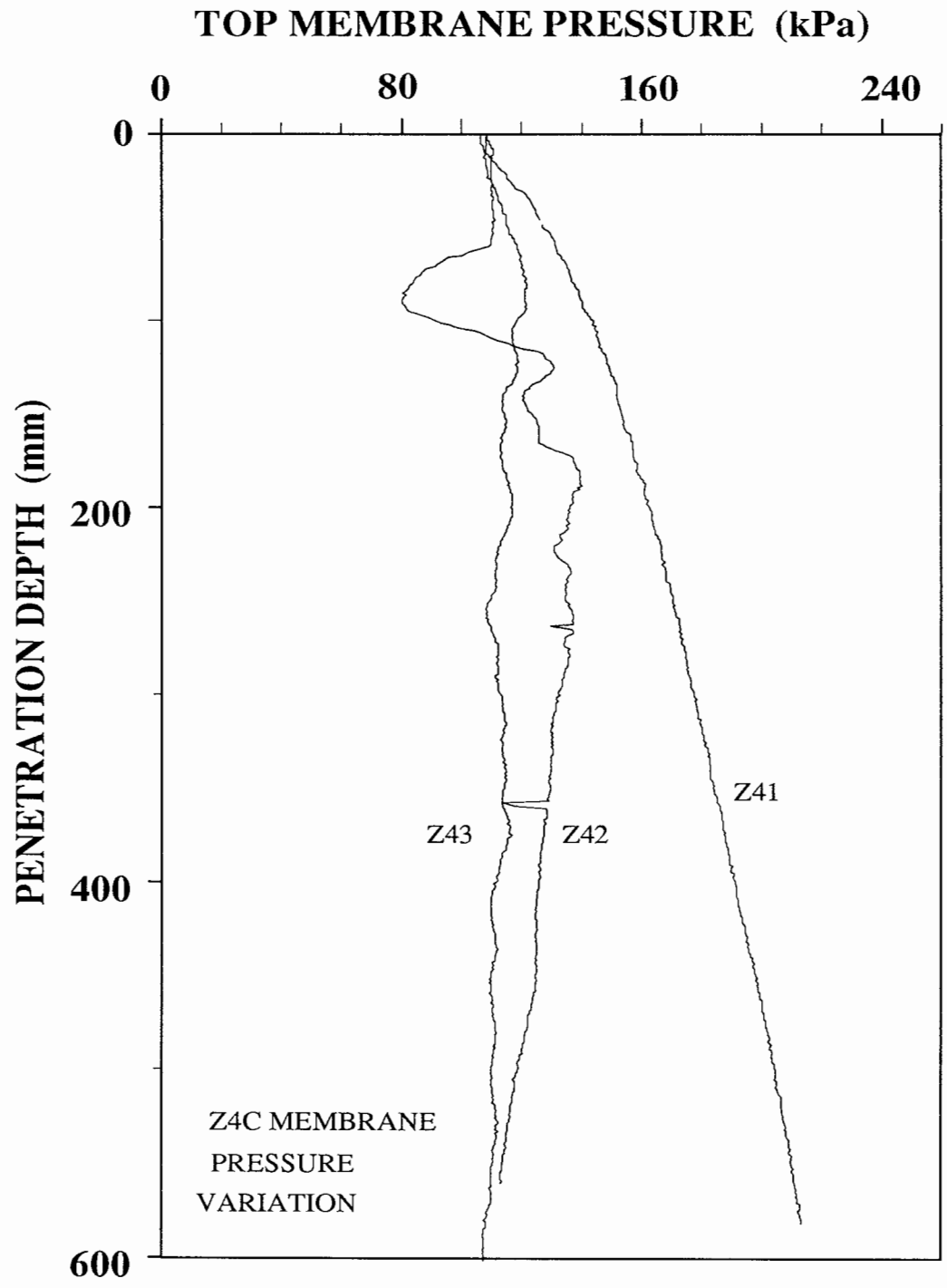

Figure 5.3 Variation of vertical stresses at the stress-controlled boundary during penetration, Z4C series.

6 CHAMBER AND LABORATORY TEST RESULTS

This research programme consisted of 36 chamber tests, 39 CIU triaxial tests, 26 restricted flow consolidation tests and 26 permeability tests. In this chapter, results from these tests will be reported, starting with discussion on sample quality.

6.1 Sample Quality

In Chapter 4, the careful preparation of the sample was described. This section will report on the results of the preparations. Two main methods were used to quantify the quality of the samples prepared. These were:

1. Shear strength profiles
2. Moisture content distribution.

In addition the samples were examined visually. The results of a visual examination are very subjective but it is fair to say that a well mixed slurry consolidates into a sample of uniform consistency. Hence there was great effort to ensure that the slurry was well mixed under vacuum at all times. The final slurry was well mixed, smooth when felt between fingers, and free of air bubbles.

6.1.1 Shear strength profiles

Shear vane tests, which were carried out through one of the five access ports, provided another indication of sample quality. This was achieved by examining the variability of shear strength with depth.

The results to be reported are presented in Figures 6.1 to 6.4. They have been compiled by two methods, the first being by chamber size. Thus, Figures 6.1 and 6.2 illustrate results from

small chambers (diameter 0.58 m) with a final sample depth of about 350 mm, and Figure 6.3 and 6.4 present results from the large chamber (1.0 m diameter) with a final sample depth of approximately 700 mm.

The second method of presentation is by sample consolidation pressure (see Section 2.4.3). Small chamber samples in the lower consolidation pressure category (that is initial consolidation pressure up to 650 kPa) are illustrated in Figure 6.1 and the ones in the higher category (that is initial consolidation pressure between 650 and 900 kPa) in Figure 6.2. For the large chamber samples, Figure 6.3 illustrates results from both consolidation categories, while Figure 6.4 illustrates results from the lower consolidation category. In Figure 6.3, Z4C and Z7C samples were of the lower and higher consolidation categories respectively.

In Figure 6.1, both Z5B and Z11B show uniform shear strength profiles indicating the homogeneous nature of the samples. The profile for Z3A shows uniform shear strength down to 200 mm depth. At 300 mm the shear strength is slightly higher.

In Figure 6.2, the same uniform pattern is observed for Z6A and Z8B, while Z10A shows a uniform strength to a depth of 250 mm with a slight drop at 300 mm. In general, the results from the small chambers were similar and did not depend upon the consolidation pressure category.

Results of Z7C (OCR 9.1) in Figure 6.3 show a small increase of shear strength with depth. Over the middle region (between 250-550 mm depth) the change in shear strength was 25% of the maximum. The profile for Z4C (OCR 5) also increased gradually but the change in shear strength over the middle half was much less.

The results in Figure 6.4, for tests Z9C and Z12C with OCR's of 1.3 and 3 respectively, show a clear pattern of increasing shear strength with depth up to about 200 mm. Thereafter the strength is constant up to a depth of 550 mm, giving a uniform shear strength throughout the middle half region.

In summary, small chamber samples from both categories exhibited uniform shear strength throughout the sample depth tests. Large chamber samples exhibited near uniform strengths in the middle half region of the sample's final depth. Low OCR samples in the large chamber, while exhibiting uniform strengths in the middle half of the sample's final depth, showed non-uniform strengths in the first 200 mm of depth.

6.1.2 Moisture content variation

The purpose of the moisture content variation check was to identify possible trends in the stress distribution across the sample. This was essentially a check for homogeneity of the sample.

Results illustrated in Figure 6.5 to 6.7 were determined in accordance with BS 1377 (1975). The low and high consolidation pressure category samples results are illustrated in Figure 6.5 and 6.6 respectively for small chamber results. All large chamber results are illustrated in Figure 6.7.

The Figures illustrate the variation of moisture content in each sample cake with depth, and at each depth with radial distance from the centre of the sample.

Moisture content was found to vary very little in the samples prepared. Radially, the samples which varied most were Z5B and Z4C, where the maximum difference was less than 2% in

both samples (Figures 6.5 and 6.6 respectively). The variation of moisture content in all samples could not be attributed to either consolidation category. They all show some variation but all within acceptable limits as indicated by the maximum variation above.

Moisture content variation with depth was much the same as that with radial distance from the centre. There was no apparent pattern of behaviour which could point to predominant variation with depth or radial distance.

These results indicate that moisture content variation was very small and, when seen in the light of the shear strength profiles discussed in Section 6.1, they indicate that the sample quality was good for the purpose of the penetration tests which were carried out in them.

6.2 Vertical Boundary Stresses

Total stress transducers installed on the piston (see Chapter 3) revealed that there was a distinct pattern of vertical stress distribution during consolidation and swelling. The results from Z2B illustrated in Figure 6.8 are typical of all the other samples.

Figure 6.8 shows two sets of results, the first at the end of consolidation and the other following completion of swelling. The positions of total stress transducers are shown relative to the centre of the piston. The two penetration testing positions are also shown. The position of the horizontal boundary is also shown. The dotted line joins the total stress measurements at the three positions on the displacement controlled boundary, and the solid line shows the uniform stress measured on the stress controlled boundary.

At the end of consolidation, the result on the displacement controlled boundary shows a marked stress increase at the boundary, i.e. 245 mm from the centre, with a difference of nearly 200 kPa or 29% of the stress at the centre. The increase at the transducer positioned at

160 mm from the centre, was only 8% of the one at the centre. The pressure difference between the transducer at the centre of the displacement boundary and the stress controlled boundary at the top of the sample was nearly 100 kPa or 16% of the smaller value.

The measured variation in pressure may be explained by the higher force needed to overcome friction on the side walls while providing a uniform displacement. The larger difference in pressure between the middle transducer and the outer transducer prompted further tests to investigate the sample in the regions of line A and B as shown in the Figure 6.8.

The investigation was to focus on whether or not there were significant differences between the sample in the region of line A and that of line B. Effectively, this was a check of sample homogeneity in the horizontal plane since it has already been established that the samples were homogeneous with depth, (see Section 6.1).

A series of Pilcon vane tests were carried out on the extruded sample Z3A in the horizontal plane. The tests were carried out at 90 mm and 180 mm from the circumference to coincide with the middle of line B and to be within the region of line A respectively (Figure 6.8).

Results of this investigation are illustrated in Figure 6.9. The Pilcon vane index provides a measure of sample homogeneity at the two distances at which they were obtained in the horizontal plane. Figure 6.9 shows clearly that there was no appreciable difference between the results from the two positions.

This result suggests that stresses in region A and, at least to the middle of region B were similar, thereby indicating that the regions of high stresses during consolidation were confined to a comparatively narrow band within, at most, 90 mm from the chamber boundary.

At the end of the swelling stage (Figure 6.8), the stresses had evened out. Friction between the soil and the side wall during the swelling stage acted in the reverse direction to that set up during consolidation. This reduced the measured stresses on the displacement controlled boundary to such an extent that there was no evidence of a variation in stress on the boundary. The difference between the stresses on the displacement and stress controlled boundaries were also insignificant.

The fact that there were different vertical stresses at the top and bottom boundaries during and at the end of the consolidation stage posed the question as to which measured stress should be used in evaluating mechanical over consolidation. However, it was decided to use the pressure measured at the stress controlled boundary because it was a measurement of a more uniformly distributed stress than that at the displacement controlled boundary.

6.3 Summary of Geotechnical Properties

Geotechnical properties of all the samples tested during the research programme are presented in Table 6.1

The testing pressure recorded in the table is the pressure at the stress controlled boundary after the swelling stages which was maintained during penetration testing and shear vane testing. Likewise, the horizontal stress used in obtaining the K_0 value is that recorded by the horizontal boundary total stress transducer after the swelling stage.

The shear vane strength recorded is the average strength in the steady state region of the profiles discussed in Section 6.1, while the triaxial shear strengths were peak strengths of consolidated undrained tests on sub samples re-consolidated to the same mean effective stress conditions which existed during the chamber test.

The coefficient of consolidation in the horizontal direction (c_h) was obtained from the results of restricted flow consolidation and permeability tests on samples oriented at 90° to the vertical.

6.4 Tip Resistance Response

Up to a maximum of four penetration tests were carried out on each sample prepared. These tests were made in such a way that the final penetration depth was about 100 mm from the displacement boundary at the base. Stopping the piezocone at this level avoided bottom boundary effects on the measured parameters. In the large chamber, this was easily achieved since the final sample depth was about 700 mm and the piezocone penetration travel was only 550 mm. In the small chamber, where the final sample depth was about 350 mm, the penetration depth was set for 280 mm.

The tip resistance reported in this thesis is the corrected tip resistance q_t . Therefore tests which did not include a cone shoulder pore water pressure measurement have been excluded from this report. The correction factor α was determined at the beginning of every test series, as discussed in Chapter 5.

Tip resistance results from all test series are illustrated in Figures 6.10 to 6.19. The test numbers in each series reflect the order in which the tests were carried out. Figures 6.10 to 6.13 inclusive are from large chamber tests with the 5 cm^2 piezocone, and only tip resistance is reported. Figure 6.14 illustrates tip resistance and shoulder pore water pressure results from the large chamber where the tests were carried out with the 1 cm^2 piezocone. Figures 6.15 to 6.19 report results from small chamber tests using the 1 cm^2 piezocone and include both tip

resistance and shoulder pore water pressure responses. Figures 6.14, 6.15 and 6.16 were made from data extrapolated from chart records because the automatic data recording system malfunctioned during the test series.

Figure 6.10 shows typical tip resistance responses in the large chamber. At the beginning of penetration the tip resistance rises sharply to a value of about 700 kPa after a penetration of less than 50 mm. After this depth there is a divergence in response for the three tests. Whilst Z41C shows a drop in response down to 200 kPa before another sharp rise back to its original high value at 100 mm depth, Z42C shows a steady response which starts to increase at about 150 mm depth and Z43C continues to rise, albeit less sharply, to 1000 kPa at about 60 mm depth before dropping down to a steady value at 200 mm depth. By the time the penetration reached 300 mm, all three tip resistance responses were steady and showing the same tip resistance. Thereafter, a near uniform (steady state) response was recorded over the remaining penetration depth.

The initial response recorded for Z71C in Figure 6.11 has a physical explanation in that the first 120 mm was penetrated twice because the piezocone was in the first instance erroneously driven down to a depth of 120 mm without switching on the data logger. This is why the sharp response starts at that depth where undisturbed soil was encountered. The decision to continue with the test was vindicated by fact that the steady state response was the same as the rest of the tests in the series.

Tip resistance results with the 1 cm^2 piezocone in the large chamber, illustrated in Figure 6.14, and in small chambers, illustrated in Figures 6.15 to 6.19, have a similar response pattern to those with the 5 cm^2 piezocone in the large chamber described above. However, the

1 cm^2 piezocone results reached a steady state response earlier, at 100 mm depth, than the 5 cm^2 piezocone. It is interesting to note that these distances are approximately 10 piezocone diameters in each case.

In some results, such as Z41C in Figure 6.10, the initial response rose to a high value and dropped before rising again to reach the steady value. In others the initial response was high but dropped or increased gradually to the steady state value as in Z72C, Z73C and Z74C in Figure 6.11. The explanation for this variation in the type of response may be found in the penetration mechanism in the access port which is described below.

Initially, the tip of the piezocone was resting at the bottom of the access port, ie zero depth. In the early stages of penetration, the tip resistance increased sharply, as would be expected, but the soil heaved into the port. As the cone shoulder approached the base of the port, the soil was squeezed against the port wall, sharply increasing the resistance to penetration. The true tip resistance of the soil in the chamber was only realised after the shoulder had gone past the base of the port. Where there was already some soil in the access port, the sharp increase in tip resistance was greater. In some test series, such as Z1C in Figure 6.14, and Z3A in Figure 6.15, water was poured into the ports to maintain the saturation of the filter element after the piezocone had been manoeuvred into place. In these cases, the soil swelled into the ports and increased the tendency described above.

6.4.1 Repeatability of results

In illustrating the repeatability of chamber tests results, Figure 6.13 will be used because not only is Z12C series typical of the results obtained, but it also contains results from all the four possible penetration tests in a series. This series did not show the common high pressure response at the beginning because the first 30 mm or so of the sample was disturbed when cutting the top filter which had shifted from its original position during consolidation.

As a result, all the four tests started with near zero tip resistance but rose sharply to about 600 kPa after penetrating undisturbed soil at about 50 mm depth. From 50 mm onwards the trend is similar to the others, rising to the steady state value at around 200 mm depth and then a near constant response until the end of penetration.

It can also be seen in Figure 6.13 that the steady state value for all four tests was very similar regardless of the testing position. This is also reflected in all the test results, both in the small and large chamber. The implication is that the results of tip resistance from the centre port were repeatable in the side ports, which means that the boundary conditions affected the results equally at both testing positions. Therefore penetration test results from any of the four testing positions in each series, were representative of the sample.

In summary, tip resistance, in either test chamber, reached a steady state response with depth after 10 piezocone diameters of penetration. In this steady state region, the value of tip resistance from any of the test positions was effectively the same. This implies that the boundary conditions applied equally at the four testing positions for both sizes of piezocone.

6.5 Pore Water Pressure Response

The pore water pressure was measured at the shoulder on the 1 cm^2 piezocone and at four positions, (on the cone face, the cone shoulder, half way on the friction sleeve and at the top of the friction sleeve), on the 5 cm^2 piezocone. The distances to the various pore water pressure measuring positions with respect to the tip, on the 5 cm^2 piezocone, were illustrated in Figure 3.1.

Results of pore pressure response during penetration are presented in Figures 6.14 to 6.29. Pore pressure responses for the 1 cm^2 piezocone, i.e. shoulder pore water pressure, are illustrated in Figures 6.14 to 6.19 and those from the 5 cm^2 piezocone in Figures 6.20 to 6.29.

The initial response of pore water pressure is affected, in a similar way to the tip resistance, by the penetration mechanism in the access port as described above. In pore pressure measurement the initial sharp response is also a good indication of the level of saturation of the filter element. Figures 6.14 and 6.16 are examples of good filter saturation while Figure 6.18 shows the difference between well and poorly saturated filter elements. Z81B and Z82B in Figure 6.18 show very sharp response of pore water pressure due to the rapid increase of total stress as shown by the corresponding tip resistance response, yet Z84B shows a sluggish response indicating that the filter element had lost full saturation before the piezocone was driven into the clay sample.

Lack of saturation of the pore water filter element, as shown in the slow early response of pore water pressure in Z33A of Figure 6.15, Z61A of Figure 6.17 or Z84B of Figure 6.18, did not seem to affect the final response in the steady state region. A possible explanation for this behaviour may be that the air in the pore pressure measuring system goes into solution as the pore pressure increases. This, therefore, allows the pore pressure transducer response to improve as the pressure increases until all the air has gone into solution.

Figure 6.20 is a typical pore pressure response from the 5 cm^2 piezocone. In this case only the pore pressure measured at the cone face (U_1) and cone shoulder (U_{shld}) are affected by the penetration mechanism in the access port. The fact that the pore pressures at both U_1 and U_{shld} start increasing at the same time is an indication that there was clay in the access port at the beginning of the test. The good saturation of the filter elements for the two transducers in question is shown by the steep rise in response after the initial drop. This is in contrast with the mid-sleeve pore water pressure response (U_3) which shows a more gradual response. The top-sleeve pore water pressure (U_4) shows good saturation.

The response pattern of each of the four pore water pressure transducers is similar to that of the tip resistance response described earlier. The sharp response occurs just above the steady state region, and then rises slowly to the steady state value where it remains until the end of penetration. In all the tests carried out with the 5 cm^2 piezocone, the pore water pressure on the cone face was the highest, followed by that at the cone shoulder. The pore water pressures U_3 and U_4 were always very close to each other in magnitude, although U_3 was always greater than U_4. This is in agreement with the results reported in literature using the same instrument by May, (1987) and Sills et al, (1988a) and, using similar equipment, by Baligh and Levadoux, (1980), to mention a few.

It is clear from the results of the 1 cm^2 piezocone (Figures 6.14 to 6.19), where it was possible to plot a series response on the same graph, that in the steady state region there was no appreciable difference in the measured shoulder pore water pressure for any of the testing positions. The 5 cm^2 piezocone pore water pressure responses have been presented in tabular form for this purpose in Table 6.2.

Table 6.2 lists average results from all tests which were carried out successfully during the research programme. The averages were taken over the same range of depths in the steady state region of each test series for all the parameters tabulated. From Table 6.2 it can seen that the pore pressures measured on the face and the shoulder showed some variation within individual series.

In the case of position U_1, the test result of Z122C in the Z12C series was over 17% below the series average. The other two test results in the series were within 9% of the series average. The variation in the results from position U_1 in other series were within 4%, 16%, and 5% of the series average for Z4C, Z7C, and Z9C respectively.

In the case of position U_{shld}, the test result of Z41C in the Z4C series was 11% above the series average, whereas Z42C and Z43C were within 7% and 4% of the average, respectively. Results from the other test series were within 6%, 3%, 8%, of their series averages for Z7C, Z9C and Z12C respectively.

Results at position U_3 were similarly analysed and were found to be within 12%, 6%, 3% and 8% of the individual series averages for Z4C, Z7C, Z9C and Z12C tests series respectively. At position U_4, results in Z4C series showed considerable scatter, taking the variability band to within 24% of the series average. The variability of the results about the series averages in Z7C, Z9C and Z12C series were, 10%, 5% and 5%, respectively.

In summary, the scatter of pore pressure results on the 5 cm^2 piezocone was most evident on the cone face and on the top-sleeve positions. It is interesting to note that the greatest variation in the results at all four positions were those tests with low over consolidation ratios. The general tendency of all pore water pressure results in the same series was to decrease with the number of tests already carried out on the sample and this was more prevalent in the results from pore pressures above the cone shoulder.

6.5.1 Excess pore pressure in the sample

During the description of sample preparation in Section 4.4, it was mentioned that miniature pressure transducers, specially designed to measure pore water pressure, were embedded in the sample before the final consolidation pressure was applied. One typical result from these miniature pressure transducers during the penetration stage is presented in Figure 6.30. The Figure shows results, SPP1 and SPP2, of two transducers, 1 and 2 embedded at the depths shown by the arrows on the Figure. Their respective distances from the vertical axis of the

piezocone were 3D and 7D, where D is the piezocone diameter. The results shown are excess pore pressures experienced in the sample at the two distances from the piezocone centre line as it penetrated the soil.

At the time when the cone face filter location passes through the horizontal plane of transducer 1, the excess pore pressure experienced at the cone face was approximately 850 kPa (Figure 6.28), while that at the miniature pressure transducer was only 34 kPa. This gives a pressure drop of 10 kPa/mm in the horizontal direction assumming a linear profile. When the piezocone was passing through the horizontal plane of transducer 2, excess pore pressure at the cone face was 870 kPa and 5 kPa at a distance of 7D from the piezocone vertical axis, giving a drop of 4.8 kPa/mm. It is known from cavity expansion analysis that this excess pore pressure distribution is not linear and that the pressure drop is steeper nearer the piezocone, becoming shallower with distance away from it (Baligh and Levadoux 1980). This means that the pressure drop near the piezocone was much higher than that indicated by the Figures presented, thus showing a very high local pressure gradient in the horizontal direction.

The second observation is that the excess pore pressure at both transducer locations continues to increase until the piezocone tip has gone 2.5D past the horizontal plane of the transducers. Part of this increase, up to a depth of 0.87D below the transducer, is due to increased total stress as the piezocone tip advanced and the cavity expanded to the piezocone diameter D at that level. Between 0.87D and 2.5D, the continuing increase in excess pressure must be due to pore water flow generated by the high pore pressure gradient between the advancing piezocone and the transducer. This result shows that there is an outward movement of pore water from the piezocone tip as it advances into the soil.

6.6 Sleeve Friction Response

Sleeve friction was measured on the 5 cm^2 piezocone and the boundary effects described in Section 6.4, for tip resistance, also affected skin friction responses. The general pattern was for a sharp rise in sleeve friction as the cone shoulder exits the access port, then a reduction to a steady state value. The sharp increase was due to the soil in the access ports being squeezed against the sides of the ports as described earlier.

Figure 6.31 shows a typical test series sleeve friction response with depth. The values of skin friction obtained during these tests were small, as can be seen in Figure 6.31 where the maximum steady state value is about 40 kPa. With the electrical noise problems encountered during the test programme, these small values would be susceptible to margins of error which may not be acceptable.

In Figure 6.31, the pattern of skin friction results in individual tests is consistent except in test Z71C where there is a gradual decrease in response from a depth of 200 mm to 400 mm before rising to the final value at a depth of 500 mm. The results of Z72C and Z74C are close to each other but those of Z71C and Z73C are quite different, and the variation of the steady state averages from each test about the series mean ranges from 64% for Z73C down to 1% for Z71C.

The reason for this variability may lie in the design for the measurement of skin friction on this particular instrument. Skin friction force is the difference between the total load and tip load. These two load cells each have a design maximum load capacity of 2.5 tonnes and yet the maximum load in the laboratory was hardly more than 1 kN. The variability must come from the fact that skin friction result is the small difference of very small outputs from the load cells in an electrically noisy environment. The electrical noise was greatly reduced so

that it was insignificant when compared to the level of output for the tip and total resistance but could not be guaranteed to be low enough for these small responses. Consequently skin friction results will not be used in any further analysis.

6.7 Pore Pressure Factors

Two factors, B_q , β , were studied during the test programme. These factors were originally suggested by Senneset et al (1982) and May (1987) respectively, as being suitable for correlation with over consolidation ratio. This section will deal with the measurement of these factors. Their possible correlation with over consolidation ratio will discussed in a later chapter.

6.7.1 Pore pressure factor β

The factor β was defined by May (1987) as follows:

$$\beta = \frac{\Delta U_{shoulder}}{\Delta U_{face}} \qquad [6.1]$$

ΔU_{face} , (or U_1 in the laboratory results) is the excess pore pressure measurement on the cone face where maximum stress occurs during penetration (Zuidberg et al (1982) and $\Delta U_{shoulder}$,(or U_{shld} in the laboratory results) is the excess pore pressure measured at the cone shoulder.

It is necessary to know the exact positions on the piezocone of the filter elements for measuring ΔU_{face} and $\Delta U_{shoulder}$ when comparing results from different instruments. The measured values of ΔU_{face} and $\Delta U_{shoulder}$ for any particular soil will vary with their position on the cone face and cone shoulder respectively, as has been shown by Baligh and Levadoux

(1980) in their theoretical pore pressure distribution along the piezocone shaft. Therefore the value of β is a function of both the instrument and the soil. In dilatant or highly over consolidated soils where $\Delta U_{shoulder}$ is very small or negative, this factor may only serve to confirm the identity of such a soil and not give any information on the over consolidation ratio of the soil.

Hydrostatic pressures in the laboratory are very small compared with the generated excess pore pressures during cone penetration. Therefore, in the discussion below, all the pore pressures are excess pore pressures.

The results from the four 5 cm^2 piezocone test series are illustrated in Figures 6.32 to 6.36. Over consolidation ratios for these series are 5, 9.1, 1.3 and 3 respectively. The initial high values of β , such as those in the results of Z41C in Figure 6.32 and Z121C or Z124C in Figure 6.35 are due to the interaction of the piezocone with the soil in the access ports prior to the test, as discussed in an earlier section.

In all the four test series, there is an identifiable value of β for each individual test result which is a value in the steady state region. In Figure 6.32, the results of Z41C and Z43C show a β value which is virtually the same throughout the steady state region. The result of Z42C, on the other hand, takes much longer to reach a steady state condition. When it does reach steady state, the β value is slightly different from that of tests Z41C and Z43C. Therefore in this series β values for each test are averaged over the depth of 400 mm to the end of penetration.

The results of the Z7C series shown in Figure 6.33 are a good example of individual tests following very different routes to reach their individual steady state conditions. The result of Z71C shows an initial response which indicates that U_{shld} was much greater than U_1. The

explanation for this is that the first 150 mm were already penetrated in error (see Section 6.4) so that during this second penetration the cone face was not in contact with intact clay until after this depth. Hence β values greater than unity resulted. When the piezocone started to penetrate intact clay, β begun to recover, but took a while to reach a steady value. The β result of Z72C initially rises to a value near unity before it also reduces to a steady value which is near that of Z71C. However it is difficult to explain this initial rise in the result Z72C because this test was carried without any noticeable difficulty. All four test results seem to be tending towards a common value but the two sets (Z71C, Z72C and Z73C, Z74C) do not quite arrive at the same value. In this series, therefore, the averages were also taken over the depth of 400 mm to the end of penetration in each test.

Test series results for Z9C, shown in Figure 6.34, are a good example of test results which followed the same trend and finished at approximately the same value. The average β values for individual tests were also calculated over the same depths of 400 mm to the end of penetration. Figure 6.35 illustrates results of test series Z12C. The results of three tests Z121C, Z123C and Z124C converge on to about the same value of β in the steady state region. The result of Z122C is uncharacteristically higher than the others but the form of the response curve is similar. The average β value for each test was calculated as above.

The averages of the results were combined on a summary graph illustrated in Figure 6.36. This graph shows β decreasing in value with over consolidation ratio. The difference in the value of β between over consolidation ratios 5 and 9.1 was not as large as that between over consolidation ratios of 1.3 and 5, which suggests that a non linear relationship may exist. In the over consolidation ratio range considered, the trend can be represented by a power function, with a correlation coefficient (R^2) of 0.84, as follows:

$$\beta = 0.76(OCR)^{-0.074} \qquad [6.2]$$

where (OCR) is the over consolidation ratio.

6.7.2 Pore pressure factor B_q

The pore pressure factor B_q was defined as follows by Senneset and Janbu (1982):

$$B_q = \frac{\Delta U_{shld}}{q_t - \sigma_{v0}} \qquad [6.3]$$

Some authors, such as Powell et al (1988), have used the excess pore pressure at the cone face (ΔU_{face}) in defining B_q . This obviously produces higher values of the factor which cannot then be used in conjunction with the standard values using ΔU_{shld} . The main advantage for using the pore pressure measured at the cone face rather that on the cone shoulder is that the factor could then be used in dilatant soils as well, since the shoulder pore pressure tends to be negative in this type of soil. Therefore, for clarity, it is important to state the position from which the excess pore pressure being used in the equation is measured or, better still, to give the other factor a new symbol.

The results of B_q from the test programme are illustrated in Figures 6.37 to 6.46, covering the full range of over consolidation ratios. B_q results in individual tests, like others discussed so far, were characterised by two types of response; namely, a very high initial response followed by a reduction to a steady state with depth, or a sharp response followed by an

increase to a steady state with depth. Figure 6.37 shows both types of response. Z91C and Z94C illustrate the type of result which combines a very sharp and very high initial response which quickly reduces to a well defined steady state region. The result of test Z93C also indicates a sharp initial response, but continues to increase, until it reaches a plateau or a steady state. In this particular series all individual tests results reached nearly the same steady state value.

Other test results similar to those of Z91C or Z94C are the results of Z2B in Figure 6.38, Z1C in Figure 6.41 and some individual results of Z12C in Figure 6.44. The rest of the results were more like those of Z91C in Figure 6.37, of which the results of test series Z4C in Figure 6.39 and Z7C in Figure 6.40 are typical examples. The variation of the averaged steady state B_q values about the series mean ranged from 3% in Z9C series (Figure 6.37), to 17% in Z6A series (Figure 6.45).

Individual results in the series were then combined in order to correlate them to their series over consolidation ratios. The summary of these results, presented in Figure 6.47, shows that B_q decreases with increasing over consolidation ratio. The decrease is prominent up to an over consolidation ratio of about five. After this, the change in B_q per unit change in over consolidation ratio is much smaller, almost tending to an asymptote, as indicated by the results of the four test series with over consolidation ratios greater than six. The scatter in the results did not allow for a good correlation coefficient when curve fitting was attempted. The best curve to fit the data was a power function with a correlation coefficient (R^2) of 0.77. The correlation equation is given below.

$$B_q = 0.88(OCR)^{-0.33} \qquad [6.4]$$

6.8 Tip Resistance Factor Q

As was shown in Chapter 1, the tip resistance factor Q is one of the latest parameters to be used in interpretation of piezocone data, although the idea had been suggested as early as 1982 by Senneset et al, in another form. The parameter, in its present form, was defined by Mayne (1986):

$$Q = \frac{q_t - \sigma_{v0}}{\sigma_v'} \qquad [6.5]$$

In the laboratory, σ_v' and σ_{v0} are only separated by a small hydrostatic pressure within the sample. As a result, σ_{v0} is virtually equal to σ'_v at any particular depth. Therefore the factor effectively becomes:

$$Q \approx \frac{q_t}{\sigma_v'} - 1 \qquad [6.6]$$

Equation 6.6 shows clearly that Q in the laboratory situation, or any similar situation, is a function of both q_t and σ'_v. Variations in q_t, at a constant σ_v', will affect the value of Q more where the changes are significantly greater than the value of σ_v'. This means that results of tests series with low values of σ_v', i.e. higher over consolidation ratios, were susceptible to greater variations in the value of Q.

The results of Q from tests carried out in the present programme are illustrated in Figures 6.48 to 6.58. (It should be noted that the scales of the Figures are only unique to each test series).

Results within each series largely show close agreement with each other. As an example, the results of Z9C in Figure 6.48 have a difference between the highest and lowest mean of Q, from the four individual test averages, of 0.19, which is 4% of the combined mean for the series. Results of Q for Z12C illustrated in Figure 6.49, and Z11B shown in Figure 6.50, when similarly analysed, produce scatters of 10% and 9% respectively. Other test series Q results were similarly close to each other.

However, there were two sets of test results which posed a problem of interpretation. It was difficult to find an explanation for the large variation of Q between individual tests in series Z10A illustrated in Figure 6.57. For example, the mean of the results of Z103A was 25% below the series average. The difference between the highest and lowest test average Q in this series was nearly six, or 42% of the series mean or five standard deviations. Similarly, no explanation could be found for the Q result of Z64A illustrated in Figure 6.54 where the other three results were very similar.

The averages in each test were correlated with the over consolidation ratios of each series and the result is illustrated in Figure 6.58. On the graph, it can be seen that Q relates well to over consolidation ratio when compared to the other two parameters discussed in previous sections. The fact that this relationship is of the form where Q increases with increasing over consolidation ratio is already different from B_q or β which decrease with over consolidation ratio. The results from each test series are seen to be close to each other except for the results

of Z10A which range from 9.8 to 15.4. Z10A series results, although shown, are not included in any further analysis relating to tip resistance. The best curve to fit the data was found to be a power function shown below with a correlation coefficient (R^2) of 0.92.

$$Q = 2.17(OCR)^{0.69} \qquad [6.7]$$

6.9 Dissipation Test Results

Dissipation tests were carried out to investigate excess pore pressure dissipation at various positions on the piezocone shaft and to compare the consolidation coefficient c_h obtained from piezocone data and that from restricted flow consolidation tests in the laboratory. During dissipation, the piezocone was clamped in one position.

6.9.1 Pore pressure dissipation

During penetration testing and in the early stages of dissipation testing, data from all channels were simultaneously recorded at a delay between readings of 50 milliseconds as described in Chapter 5. At this rate of data collection, it was possible to capture the behaviour of the excess pore pressure regimes at the filter locations on the piezocone during the early stages of the dissipation process. Typical dissipation test results are illustrated in Figures 6.59 to 6.64 with excess pore pressure plotted against the square root of time. Figures 6.59 and 6.60 present results of excess pore pressure dissipation from tests carried out with the 1 cm^2 piezocone with the filter element on the cone shoulder in the small chamber. Figures 6.61 to 6.64 illustrate the results of tests carried out with the 5 cm^2 piezocone with four pore pressure measuring locations, in the large chamber. Figures 6.61 to 6.64 are also arranged in the order of increasing over consolidation ratio.

From Figure 6.59 and 6.64 the dissipation of excess pore pressure at the cone shoulder are similar regardless of the size of the piezocone. In the results from the 5 cm^2 piezocone the cone shoulder dissipation results can be seen to be similar to that at the cone face shown in Figures 6.61 to 6.64, except for the initial few seconds when they very different. This is better seen in Figure 6.65 which is an enlarged version of Figure 6.63 over the first nine minutes of the dissipation during Z41C test. The initial slope of the cone shoulder excess pore pressure dissipation curve is shallower than that at the cone face. This very quick initial dissipation at the cone face could also be seen as an initial drop in excess pore pressure due to reduction in vertical stress, which occurs when the piezocone stops.

The pattern of the dissipation curve for the pore pressure locations above the cone shoulder, in Figures 6.61 to 6.64, is the same in all the tests, regardless of over consolidation ratio. They all show an increase in pressure before they start to dissipate. The results of test Z121C in Figure 6.62 illustrate this initial increase clearly. The fact that the increase starts immediately after the piezocone stops is an indication that the sample is fully saturated. The increase in excess pore pressure is due to a wave of migrating pore water from the localised high pore pressure area at the cone face. This is driven by the high pore pressure gradients that exist between the cone face area and the low excess pore pressure areas well above the cone shoulder. This flow of pore water was also seen to increase the excess pore pressure at the two pressure transducers embedded in the soil sample described earlier. This explains the shallow initial slope of the cone shoulder dissipation curve since the initial dissipation is counteracted by the pressure from the migrating pore water.

6.9.2 Evaluation of the coefficient of consolidation

The evaluation of the coefficient of consolidation involves the fitting of theoretical dissipation data to experimental data. However, as has been seen in the dissipation results discussed in

the previous section, the dissipation pattern is different at each location of the filter element on the piezocone. Therefore, great care has to be exercised in choosing the type of theoretical solution to fit the data.

The two theoretical dissipation solutions used in the evaluation of the consolidation coefficient c_h were developed by Baligh and Levadoux (1980) and Teh (1987). The former solution is for filter elements on the cone face, the cone shoulder and a position on the shaft, 5D from the cone tip. These filter locations are different from those on the piezocone used in the present programme where they are located at 3.65D and 6.25D from the cone tip (see Figure 3.1). However, in this region, as has been seen in Figures 6.20 to 6.29, the difference in excess pore pressure responses are not very significant. Therefore the theoretical solution for the shaft position was used knowing that there would only be a slight error in the resulting coefficients of consolidation. Teh's shaft position solution was similarly used when analysing the dissipation at the top of the friction sleeve because it is for a position 3.4D from the cone tip, which is nearer to the location of the mid-sleeve pore pressure filter element.

In fitting the theory to the experimental data, a spread sheet programme, Lotus 123, was used and it was necessary for theoretical data to be in digital form. The time factor T was used as standard for Baligh and Levadoux's solutions but Teh's time factor had to be converted to the standard factor by multiplying by the rigidity index or the ratio of the shear modulus G to the undrained shear strength s_u. The shear modulus was obtained from the initial slope of the stress strain curve of consolidated undrained triaxial tests and the undrained strength from the peak value of the same curve. These tests were carried out on sub-samples from the main series chamber sample and re-consolidated to mean stress levels existing at the time of the penetration test.

$$T = \frac{c_h t}{R^2} \quad \text{(standard)}$$

$$T = T^* \sqrt{I_r} \qquad [6.8]$$

For the experimental results, the measured excess pore pressure during dissipation were normalised by the the initial pore pressure, which is the pore pressure at the instant when the piezocone was stopped. In order to convert real time to the time factor T, c_h was taken to be 1 m^2/min and the time t and piezocone radius R in minutes and metres, respectively. The two sets of data were then plotted using the same scale on the same graph, as illustrated in a typical case for cone shoulder analysis in Figure 6.66. The two curves are separated by the actual value of c_h . By trial and error, either the experimental or theoretical data were factored by an appropriate value of c_h , until a value is found which allows the two curves to match.

In order to illustrate the above process and to compare the results obtained using the two theoretical solutions, the complete results of one 5 cm^2 dissipation test are illustrated in Figures 6.67 to 6.74. The Figures have been arranged in pairs for ease of comparison between the two solutions. Therefore Figures 6.67 and 6.68 are for the analysis at the cone face, Figures 6.69 and 6.70 for the cone shoulder, Figures 6.71 and 6.72 for the mid-sleeve position and Figures 6.73 and 6.74 for the top-sleeve position. In each pair the first Figure uses Baligh and Levadoux's solution and Teh's solution is used in the second Figure. As an example, in the analysis using Teh's solution in Figure 6.70, the experimental data were factored by trial and error until a c_h value of 2.5×10^{-4} m^2/min produced an experimental curve with which the theoretical one coincided.

The first observation is that c_h values by Teh (1987) are lower than those by Baligh and Levadoux (1980) by up to a factor of three. This makes them closer to values of c_h obtained in the laboratory, as indicated by Sills et al (1988a) who reported that c_h values derived from piezocone data using Baligh and Levadoux's method were greater than those obtained by laboratory means by up to a factor of six. This fact is also confirmed by the results of c_h derived from restricted flow and permeability tests carried out by the author and summarised in Table 6.4, together with the rest of the c_h values from other dissipation tests.

As far as the prediction of the dissipation pattern is concerned, both solutions predict the cone shoulder dissipation curve satisfactorily, as can be seen in Figures 6.69 and 6.70. They initially over-predict the cone face dissipation, which means that only the bottom curve could be fitted with confidence. The use of T_{50} and T_{90} for the calculation of c_h may yield the same result as fitting the whole curve. However, neither solution predicts the initial rise in pore pressure at the locations on the piezocone shaft in Figures 6.71 and 6.74. (See Figures 6.61 to 6.65)

6.9.3 Tip resistance during the dissipation stage

One observation made at an early stage of this test programme was that the tip resistance did not remain constant after penetration had stopped. The trend in all the tests had been for the tip resistance to drop immediately after stopping. There then followed a continuing decrease before rising again to a value about 80% of its original value. To distinguish between tip resistance during driving and that immediately after stopping, the former can be referred to as the dynamic and the latter as the static tip resistance. A further distinction can also be made between the static value immediately after stopping and the final value risen to after dissipation. These can be distinguished as the undrained and drained static tip resistance

respectively.

Figure 6.75 shows the tip resistance plotted against time, for the first 60 seconds, from test Z41C which was carried out with the 5 cm^2 piezocone in the 1m testing chamber. The initial drop in tip resistance is very evident. Figure 6.76 shows the dissipation of shoulder pore water pressure from the 1 cm^2 piezocone from test Z14C carried out in the same chamber as above. On the same graph was plotted the tip resistance with time after penetration had stopped. In this Figure, the initial drop is not clear but continuing decrease in tip resistance can been seen to reach a minimum after approximately 100 seconds, when it had reached about 55% of its dynamic value. The tip resistance then increased gradually until it reached its drained static value, after another 15 minutes.

The initial drop is due to the relaxation of the pressure of the soil on the piezocone due to the loss of momentum of the soil when the piezocone stops. The continuing decrease in tip resistance suggests a consolidation process taking place within the soil mass around the cone, while the subsequent increase seems to indicate that the soil is swelling back. The water aiding the swell back will be that flowing away from the cone tip area due to high hydraulic gradients. The two processes could have been continuous, except that the consolidation process could be seen to be more dominant during the time the tip resistance is dropping and the swelling more dominant when the tip resistance increases.

Table 6.1 Geotechnical properties of test samples

Test Series No.	Testing Pressure σ_v' kPa	OCR	K_0	Shear vane Strength s_{uv} kPa	Triaxial Shear Strength s_{uciu} kPa	c_h 10^{-6} m^2/min
Z1C	537	1.6	0.85			
Z2B	222	2.6	0.93	121	91	72.3
Z3A	194	3.2	1.1	103	96	
Z4C	95	5.0	1.0	70	55	116
Z5B	68	8.9	1.4	47	49	
Z6A	131	6.7	0.83	78	63	55.6
Z7C	81	9.1	1.2	90	57	350
Z8B	524	1.4	0.78	167	132	31.8
Z9C	580	1.3	0.68	178	155	191.3
Z10A	92	8.4	1.0	132	-	112.4
Z11B	81	6.1	1.2	62	-	23.5
Z12C	200	3.0	0.86	99	-	81.4

Table 6.2A Results of penetration tests

Test Series No.	q_t kPa	Skin Friction kPa	U_1 kPa	U_{Shld} kPa	U_3 kPa	U_4 kPa
Z14C Z13C	2370 2462			1157 1289		
Z21B Z22B	1824 1420			948 790		
Z33A Z34A	1450 1500			634 680		
Z41C Z42C Z43C	943 912 888		631 604 588	422 355 367	291 266 233	251 186 170
Z53B Z54B	824 832			317 304		
Z61A Z62A Z63A	951 829 832			369 356 352		

Table 6.2B Results of penetration tests (continued)

Test Series No.	q_t kPa	Skin Friction kPa	U_{Face} kPa	U_{Shld} kPa	$U_{M.sleeve}$ kPa	$U_{T.sleeve}$ kPa
Z71C	1190	24	716	558	256	154
Z72C	1255	18	646	511	265	178
Z73C	1213	39	832	524	250	177
Z74C	1279	14	870	487	278	182
Z81B	2086			1185		
Z82B	1899			1170		
Z84B	2123			1062		
Z91C	1973	13.5	1638	1236	930	712
Z92C	2077	11	1724	1264	911	699
Z93C	1967	8.5	1632	1186	898	640
Z94C	1943	11	1605	1205	870	661
Z101A	1453			563		
Z102A	1530			529		
Z103A	958			522		
Z104A	1165			459		
Z111B	787			308		
Z112B	764			268		
Z113B	738			280		
Z114B	747			221		
Z121C	1112	9.3	874	635	409	281
Z122C	1054	8.6	657	545	376	260
Z123C	1019	5.6	812	567	390	267
Z124C	1035	6.1	837	610	353	261

Table 6.3A Factors derived from penetration results

Test Series No.	OCR	β	B_q	Q
Z13C Z14C	1.6 1.6		0.67 0.68	2.8 3.3
Z21B Z22B	2.6 2.6		0.61 0.67	5.6 5.4
Z33A Z34A	3.2 3.2		0.52 0.53	5.5 5.7
Z41C Z42C Z43C	5.0 5.0 5.0	0.68 0.64 0.66	0.50 0.49 0.50	7.6 7.5 7.0
Z53B Z54B	8.9 8.9		0.42 0.40	11.1 11.2
z61A Z62A Z63A	8.3 6.7 6.7		0.37 0.49 0.48	7.5 6.7 6.7

Table 6.3B Factors derived from penetration results (continued)

Test Series No.	OCR	β	B_q	Q
Z71C	9.1	0.28	0.52	10.6
Z72C	9.1	0.69	0.48	9.6
Z73C	9.1	0.64	0.48	11.4
Z74C	9.1	0.61	0.45	9.6
Z81B	1.4		0.75	3.1
Z82B	1.4		0.84	2.7
Z84B	1.4		0.66	3.1
Z91C	1.3	0.76	0.91	2.3
Z92C	1.3	0.73	0.86	2.4
Z93C	1.3	0.73	0.87	2.2
Z94C	1.3	0.75	0.90	2.2
Z101A	7.9		0.46	15.2
Z102A	8.5		0.42	15.4
Z103A	8.4		0.60	9.8
Z104A	8.5		0.43	12.0
Z111B	6.2		0.38	8.1
Z112B	6.1		0.40	7.4
Z113B	6.1		0.43	7.4
Z114B	5.7		0.34	7.5
Z121C	3.0	0.73	0.70	4.5
Z122C	3.0	0.83	0.64	4.2
Z123C	3.0	0.70	0.70	4.1
Z124C	3.0	0.72	0.74	4.1

Table 6.4 Consolidation coefficients

Test Series No.	c_h(10^{-6}m^2/min)								
	U_1 (BL)	U_1 (T)	U_{Shld} (BL)	U_{Shld} (T)	U_3 (BL)	U_3 (T)	U_4 (BL)	U_4 (T)	c_h (Lab)
Z2B			500.0						72.3
Z4C	900	465	454.5	308.0	900	465	900	465	116.0
Z6A			293.0	90.0					55.6
Z7C	1754	833	714.0	667.0	1667	952	909	556	350.0
Z8B			175.4	53.5					31.8
Z9C	833.3	181.8	588.3	181.8	1250	400	1250	308	191.3
Z10A									112.4
Z11B									23.5
Z12C	1000	333	667.0	286.0	1250	500	833	287	81.4

BL Baligh and Levadoux (1980)
T Teh (1987)
Lab c_h values from restricted flow consolidation and permeability tests on 90 samples

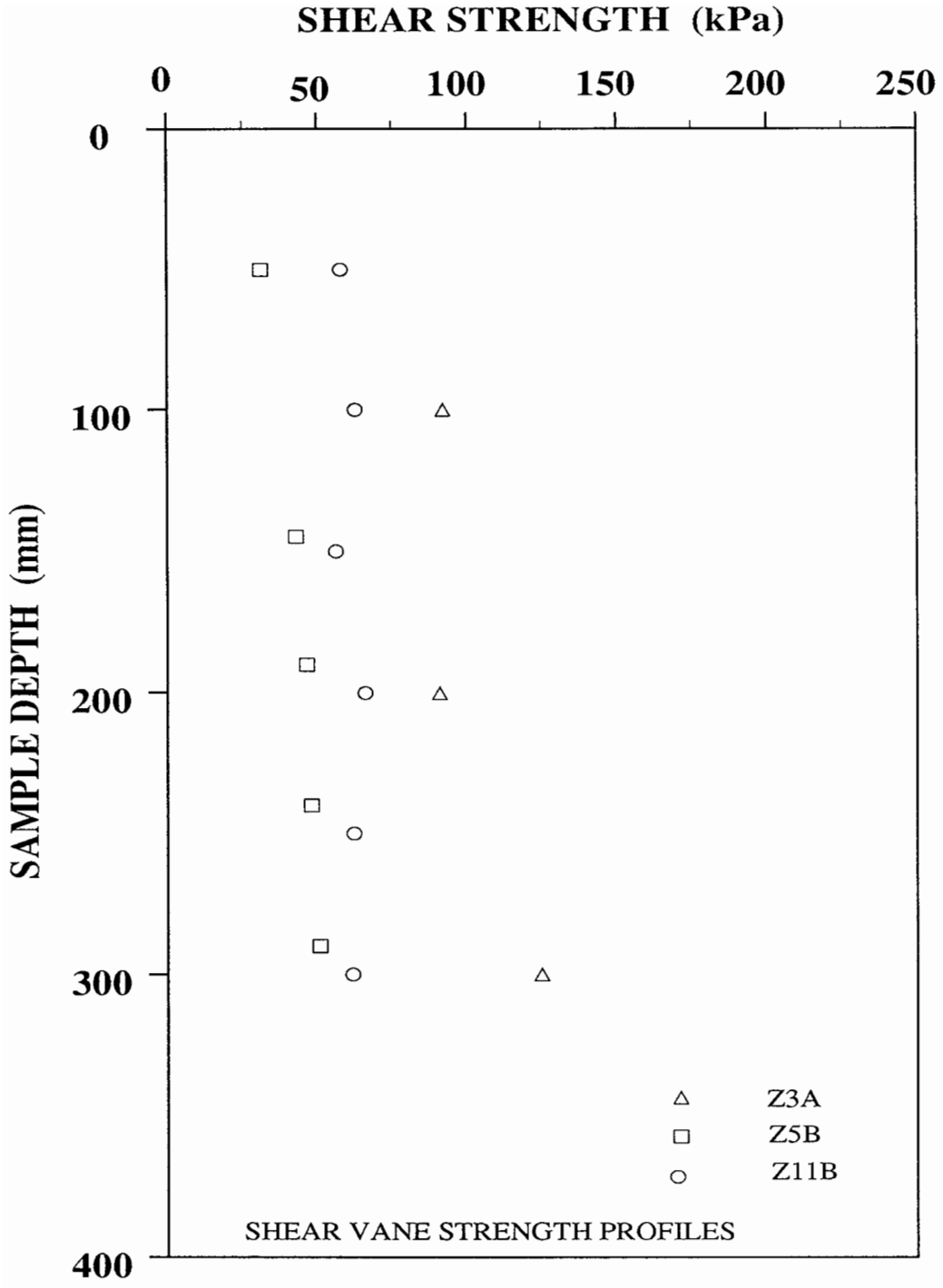

Figure 6.1 Shear strength profiles for samples Z3A, Z5B and Z11B.

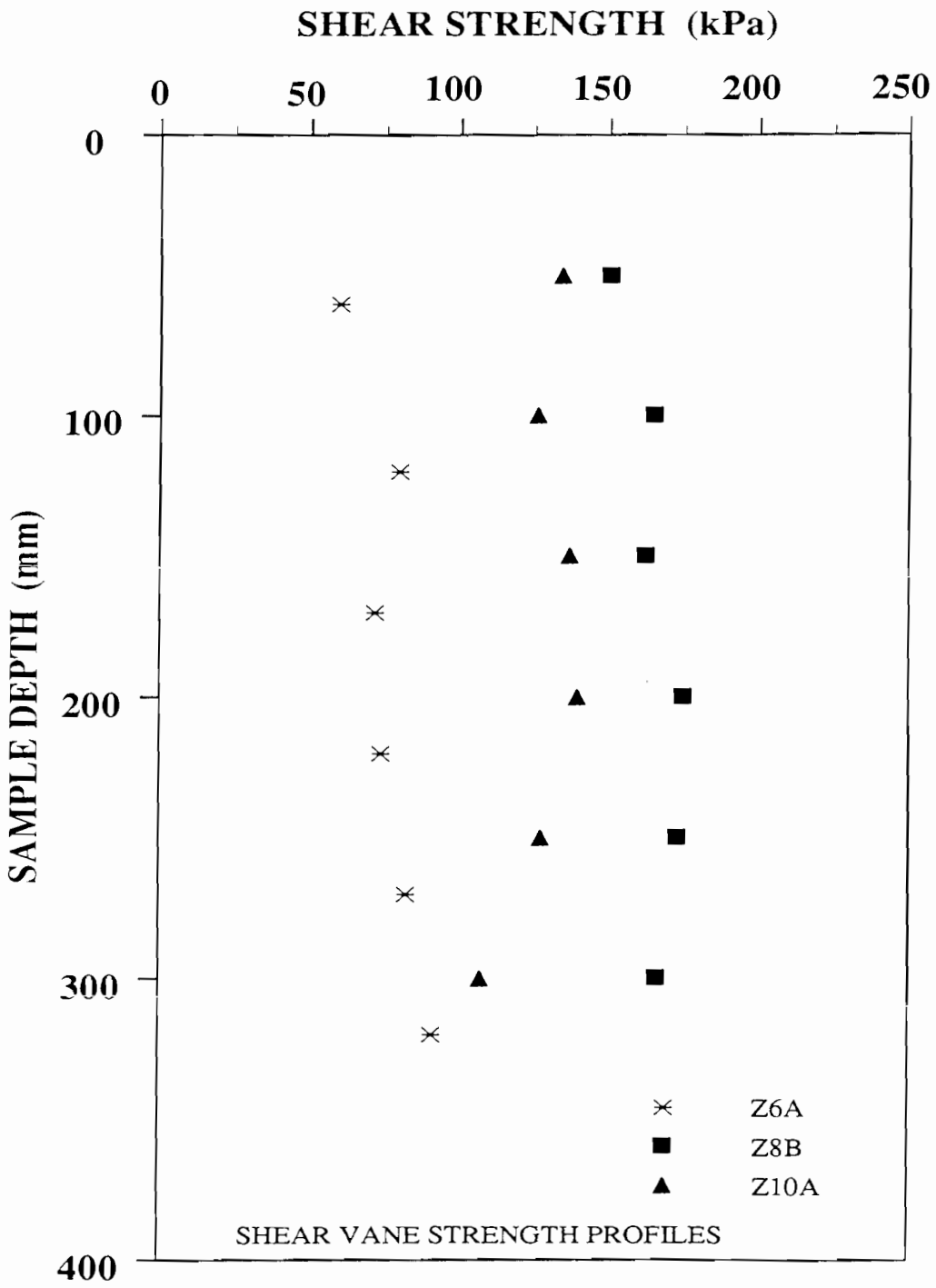

Figure 6.2 Shear strength profiles for samples Z6A, Z8B and Z10A.

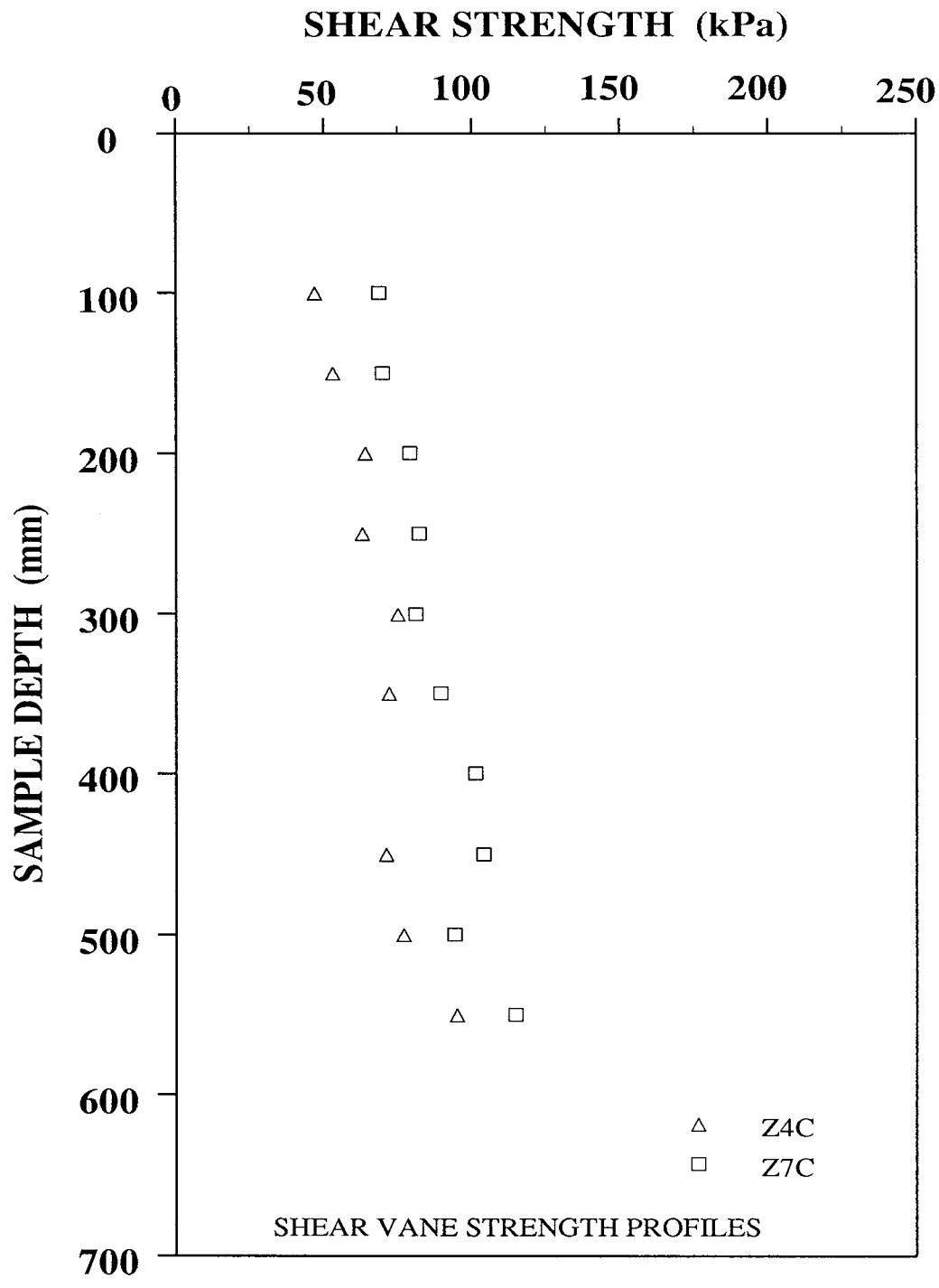

Figure 6.3 Shear strength profiles for samples for Z4C and Z7C.

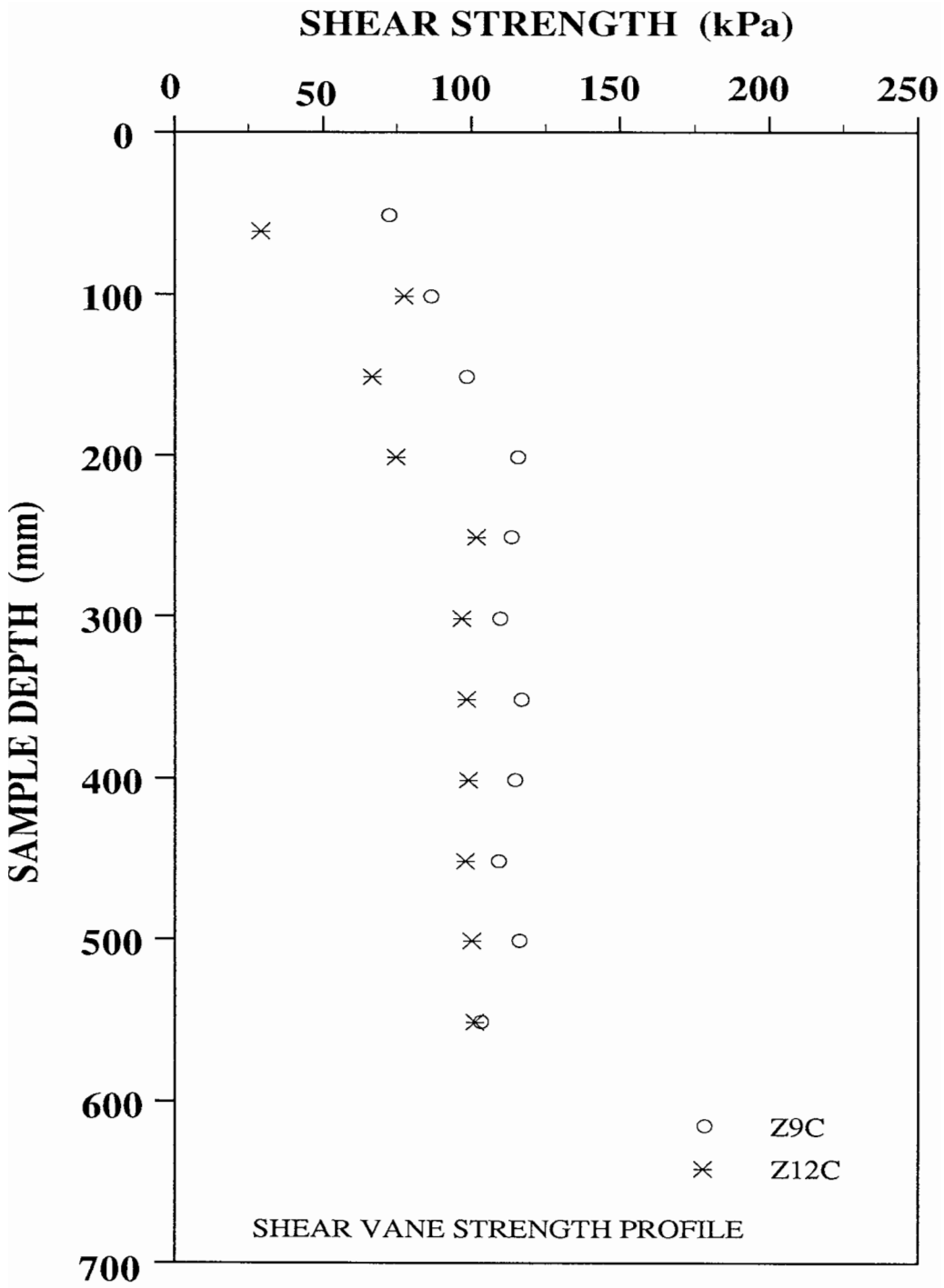

Figure 6.4 Shear strength profiles for samples for Z9C and Z12C.

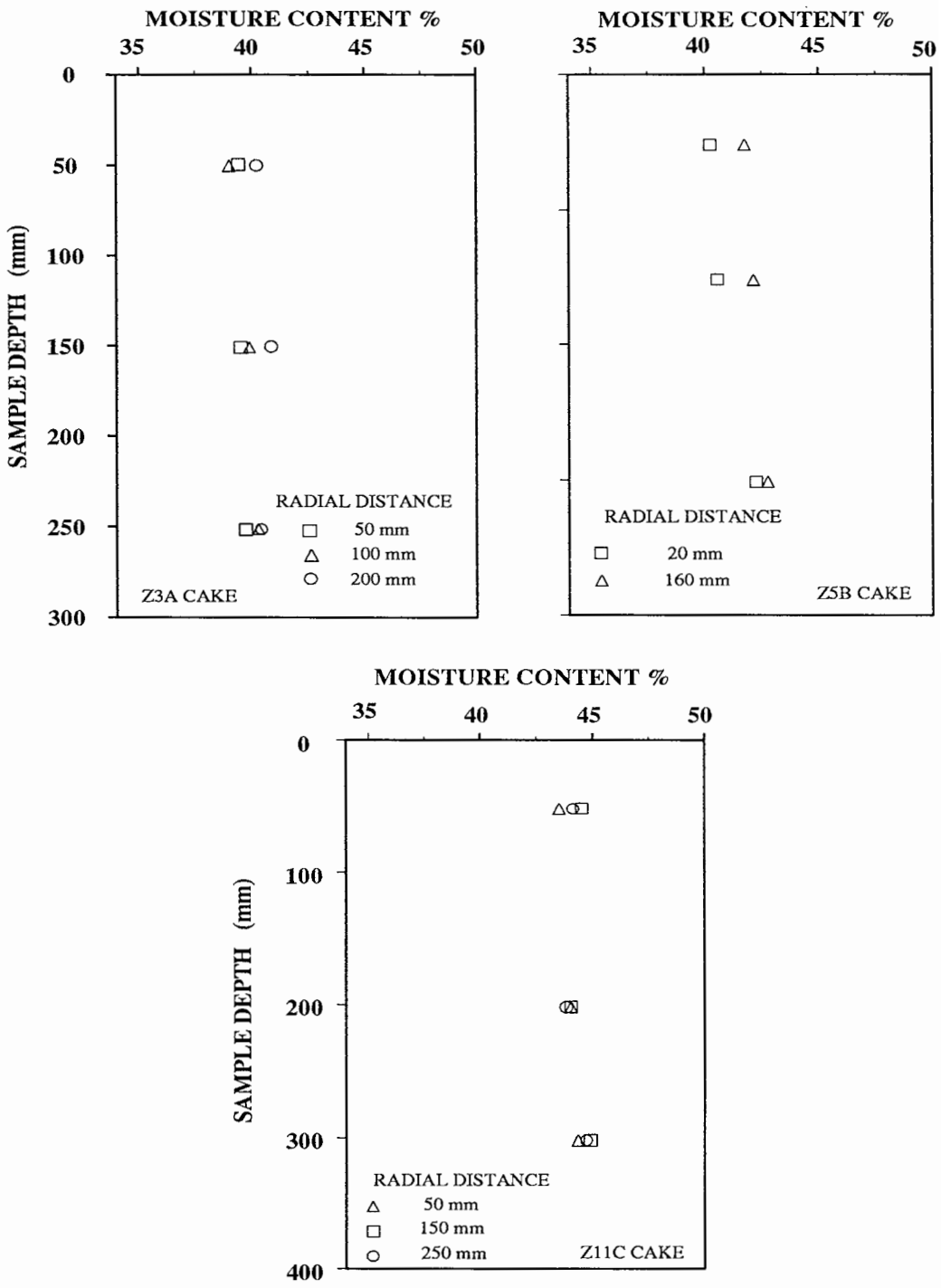

Figure 6.5 Moisture content variation in samples Z3A, Z5B and Z11B.

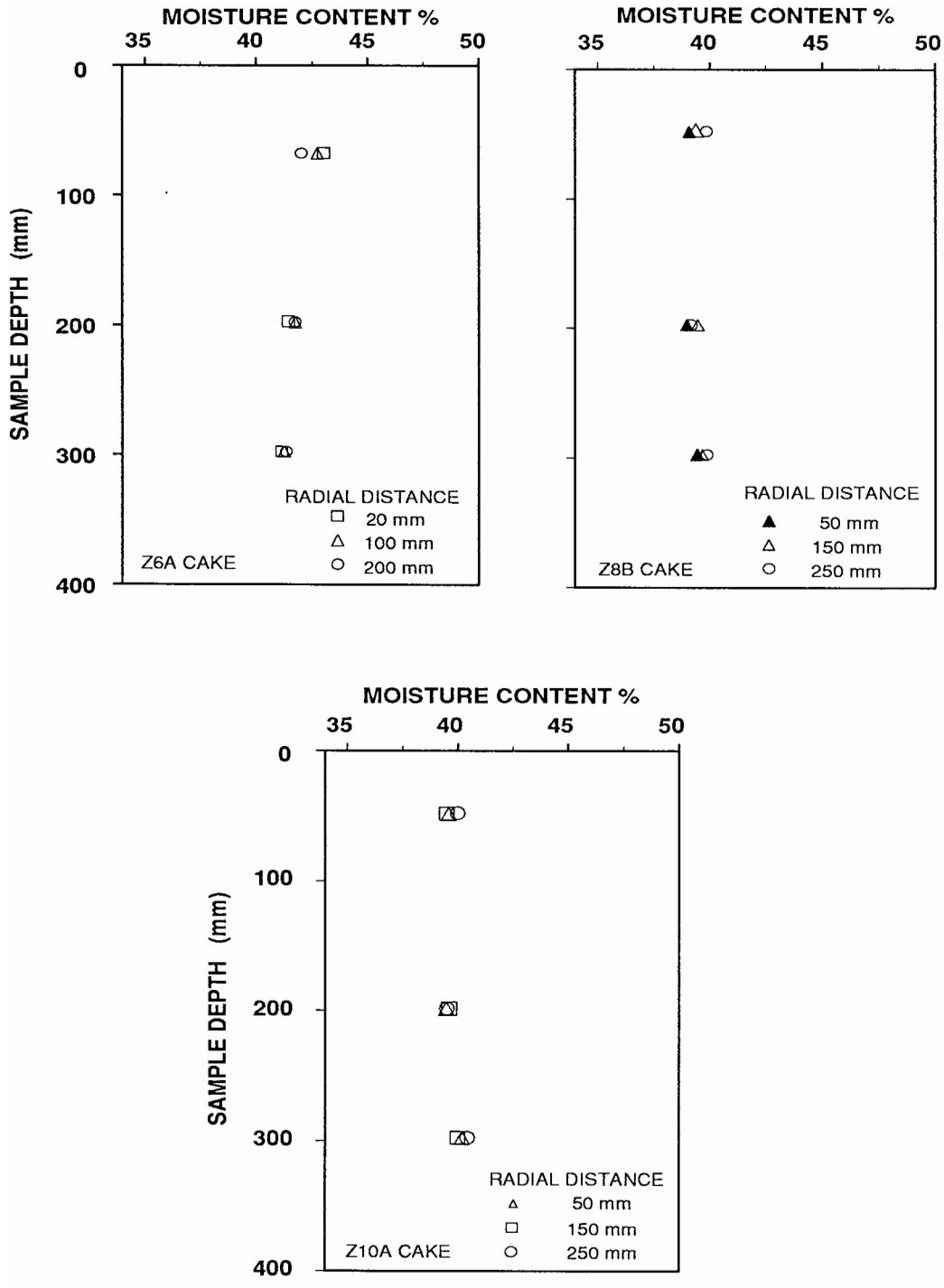

Figure 6.6 Moisture content variation in samples Z6A, Z8B and Z10A.

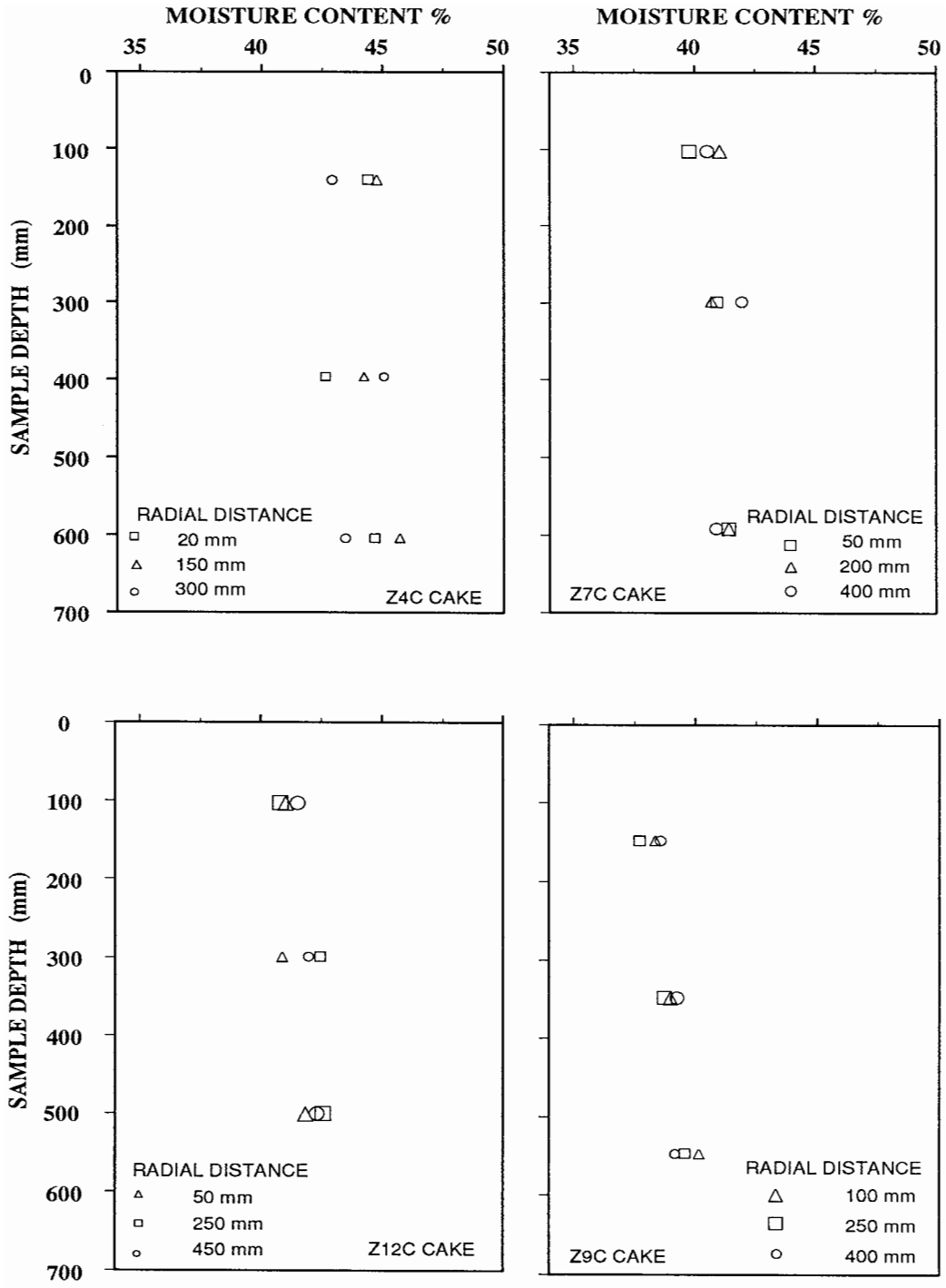

Figure 6.7 Moisture content variation in samples Z4C, Z7C and Z12C.

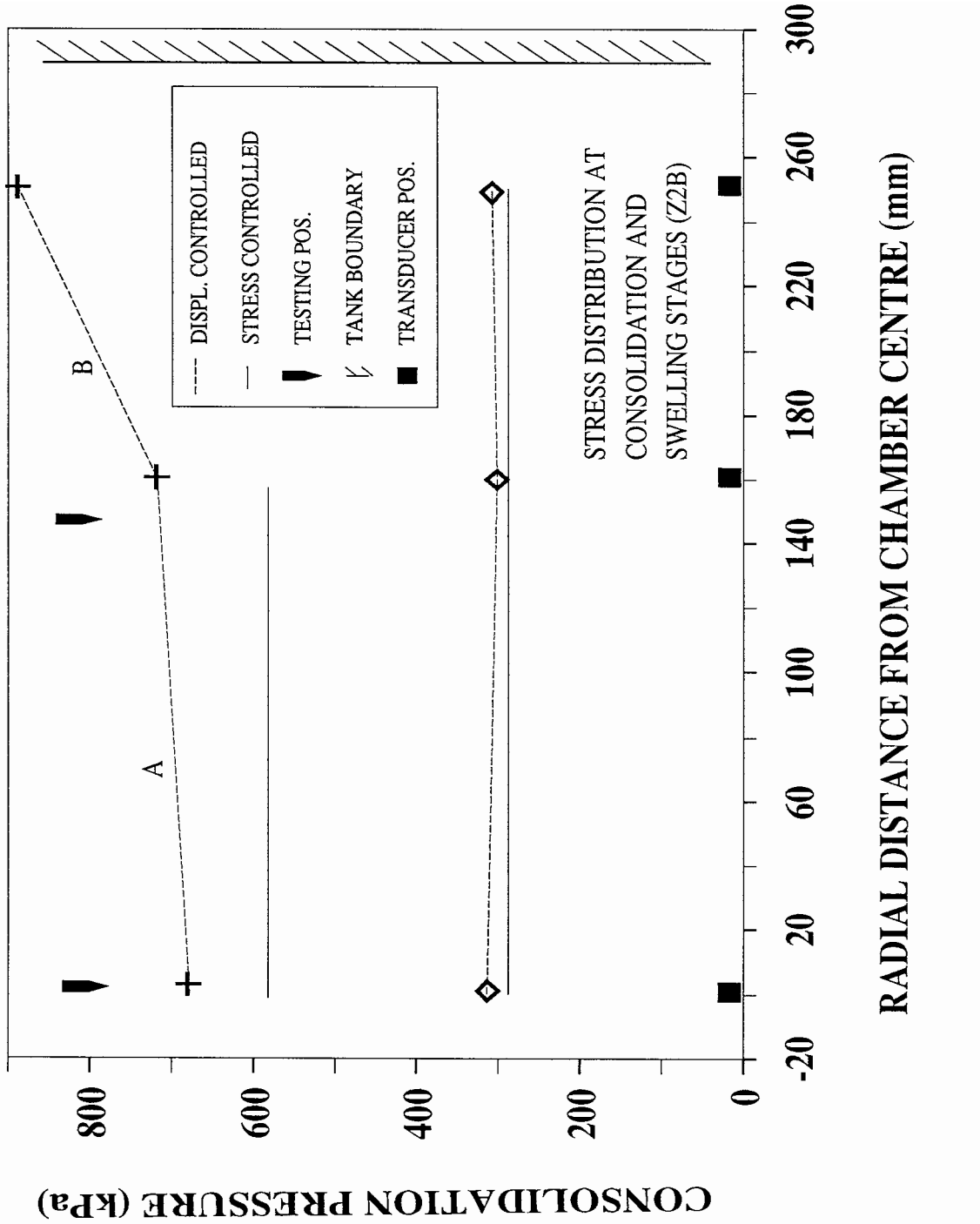

Figure 6.8 Vertical stress distribution before and after the swelling stage for sample Z2B.

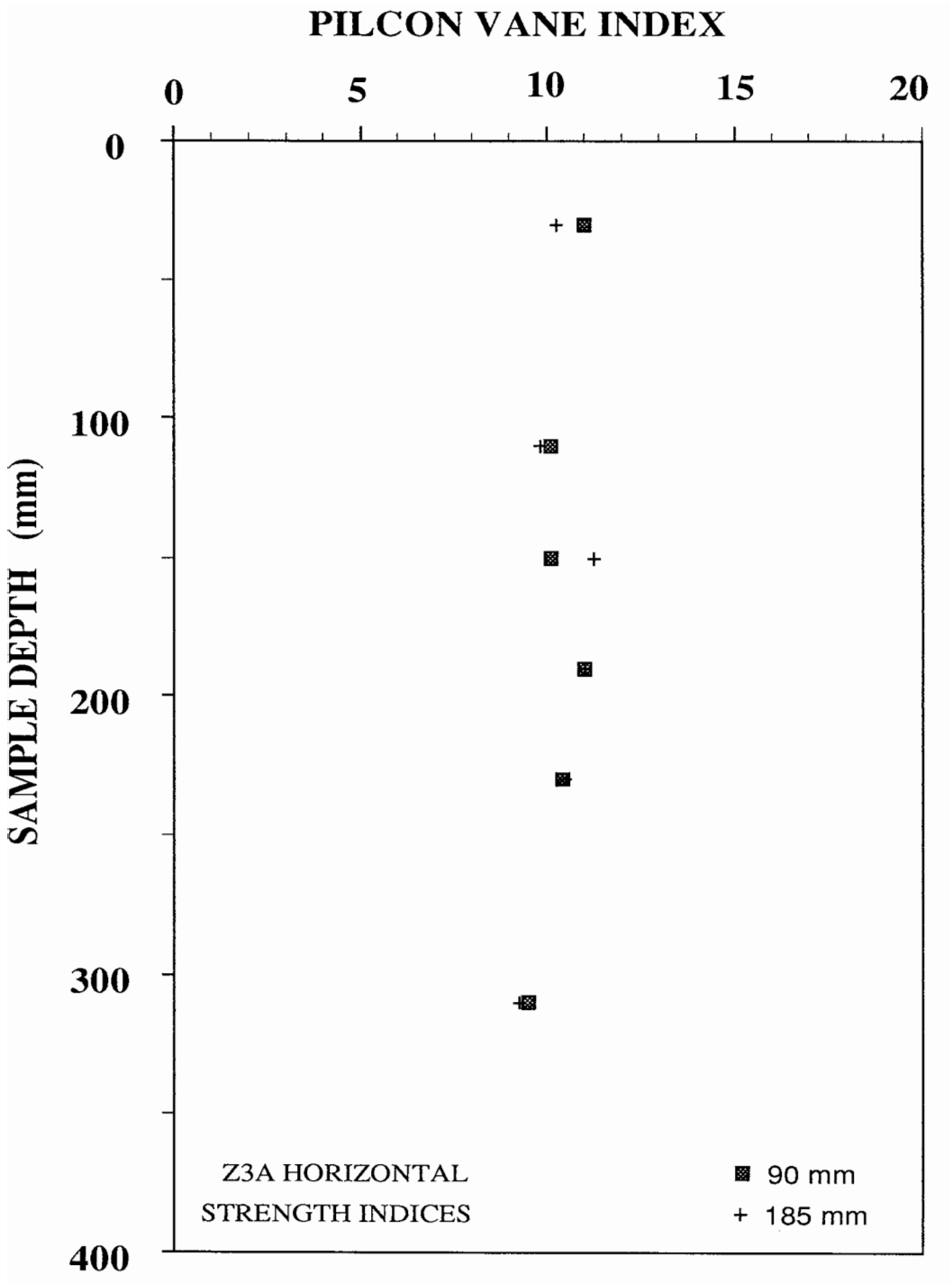

Figure 6.9 Horizontal shear strength index for sample Z3A.

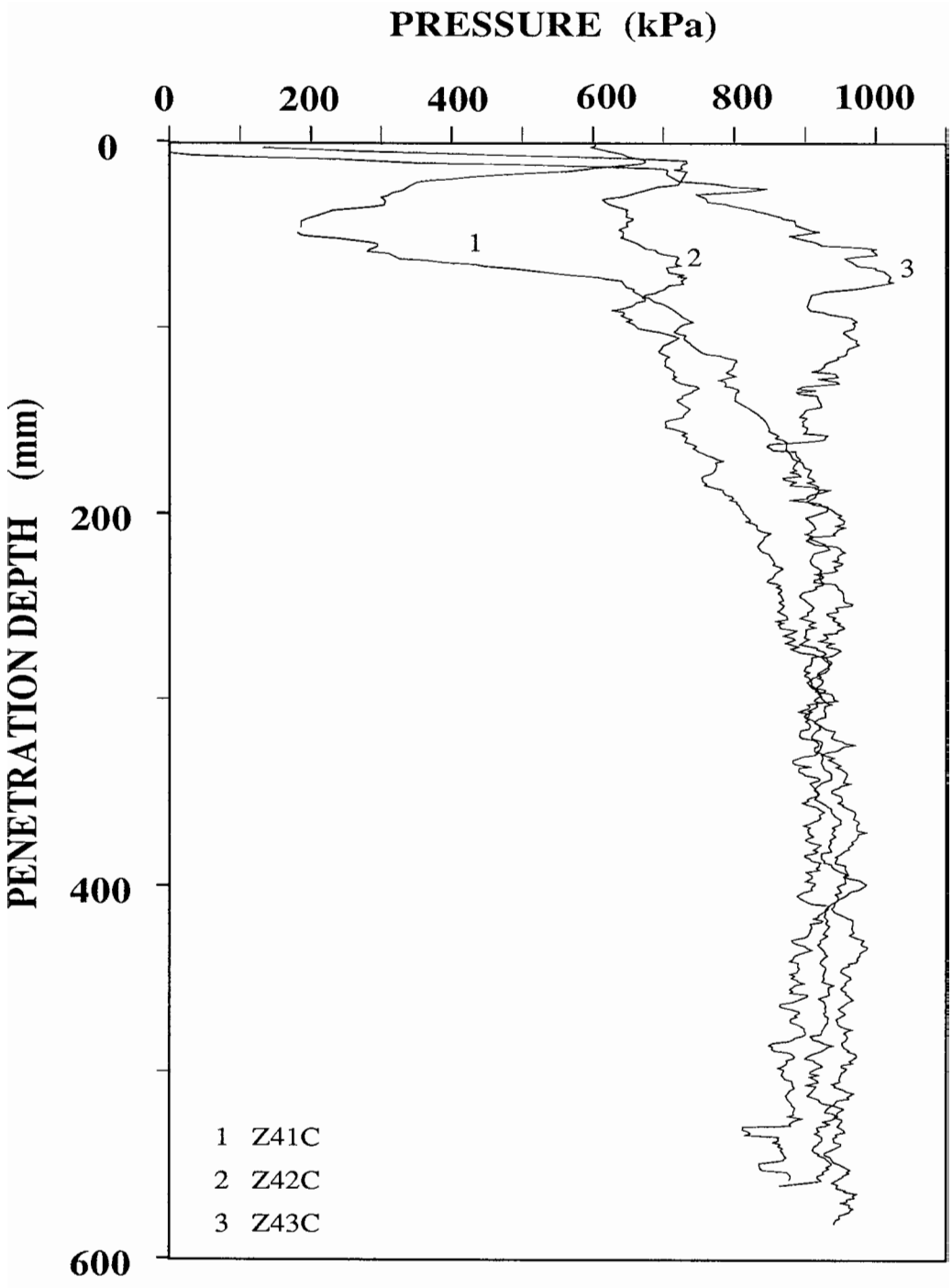

Figure 6.10 Tip resistance responses for test series Z4C.

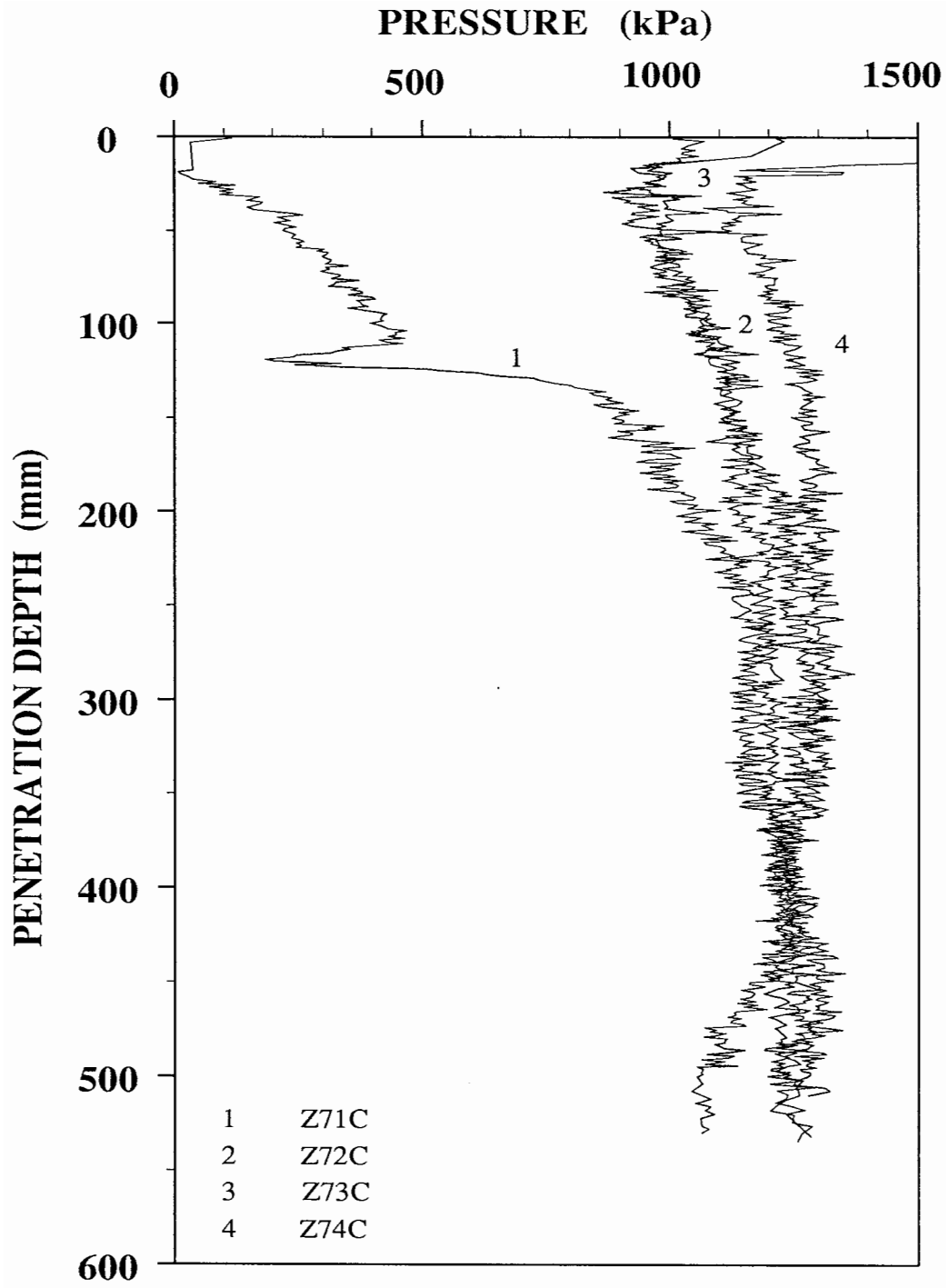

Figure 6.11 Tip resistance responses for test series Z7C.

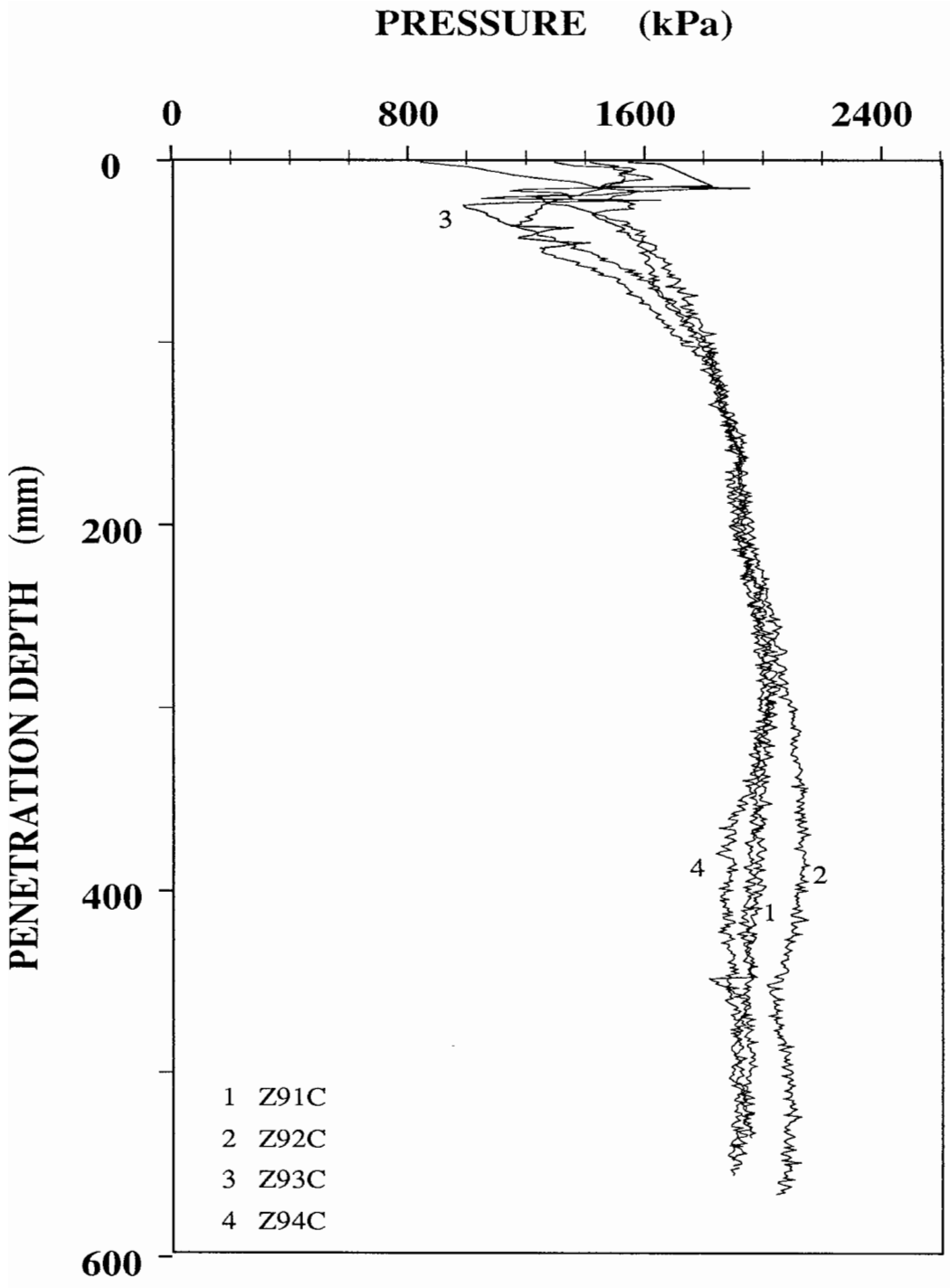

Figure 6.12 Tip resistance responses for test series Z9C.

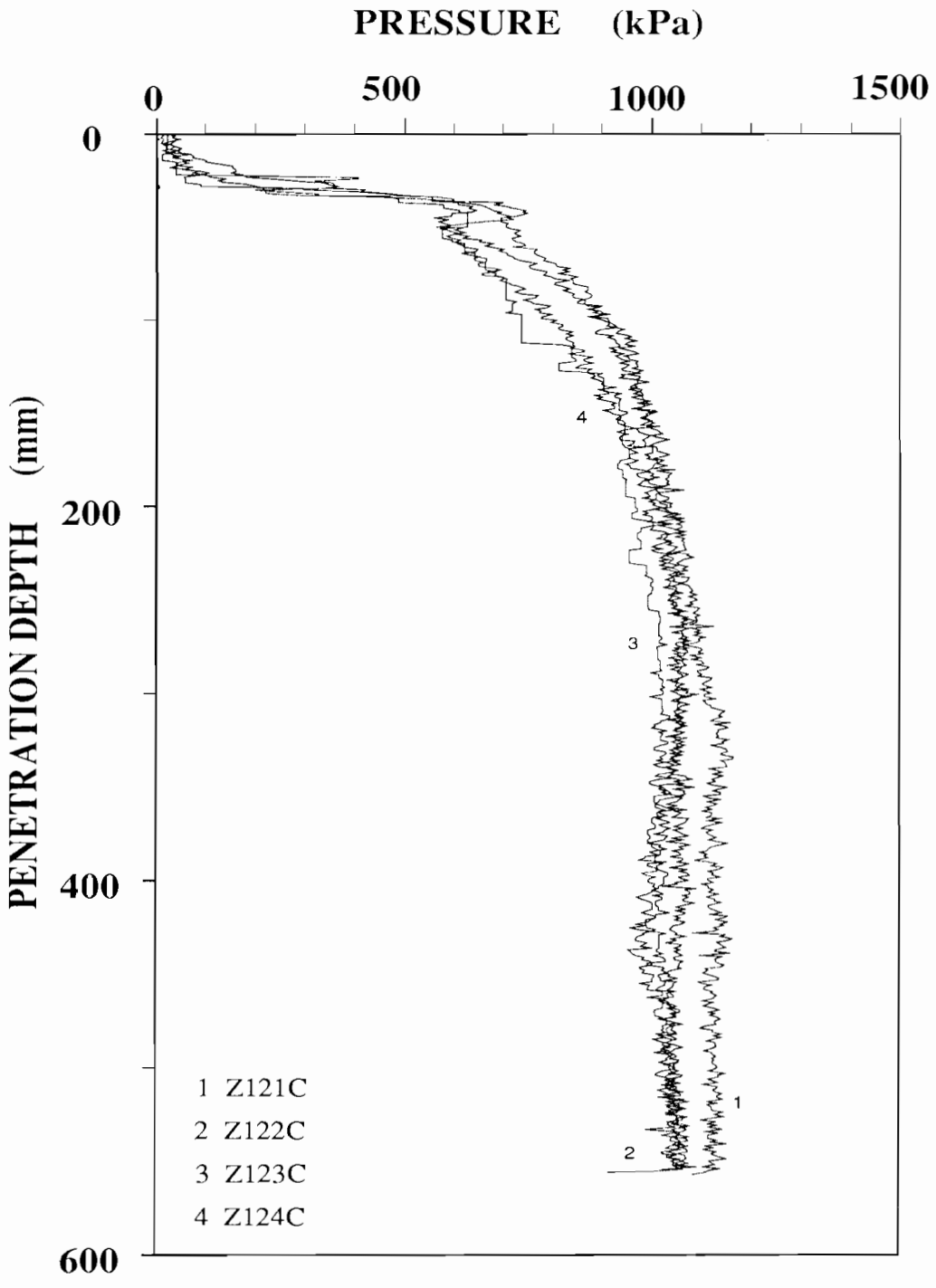

Figure 6.13 Tip resistance responses for test series Z12C.

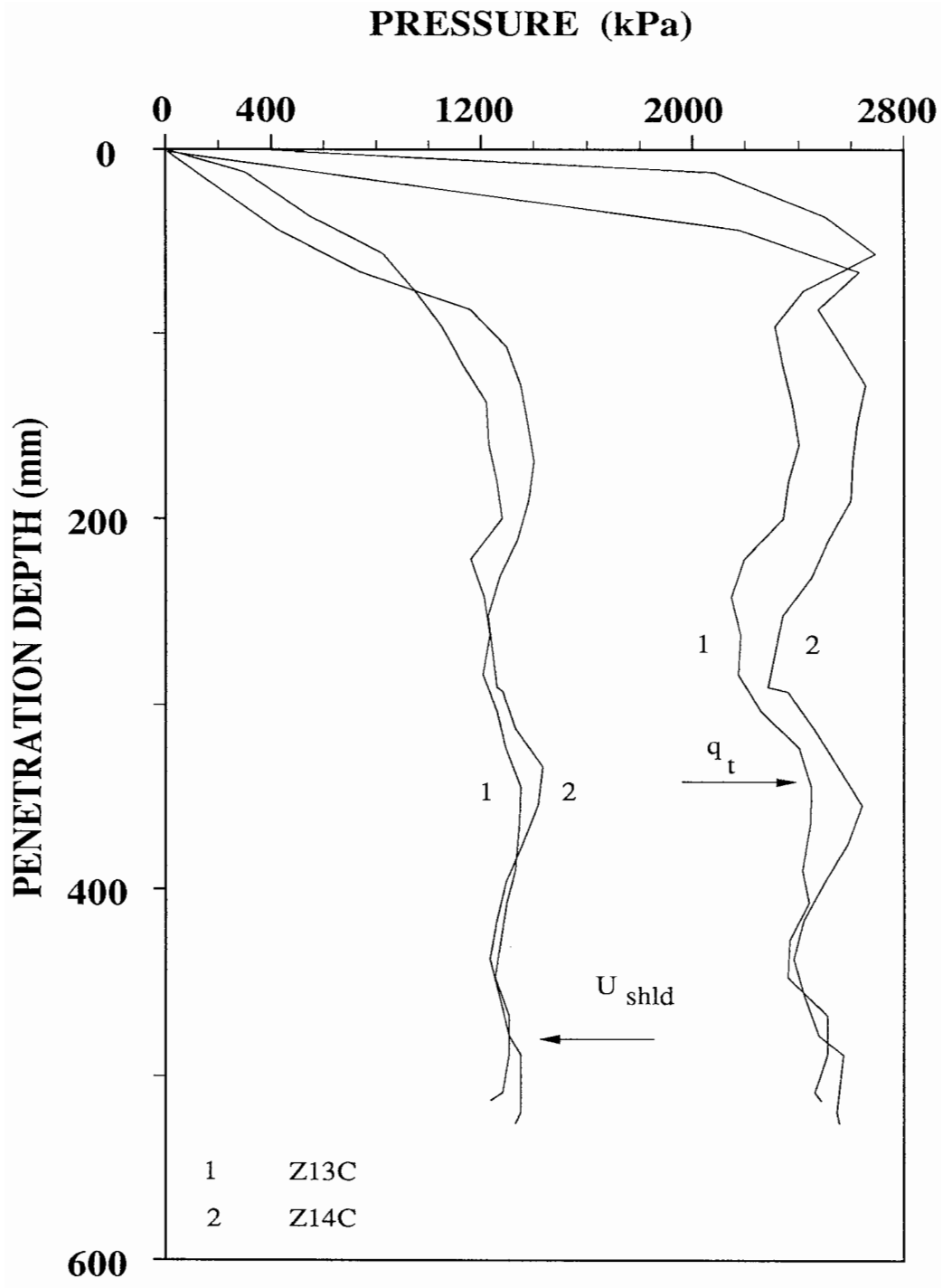

Figure 6.14 Tip resistance and shoulder pore water pressure responses for test series Z1C.

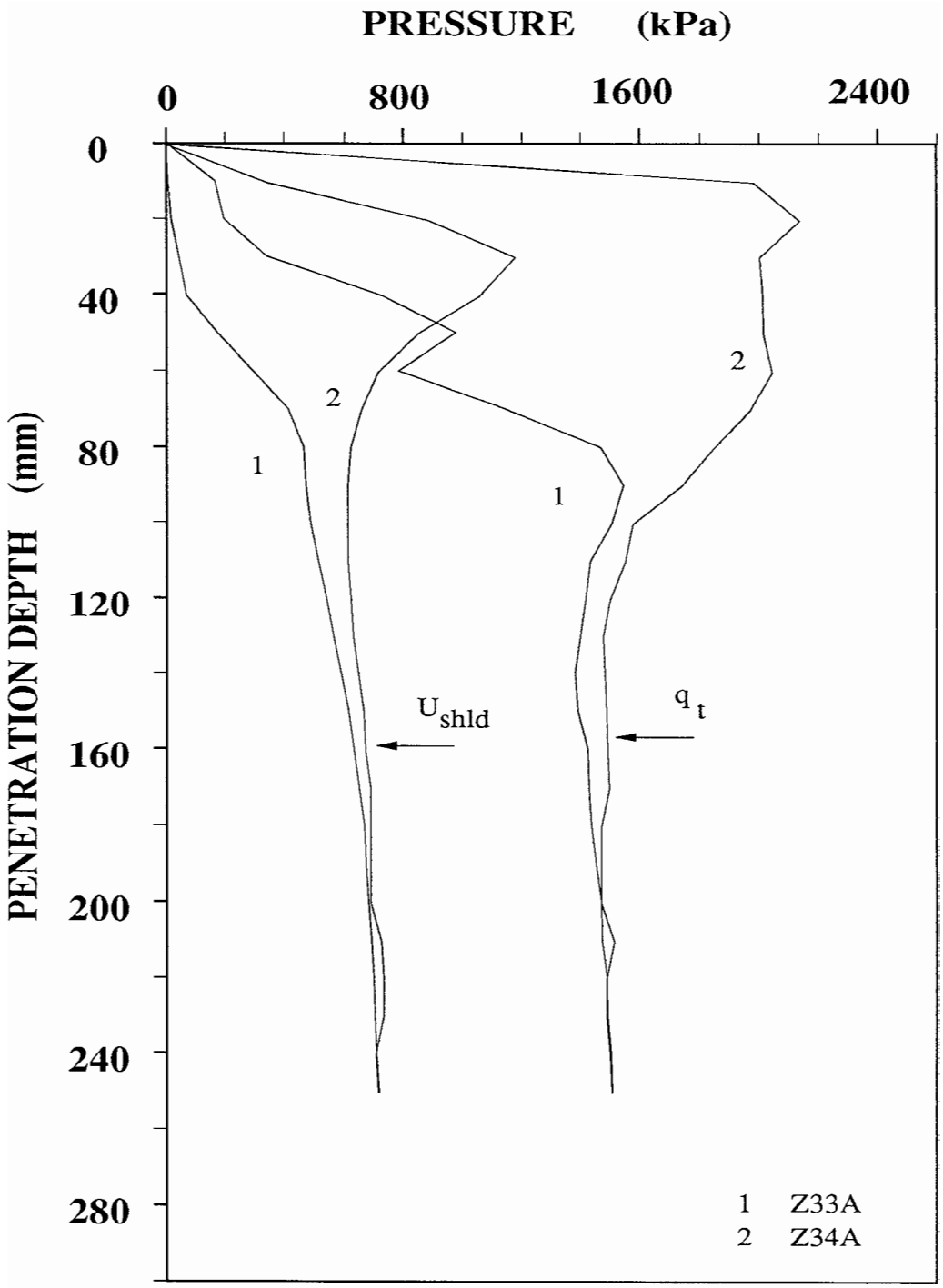

Figure 6.15 Tip resistance and shoulder pore water pressure responses for test series Z3A.

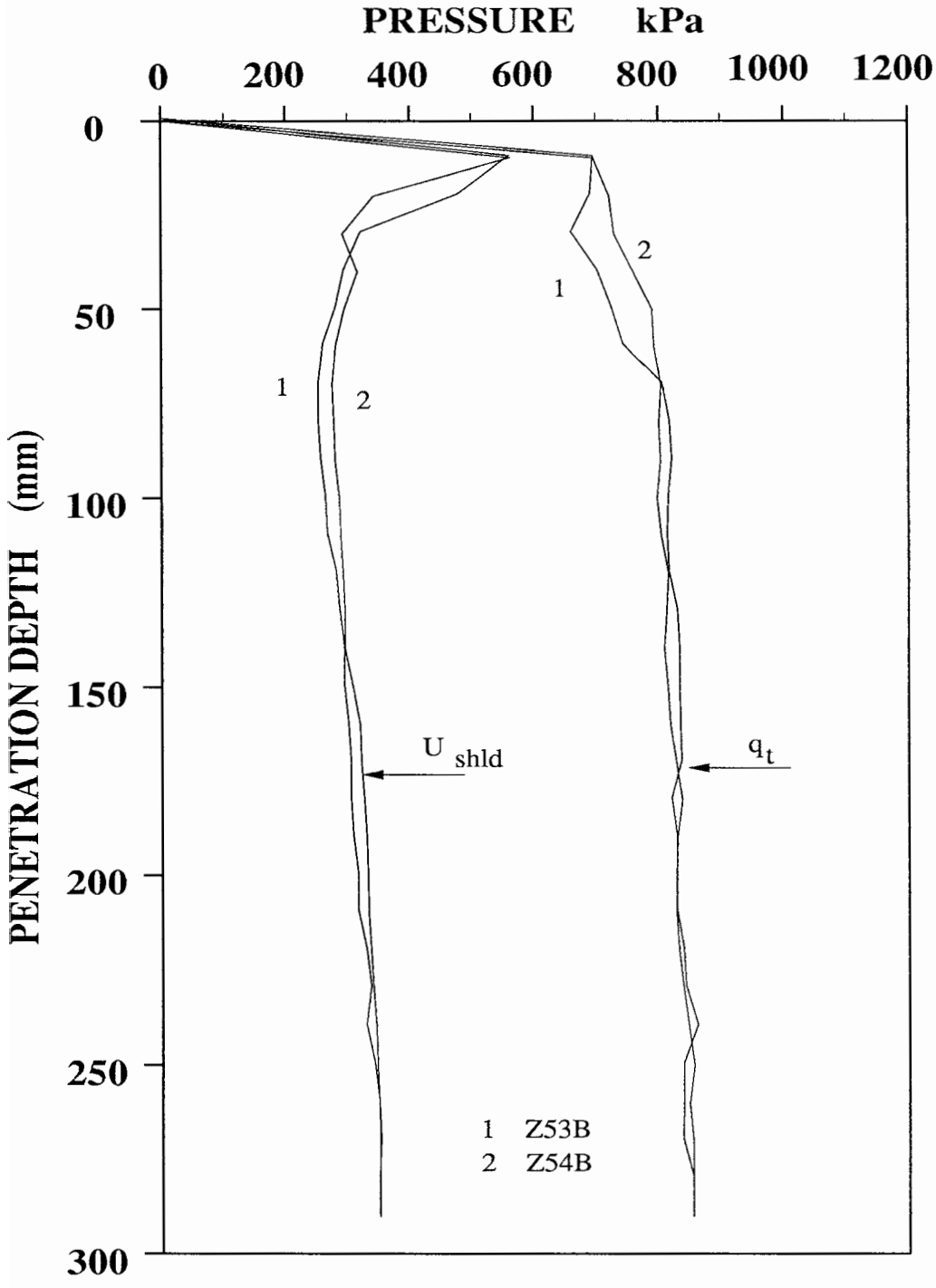

Figure 6.16 Tip resistance and shoulder pore water pressure responses for test series Z5B.

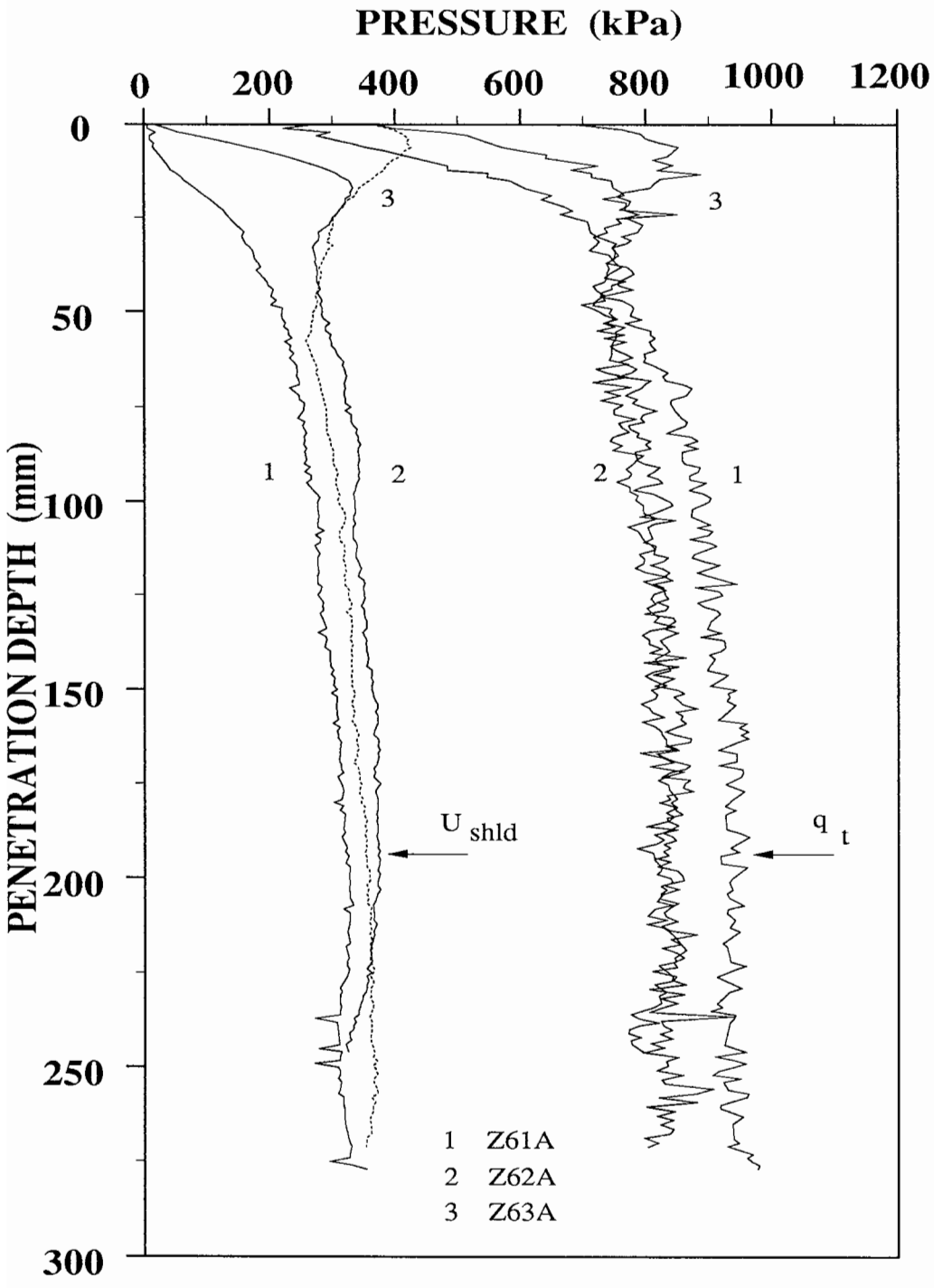

Figure 6.17 Tip resistance and shoulder pore water pressure responses for test series Z6A.

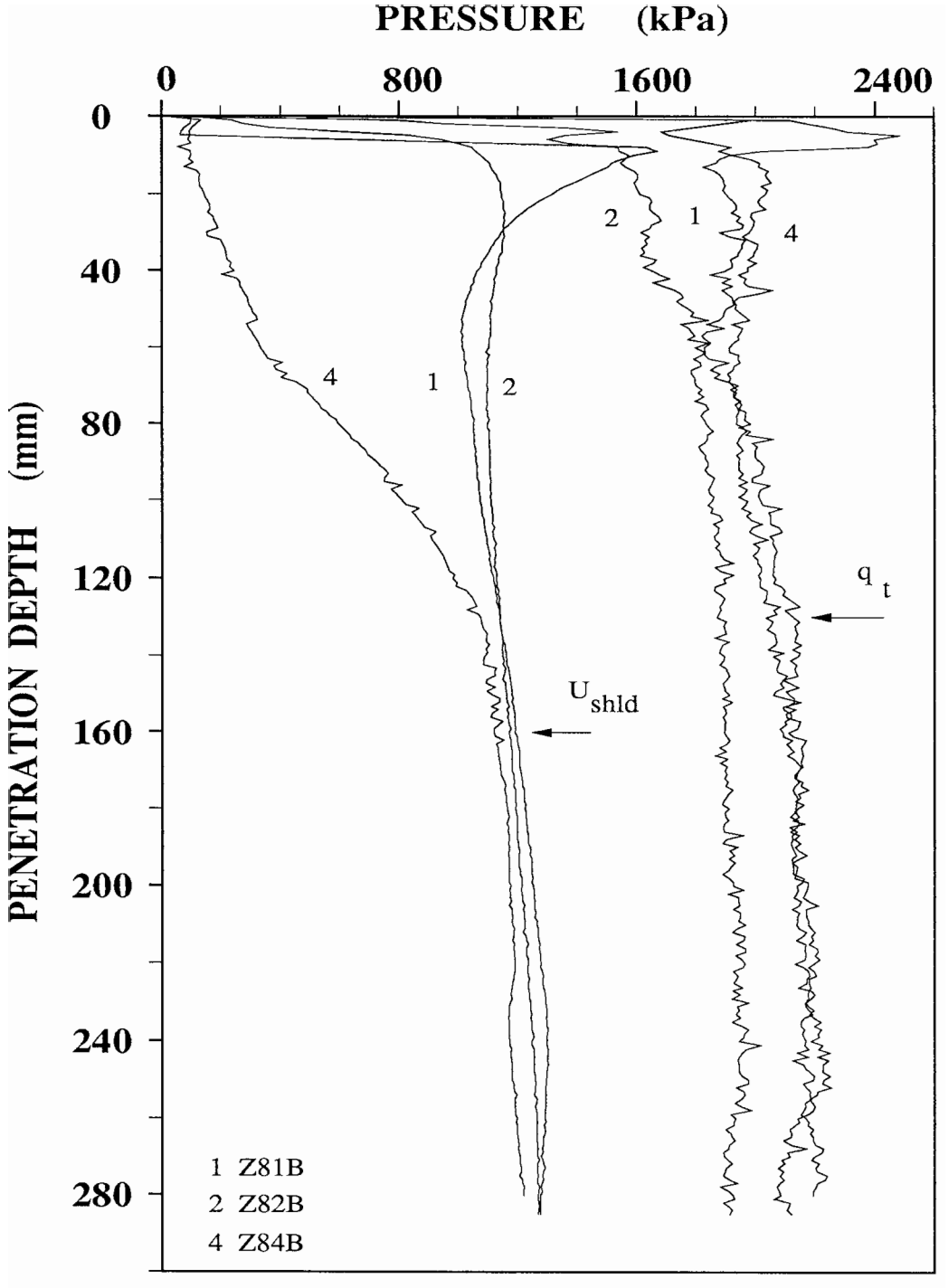

Figure 6.18 Tip resistance and shoulder pore water pressure responses for test series Z8B.

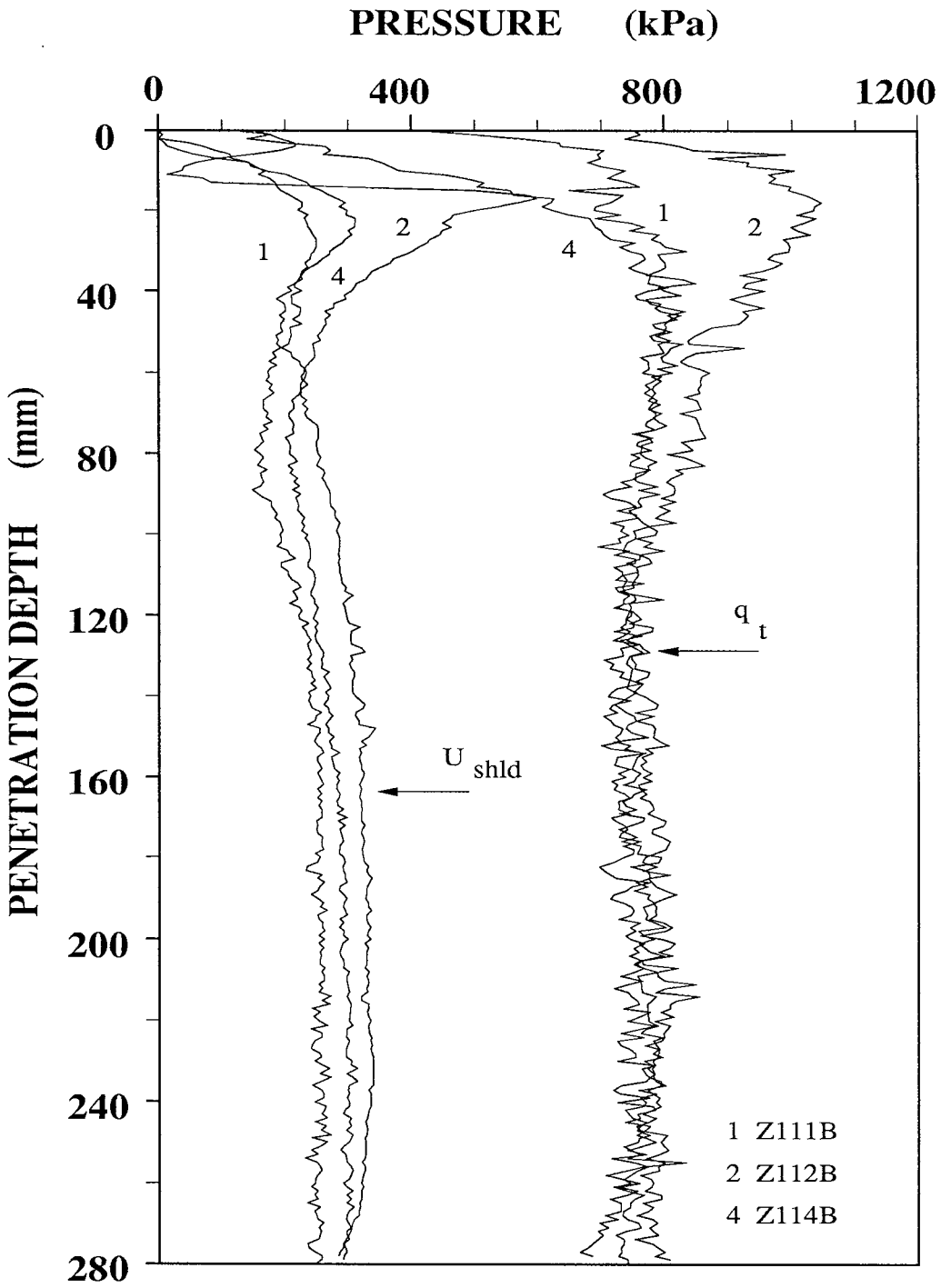

Figure 6.19 Tip resistance and shoulder pore water pressure responses for test series Z11B.

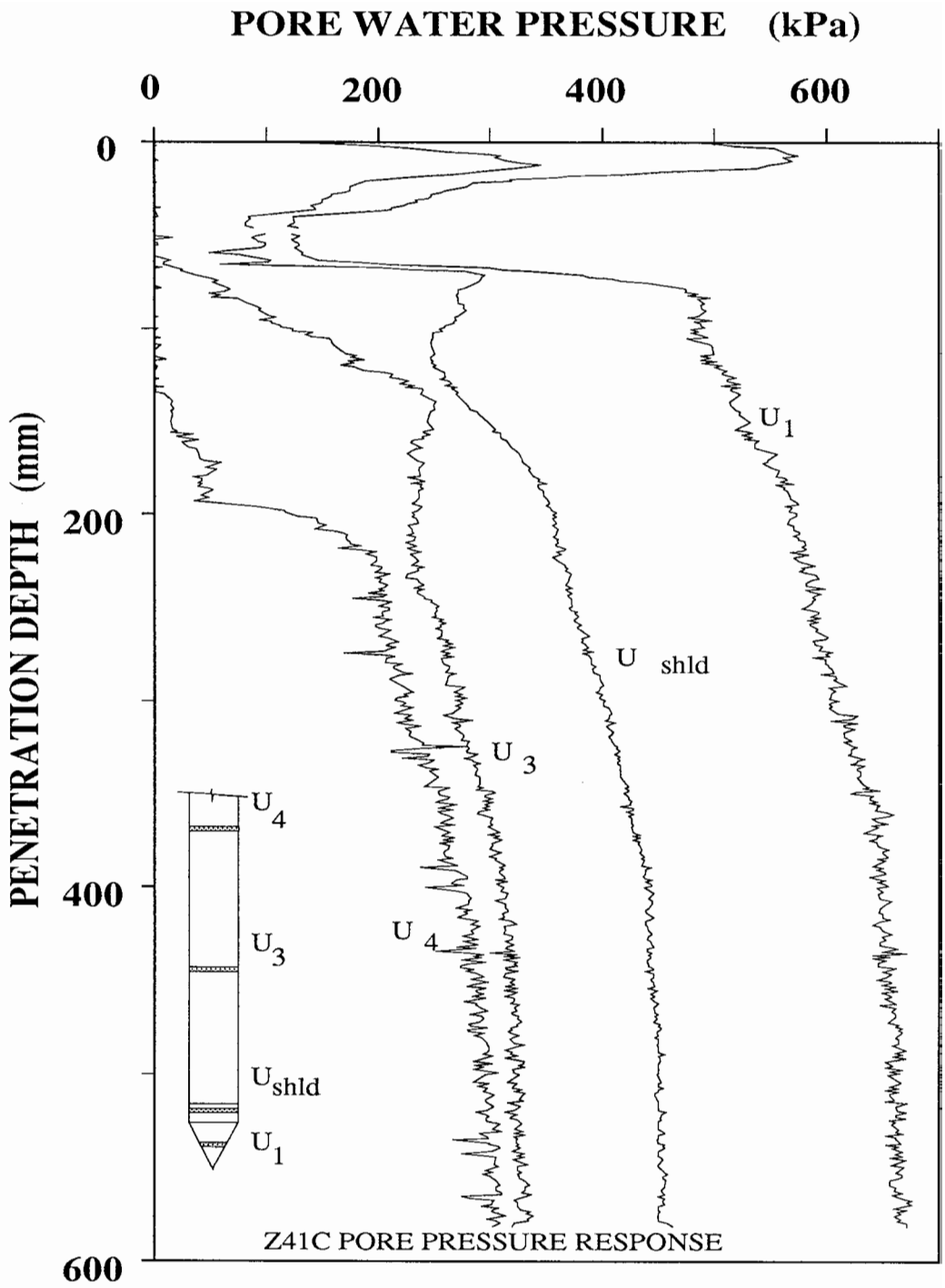

Figure 6.20 Pore water pressure during penetration in test Z41C.

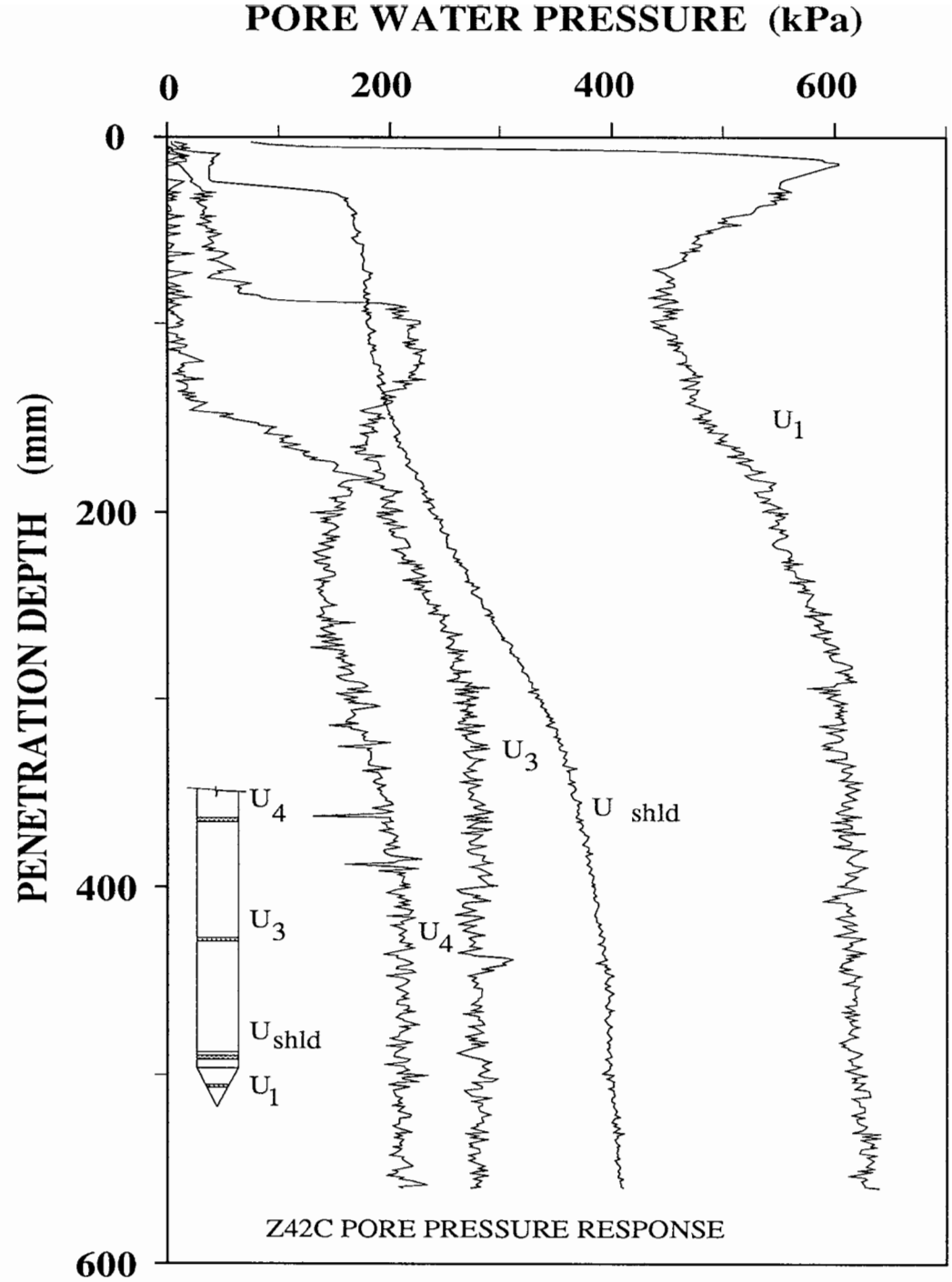

Figure 6.21 Pore water pressure during penetration in test Z42C.

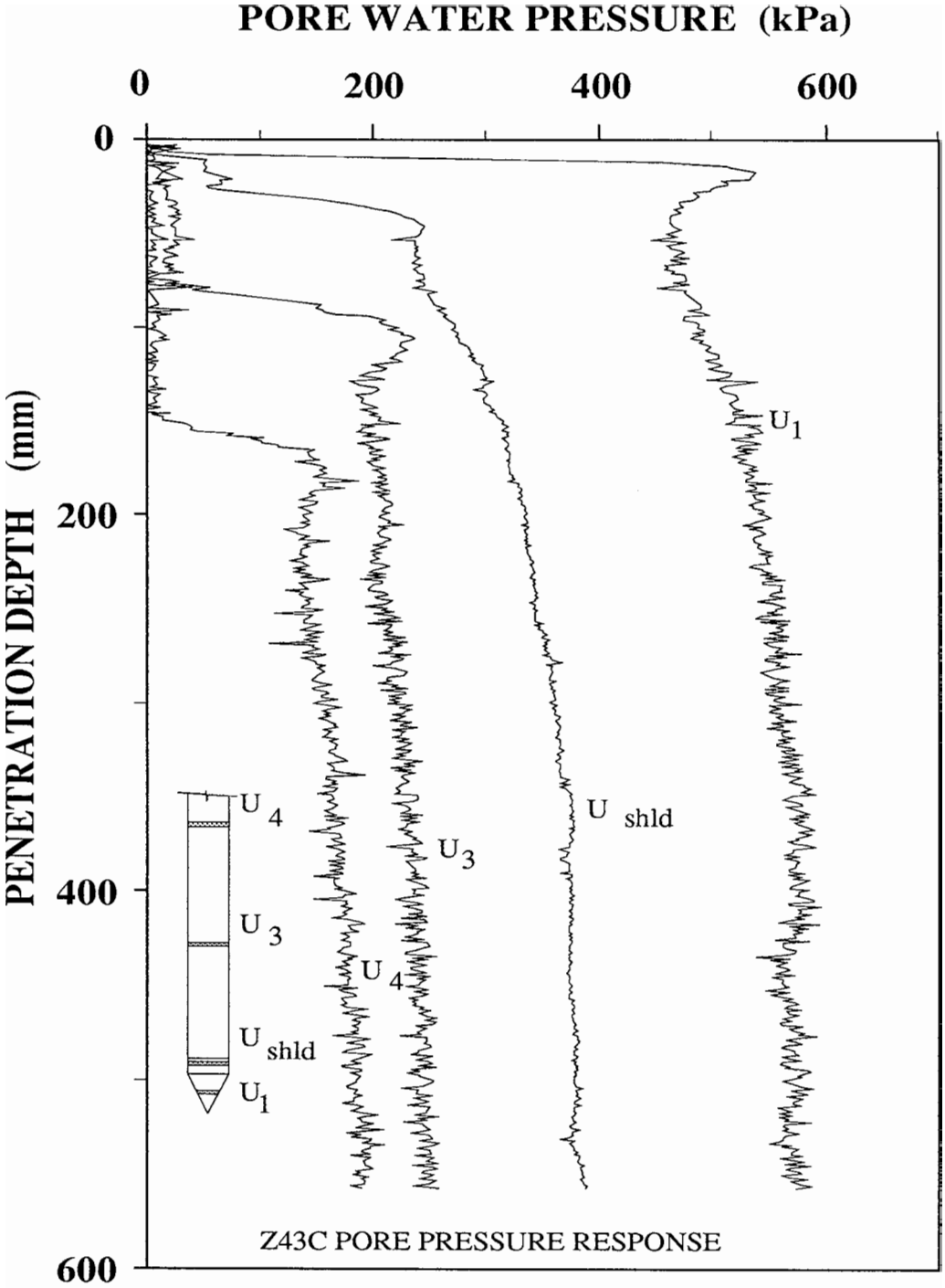

Figure 6.22 Pore water pressure during penetration in test Z43C.

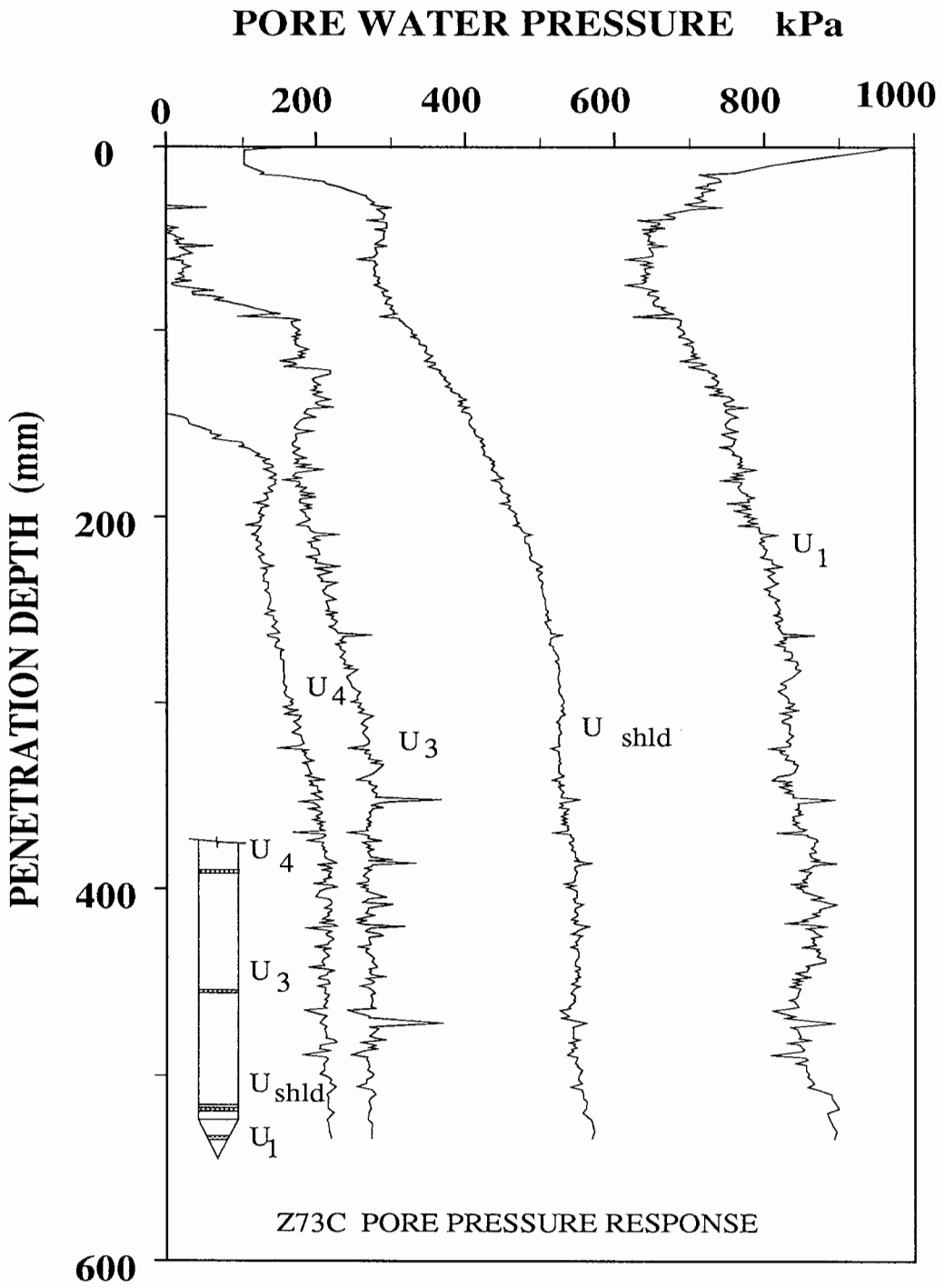

Figure 6.23 Pore water pressure during penetration in test Z73C.

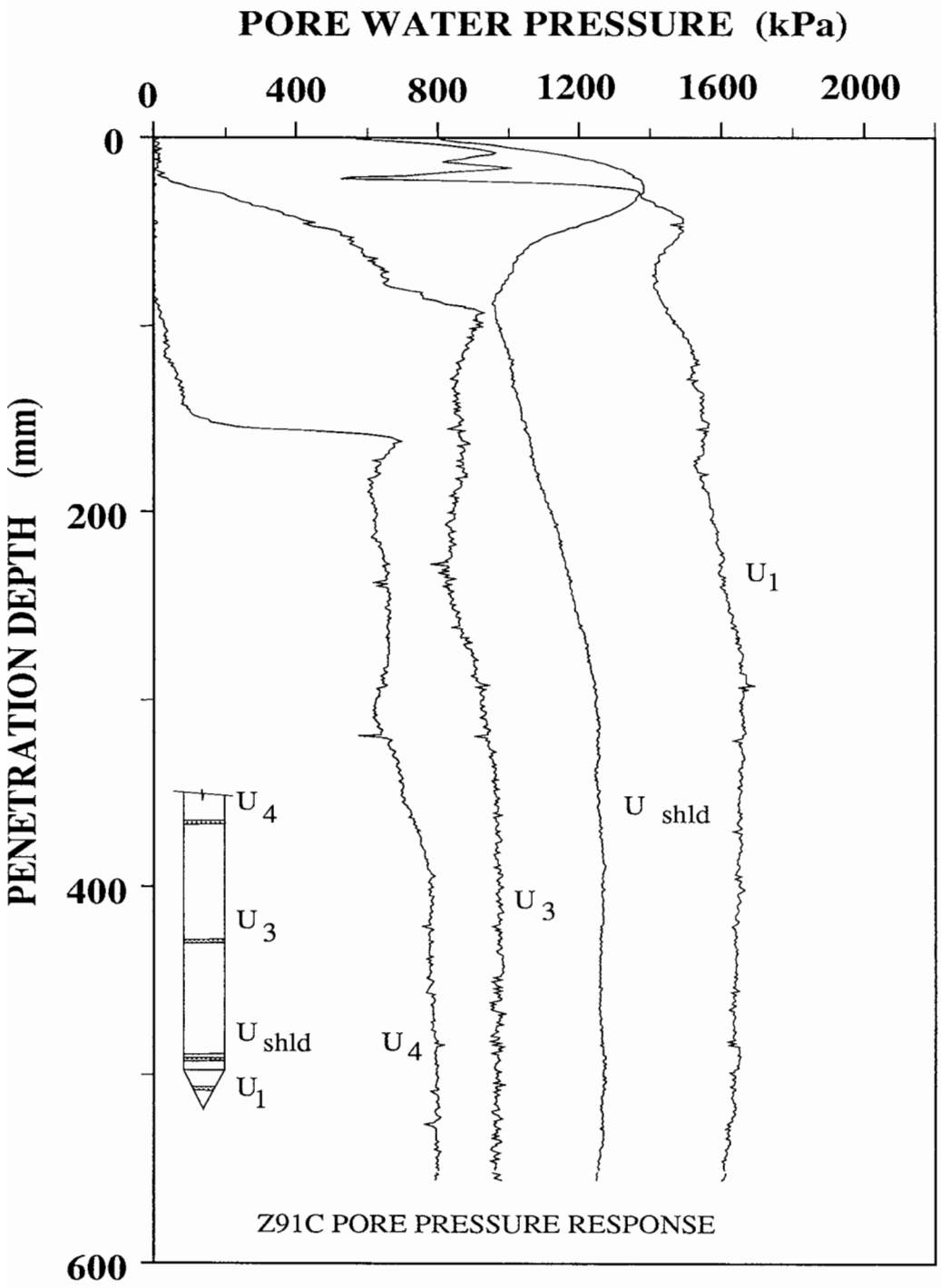

Figure 6.24 Pore water pressure during penetration in test Z91C.

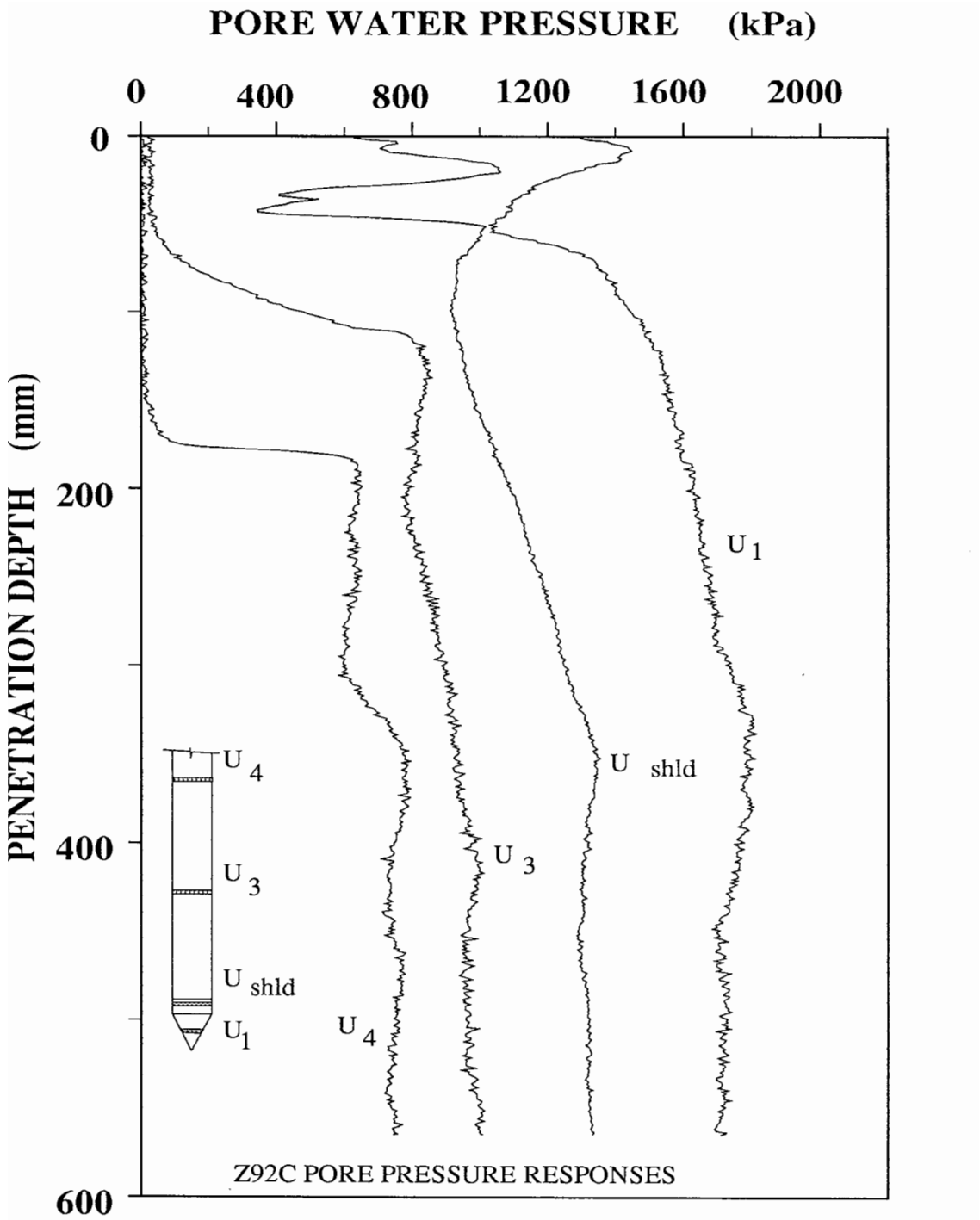

Figure 6.25 Pore water pressure during penetration in test Z92C.

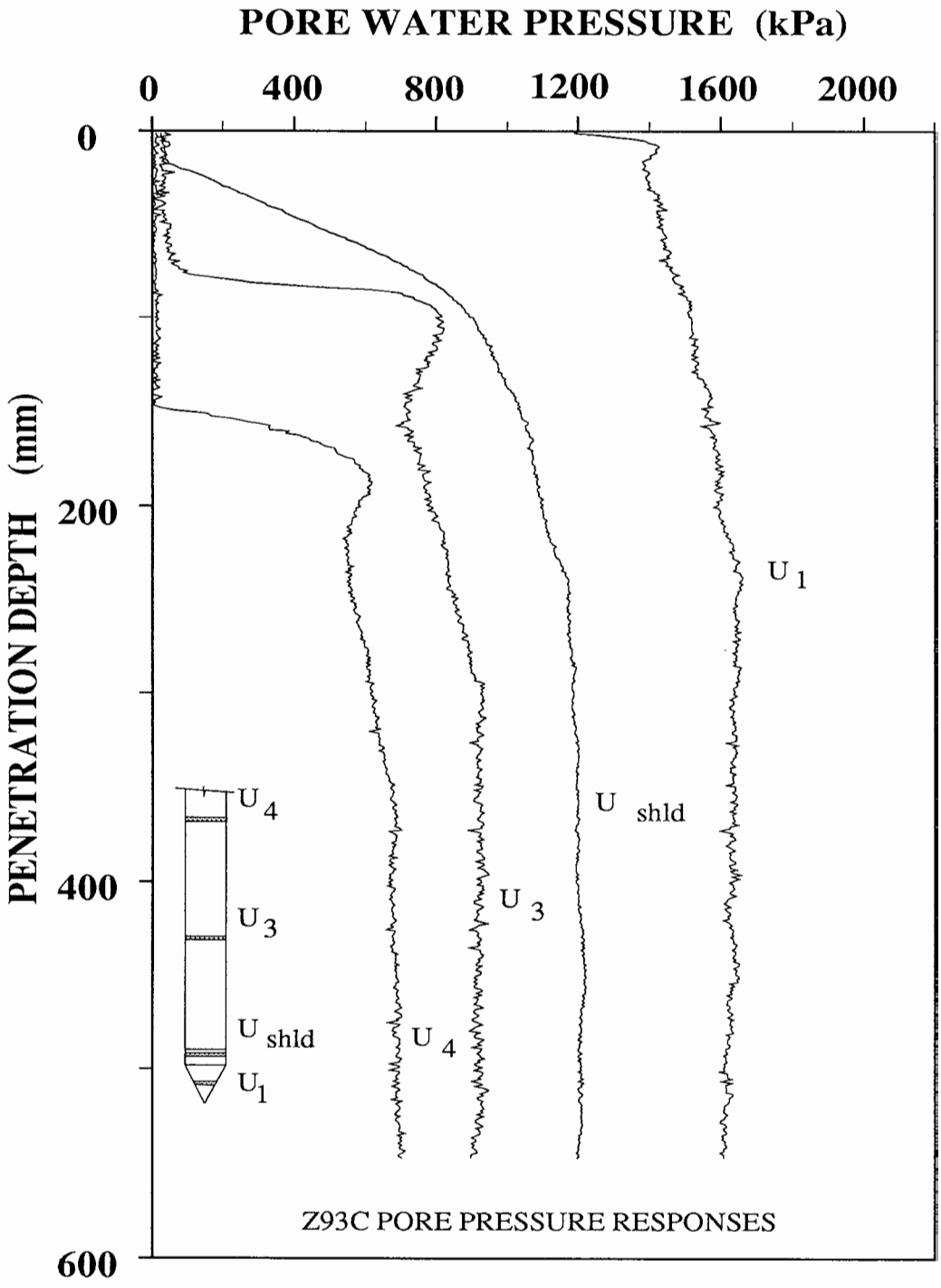

Figure 6.26 Pore water pressure during penetration in test Z93C.

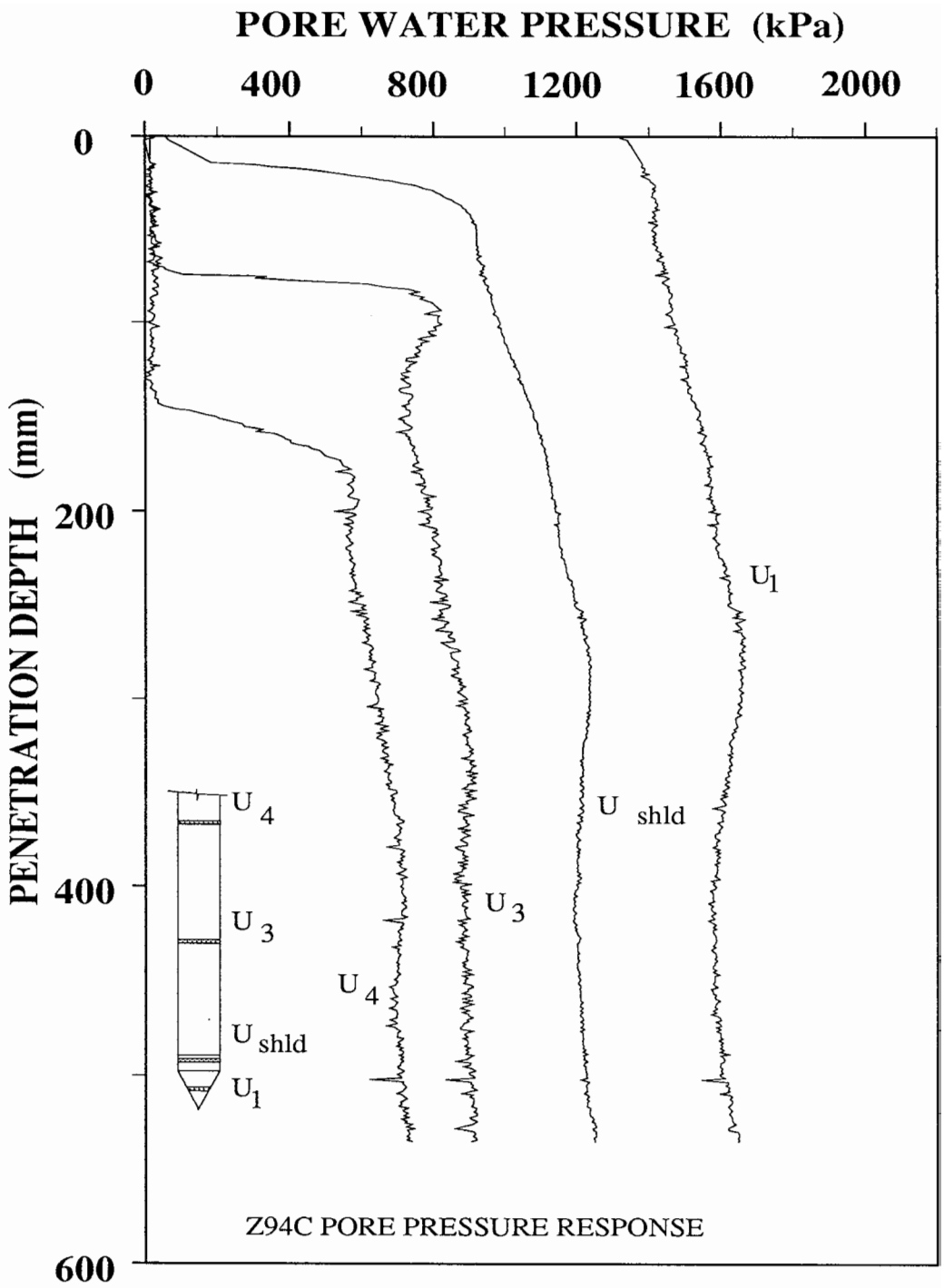

Figure 6.27 Pore water pressure during penetration in test Z94C.

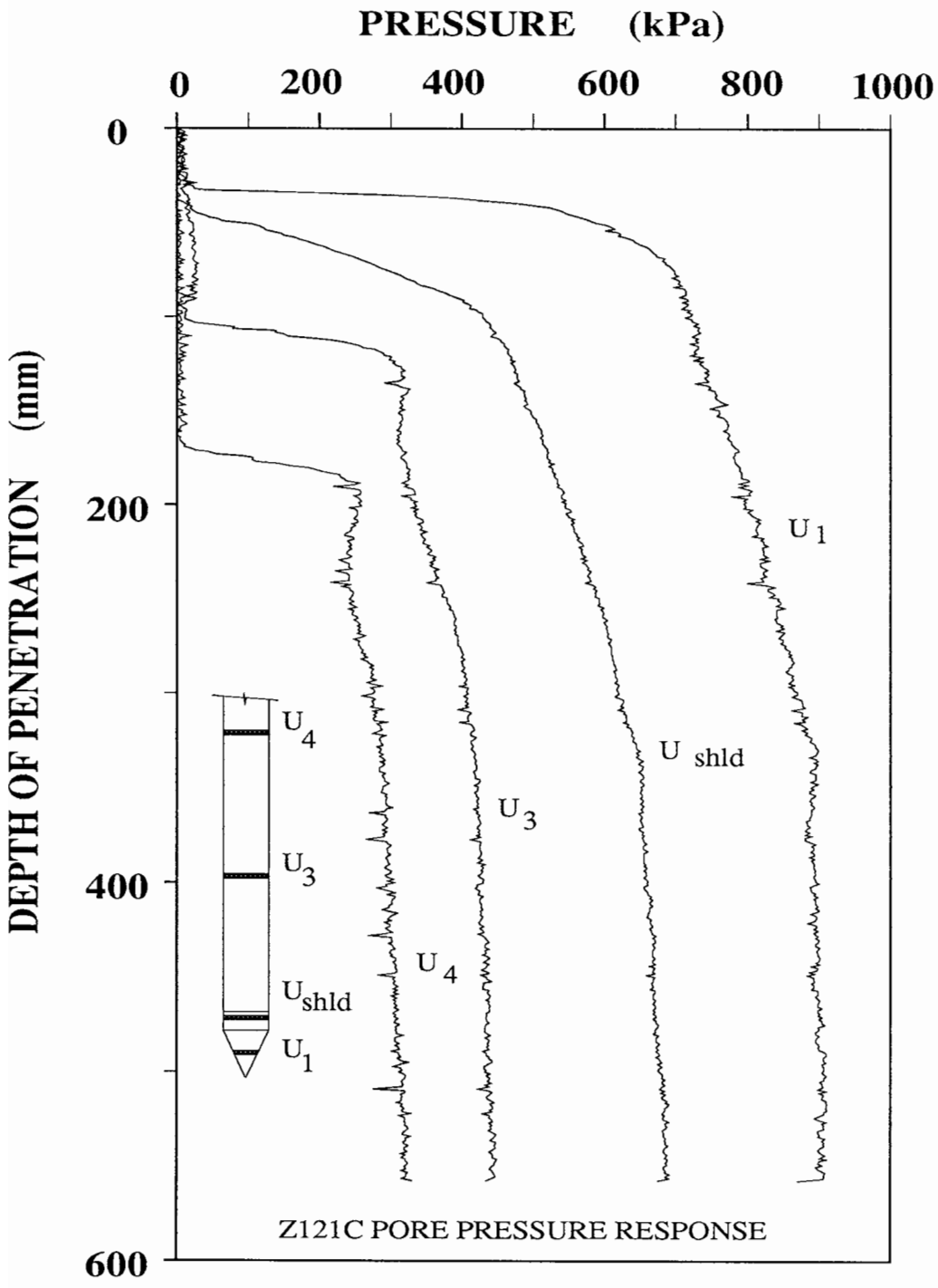

Figure 6.28 Pore water pressure during penetration in test Z121C.

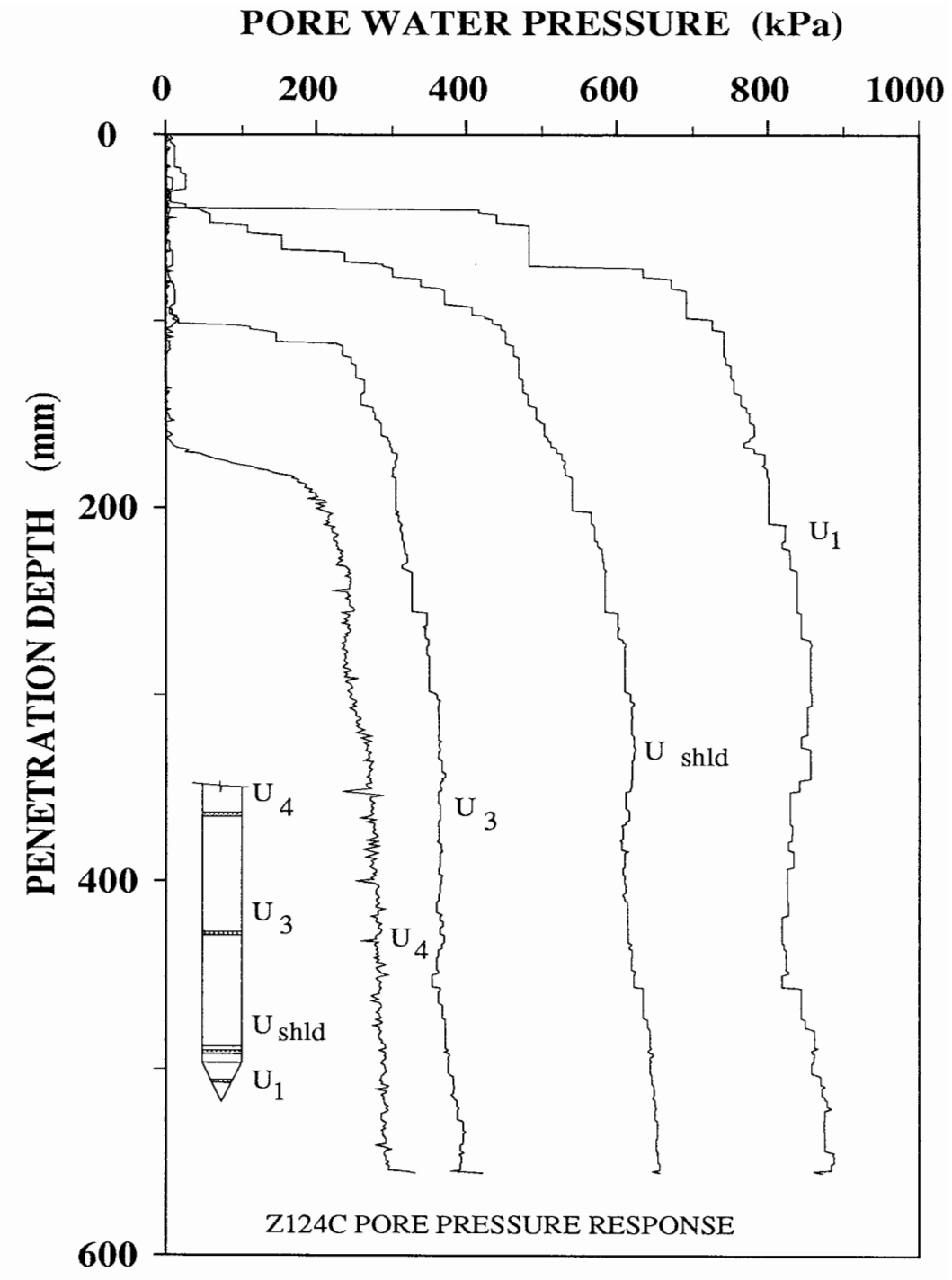

Figure 6.29 Pore water pressure during penetration in test Z124C.

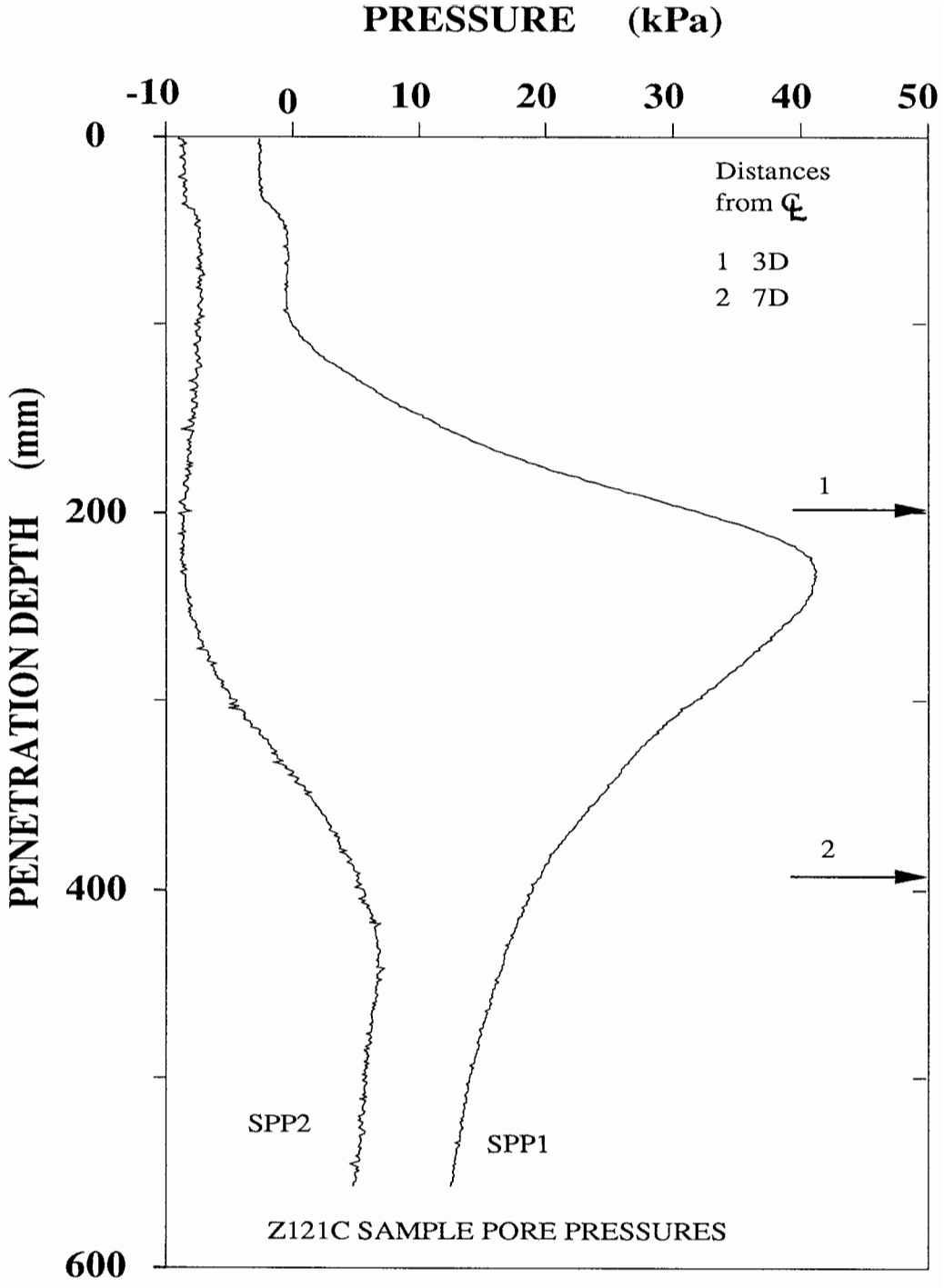

Figure 6.30 Excess pore pressures in the soil sample during penetration test Z121C.

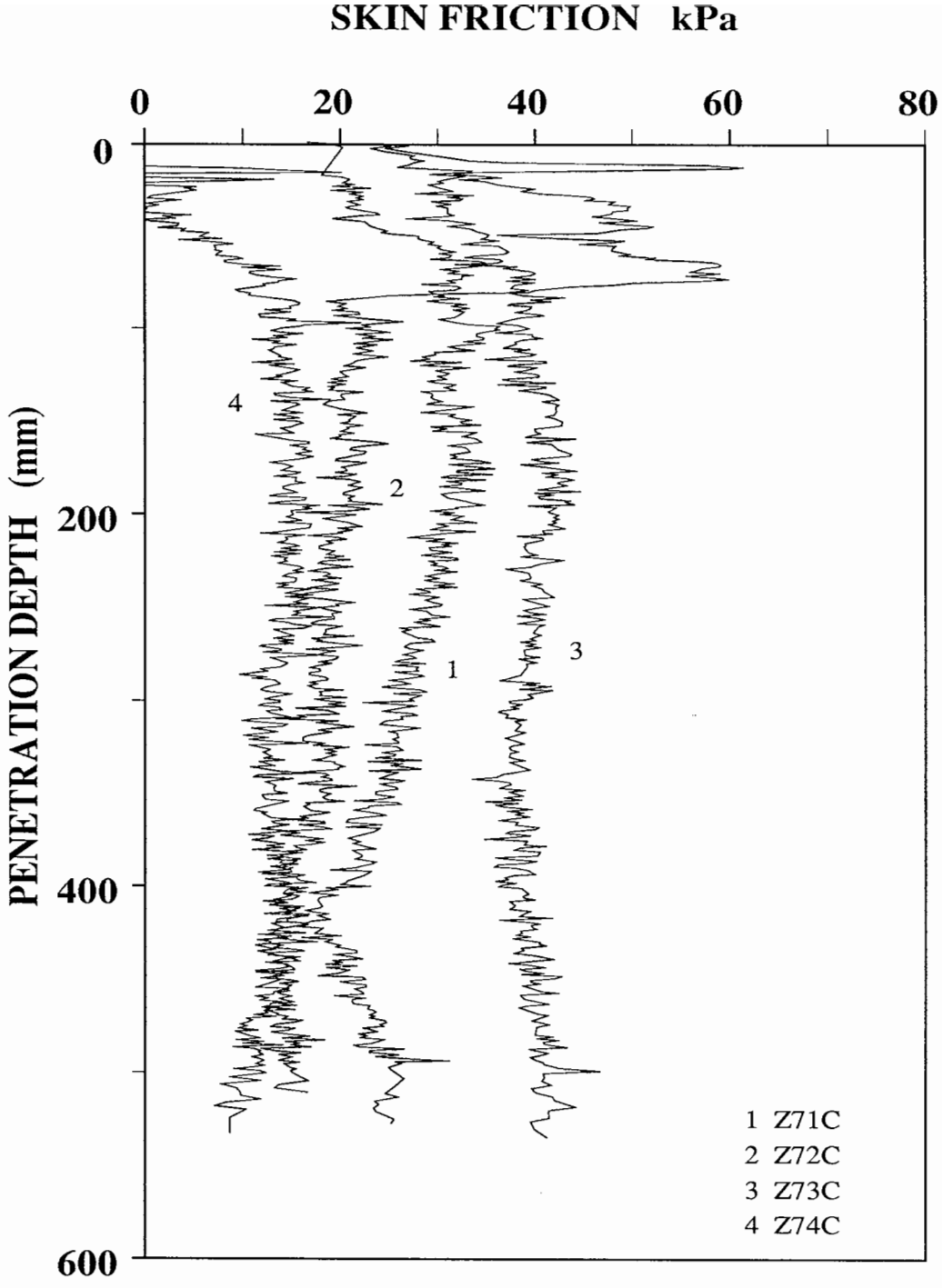

Figure 6.31 Skin friction response during test series Z7C.

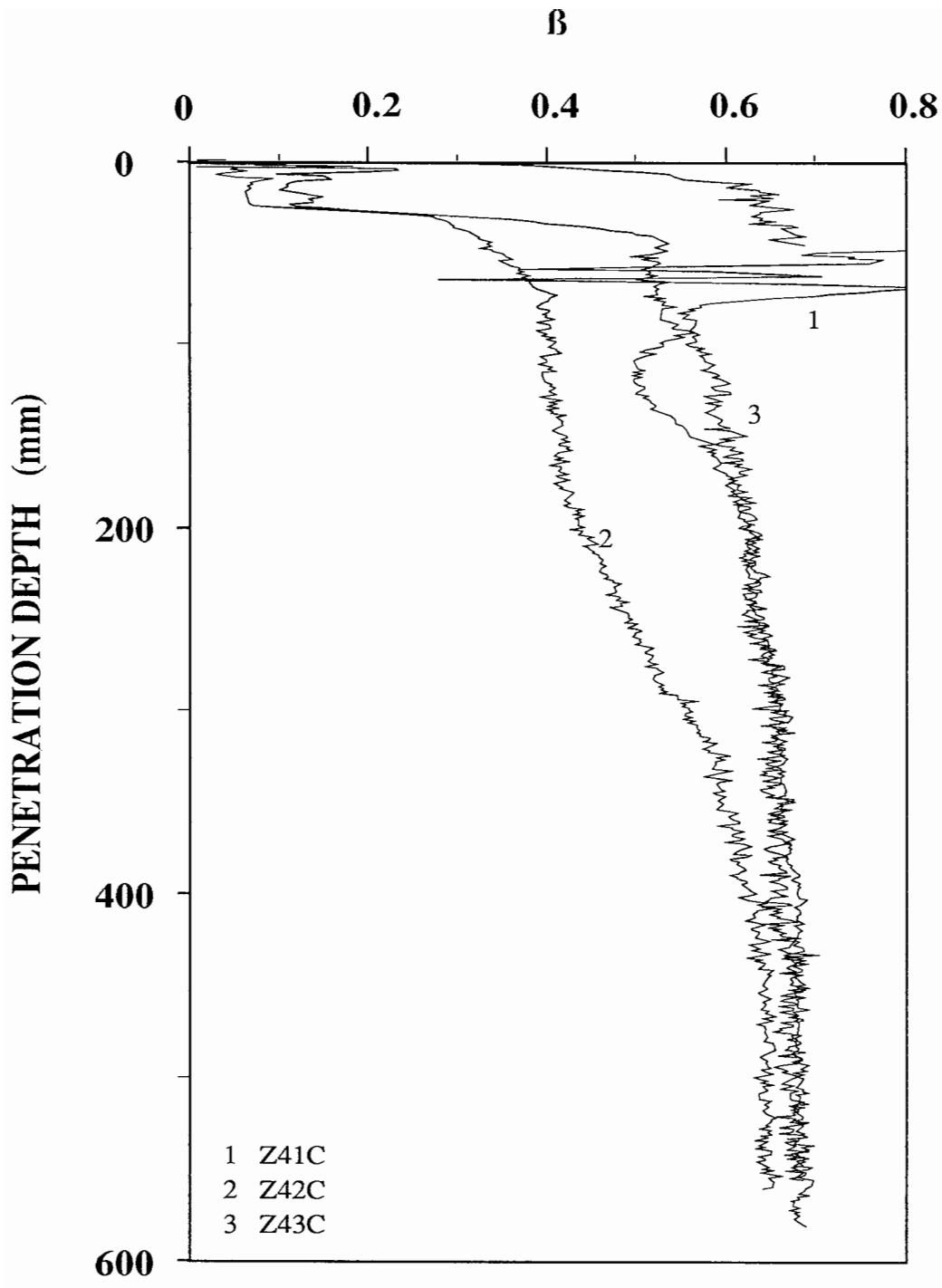

Figure 6.32 β with penetration depth during test series Z4C.

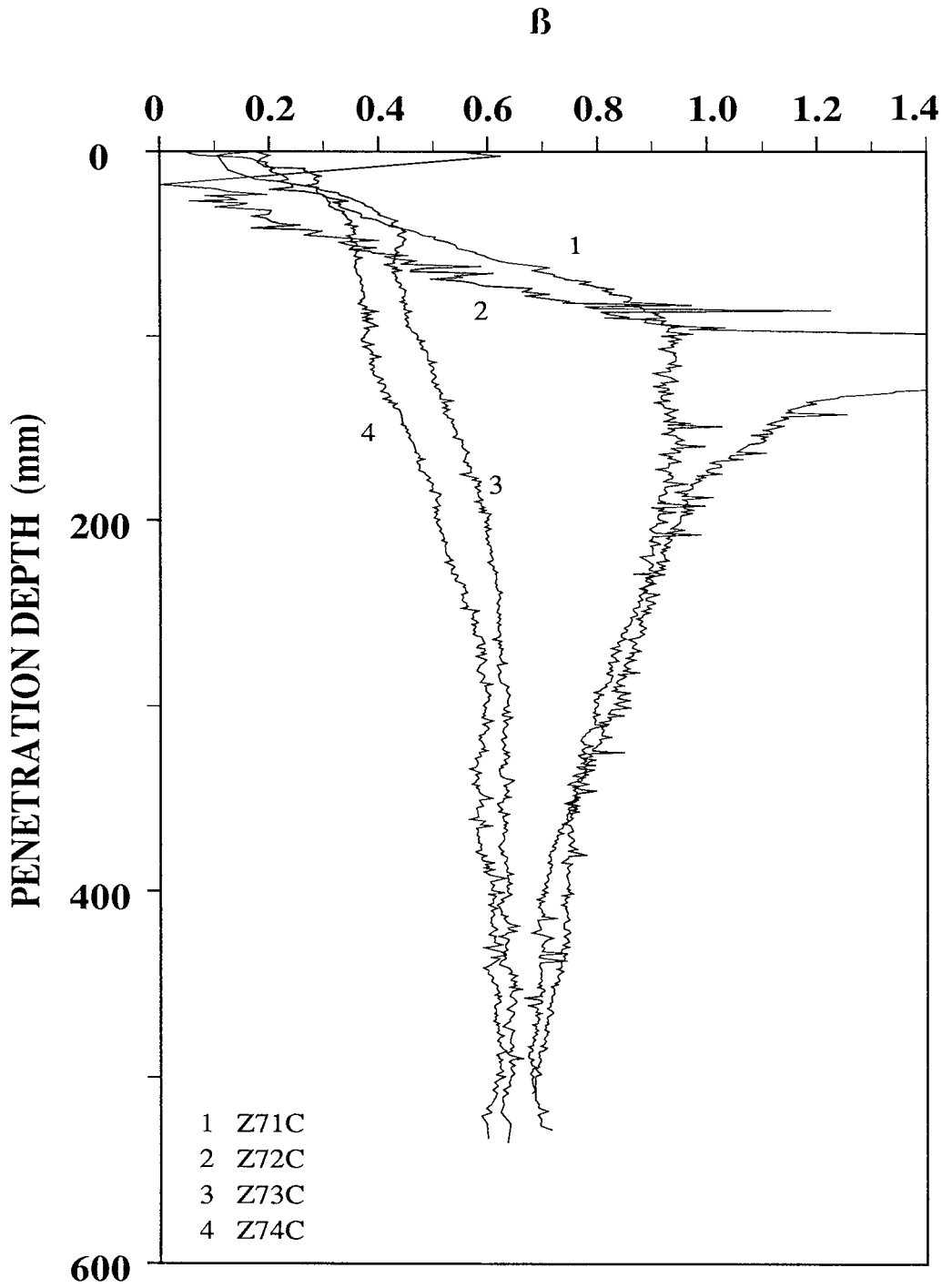

Figure 6.33 β with penetration depth during test series Z7C.

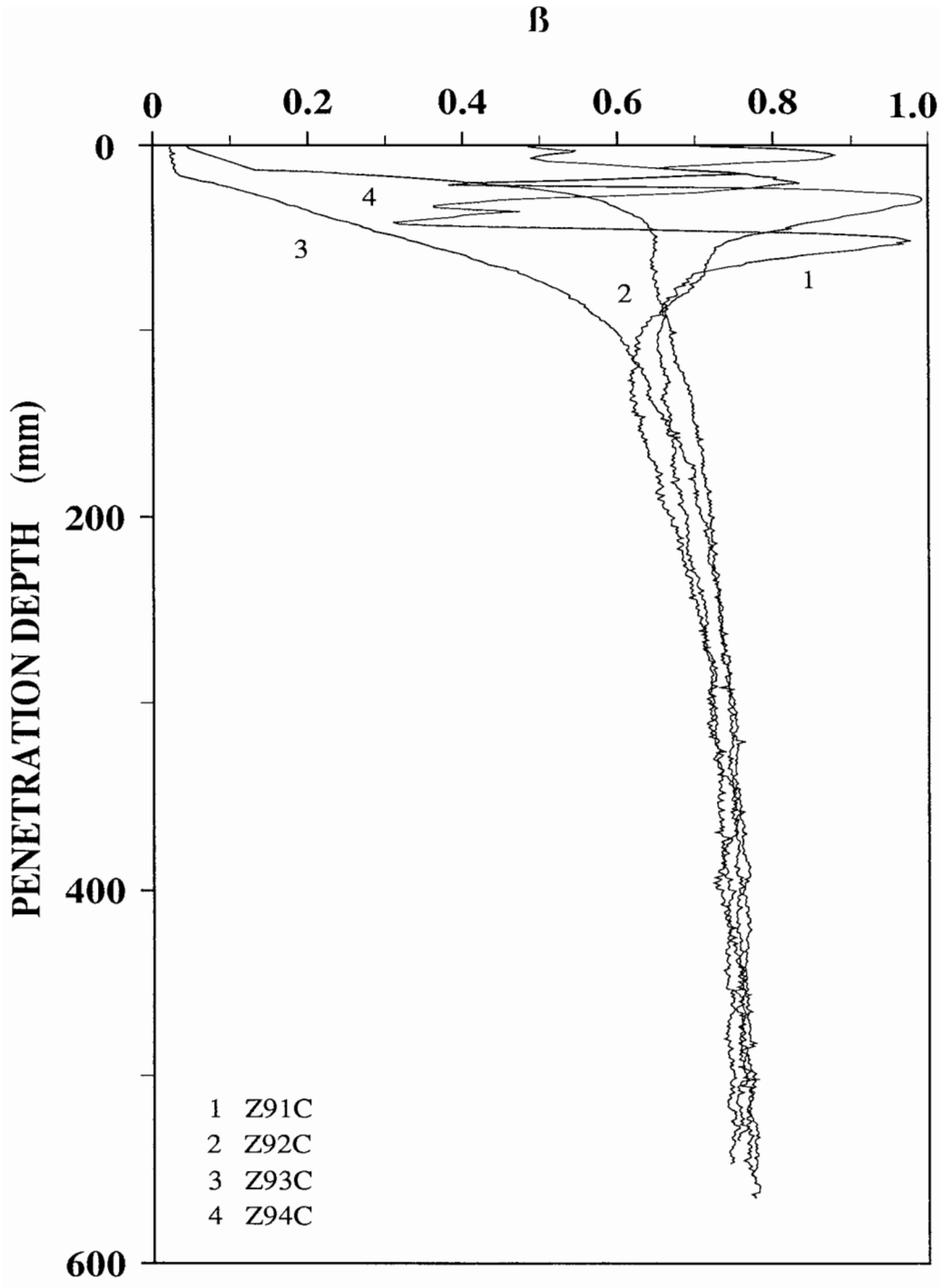

Figure 6.34 β with penetration depth during test series Z9C.

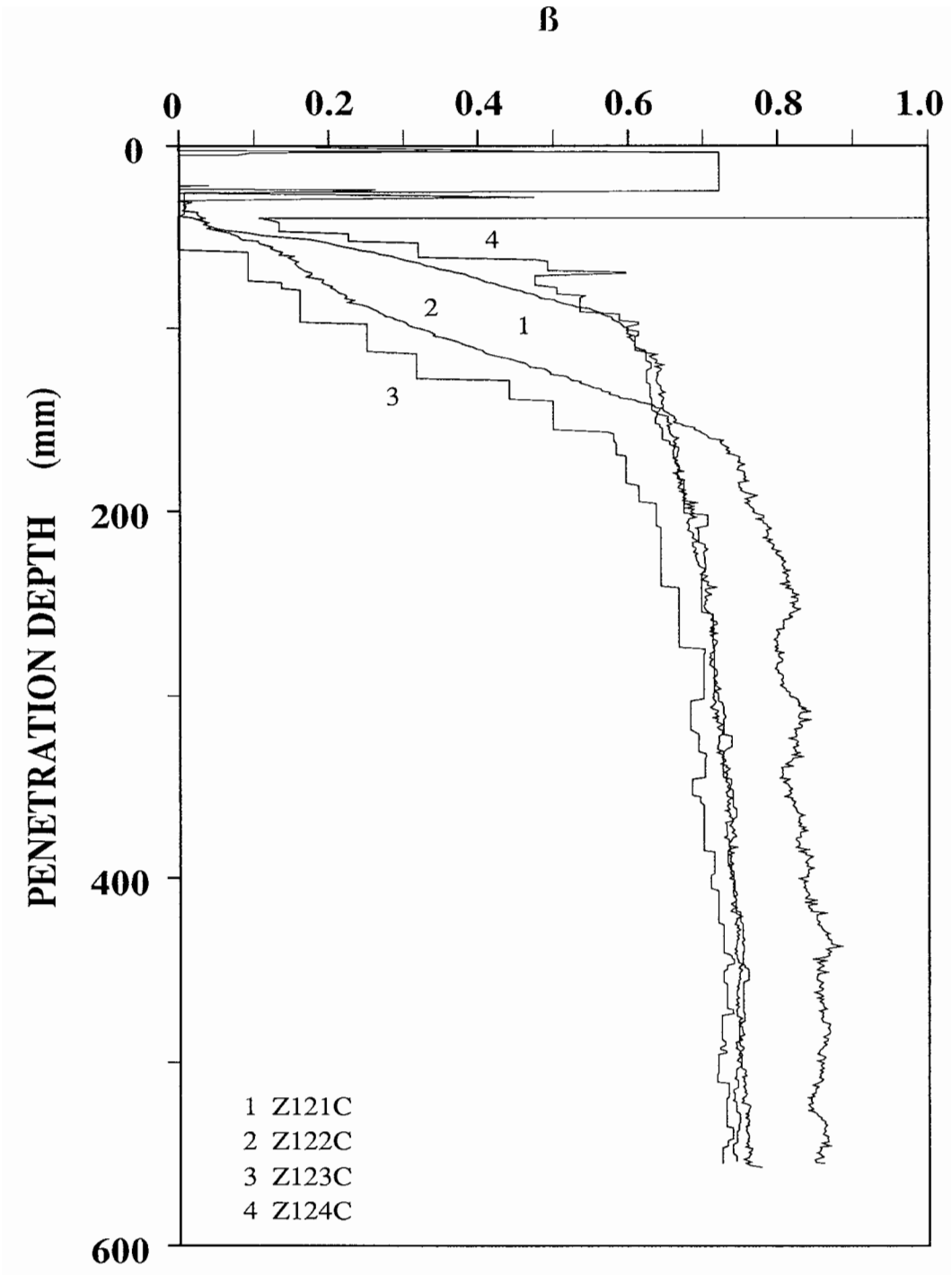

Figure 6.35 β with penetration depth during test series Z12C.

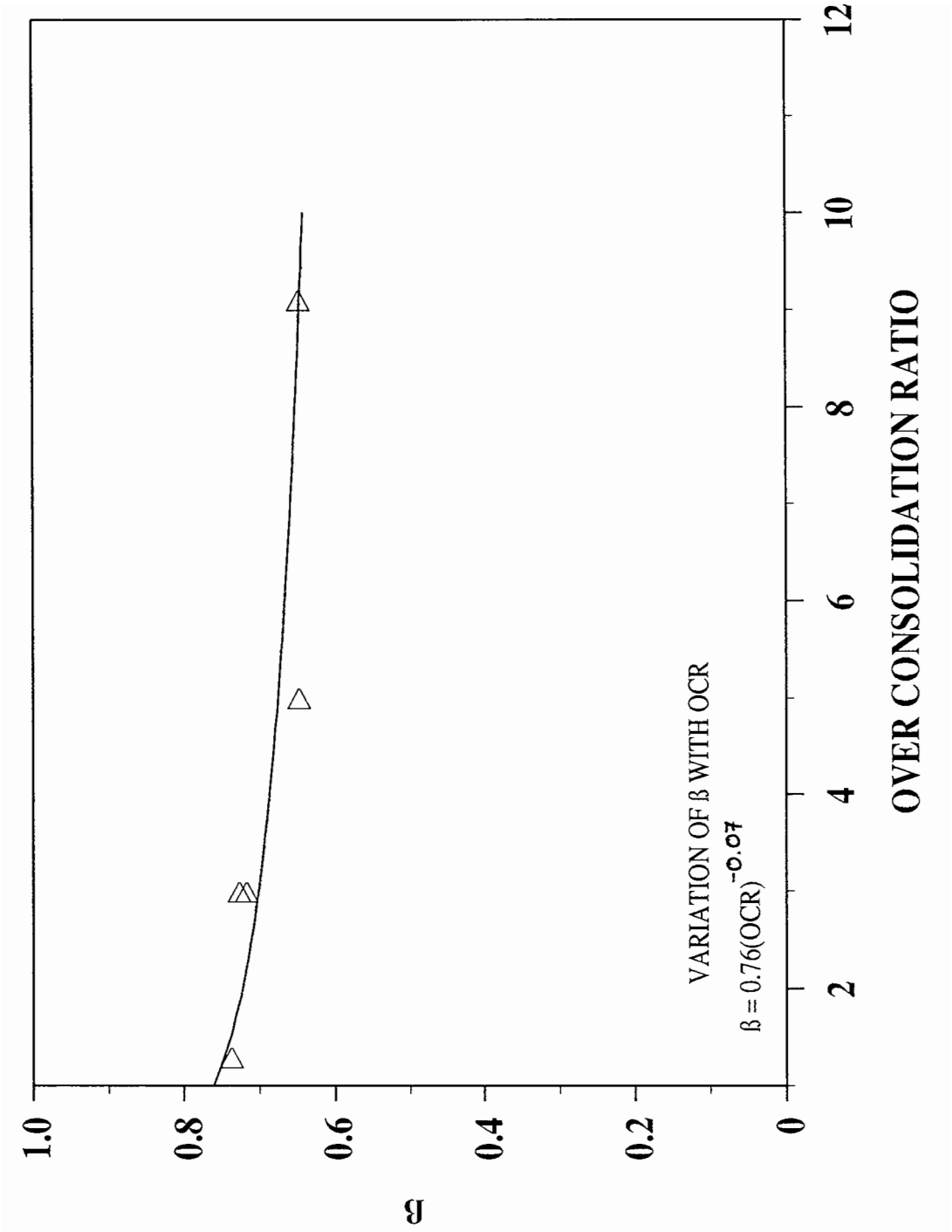

Figure 6.36 Variation of β with overconsolidation ratio for test series Z9C, Z12C, Z4C and Z7C in order of increasing OCR.

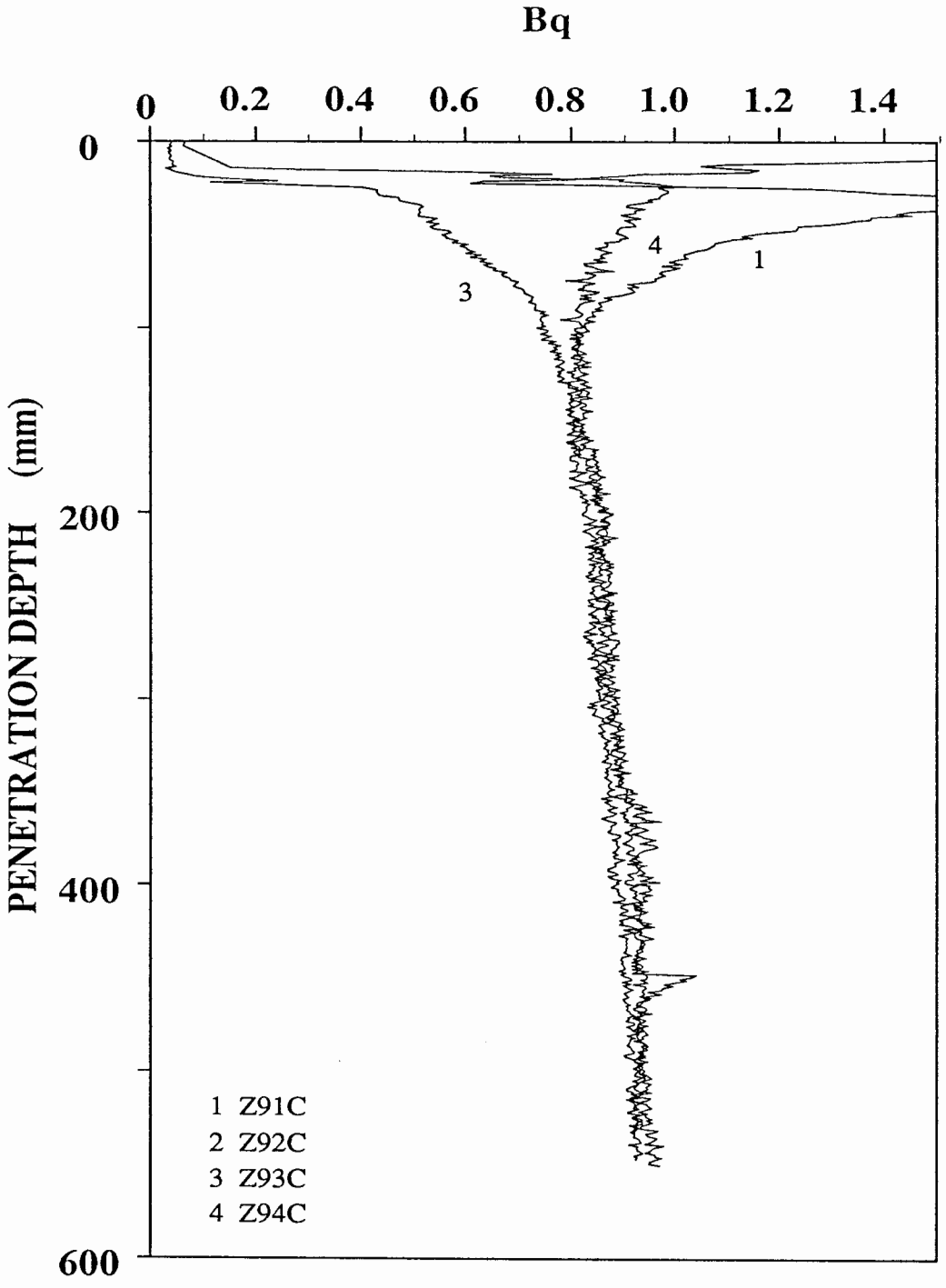

Figure 6.37 Pore pressure factor B_q with penetration depth during test series Z9C.

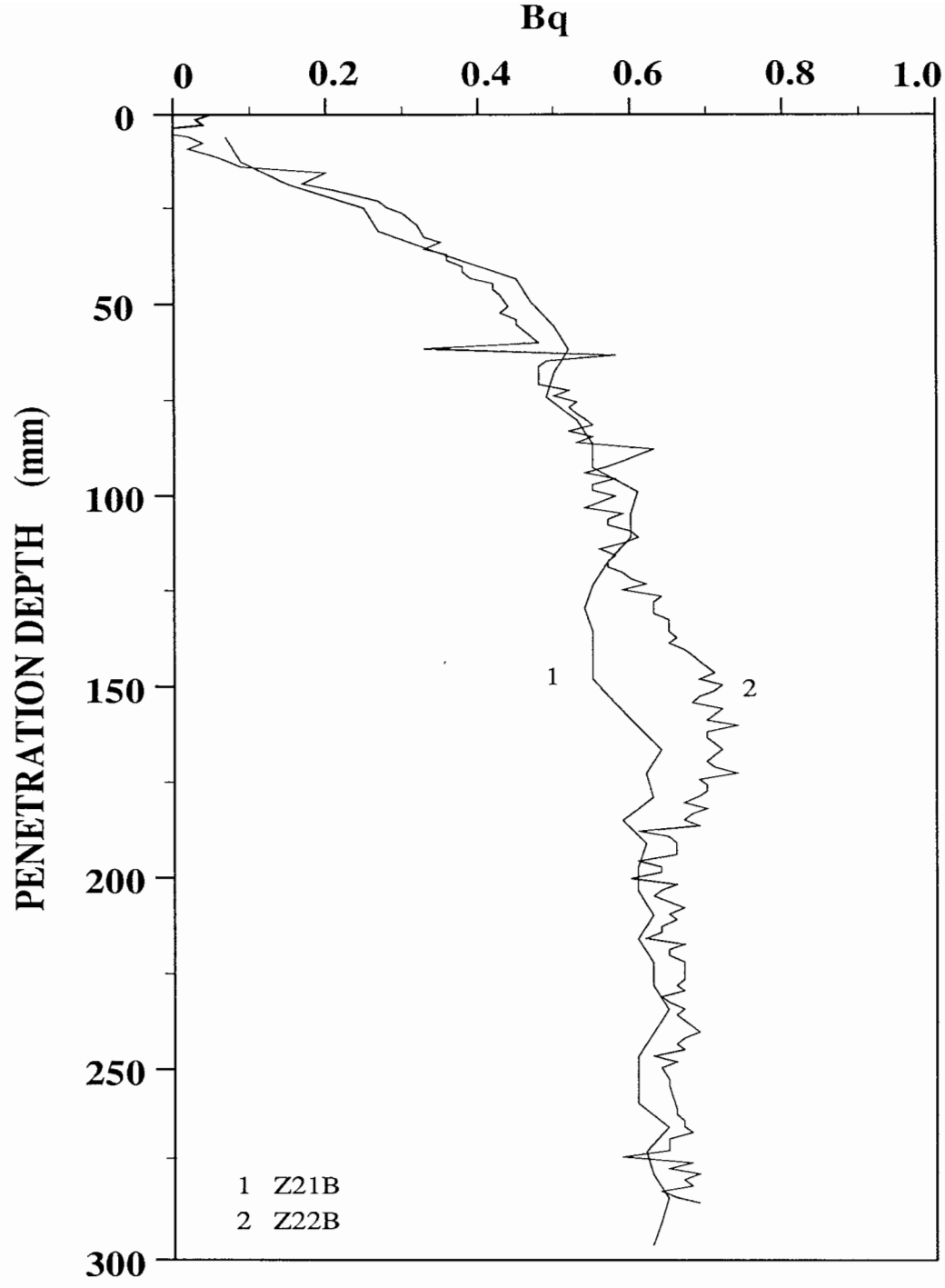

Figure 6.38 Pore pressure factor B_q with penetration depth during test series Z2B.

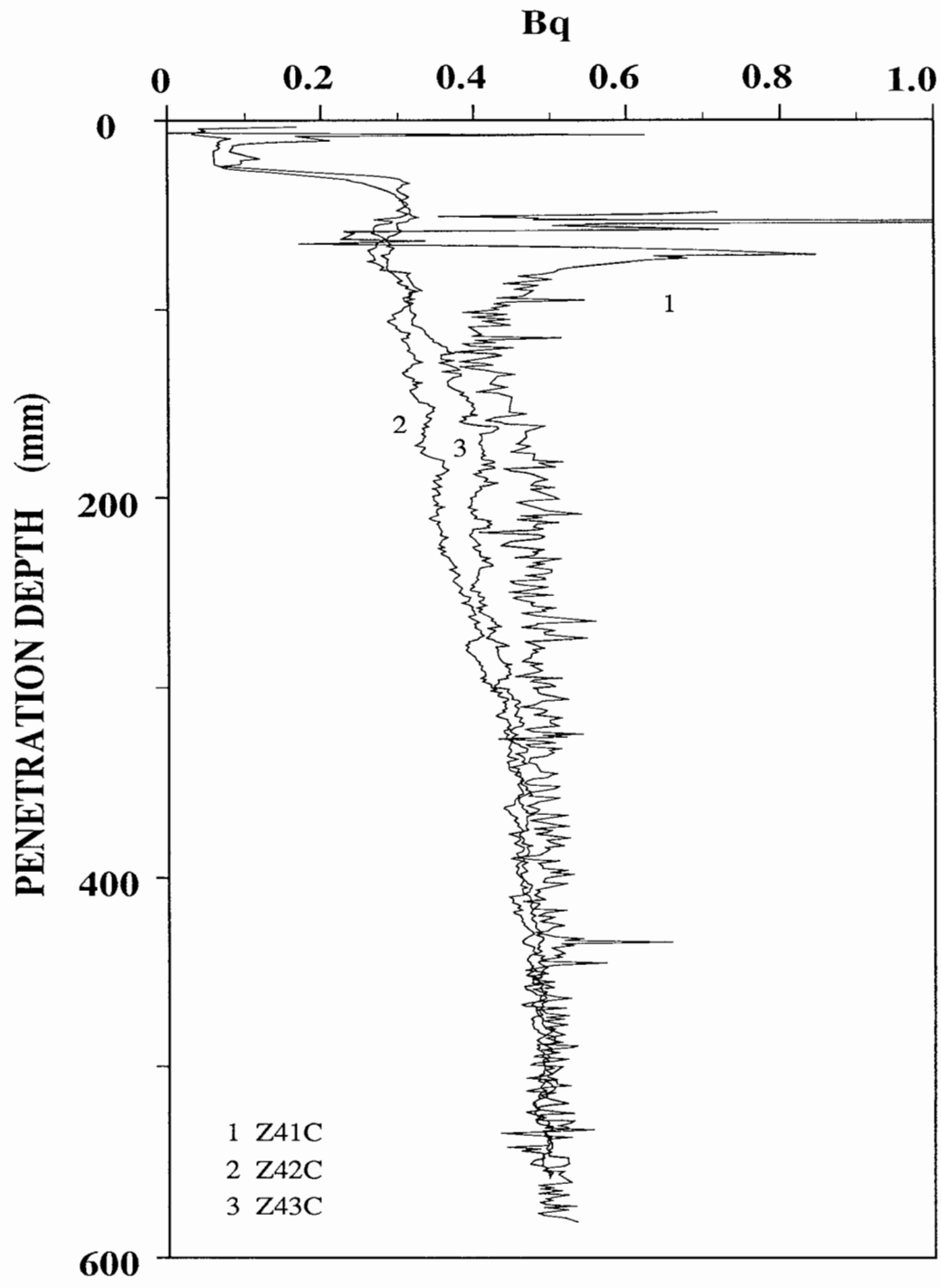

Figure 6.39 Pore pressure factor B_q with penetration depth during test series Z4C.

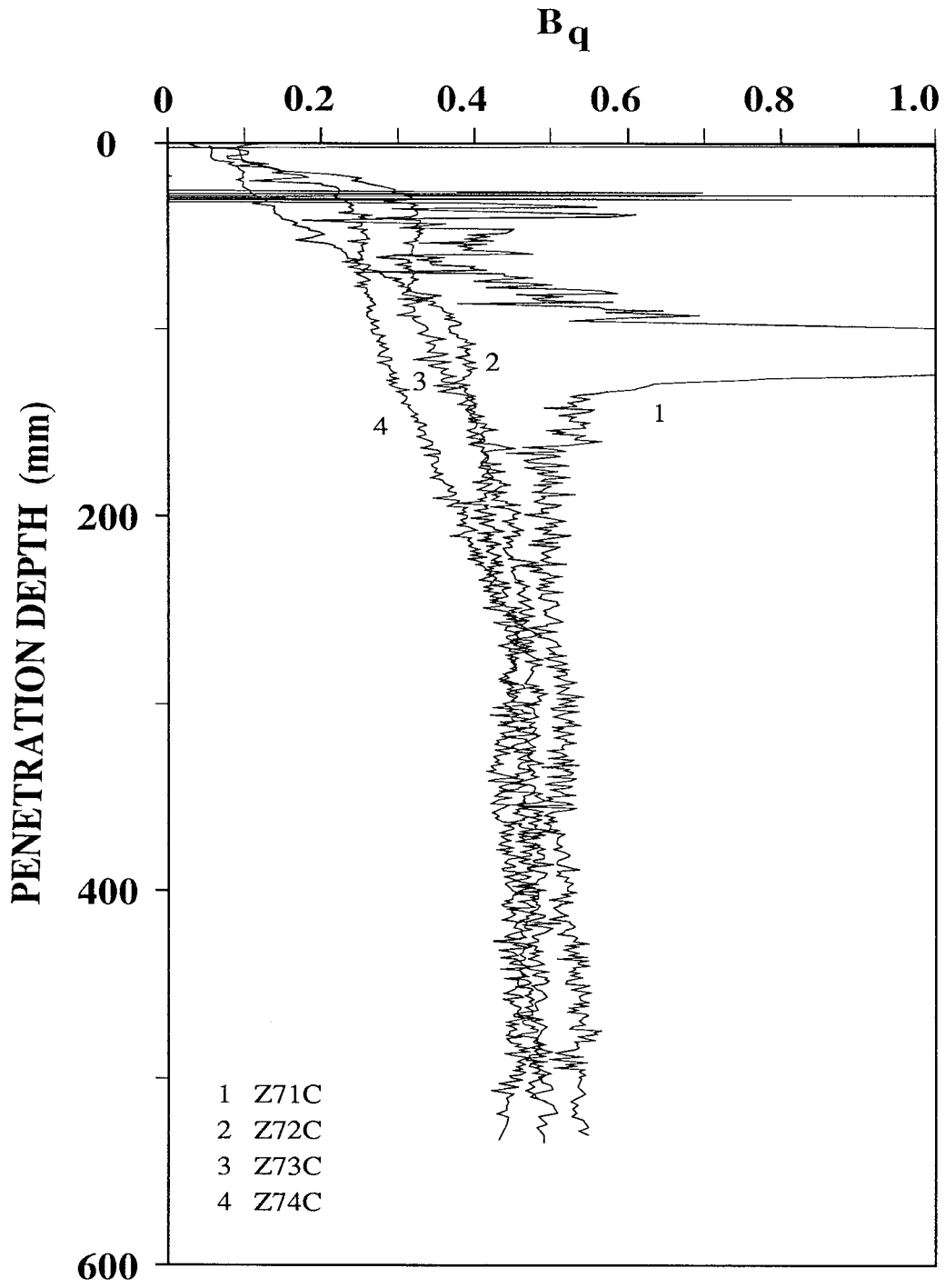

Figure 6.40 Pore pressure factor B_q with penetration depth during test series Z7C.

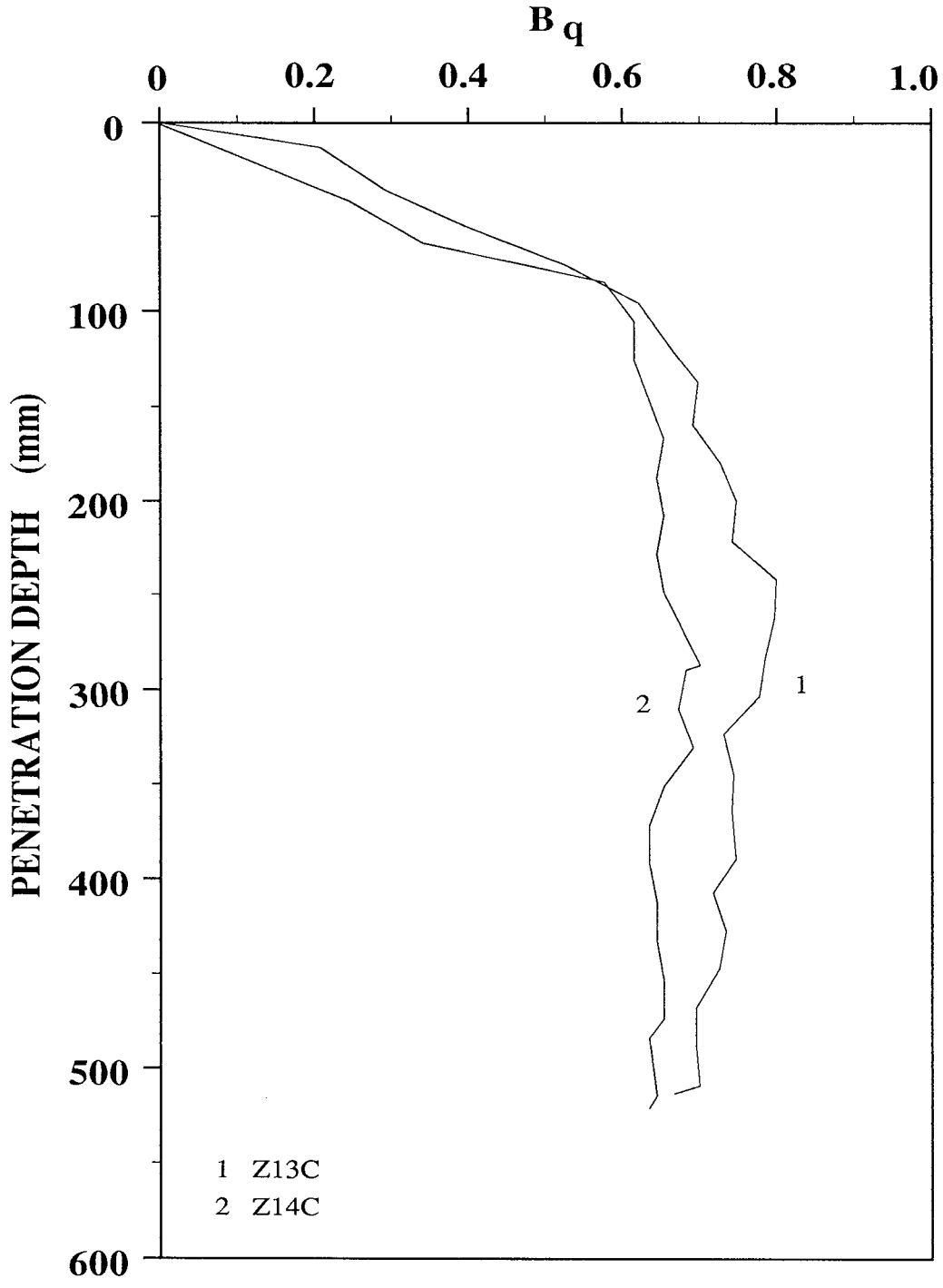

Figure 6.41 Pore pressure factor B_q with penetration depth during test series Z1C.

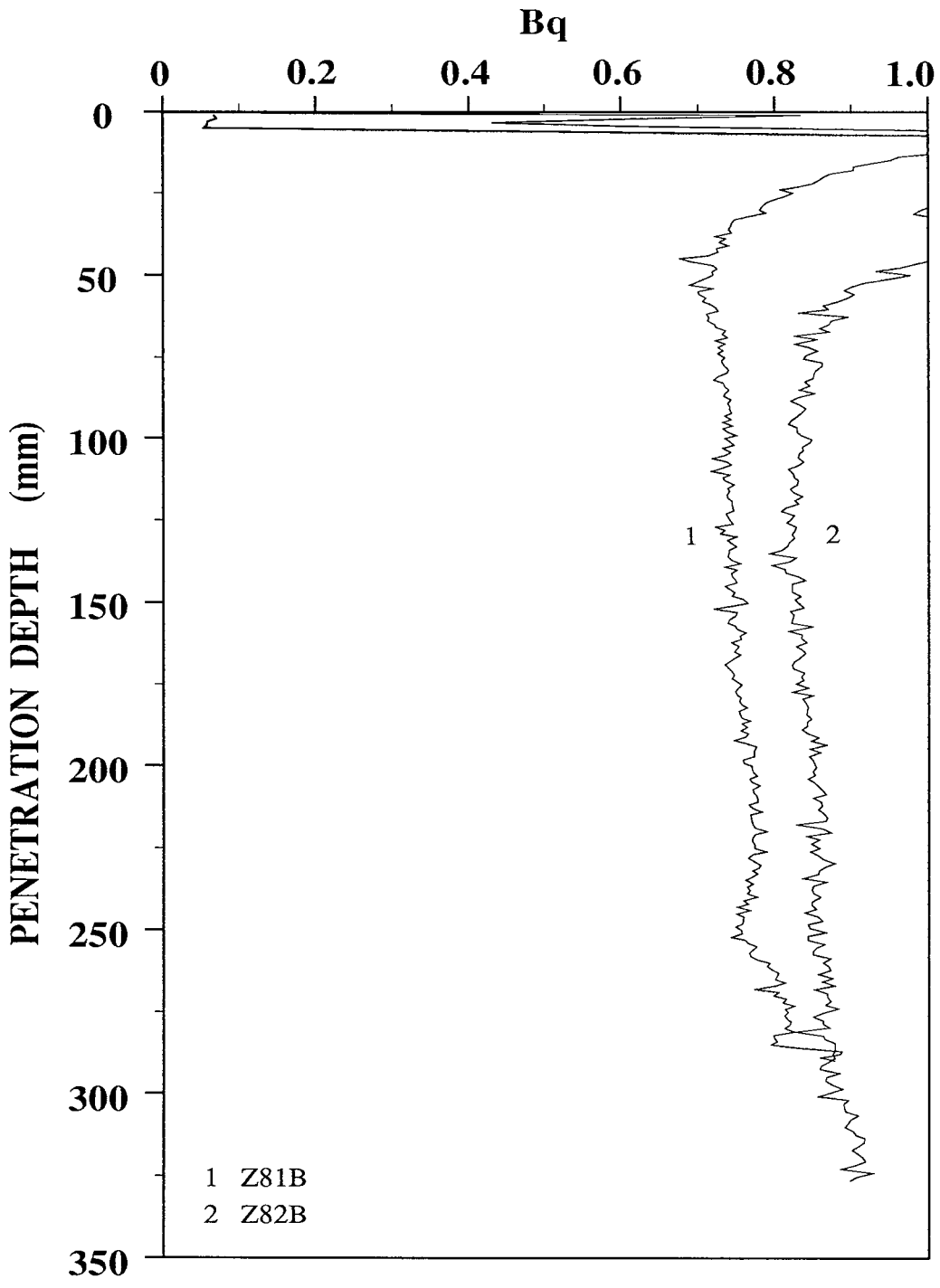

Figure 6.42 Pore pressure factor B_q with penetration depth during test series Z8B.

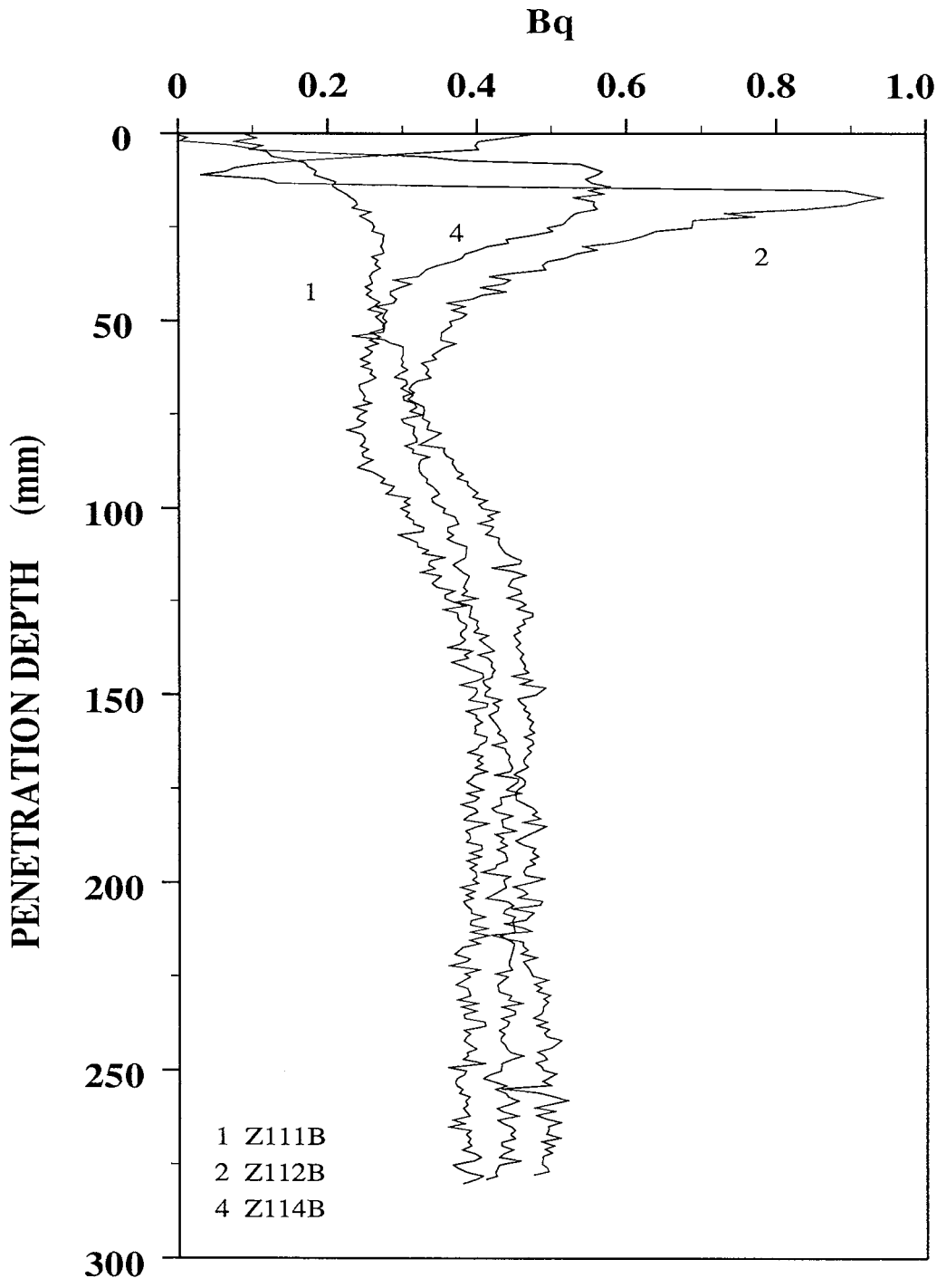

Figure 6.43 Pore pressure factor B_q with penetration depth during test series Z11B.

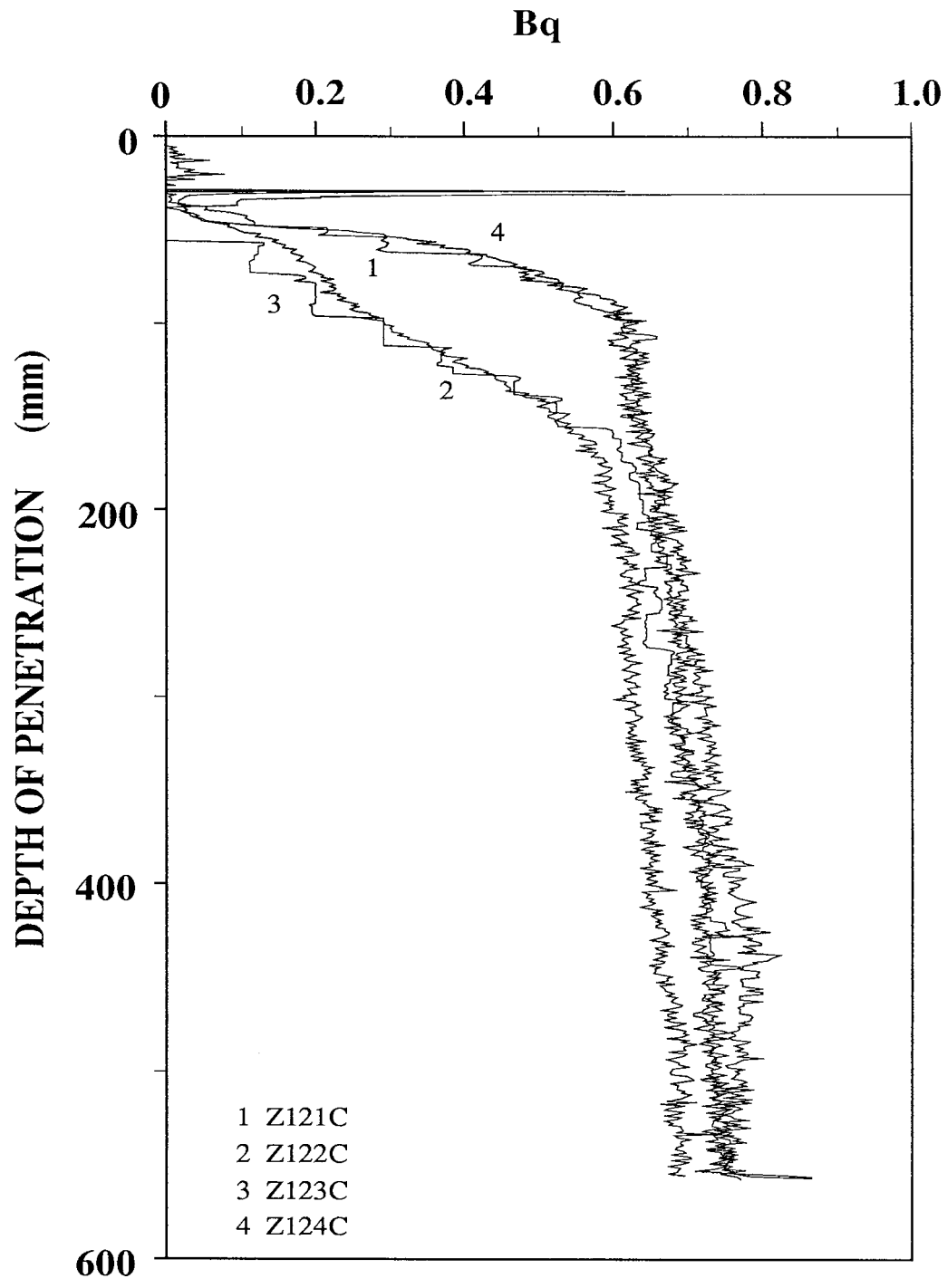

Figure 6.44 Pore pressure factor B_q with penetration depth during test series Z12C.

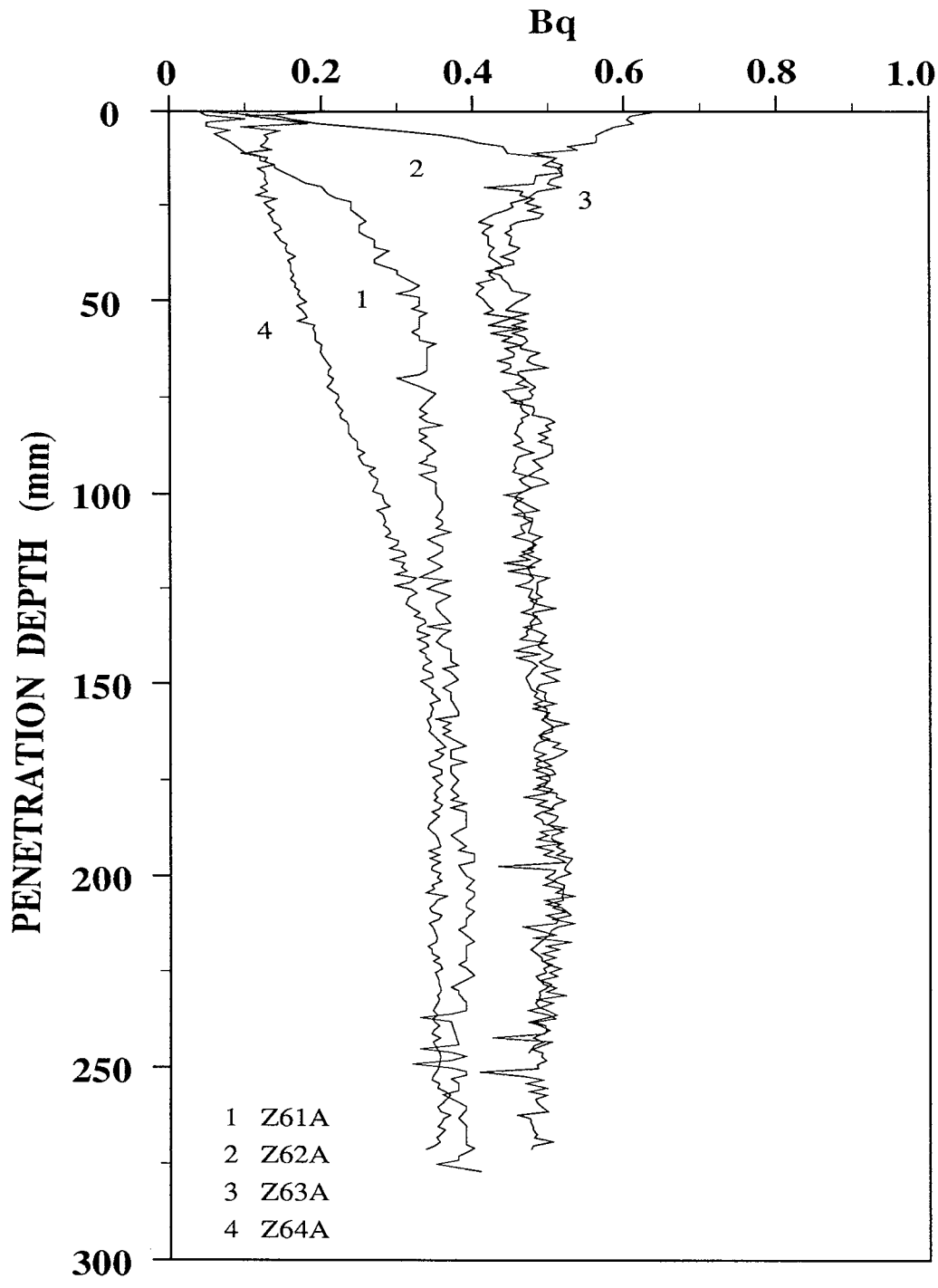

Figure 6.45 Pore pressure factor B_q with penetration depth during test series Z6A.

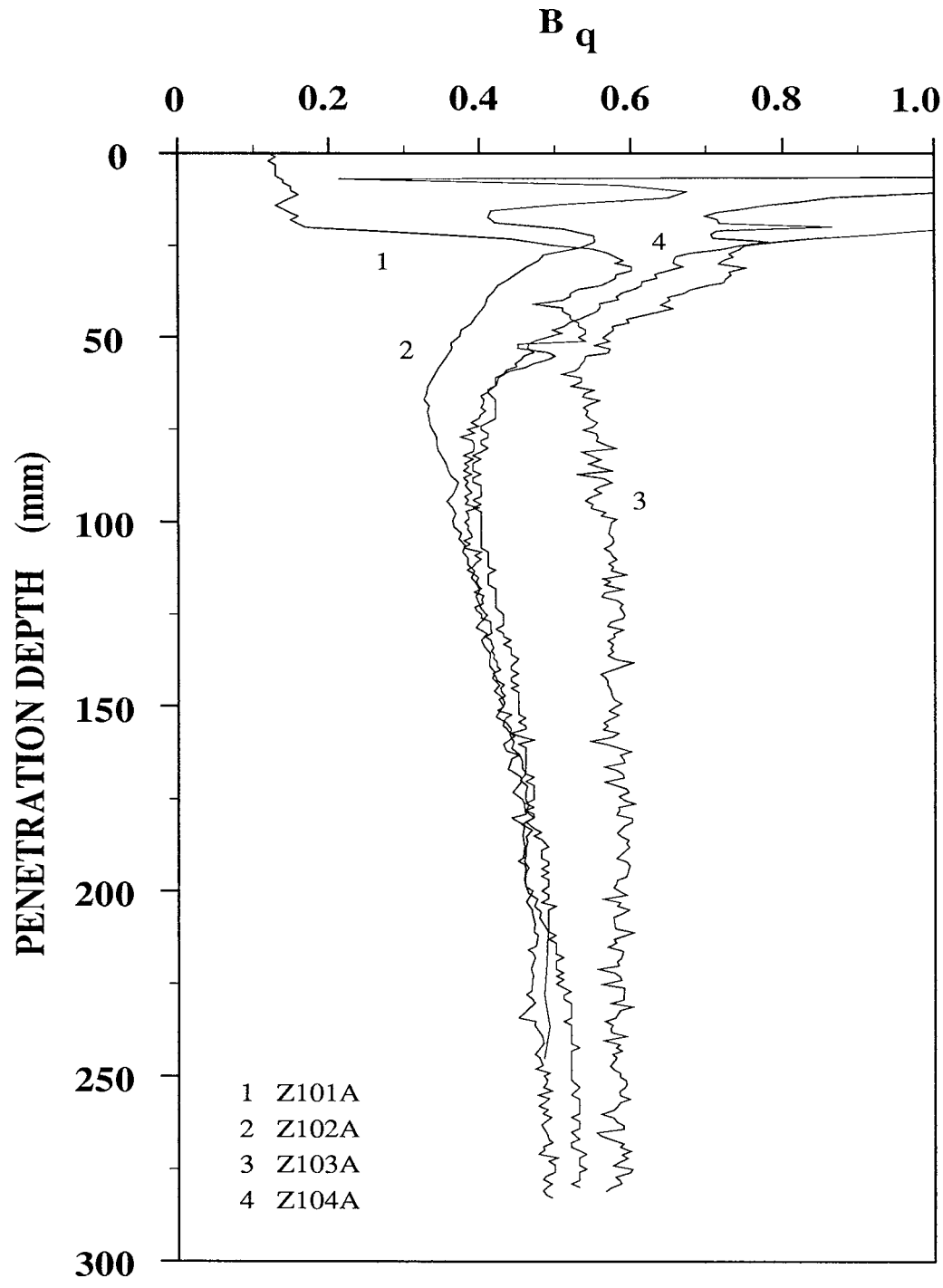

Figure 6.46 Pore pressure factor B_q with penetration depth during test series Z10A.

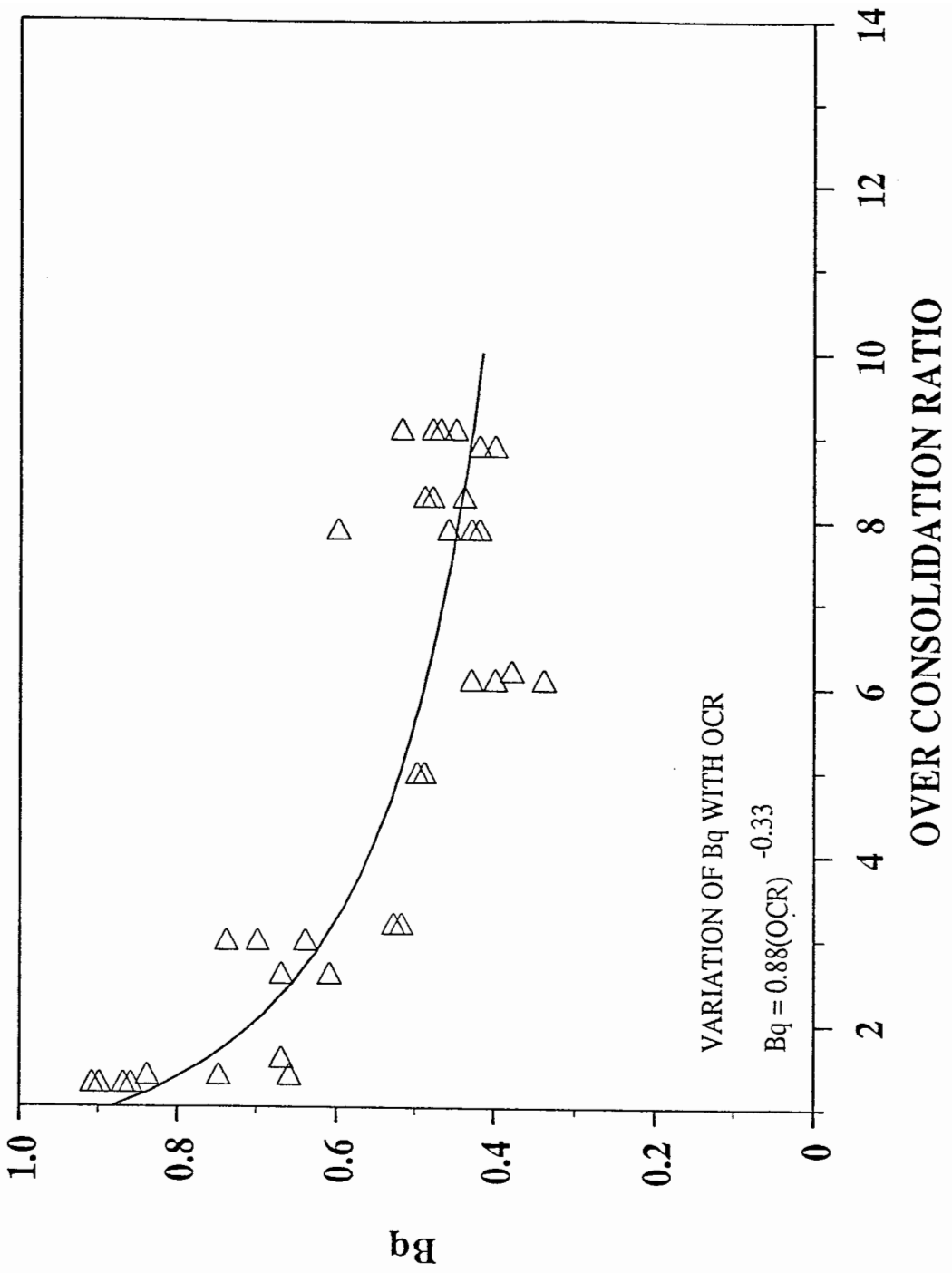

Figure 6.47 Variation of B_q with overconsolidation ratio for all laboratory test series.

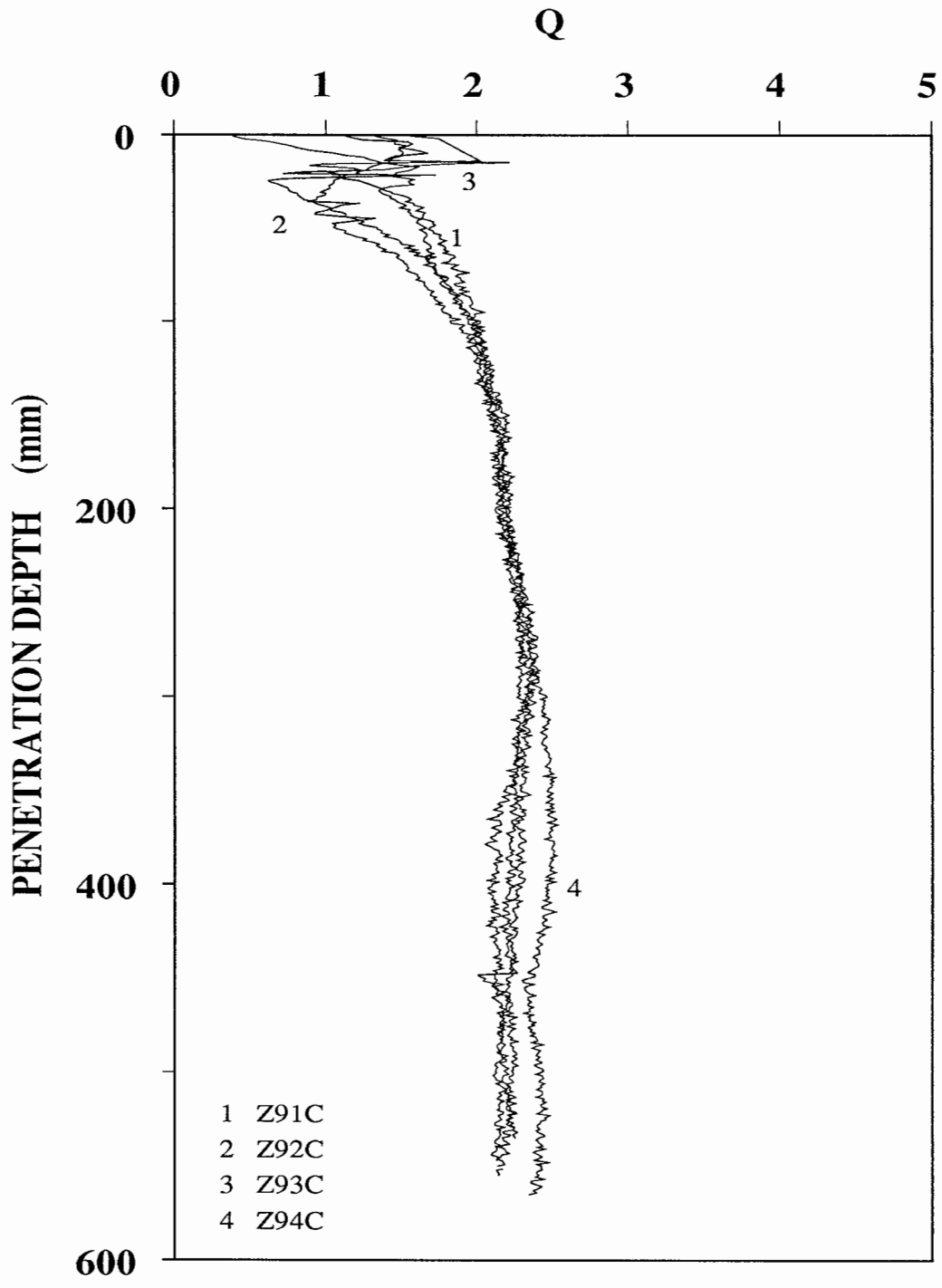

Figure 6.48 Tip resistance factor Q with penetration depth during test series Z9C.

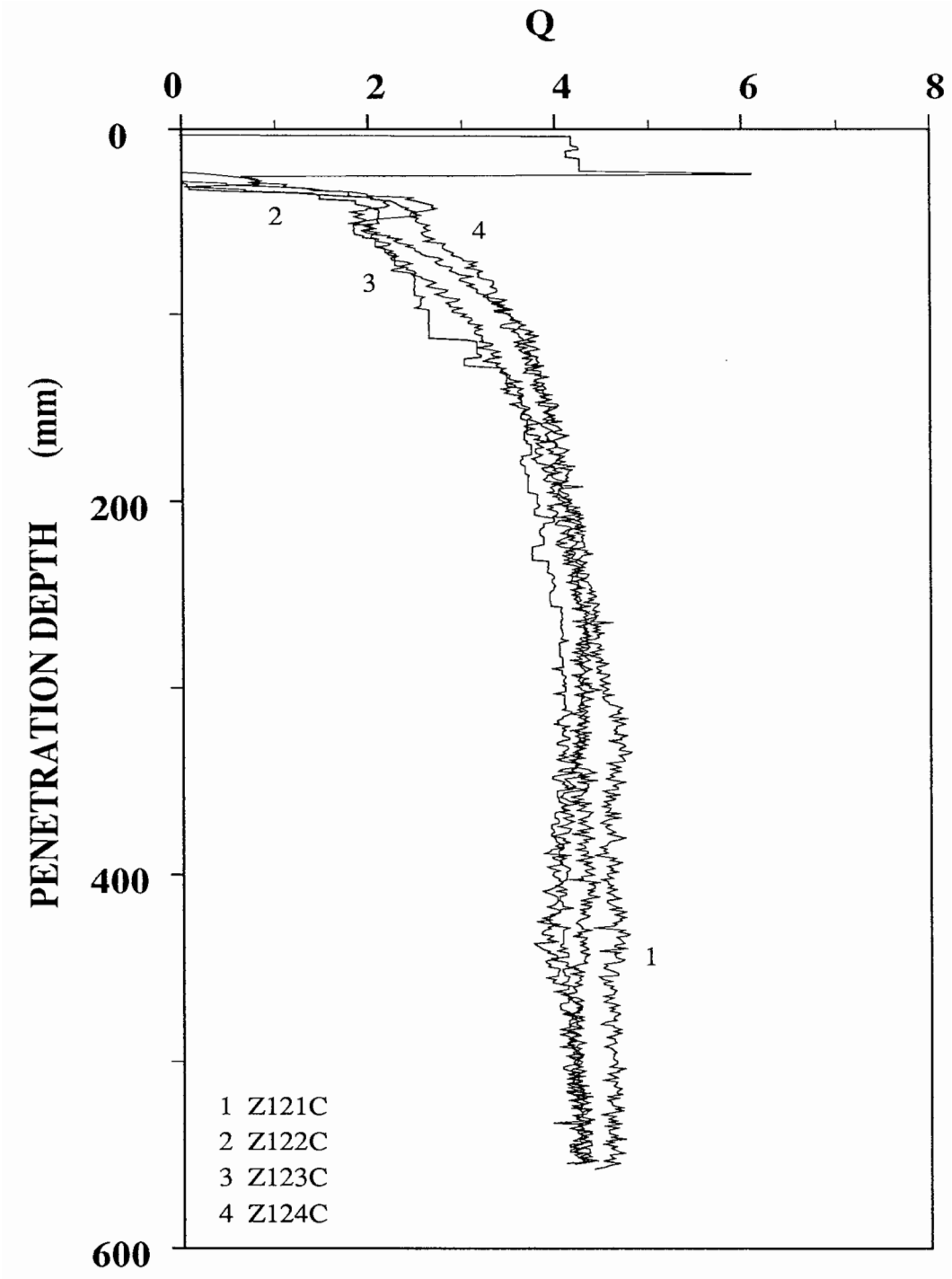

Figure 6.49 Tip resistance factor Q with penetration depth during test series Z12C.

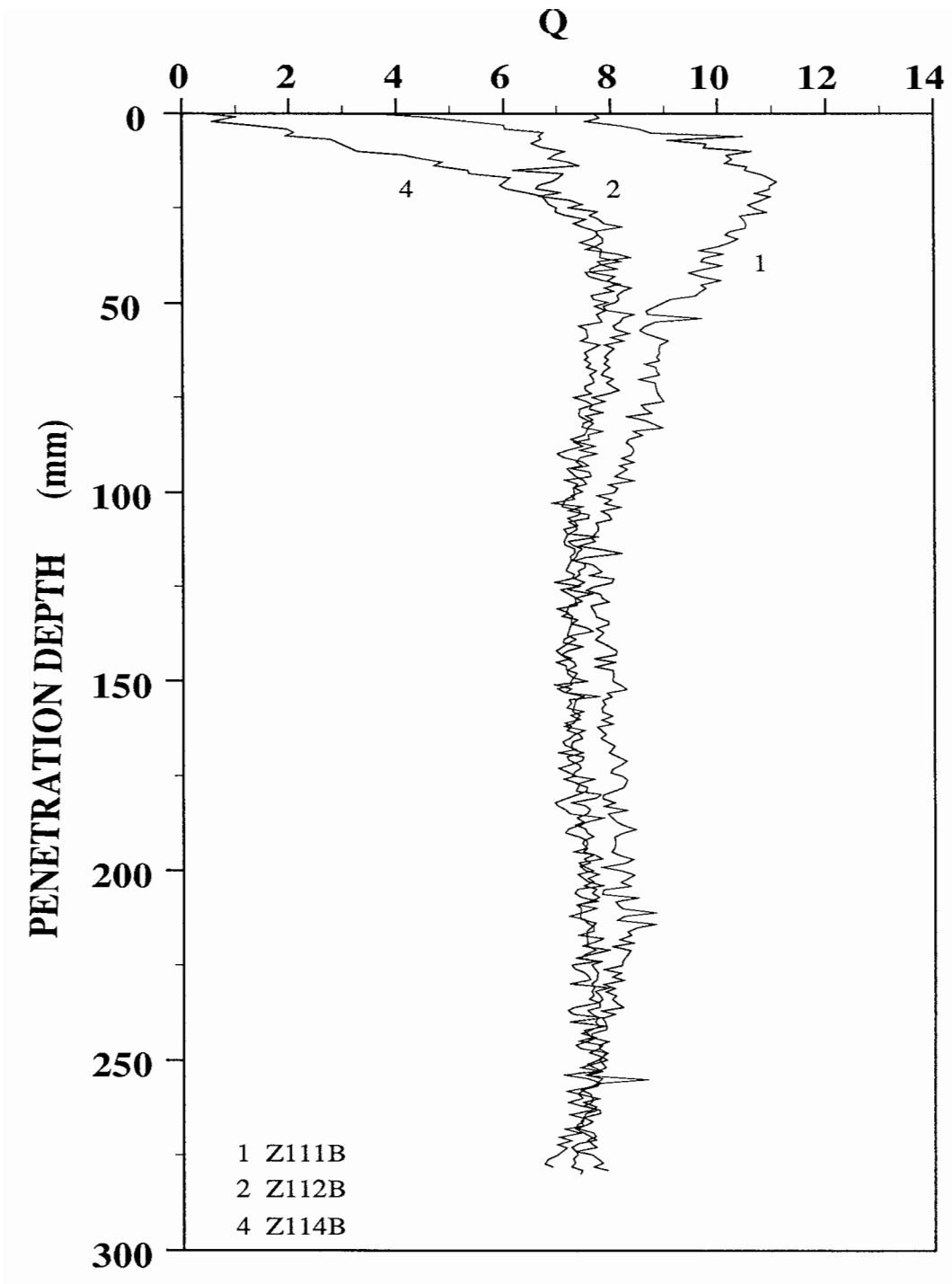

Figure 6.50 Tip resistance factor Q with penetration depth during test series Z11B.

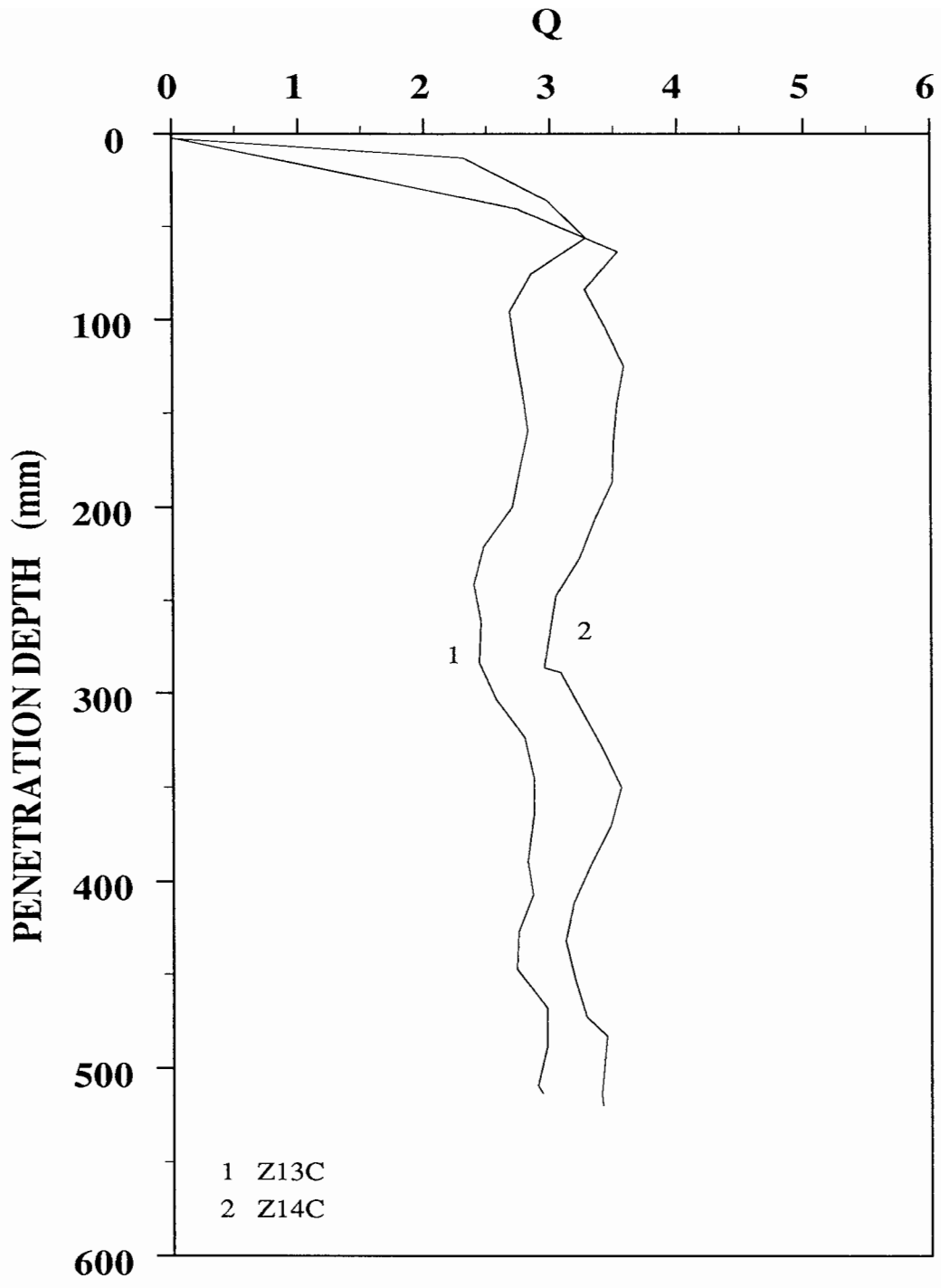

Figure 6.51 Tip resistance factor Q with penetration depth during test series Z1C.

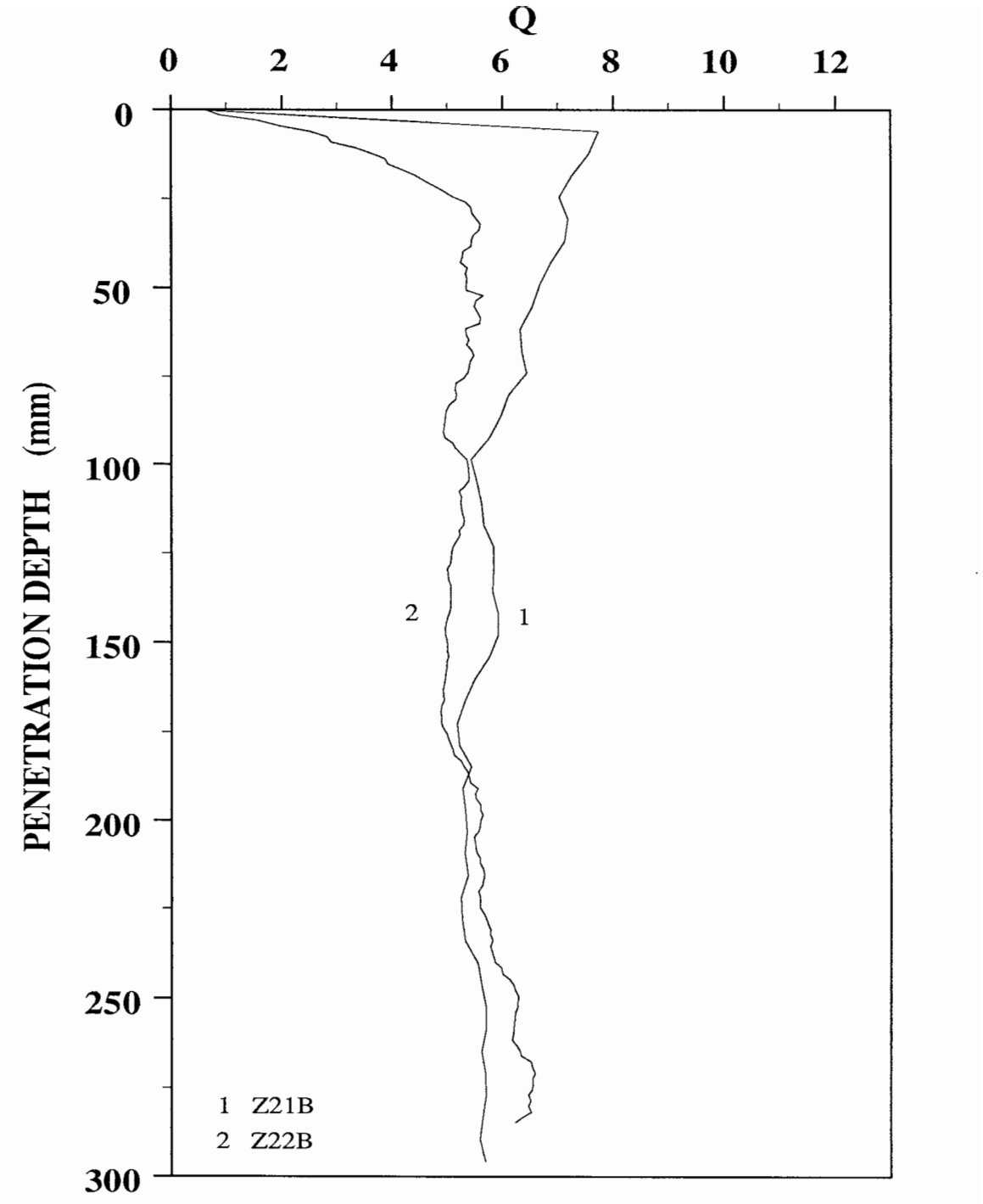

Figure 6.52 Tip resistance factor Q with penetration depth during test series Z2B.

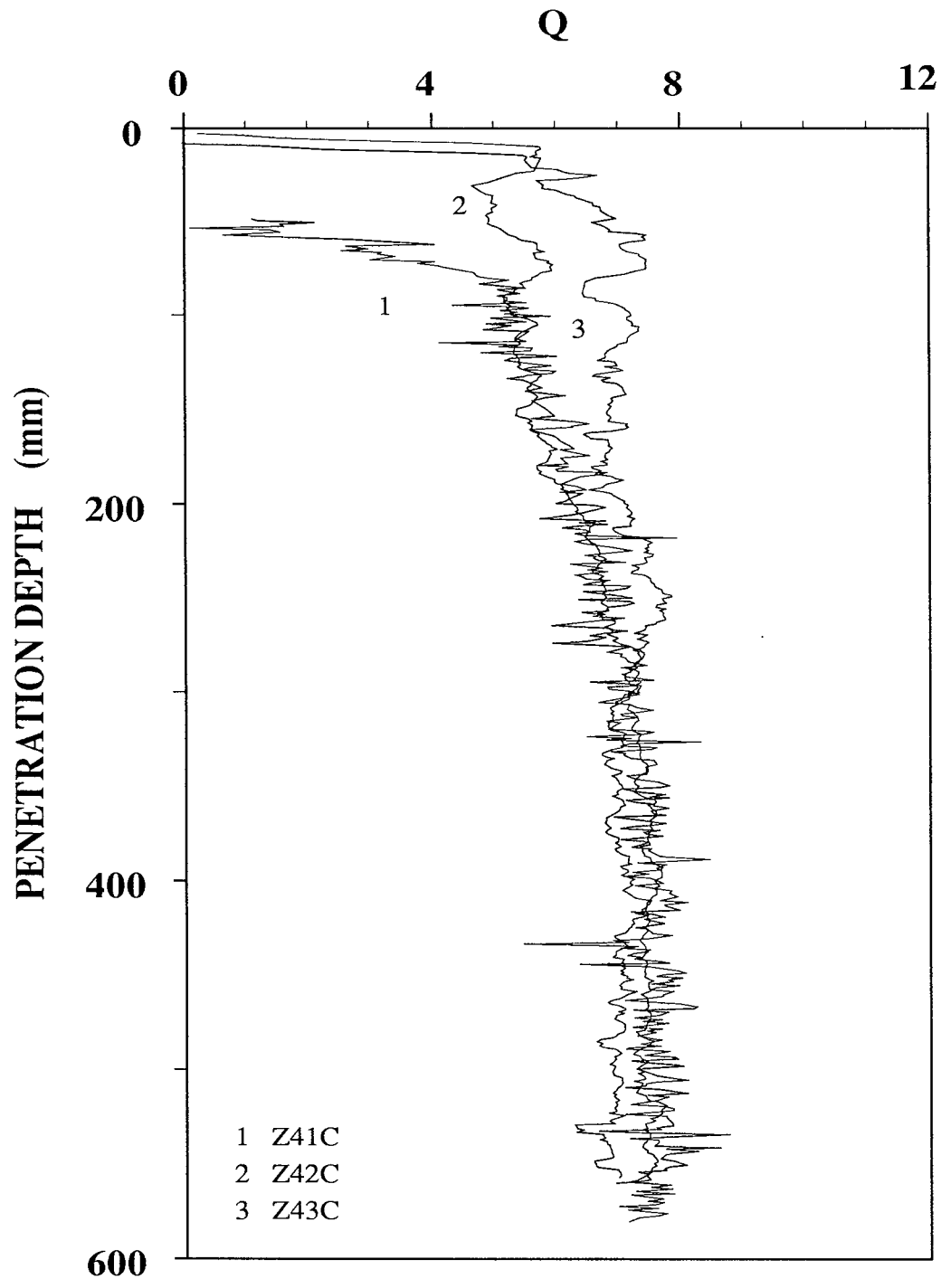

Figure 6.53 Tip resistance factor Q with penetration depth during test series Z4C.

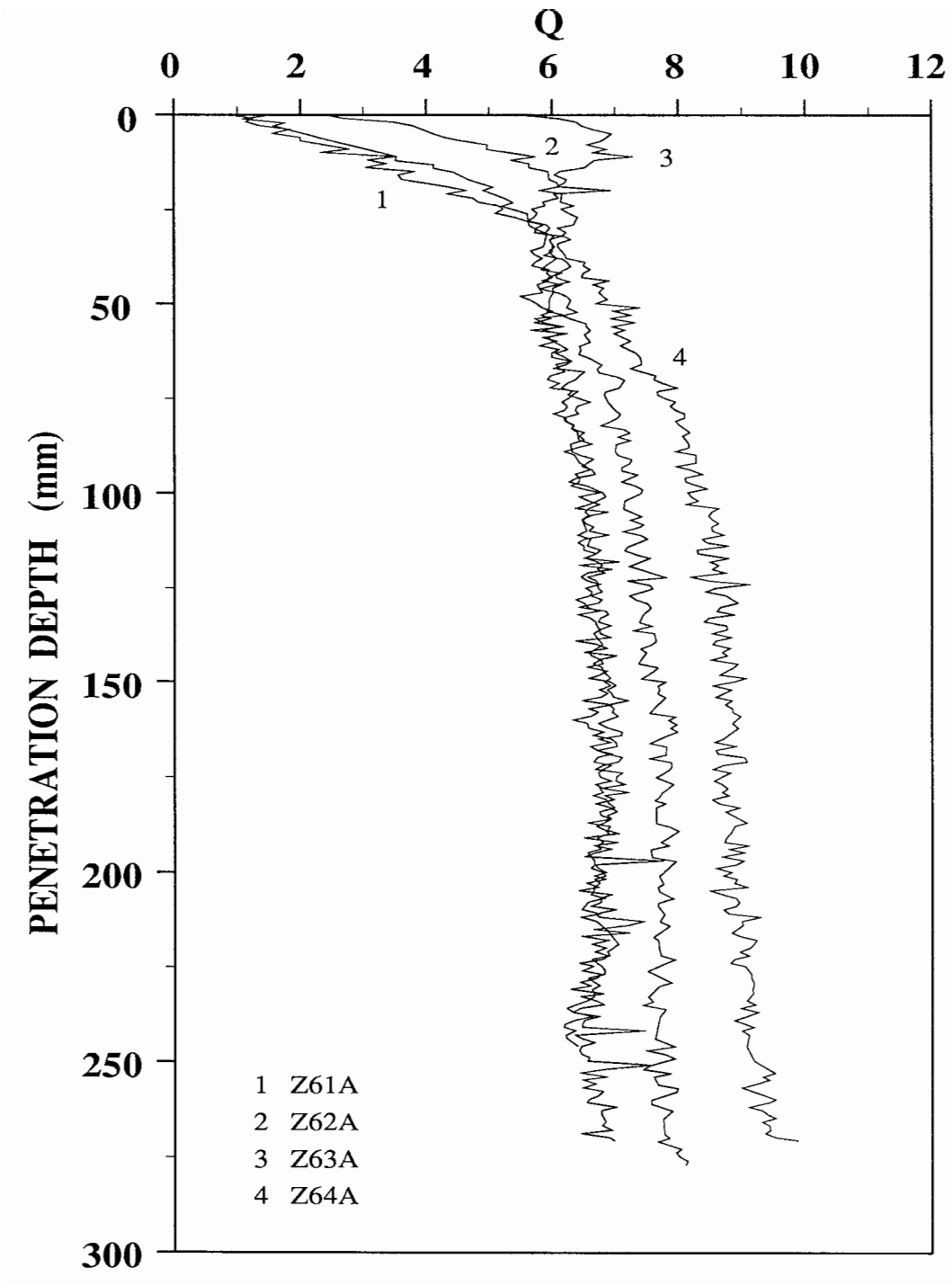

Figure 6.54 Tip resistance factor Q with penetration depth during test series Z6A.

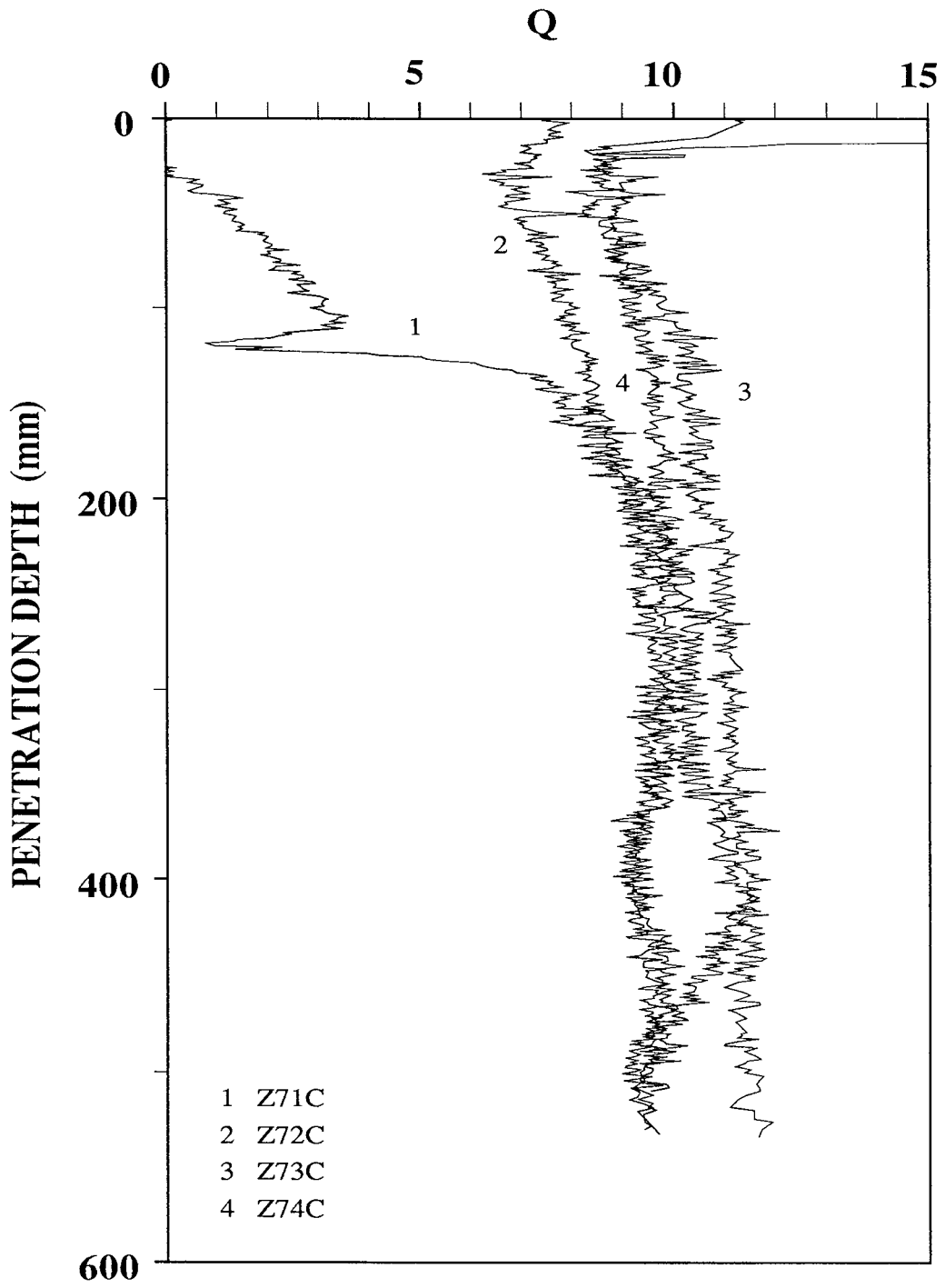

Figure 6.55 Tip resistance factor Q with penetration depth during test series Z7C.

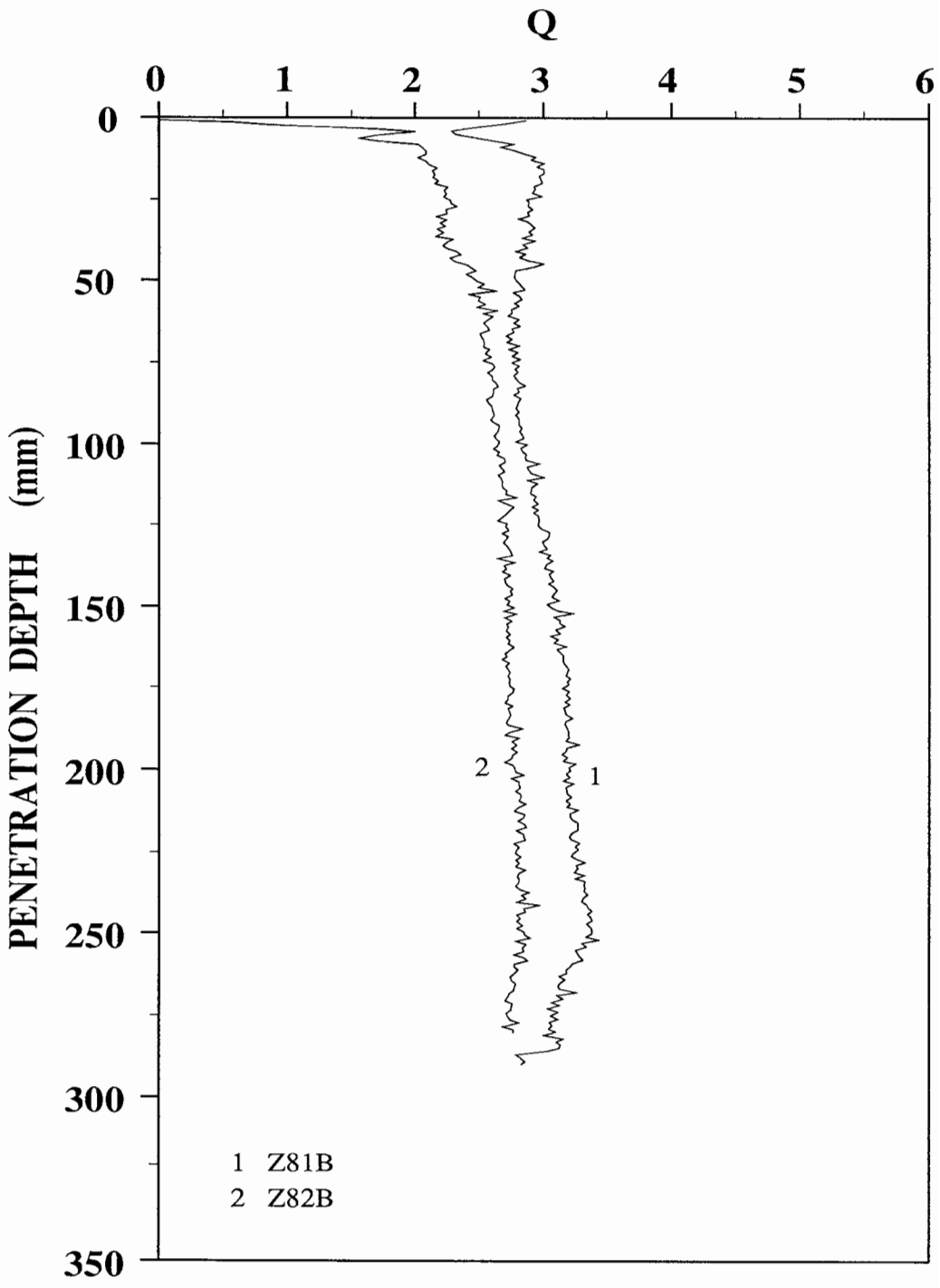

Figure 6.56 Tip resistance factor Q with penetration depth during test series Z8B.

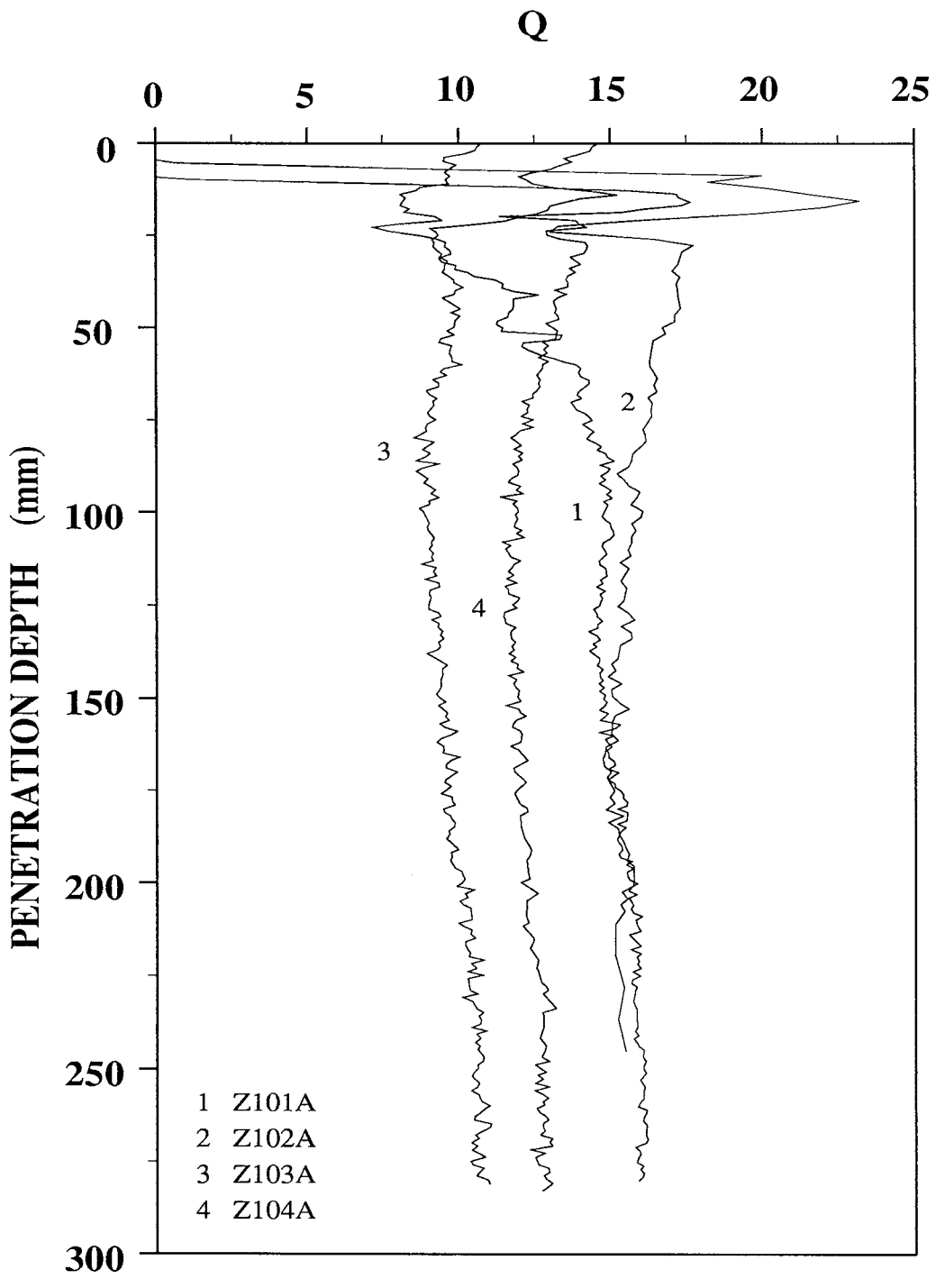

Figure 6.57 Tip resistance factor Q with penetration depth during test series Z10A

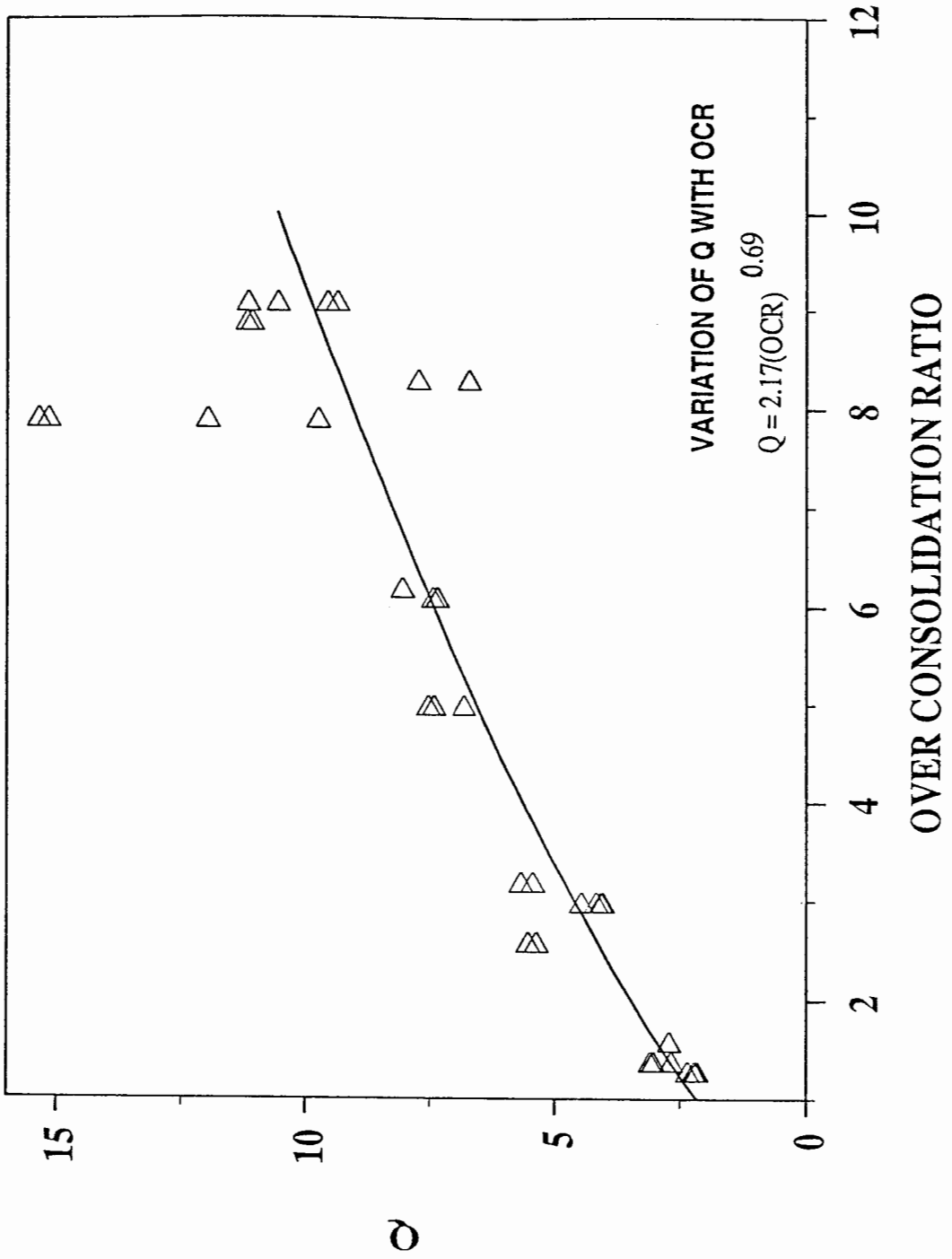

Figure 6.58 Variation of the tip resistance factor Q with over consolidation ratio for all laboratory test series.

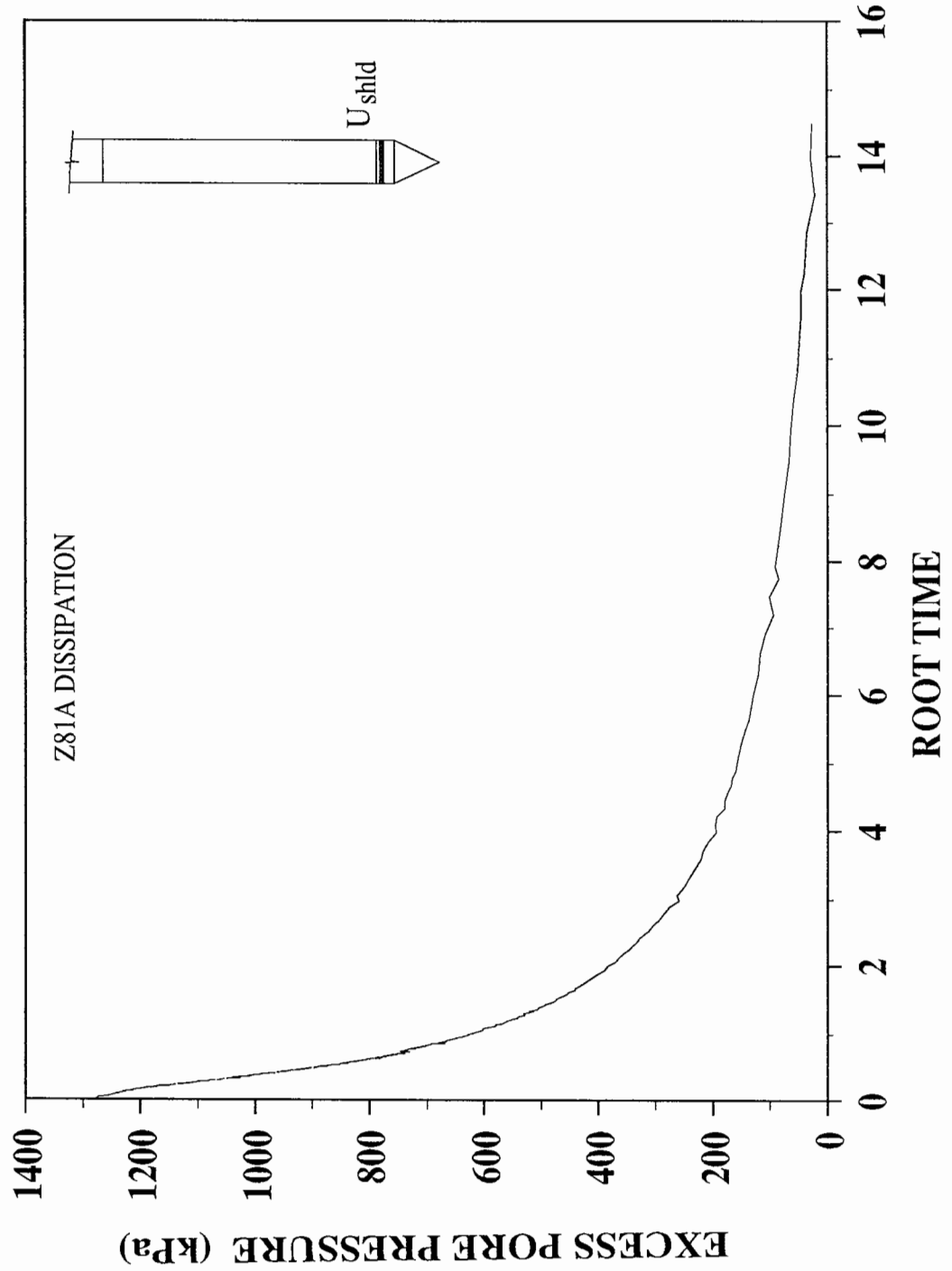

Figure 6.59 Excess pore pressure dissipation after penetration testing. Tests Z81A.

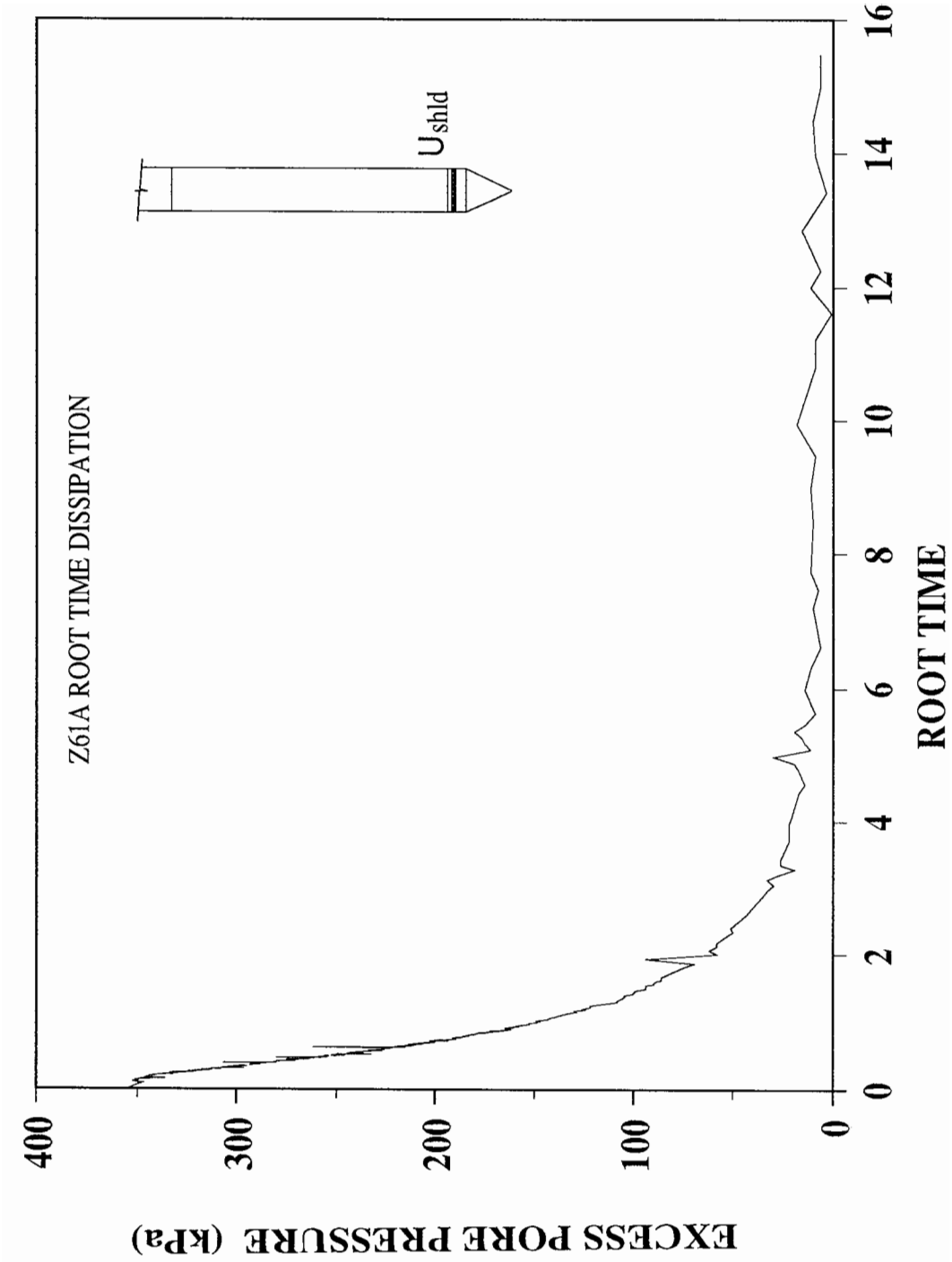

Figure 6.60 Excess pore pressure dissipation after penetration testing. Test Z61A

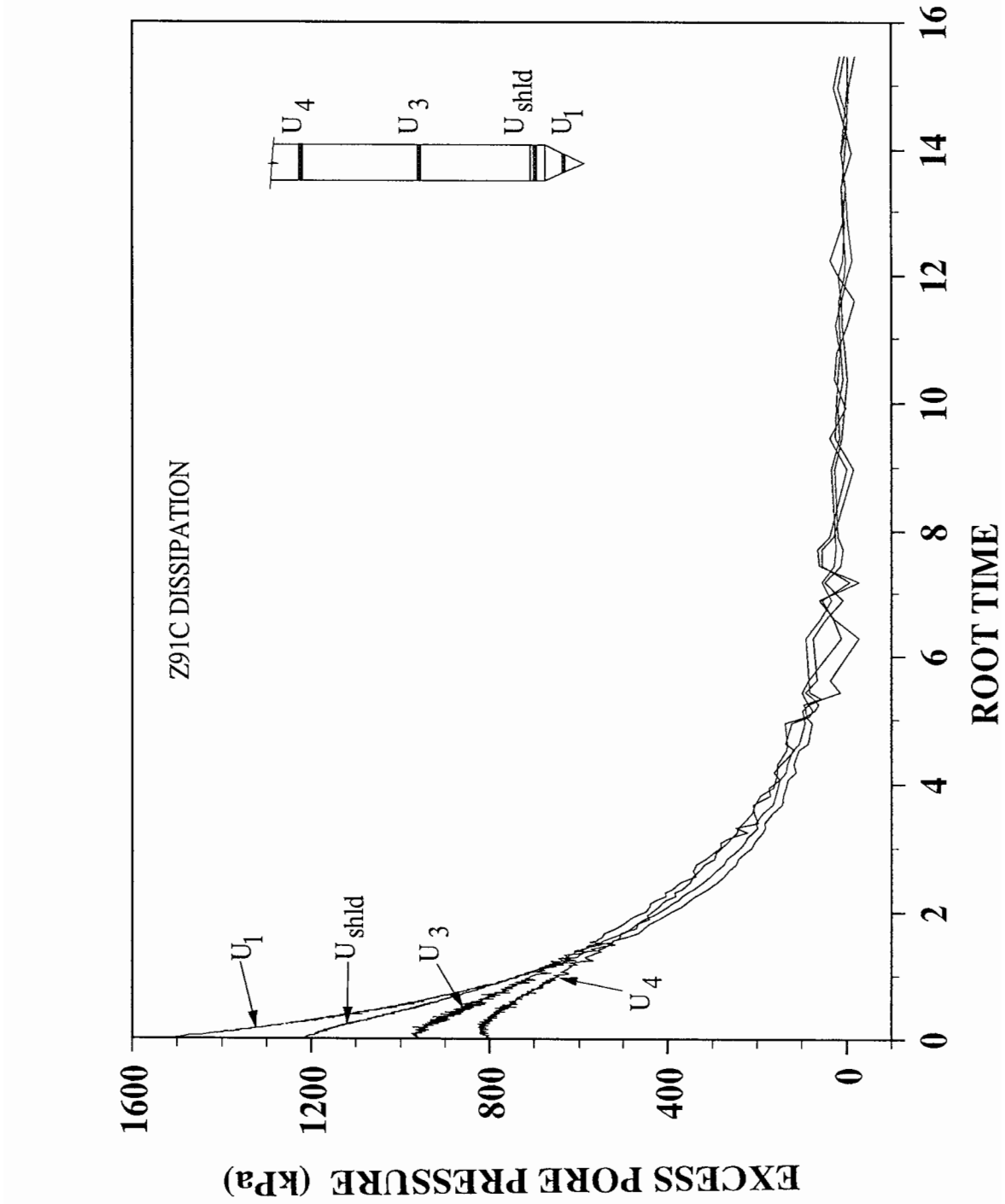

Figure 6.61 Excess pore pressure dissipation after penetration testing. Test Z91C

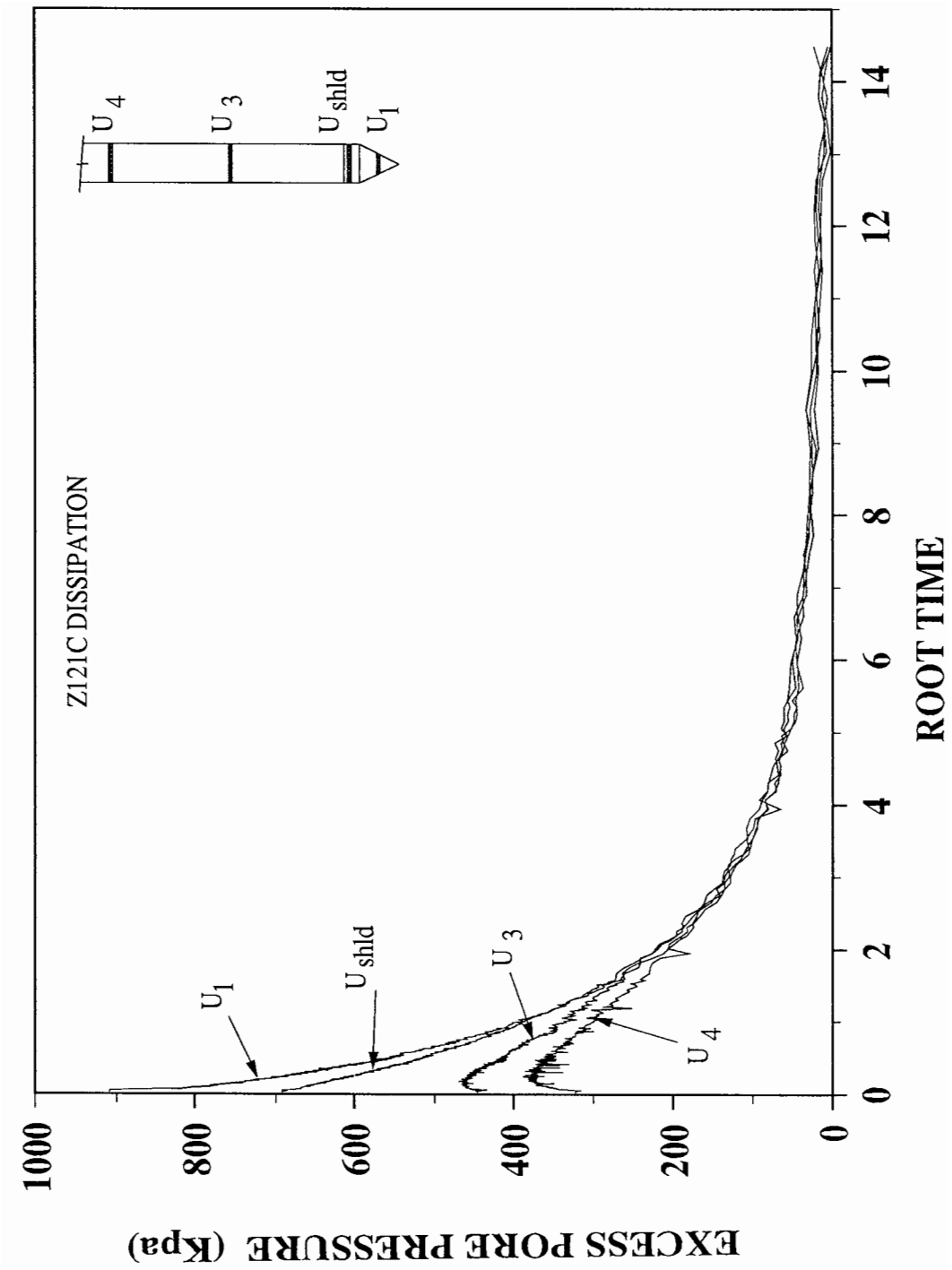

Figure 6.62 Excess pore pressure dissipation after penetration testing. Test Z121C

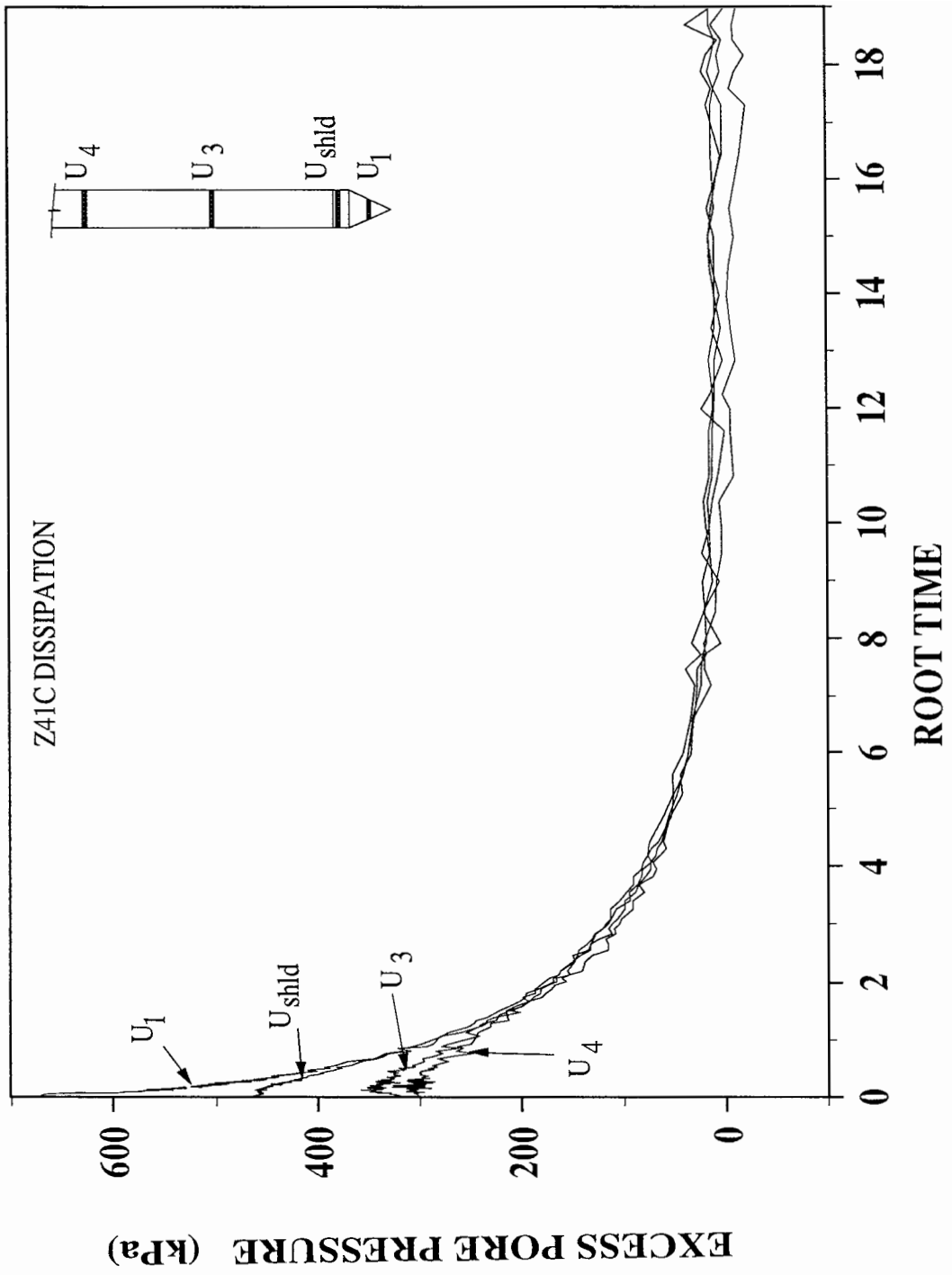

Figure 6.63 Excess pore pressure dissipation after penetration testing. Test Z41C

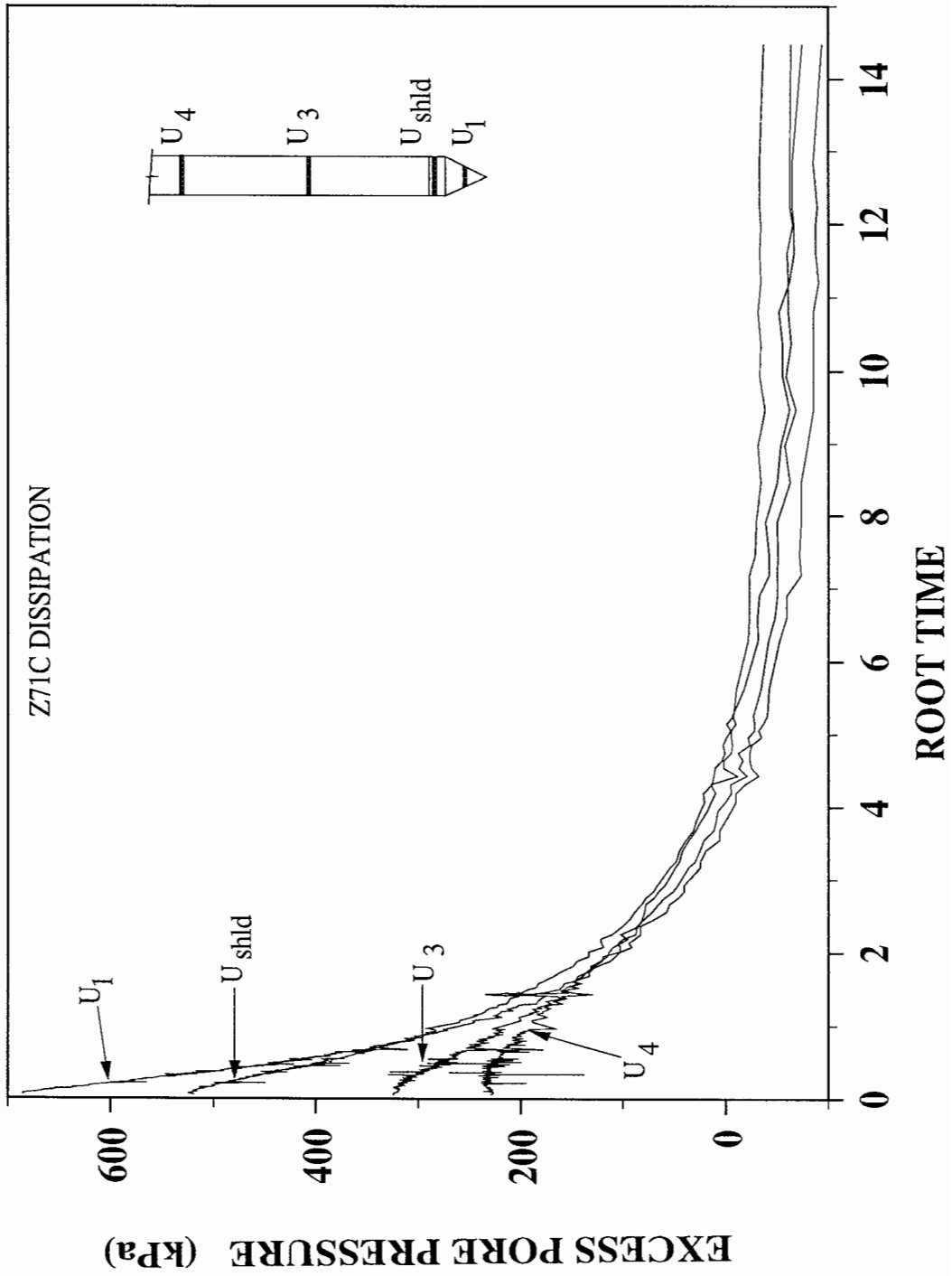

Figure 6.64 Excess pore pressure dissipation after penetration testing. Test Z71C

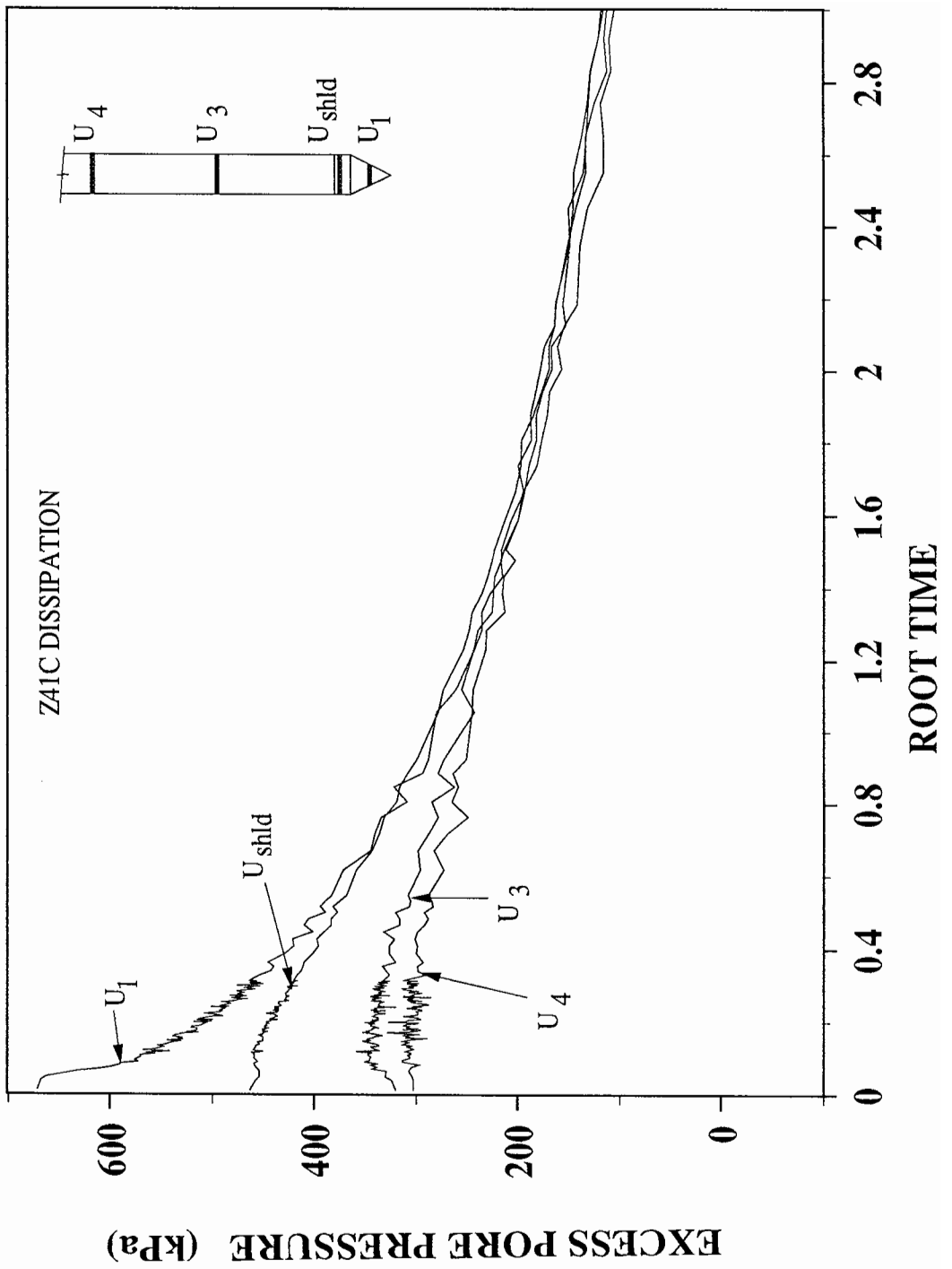

Figure 6.65 Excess pore pressure dissipation after penetration testing in the first 9 minutes. Test Z

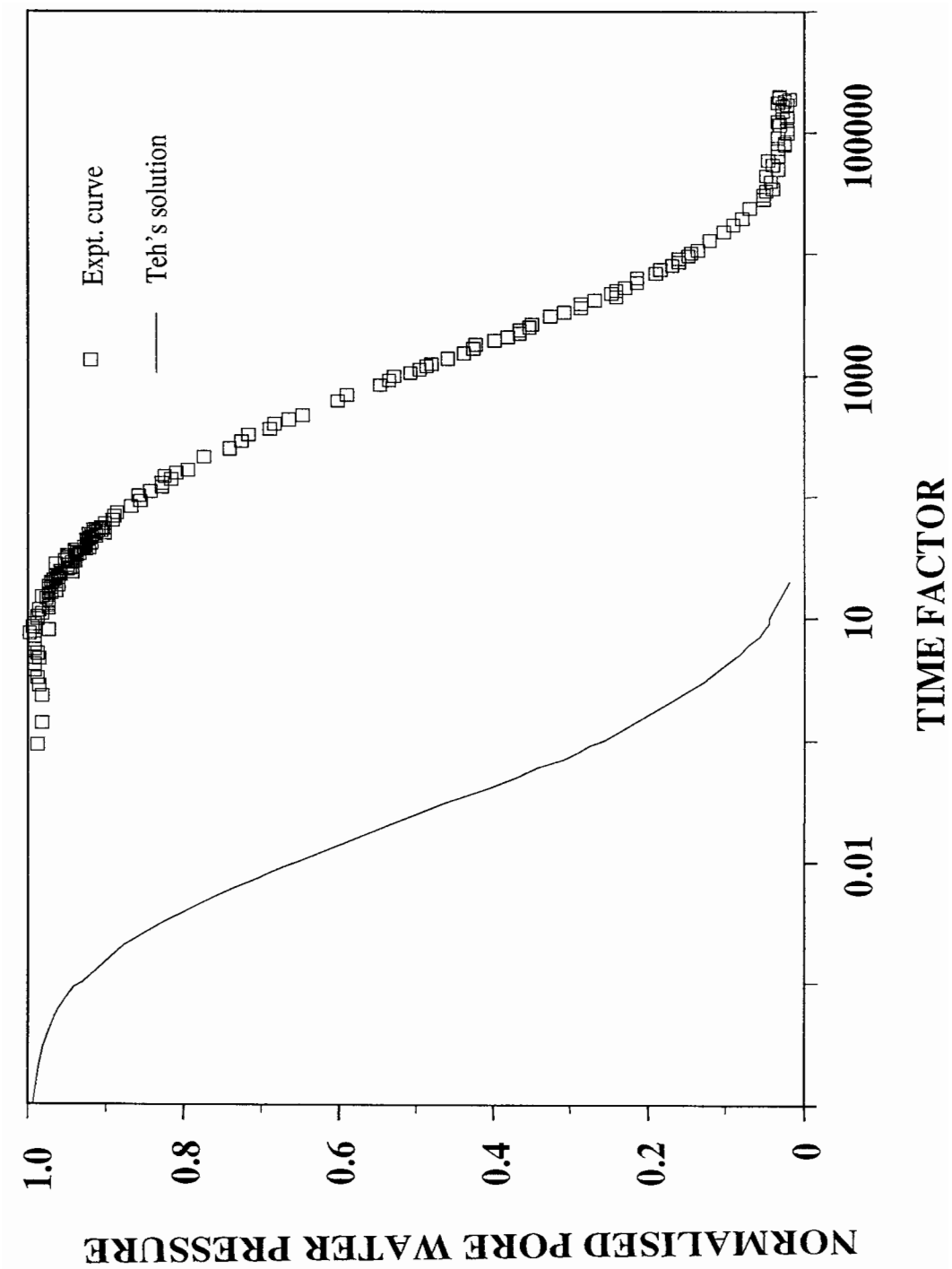

Figure 6.66 Theoretical and experimental dissipation graphs separated by c_h

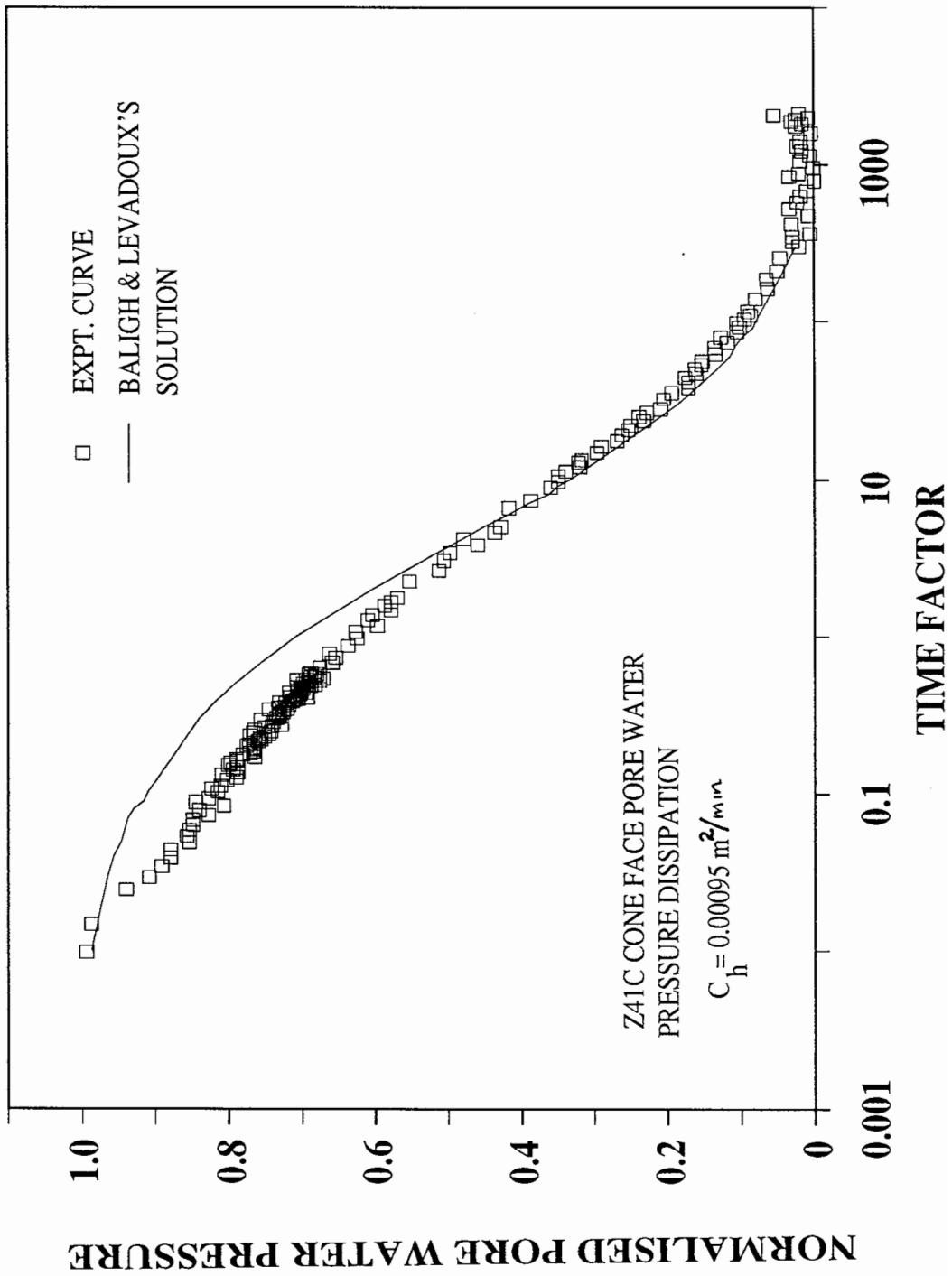

Figure 6.67 Curve fitting for cone face (U_1) excess pore pressure dissipation using solution by Baligh and Levadoux (1980). Test Z41C

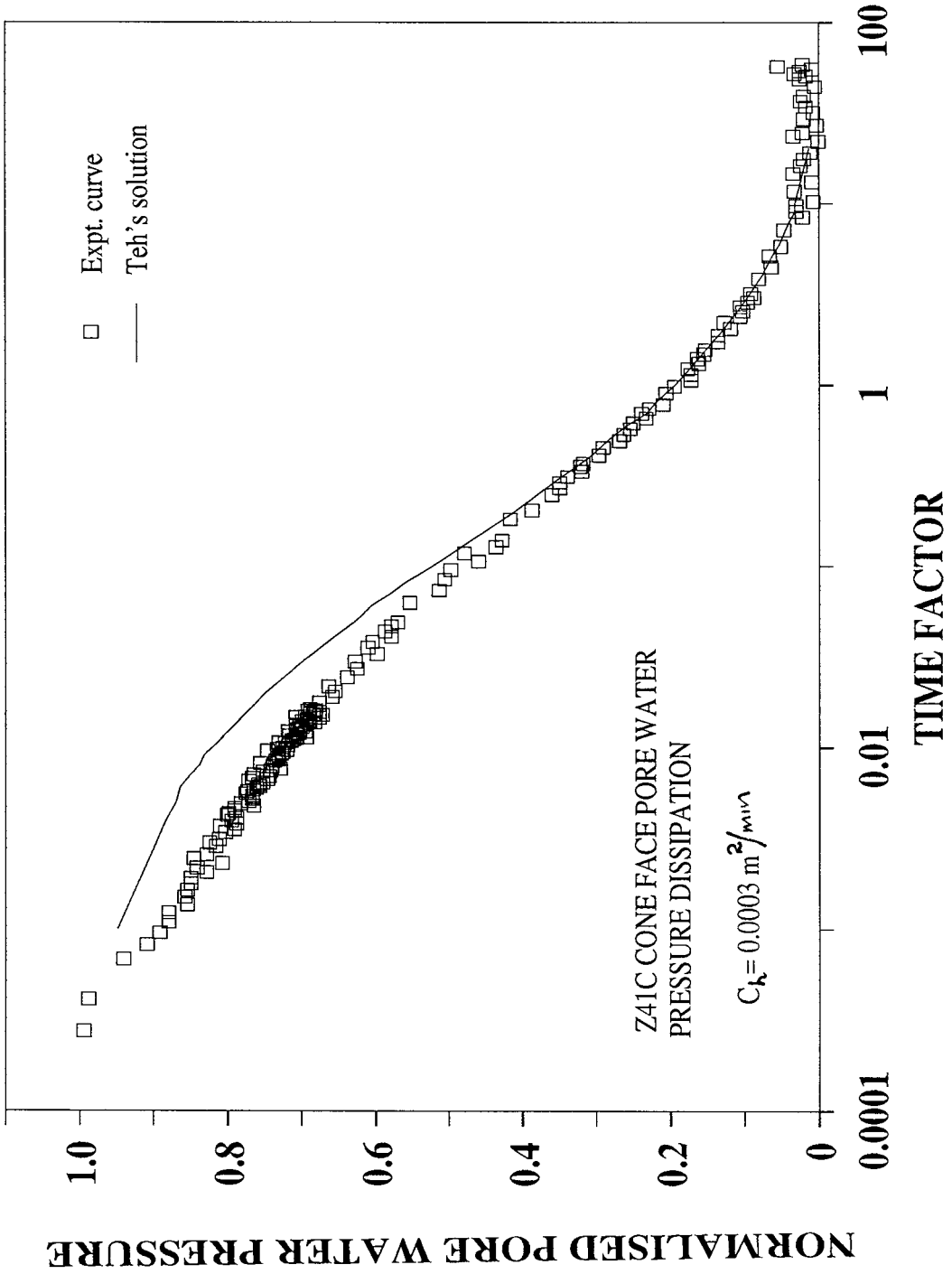

Figure 6.68 Curve fitting for cone face (U_1) excess pore pressure dissipation using the solution by Teh (1987). Tests Z41C.

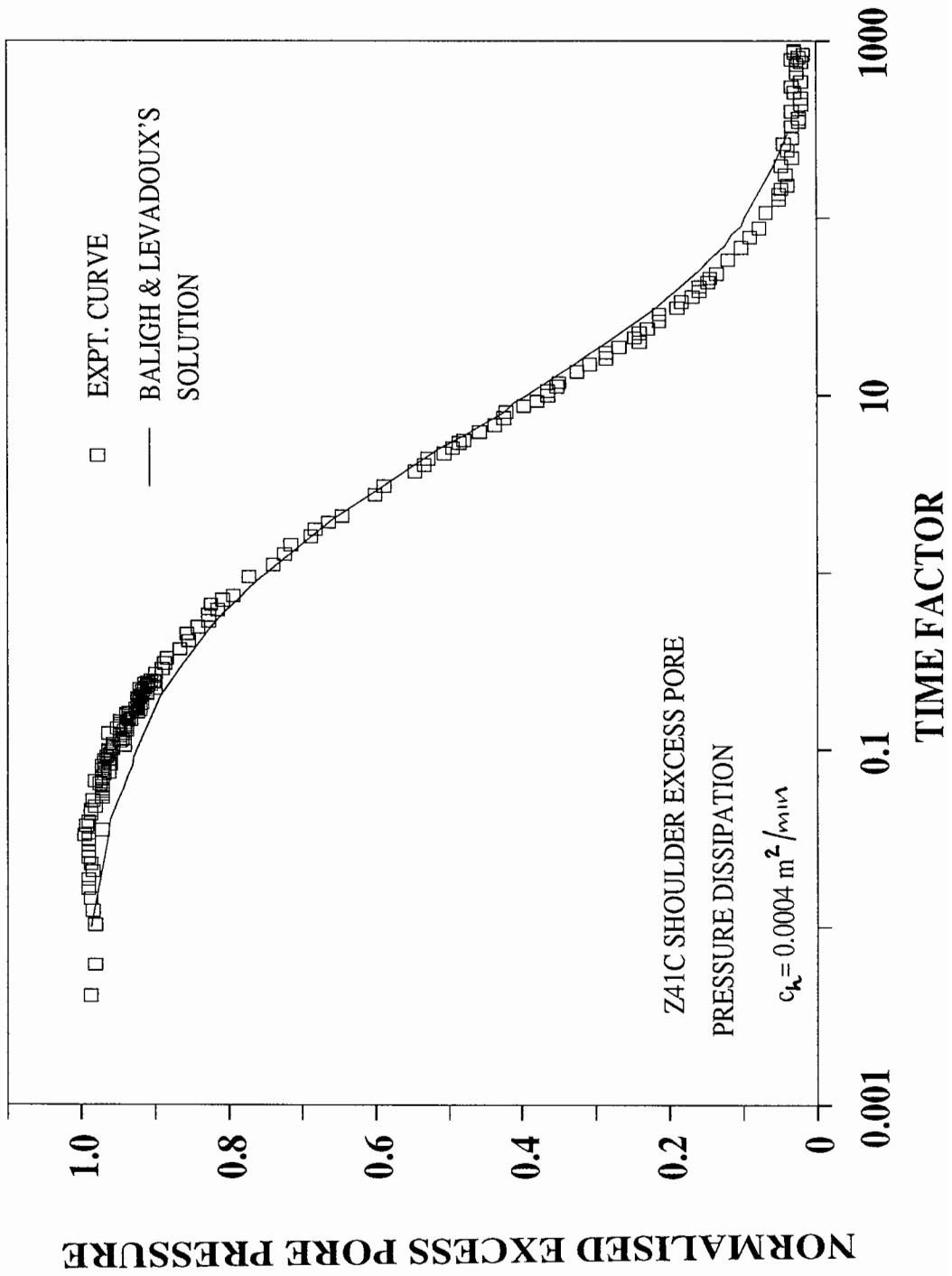

Figure 6.69 Curve fitting for cone shoulder (U_{shld}) excess pore pressure dissipation using solution by Baligh and Levadoux (1980). Test Z41C

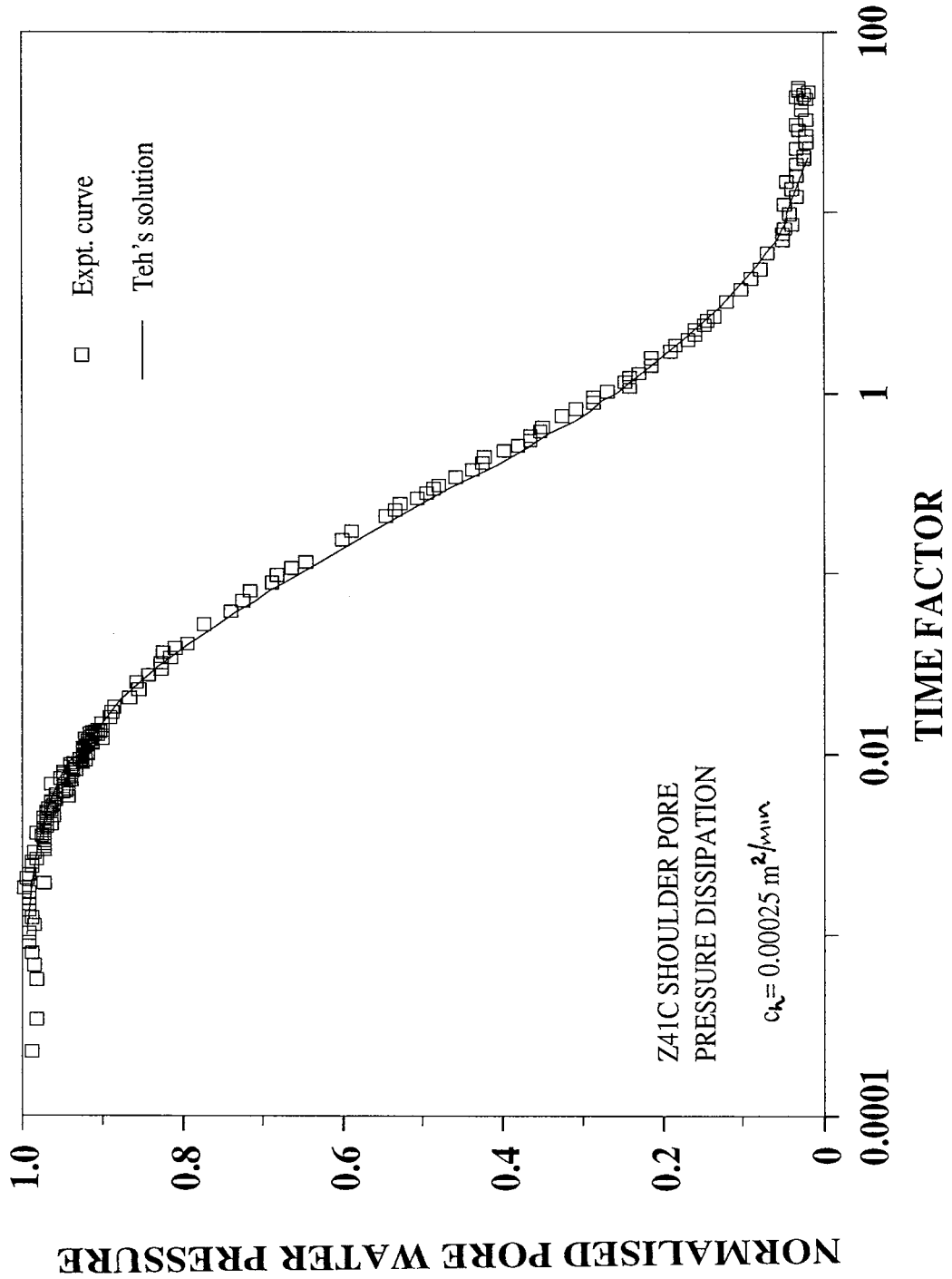

Figure 6.70 Curve fitting for cone shoulder (U_{shld}) excess pore pressure dissipation using the solution by Teh (1987). Tests Z41C.

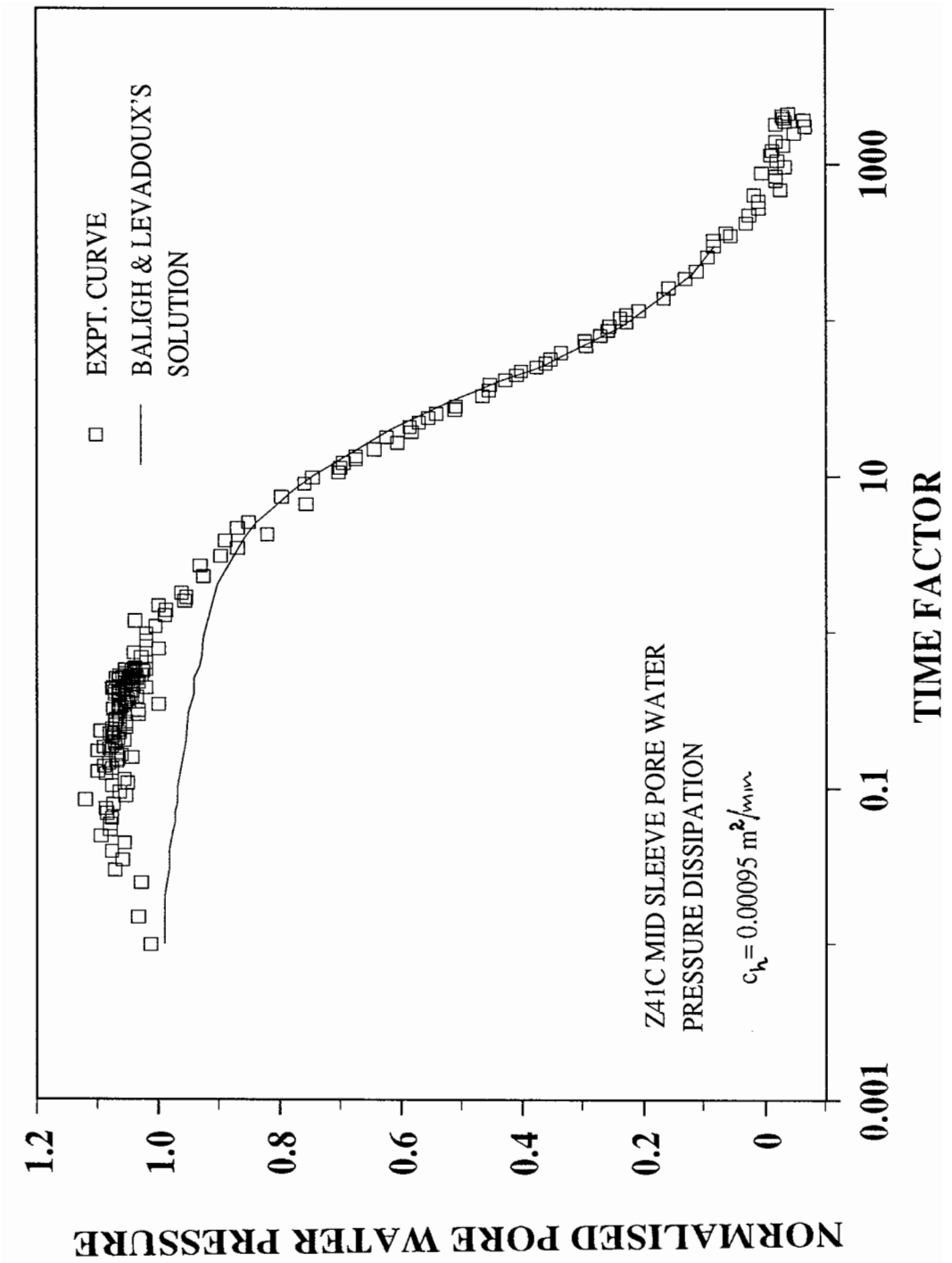

Figure 6.71 Curve fitting for mid-sleeve (U_3) excess pore pressure dissipation using solution by Baligh and Levadoux (1980). Test Z41C

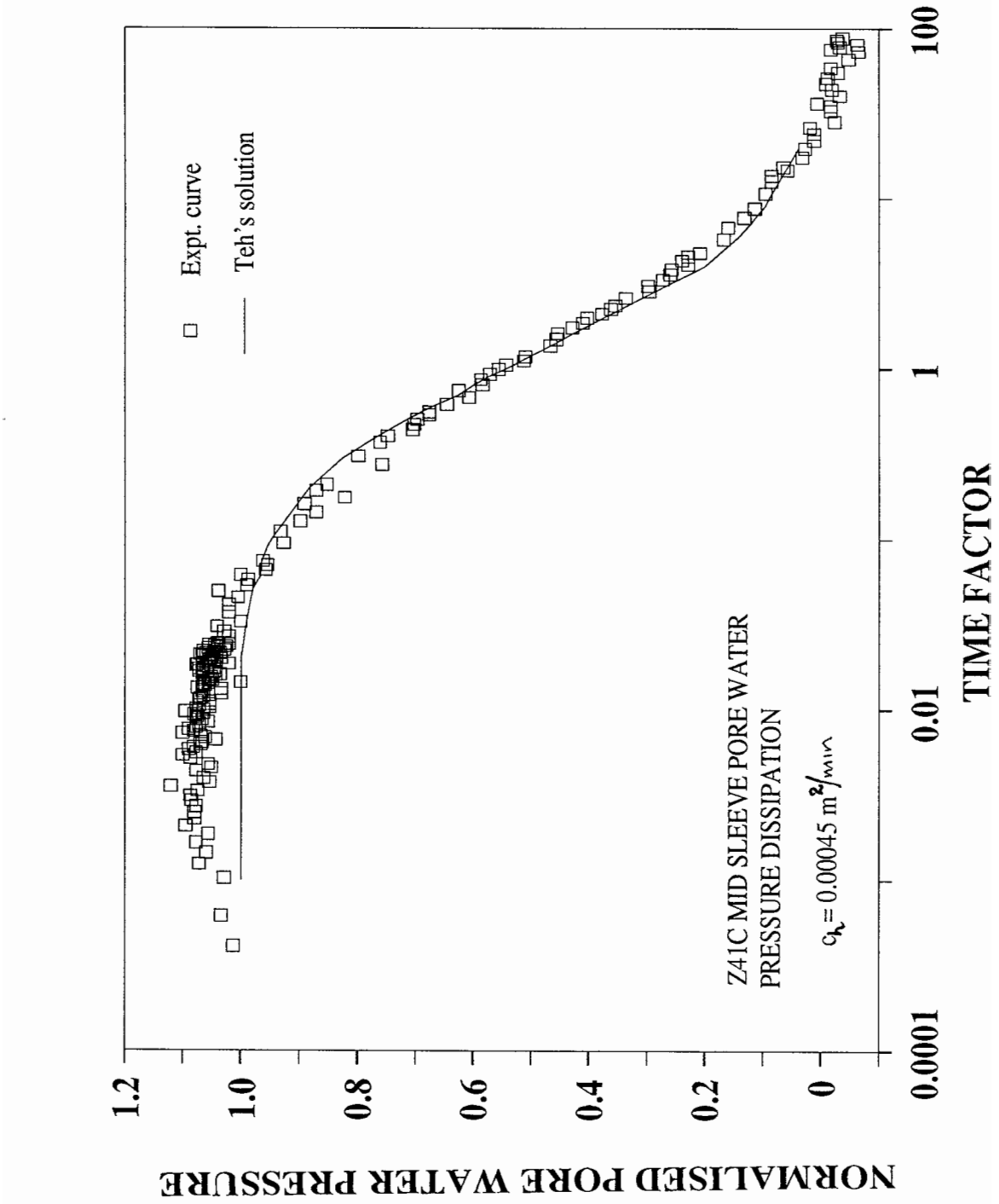

Figure 6.72 Curve fitting for mid-sleeve (U_3) excess pore pressure dissipation using the solution by Teh (1987). Tests Z41C.

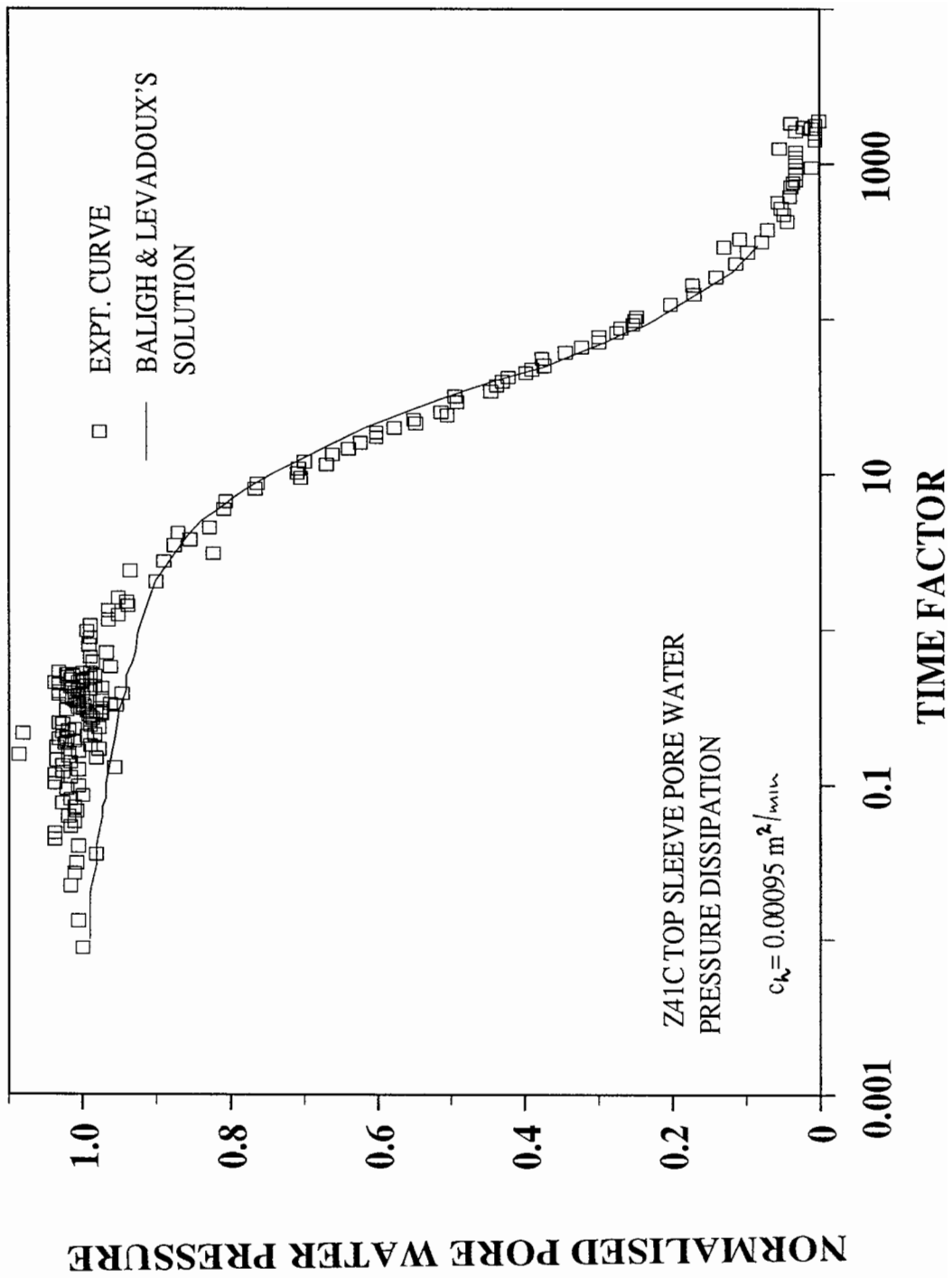

Figure 6.73 Curve fitting for top-sleeve (U_4) excess pore pressure dissipation using solution by Baligh and Levadoux (1980). Test Z41C

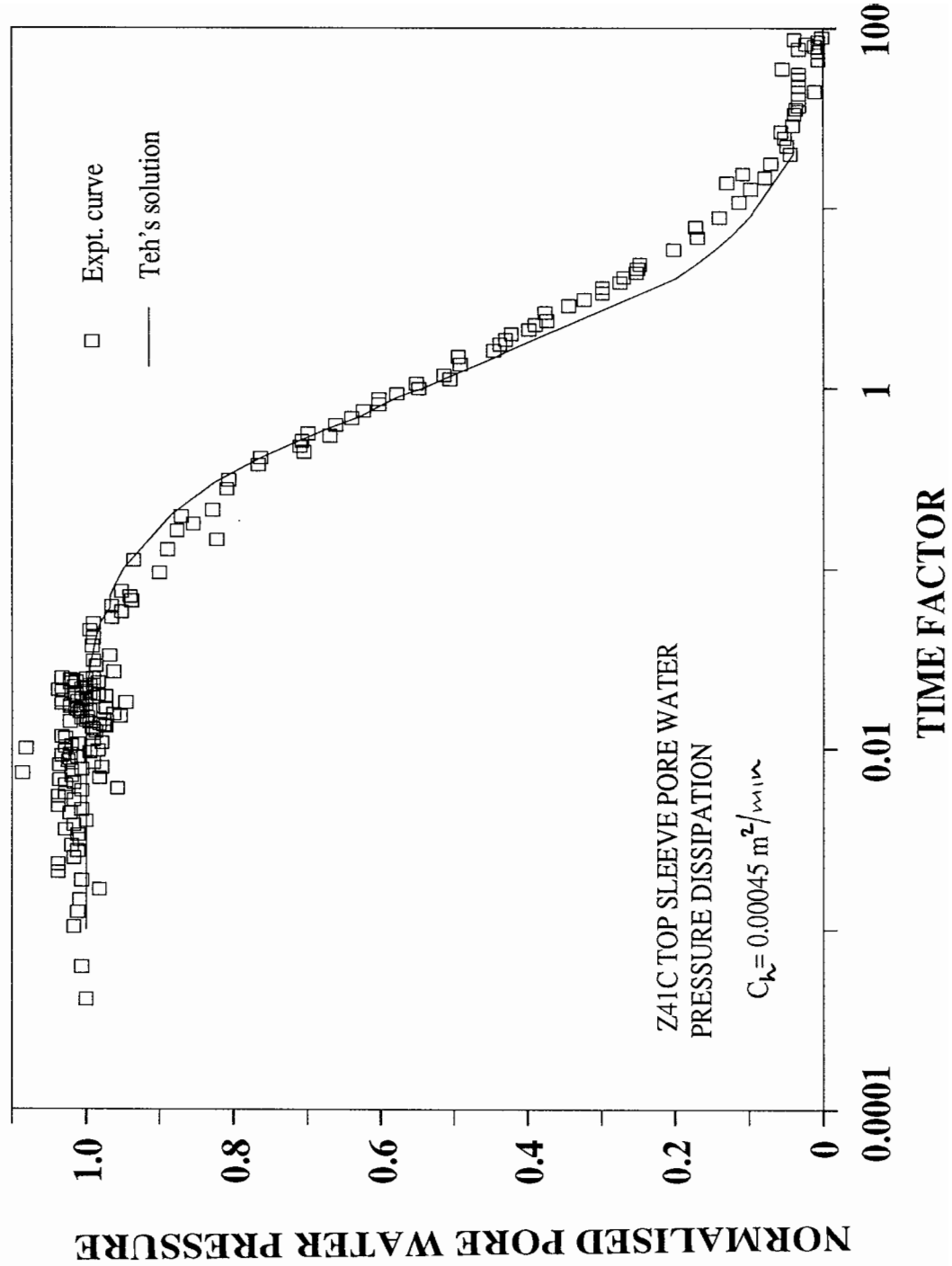

Figure 6.74 Curve fitting for top-sleeve (U_4) excess pore pressure dissipation using the solution by Teh (1987). Tests Z41C.

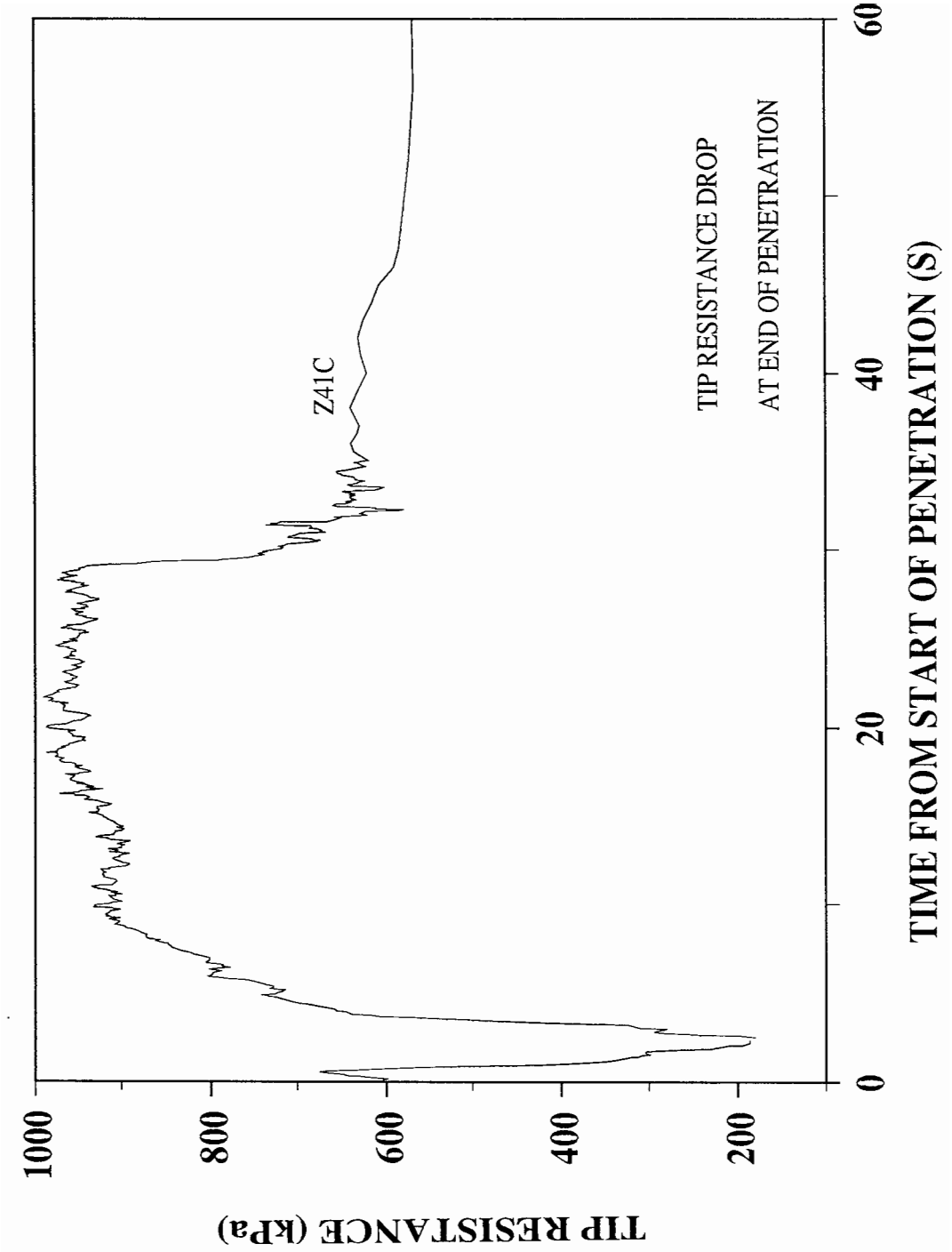

Figure 6.75 Tip resistance with time, showing the the drop in pressure when penetration stops

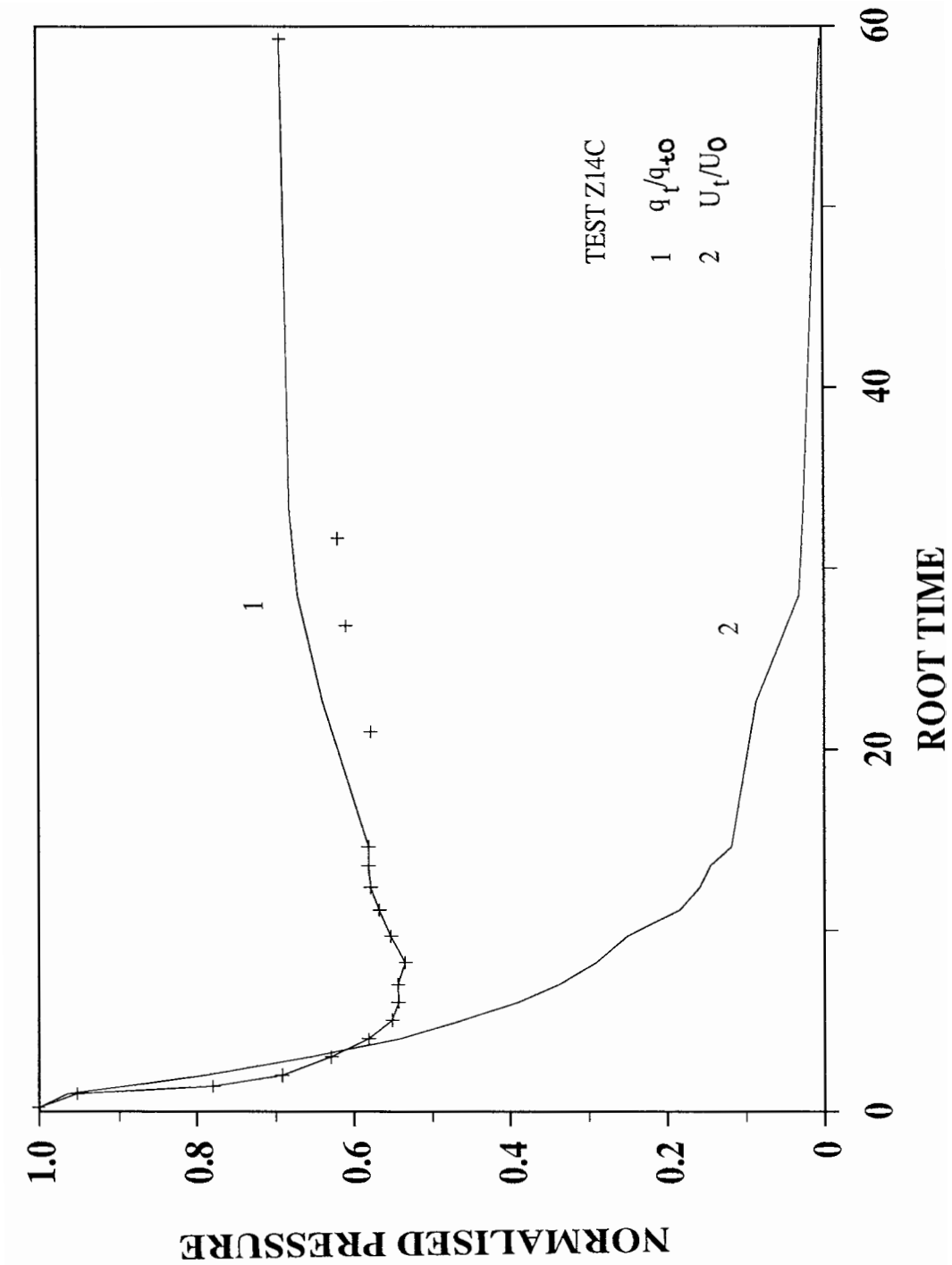

Figure 6.76 Tip resistance and shoulder pore pressure during dissipation test of Z14C.

7 INTERPRETATION OF TEST RESULTS

The piezocone test has received considerable attention in recent literature and several authors have published methods of interpreting test results. One of the recent publications, Wroth (1988), emphasised that correlations which can be used with confidence outside the immediate context in which they were formulated should ideally be:

a) based on a physical appreciation of why the properties can be expected to be related;
b) set against a background of theory, however idealised this may be;
c) expressed in terms of dimensionless variables so that advantage can be taken of the scaling laws on continuum mechanics.

In addition to these three points, the correlations should be able to be tested experimentally.

With the above in mind, this chapter will focus on the interpretation of piezocone test results obtained during the research programme from an experimental point of view. In the analyses that will follow, unless otherwise specified, all the results from the test programme were taken into account.

In the piezocone tests carried out with the 1 cm^2 piezocone, two independent measurements (tip resistance and cone shoulder pore pressure) were made. Using the 5 cm^2 piezocone, it was possible to make six independent measurements. Of these, four were pore pressure measurements at different locations, constituting one independent parameter, and the remainder were tip resistance and sleeve friction. Since the sleeve friction data were unreliable (see Chapter 6), this left two independent parameters from the piezocone for use in correlations.

From the soil sample, the vertical and horizontal effective stresses, the undrained shear strength and the over consolidation ratio were known. The influence of these soil sample parameters on the tip resistance and the excess pore pressure will be examined, leading to correlations which may be suitable for the interpretation of piezocone data.

The correlation of the measured parameters, or a combination of them, with the over consolidation ratio will be sought and, to this end, the variation of three factors, β,Q and B_q with over consolidation ratio has already been illustrated in Chapter 6. Additional discussion about these parameters will be made later in Section 7.3.

7.1 Tip Resistance

In this section, the influence of the vertical and horizontal effective stresses on tip resistance will be discussed together with the influence of the over consolidation ratio.

The influence of the horizontal effective stress (σ'_{h0}) at the time of the penetration test on the mobilised net tip resistance ($q_t - \sigma_{v0}$) was analysed by plotting the two parameters against each other. The parameters were made non dimensional by dividing by the vertical effective stress at the time of the test. Since σ'_{v_0} is used to make both ($q_t - \sigma_{v0}$) and (σ'_{h0}) dimensionless, this exercise is effectively correlating the tip resistance factor (Q) and the coefficient of earth pressure at rest (K_0). The result of the correlation is illustrated in Figure 7.1. All test results are represented in the Figure and it can be seen that four results (all from Z10A series) stand on their own while the rest form a clearly defined linear relationship. The linear function which fitted the data, excluding Z10A results, with a correlation coefficient of 0.91, is given below.

$$Q = 14.4K_0 - 7.9 \qquad [7.1]$$

Figure 7.1 shows that K_0 has a significant influence on the tip resistance factor Q and the corollary to the result is that the net tip resistance is significantly influenced by the horizontal effective stress (σ'_{h0}). This is an important result because it means that the coefficient of lateral earth pressure may be estimated from piezocone data. However, this result is from a limited range of K_0 values and extrapolation from the limits of 0.6-1.4 may cause unforeseen problems. Therefore, further work to look at this correlation, outside this range, may be required to confirm this finding.

In order to investigate the effect of the vertical effective stress at the time of the penetration test on tip resistance, it was necessary to change the parameter used to make $(q_t - \sigma_{v0})$ and σ'_{v0} non dimensional. The shear vane strength was used in this case. The resulting non-dimensional tip resistance was called the undrained tip resistance ratio, N_{kt}. The non-dimensional vertical effective stress is the undrained strength ratio (Wroth 1988). Therefore the slope of this graph, plotted in Figure 7.2, should be the parameter Q, since:

$$Q = \left(\frac{q_t - \sigma_{v_0}}{s_{u_v}}\right)\left(\frac{s_{u_v}}{\sigma'_{v_0}}\right) \qquad [7.2]$$

There are two sets of results plotted in Figure 7.2. The first set, with open triangles, is the result of the correlation of $(q_t - \sigma_{v0})/s_{uv}$ or N_{kt} with the undrained strength ratio. This result shows that there is no clear correlation between the two variables. Therefore another form of the relationship (i.e. $(q_t - \sigma_{v0} - U_{shld})/s_{uv}$ with the undrained strength), was tested and the result is shown by the shaded triangles. Although there is some indication of a decreasing tip resistance ratio with increasing undrained strength ratio, there is a lot of scatter in the results at the lower end of the undrained strength ratio and there is not enough data at the higher undrained strength ratio end to prove whether or not there is an underlying correlation. Houlsby and Hitchman (1988) also found no direct correlation between tip resistance and vertical effective stress for any density of sand.

The variation of the tip resistance factor (Q) with over consolidation ratio, illustrated in Figure 6.58, is essentially a test of the effect of the vertical effective stress ratio (pre-consolidation pressure to the present vertical effective stress) on the net tip resistance made non-dimensional by the vertical effective stress. The high correlation coefficient (0.92) is an indication that the stress ratio has a definite and direct influence on the tip resistance. The corollary is, therefore, that the tip resistance factor is a very good indicator of over consolidation ratio. The correlation of (Q) with over consolidation ratio is discussed further in Section 7.3.

In summary, the net tip resistance has been shown to be dependent on the horizontal effective stress at the time of the test and the vertical effective stress ratio. The vertical effective stress was found to have no direct correlation with the net tip resistance. The correlation of the non-dimensional net tip resistance, otherwise known as the tip resistance factor Q may lead to the possible estimation of the coefficient of lateral earth pressure, K_0, from piezocone results.

7.2 Excess Pore Pressure

Excess pore pressures from each test were made non-dimensional by the vertical effective stress so that the influence of the horizontal effective stress, which was similarly made non-dimensional, could be tested. The ratio of the excess pore pressure to the vertical effective stress has been called the pore pressure ratio, and the non-dimensional horizontal effective stress is the coefficient of lateral earth pressure at rest, K_0. The results in Figure 7.3 are for the excess pore pressure at the cone shoulder for all tests including those with the 1 cm^2 piezocone in the small chambers. Figure 7.4 illustrates results from the 5 cm^2 piezocone at the other three pore pressure positions.

The excess pore pressure at the shoulder, shown in Figure 7.3, indicates a tendency to increase with increasing K_0, showing some influence of the horizontal effective stress, but there is too much scatter in the results to give a direct correlation. In Figure 7.4 the influence

of the horizontal stress is clearly seen. The gradients of the regression lines show that the influence is greater at the cone face than on the piezocone shaft, and reduces with distance from the cone tip.

7.2.1 Excess pore pressure distribution

The distribution of pore pressure along the shaft of the piezocone has been reported by many authors, of whom Baligh and Levadoux (1980) and Teh (1987) are the notable analytical exponents. On the experimental field test front, Jamiolkowski et al (1985), Sills et al (1988a) and May (1987) have reported results of the distribution of excess pore pressure along the piezocone shaft. Sills et al (1988a) and May (1987) used the same piezocone as the one used in this test programme at sites where the over consolidation ratios were less than four. Therefore this programme, in which over consolidation ratios went up to 9.1, provides new data for the distribution of excess pore pressure along the length of the piezocone.

The results of the distribution of excess pore pressure during penetration using the 5 cm^2 piezocone are summarised in Figure 7.5. In the Figure, excess pore pressures measured at all four locations were normalised by that measured at the top of the friction sleeve (U_4). Apart from the result May C2-1 which was taken from May (1987), all the other results are averages of each test series in the current programme. The scatter about the mean is typically 0.4 at the cone face, 0.2 at the cone shoulder and less than 0.1 at mid-sleeve. The five different sets of results are from tests carried out at different over consolidation ratios, as indicated in the key for the Figure, but they were all carried out in kaolin samples in the large chamber.

Figure 7.5 also illustrates two theoretical solutions by Baligh and Levadoux (1980) and Teh (1987). The soil parameters used in Baligh and Levadoux's solution were obtained from reconstituted Boston Blue Clay with over consolidation ratios of up to three, while Teh's solution is based on a rigidity index (I_r) of 100. The values of I_r in three of the four tests

series carried out with the 5 cm^2 piezocone were: 45 for Z9C, 80 for Z7C and 170 for Z4C series. No I_r value was obtained for Z12C series because of a problem in the laboratory which led to the disconnection of the compressed air sytem for a long time.

Experimental results, shown in Figure 7.5, indicate different degrees of variation at the three filter element positions. At the cone face, there is a great spread of the results in the order of increasing over consolidation ratio. At the cone shoulder position the results are also spread out but not as much as at the cone face. The order of the spread is the same except for Z12C and Z4C which are switched but remain close. Given the scatter in the results, and the closeness of the two points,this switch is acceptable.

The mid-sleeve position (U_3) shows a close spread of the results. This is mainly because the excess pore pressure differences between this and the normalising position are very small. The range is from the two low OCR results of May C2-1 and Z91c to the high OCR result of Z73C.

It is observed that each test series has its own distribution. Since the spread of results at each position does not seem to follow in the order of the value of rigidity index, it suggests that excess pore pressure distribution on the piezocone shaft depends on the over consolidation ratio of the soil. This is more pronounced at the cone face and shoulder positions.

The two theoretical solutions estimate the normally consolidated distributions quite well. At the cone face and at the shoulder both theoretical predictions are close to the experimental ones, with Baligh and Levadoux (1980) over estimating slightly. Teh (1987) predicts the cone shoulder distribution for the normally consolidated situation very well. The reverse is true for the mid-sleeve position where Teh (1987) under estimates while Baligh and Levadoux are much closer to the experimental distribution.

In summary, the distribution of excess pore pressure along the piezocone shaft appears to depend upon the over consolidation ratio rather than the rigidity index. The theoretical distributions by Baligh and Levadoux (1980) and Teh (1987) both predict the normally consolidated situation well.

7.3 Over Consolidation Ratio

One of the increasing uses of piezocone data is in the use of the results as a tool for estimating over consolidation ratio. In this programme of research several methods were tested.

$$B_q = \frac{\Delta U}{q_t - \sigma_{v_0}} = f(OCR) \qquad [7.3]$$

$$Q = \frac{q_t - \sigma_{v_0}}{\sigma'_v} = f(OCR) \qquad [7.4]$$

$$\beta = \frac{\Delta U_{Shld}}{\Delta U_{Face}} = f(OCR) \qquad [7.5]$$

$$B_{mi} = \frac{\Delta U_i}{\sigma'_v} = f(OCR) \qquad [7.6]$$

Three of the above factors (B_q Q and β) have already been described in Chapter 6. B_q and Q are discussed further in this section together with pore pressure ratios (B_{mi}) and pore pressure differences (PPD) which are defined in Section 7.3.4.

7.3.1 B_q as indicator of OCR

The merits of this factor over the factors suggested by Smits (1982), Baligh et al (1981), Tumay et al (1981) and Campanella and Robertson (1981) were argued by Wroth (1984) but it is worth noting that Senneset et al (1982) originally suggested B_q should be used in the classification of soils. Also, in their classification table, $B_q = 0.4$ was their dividing point between silty clay and silts. Taking both Senneset et al (1982) and Wroth (1984), it would seem that in clays B_q will vary between 1 and 0.4. The question therefore, is whether or not the variation within this region is a function of over consolidation ratio.

The results illustrated in the previous chapter (Figure 6.47) showed that B_q correlated with over consolidation ratio, albeit with a poor correlation coefficient, up to an OCR of approximately six. At higher OCR's B_q tends asymptotically to a value of approximately 0.4 and therefore, can no longer be expected to correlate with OCR. This is obviously the lower value of B_q for the kaolin used in the programme. Senneset et al (1982) have reported values of B_q less than 0.4 for silts. It might therefore be expected that for a clay with a larger percentage of silts than the kaolin used in this programme, lower values of B_q would occur at higher over consolidation ratios.

7.3.2 Q as indicator of OCR

The parameter Q was shown in Figure 6.58 to correlate very well with OCR. In order to understand this result, it is necessary to break it down into a form where its correlation with OCR can be readily seen.

$$Q = N_{kt}\frac{s_u}{\sigma'_v} \qquad [7.7]$$

Equation 7.7 shows that if N_{kt} were constant, Q would be expected to correlate with OCR because (s_u/σ_v') is known to correlate with OCR in the following form (Houlsby 1988):

$$\frac{s_u}{\sigma_v'} = A(OCR)^{\Lambda} \qquad [7.8]$$

Therefore, Q expressed in a form which allows easy recognition of the type of relationship with OCR would be as follows:

$$Q = AN_{kt}(OCR)^{\Lambda} \qquad [7.9]$$

It is clear from Equation 7.9 that if N_{kt} varies with soil type then Q will also follow the same trend. On the other hand, if Q is found to correlate with OCR, regardless of the soil type, then it would follow that (AN_{kt}) is a constant. This can only be ascertained when more field data have been compared with the laboratory findings being reported in this thesis. For the laboratory situation, the correlation between Q and OCR is given in Equation 6.7, repeated here as Equation 7.10.

$$Q = 2.17(OCR)^{0.69} \qquad [7.10]$$

The values of N_{kt} resulting from this test programme are plotted against their respective over consolidation ratios in Figure 7.6. It is clear that there is no correlation with over consolidation ratio. In fact, it appears to be a constant value of approximately 11 with a lot of

scatter around it. This would give an A value of 0.2. The values of Λ and A in Equation 7.10 compare well with estimates of typical values given by Houlsby (1988) which are 0.8 and 0.25, respectively.

7.3.2.1 Comparison with field results

Three sets of published field data were used for comparison with the laboratory results. Together they represent data from 17 sites in Europe and the Americas. The first set was published by May (1987) for data at Inchinnan in Scotland. Powell et al (1988) published further data from the United Kingdom and Rad and Lunne (1988) data from the rest of Europe and the Americas.

The plasticity indices of the data set reported by Rad and Lunne (1988) ranged from eight at Emmerstad in Norway to 60 at Rio in Brazil. (These places have not been individually named on the combined graph). The plasticity indices in the soils from the United Kingdom ranged from 15 at Inchinnan to 40 at Madingley. The soil at Emmerstad is a silty quick clay while that at Madingley is a very stiff highly over consolidated clay. This provided a good spread of different types of soils. Data from Madingley, Canons Park and Brent Cross fall outside the range of over consolidation ratios considered but they were included in order to see the general trend.

The combined data were presented in Figure 7.7 and the following observations can be made about the results:

a) Laboratory data are in close agreement with field data in the range of over consolidation ratios studied, except for the results from Cowden. This is an indication that the tip resistance factor Q does not depend upon the plasticity index of the soil.

b) Inchinnan and Bothkennar are both in an area of similar geological history (Macgregor and Macgregor 1978). Their stress histories and the reported values of Q reported by different authors are virtually the same.

c) Although data from Canons Park, Madingley and Brent Cross are individually grouped, the laboratory data provides a link between these highly over consolidated clay sites and the normally consolidated clay sites at Bothkennar and Inchinnan.

d) Data from Cowden in Hull appear to be out of step with the rest of the data. However, estimation of pre-consolidation pressure was reported to be difficult to ascertain at this site (NGI 84 223-1). It may well be, therefore, that the OCRs have been underestimated.

7.3.3 B_m as an indicator of OCR

From the distribution of excess pore water pressure around the piezocone shown in Figure 7.5, the results indicate a general trend of increasing normalised excess pore pressures with OCR. It was therefore decided to investigate the correlation of pore pressures at individual locations with OCR.

The excess pore pressures were made non-dimensional by vertical effective stress σ_v'. The resulting parameter was called B_m for the particular location.

$$B_{mi} = \left(\frac{U_i - U_0}{\sigma_v'}\right) = \left(\frac{q_t - \sigma_{v0}}{\sigma_v'}\right)\left(\frac{\Delta U_i}{q_t - \sigma_{v0}}\right) = QB_{qi} \qquad [7.11]$$

As shown in the above equation, B_m is not an independent variable. It is a product of Q and B_q at the particular location of the measured pore pressure. Its relationship with OCR will

therefore be influenced by the two parameters. Since both Q and B_q have a form of correlation with OCR, it can be expected that B_m will also have its own form of correlation with OCR.

The results of this exercise are illustrated in Figures 7.8 and 7.9. Figure 7.8 incorporates the results at the cone face (U_1), mid-sleeve (U_3) and top-sleeve (U_4) pore pressure measuring locations while Figure 7.9 contains results from the cone shoulder position only.

B_m at all four locations shows varying degrees of correlation with OCR. In Figure 7.8, B_m at the cone face produced a better linear correlation (with a coefficient (R^2) of 0.94) than all other locations even though the results of Z7C showed considerable scatter. The correlation equation for this location is as follows:

$$B_{m1} = 0.87(OCR)+1.7 \qquad [7.12]$$

The results at U_3 and U_4 pore pressure measuring locations showed little scatter in the results but their slopes, at 0.24 and 0.14, were too small for their correlations to be used in estimating OCR. At the shoulder, where more tests could be incorporated, there is a definite linear correlation, even though results from three test series caused scatter of data points. The linear equation for the shoulder position with a correlation coefficient of 0.94 is as follows:

$$B_{m2} = 1.5+0.53(OCR) \qquad [7.13]$$

7.3.4 PPD as an indicator of OCR

A method similar to Sully et al (1988), pore pressure difference (PPD), was used as an alternative way of arriving at OCR. The pore pressure differences utilising all four locations on the 5 cm^2 piezocone were tested in a parametric study. The pore pressure differences (U_1-U_2), (U_1-U_3), (U_1-U_4), (U_2-U_3), (U_2-U_4), were all made non-dimensional by the vertical effective stress σ'_v and correlated with OCR. The expressions are as follows:

$$\frac{(U_1-U_2)}{\sigma'_{v0}} = f(OCR) \qquad \frac{(U_2-U_3)}{\sigma'_{v0}} = f(OCR)$$

$$\frac{(U_1-U_3)}{\sigma'_{v0}} = f(OCR) \qquad \frac{(U_2-U_4)}{\sigma'_{v0}} = f(OCR)$$

$$\frac{(U_1-U_4)}{\sigma'_{v0}} = f(OCR) \qquad [7.14]$$

The results of this exercise are illustrated in Figures 7.10 and 7.11. Figure 7.10a illustrates the correlation of the non dimensional pore pressure difference (U_1-U_2) with OCR. There is a lot of scatter in the results of test series Z7C which have the highest OCR. The results in Figures 7.10b and 7.10c for (U_1-U_3) and (U_1-U_4), respectively, also show the same scatter in the non-dimensional pore pressure difference at this high OCR. This scatter in data points in the results of Z7C is reduced when the non-dimensional PPD (U_2-U_3) and (U_2-U_4) are plotted against OCR in Figures 7.11a and 7.11b. This may be an indication that these pore pressure differences are more stable than the ones using the cone face excess pore pressure.

The pore pressure differences using the cone face excess pore pressure have the advantage of being larger than those using the cone shoulder excess pore pressure. Consequently, the slopes of the linear correlation equations are larger. In this respect, the results of (U_1-U_4), shown in Figure 7.10c, with OCR produced the highest slope at 0.74 with a correlation coefficient of 0.94. Of the two pore pressure differences using the cone shoulder, (U_2-U_4) had the best coefficient at 0.94, but the slope was only 0.43 (Figure 7.11b).

These correlations of pore pressure differences are unique to this design of piezocone. They will not be directly comparable with any other piezocone unless the positions of the filter elements are the same. Therefore their use is restricted but the concept can be extended to all piezocones.

7.4 Shear Strength from Piezocone Results

Shear strength from piezocone data has been estimated using the parameter N_{kt} from the bearing capacity relationship

$$q_t = N_{kt} s_u + \sigma_{v_0}$$

$$N_{kt} = \frac{q_t - \sigma_{v_0}}{s_u} \qquad [7.15]$$

N_{kt} was originally expected to be a constant for all clays, but has been found to vary considerably with soil type (Campanella et al, 1983) and rigidity index (Houlsby and Teh, 1988). This makes the prediction of the undrained shear strength (s_u) very difficult because of the difficulties in finding the appropriate rigidity index.

Since $s_u = f(OCR)$, it was also expected that $N_{kt} = f(OCR)$ may also be true. The results from this test programme do not support this premise (see Figure 7.6).

Houlsby and Teh (1988) have suggested an analytical solution for N_{kt} (see Equation 1.17) which requires the rigidity index (I_r). Therefore, in order to make an estimate of shear strength from piezocone data using N_{kt} , one has to have a fair knowledge about the soil under investigation. In such a situation, an estimate for shear strength would not be required if (G/s_u) were known.

This fact leads to the investigation of ways which could lead to shear strength without using N_{kt} directly. Calibration chamber work becomes very useful in such circumstances. Therefore three ways involving the undrained strength ratio were investigated. These were as follows:

a) Undrained strength ratio with OCR relationships,

b) Undrained strength ratio with non-dimensional excess pore pressure (pore pressure ratio) relationships,

c) Tip resistance factor with undrained strength ratio relationships.

7.4.1 Undrained strength ratios with OCR

One correlation that has been proposed by Maine and Kulhawy (1984) and Becker et al (1986) for estimating shear strength is that of the undrained strength ratio with OCR. The over consolidation ratio is estimated from piezocone data and the undrained strength ratio is either read from the graph or calculated from the correlation equation. This is an inexpensive way of arriving at an estimate of shear strength. The over consolidation ratio can be arrived at using any of the methods discussed above.

The results from the this test programme are illustrated in Figure 7.12. There are two sets of results shown in the Figure. Firstly the undrained strength ratio using shear vane results (s_{uv}), and secondly, that using consolidated undrained triaxial shear strengths ($s_{u\,ciu}$). The results from the shear vane are consistently higher than those from the triaxial test and individually they clearly correlate with over consolidation ratio in the range of OCRs considered. There are two shear vane results which clearly do not follow the trend. No explanation for this eas found. Therefore in lightly over consolidated soils, a knowledge of the over consolidation ratio would lead to an estimate of the undrained shear strength.

This fact leads to the investigation of ways which could lead to shear strength without using N_{kt} directly. Calibration chamber work becomes very useful in such circumstances. Therefore three ways involving the undrained strength ratio were investigated. These were as follows:

a) Undrained strength ratio with OCR relationships,

b) Undrained strength ratio with non-dimensional excess pore pressure (pore pressure ratio) relationships,

c) Tip resistance factor with undrained strength ratio relationships.

7.4.1 Undrained strength ratios with OCR

One correlation that has been proposed by Maine and Kulhawy (1984) and Becker et al (1986) for estimating shear strength is that of the undrained strength ratio with OCR. The over consolidation ratio is estimated from piezocone data and the undrained strength ratio is either read from the graph or calculated from the correlation equation. This is an inexpensive way of arriving at an estimate of shear strength. The over consolidation ratio can be arrived at using any of the methods discussed above.

The results from the this test programme are illustrated in Figure 7.12. There are two sets of results shown in the Figure. Firstly the undrained strength ratio using shear vane results (s_{uv}), and secondly, that using consolidated undrained triaxial shear strengths ($s_{u\,ciu}$). The results from the shear vane are consistently higher than those from the triaxial test and individually they clearly correlate with over consolidation ratio in the range of OCRs considered. There are two shear vane results which clearly do not follow the trend. No explanation for this was found. Therefore in lightly over consolidated soils, a knowledge of the over consolidation ratio would lead to an estimate of the undrained shear strength.

7.4.2 Shear strength from excess pore pressure

An attempt was made to correlate shear strength directly with measured excess pore pressures on the piezocone shaft. The theoretical basis stems from the fact that a greater proportion of the excess pore pressure on the shaft is induced by shear stress (Wroth, 1984). Therefore, there was a greater possibility for the excess pore pressure on the shaft to correlate with shear strength.

Both the excess pore pressures and the vane shear strength were made non-dimensional by the vertical effective stress. The results, illustrated in Figure 7.13, were from four test series and the scatter at each series is due to the variation in excess pore pressure only. Apart from the one point which does not follow the trend on the U_4 graph (at an undrained strength ratio of approximately 0.7), the result was very encouraging. The linear function which fitted U_3 data with a correlation coefficient of 0.92 was as follows:

$$\frac{\Delta U_3}{\sigma_v'} = 1.14+1.92\left(\frac{s_{u_v}}{\sigma_v'}\right) \qquad [7.16]$$

The data for U_4 were also fitted with a linear function but the aberrant data point brought the correlation coefficient down to 0.71. When it is taken out of the regression, the correlation coefficient increases to 0.91. The linear function for the latter is presented below:

$$\frac{\Delta U_4}{\sigma_v'} = 0.9+1.11\left(\frac{s_{u_v}}{\sigma_v'}\right) \qquad [7.17]$$

It is apparent from the results that the effect of the location of the pore pressure sensor is important. Clearly the use of this method would require standard positioning of the pore pressure locations. However, the results are very encouraging and ought to be pursued in further research.

7.4.3 Shear strength from Q

Tip resistance is essentially a measure of soil strength. Therefore, correlation with undrained shear strength is, according to the hierarchy suggested by Wroth (1988), a primary correlation. Therefore another correlation examined was that of the tip resistance factor Q with the undrained strength ratio (s_u/σ'_{v0}). It was shown earlier that:

$$Q = \left(\frac{q_t - \sigma_{v_0}}{\sigma'_v}\right) = \left(\frac{q_t - \sigma_{v_0}}{s_u}\right)\left(\frac{s_u}{\sigma'_v}\right) = N_{kt}\left(\frac{s_u}{\sigma'_v}\right) \qquad [7.18]$$

A direct correlation of Q with the undrained strength ratio would bypass the practical need of estimating N_{kt}. It is however. realised that the result will still be influenced by the N_{kt} value of the reference material which, in this case, is kaolin. Since the average value was that of a typical clay soil, the estimate of shear strength would be acceptable.

In order to illustrate the relationship the net tip resistance was first plotted against the shear vane strength in engineering units. These are shown in Figure 7.14. It is clear from the Figure that there is some correlation between the net tip resistance and the shear vane strength albeit with a lot of scatter in data points. The slope of this graph is N_{kt}. The correlation coefficient for the slope was very poor, at 0.65.

The non dimensional form of this relationship is obviously the tip resistance factor Q plotted against the undrained strength ratio s_{uv}/σ'_{v0}. The results of this correlation are illustrated in Figure 7.15. On the Figure there is little scatter of results except for results of Q at two undrained strength ratios. These are 1.43 and 0.69, which are the undrained strength ratios for Z10A and Z5B series. The best correlation equation that fitted all the data was a power function with a correlation coefficient of 0.90, as follows:

$$Q = 9.8\left(\frac{s_{u_v}}{\sigma'_v}\right)^{0.9} \qquad [7.19]$$

Given the scatter of the data points in Figure 7.14, the lack of significant scatter of data points in Figure 7.15 is very encouraging. This result further emphasises the importance of the tip resistance factor Q in the interpretation of piezocone data.

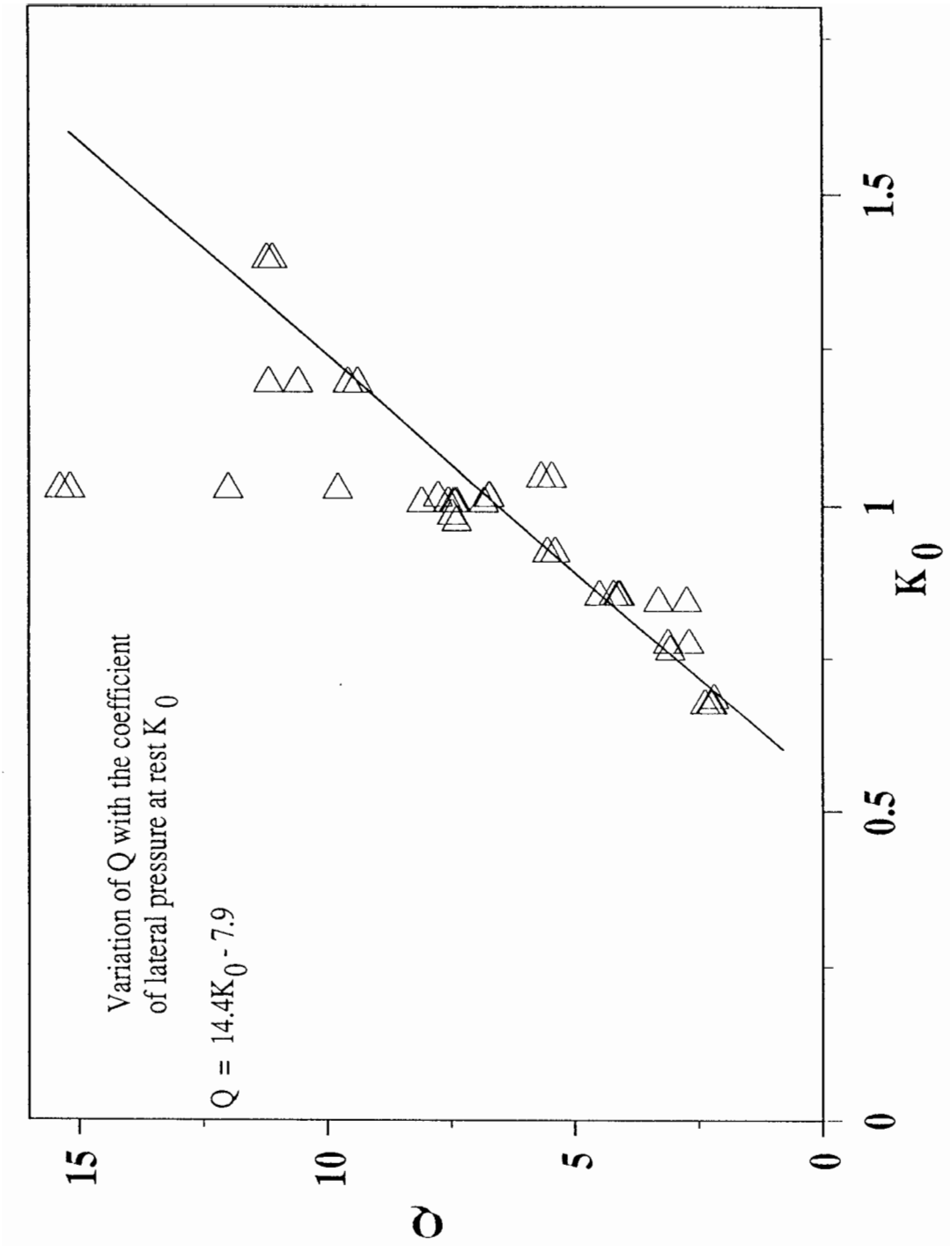

Figure 7.1 The variation of the tip resistance factor Q with the coefficient of lateral earth pressure at rest K_0.

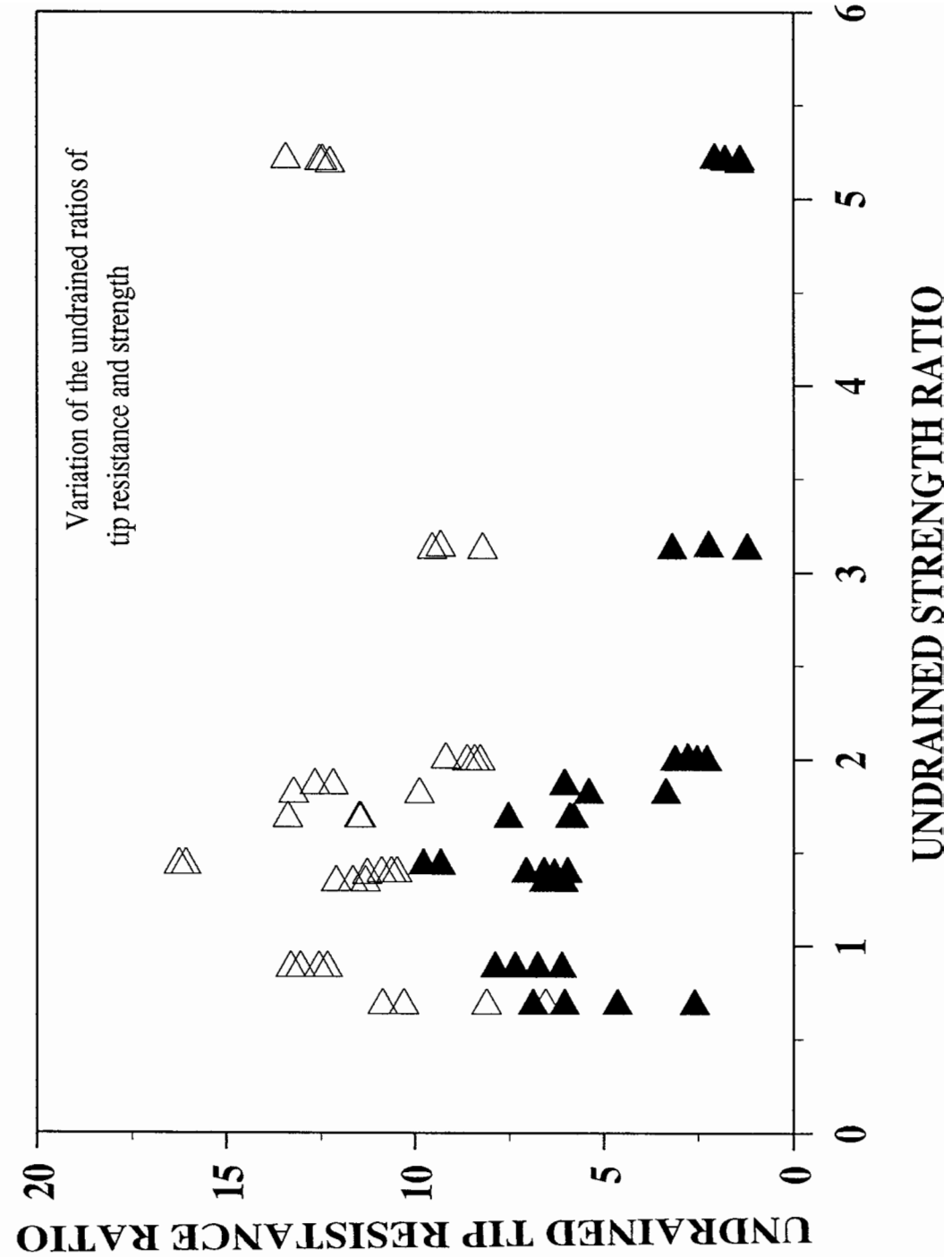

Figure 7.2 The variation of the ratios of undrained tip resistance with undrained strength.

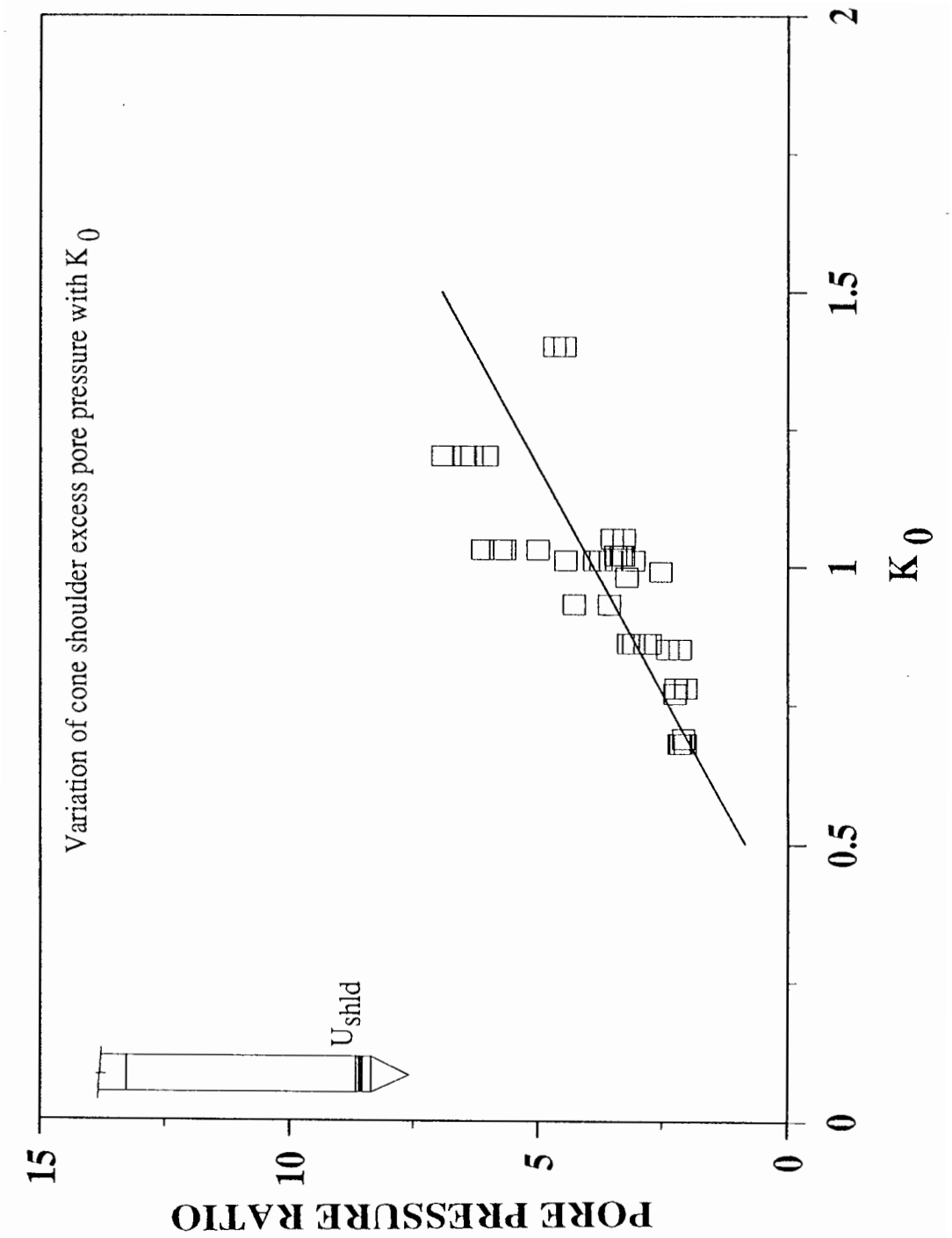

Figure 7.3 The variation of cone shoulder excess pore pressure ratio with the coefficient of lateral earth pressure at rest K_0

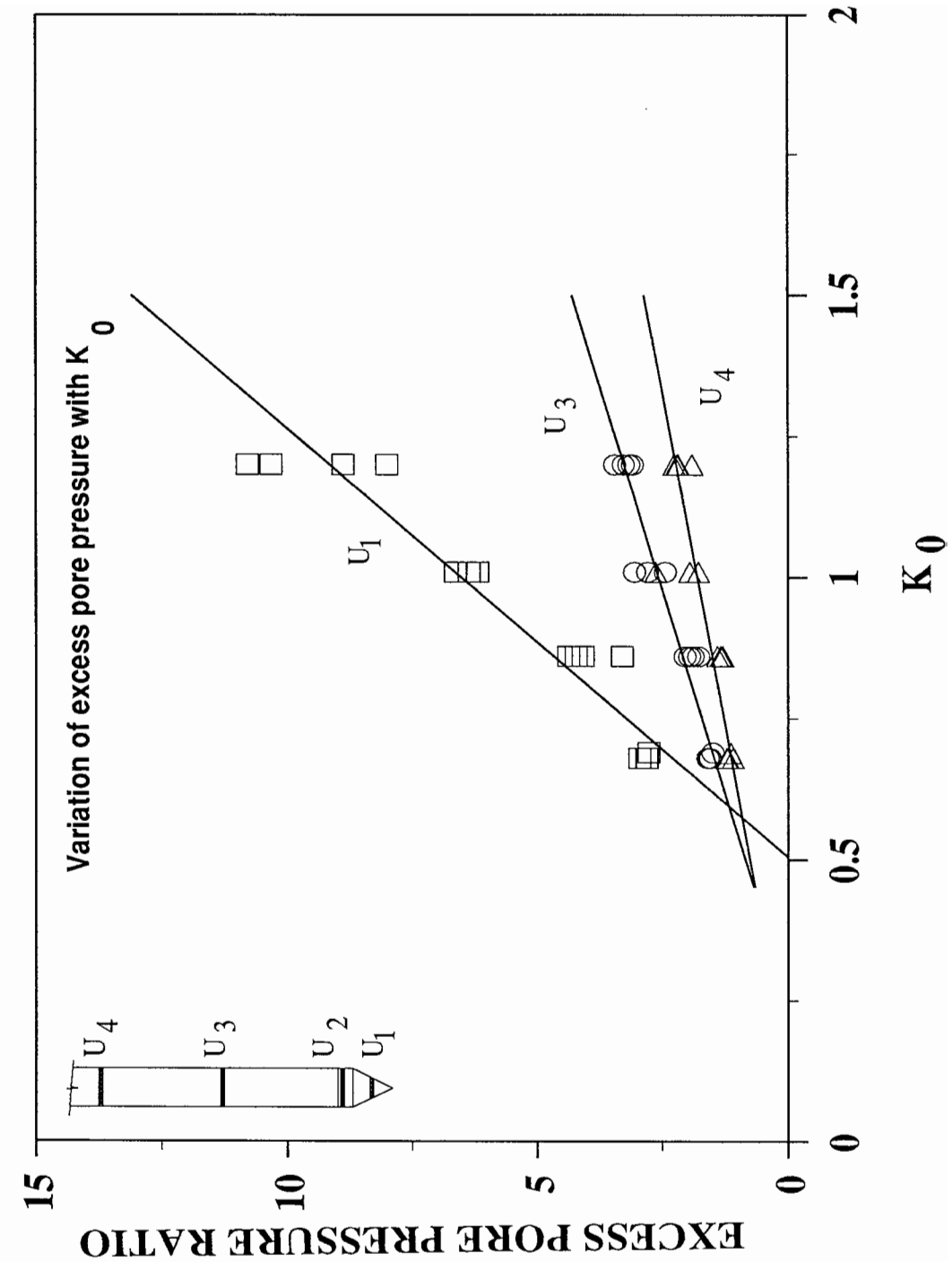

Figure 7.4 The variation of excess pore pressure ratios for $U_1, U_3,$ and U_4 with the coefficient of lateral earth pressure at rest K_0.

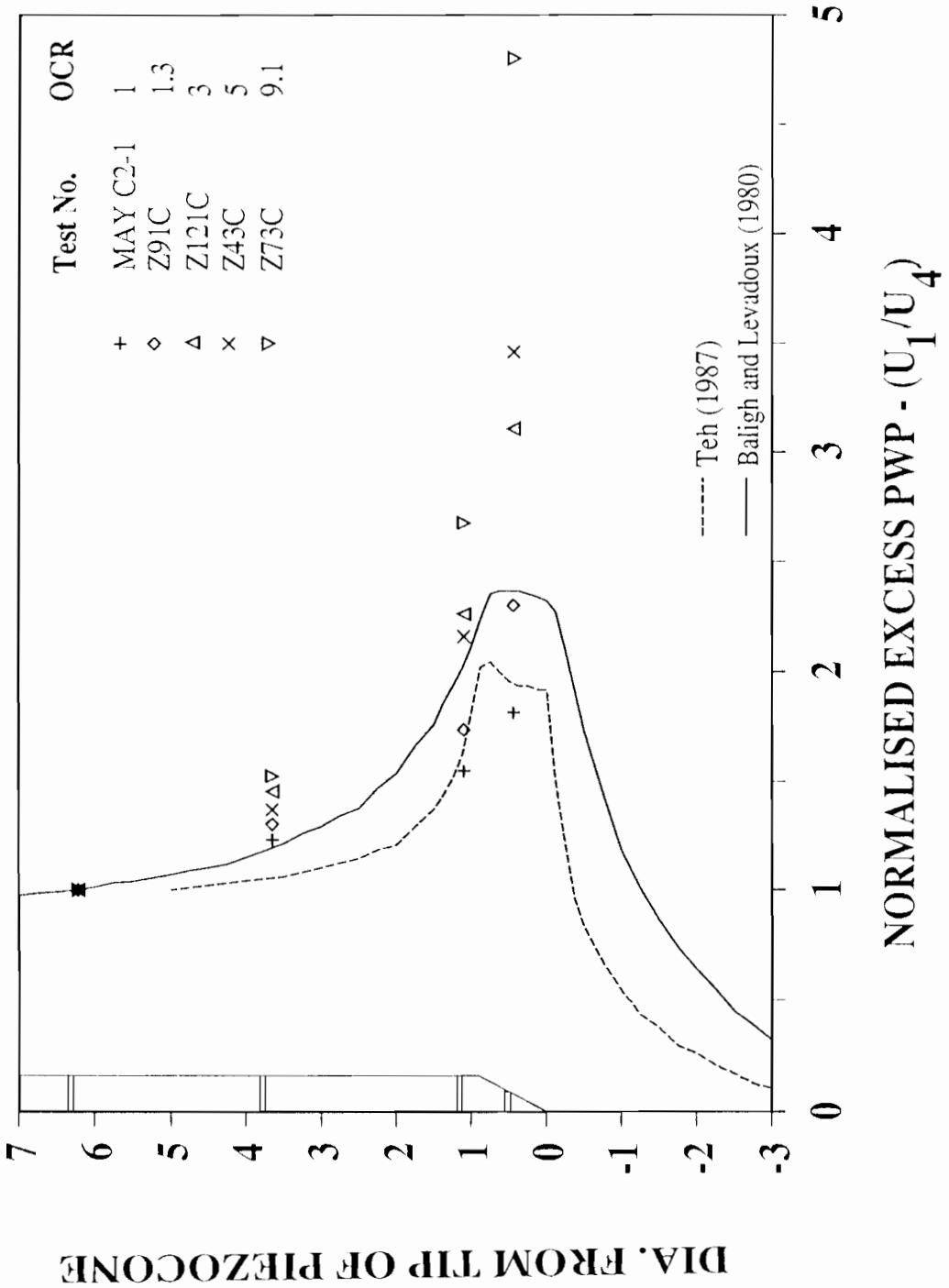

Figure 7.5 The distribution of normalised excess pore pressure along the length of the piezocone.

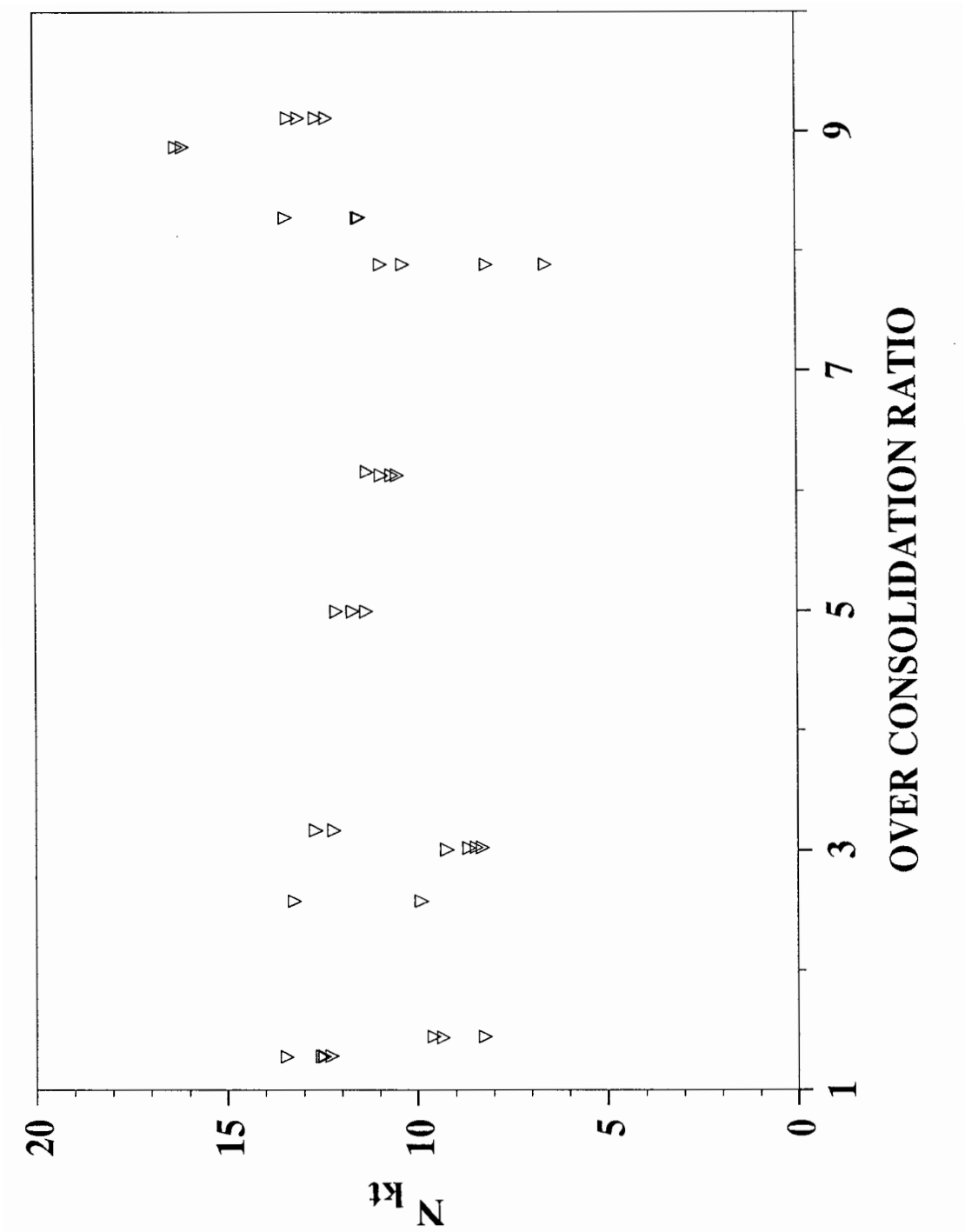

Figure 7.6 The variation of N_{kt} with over consolidation ratio.

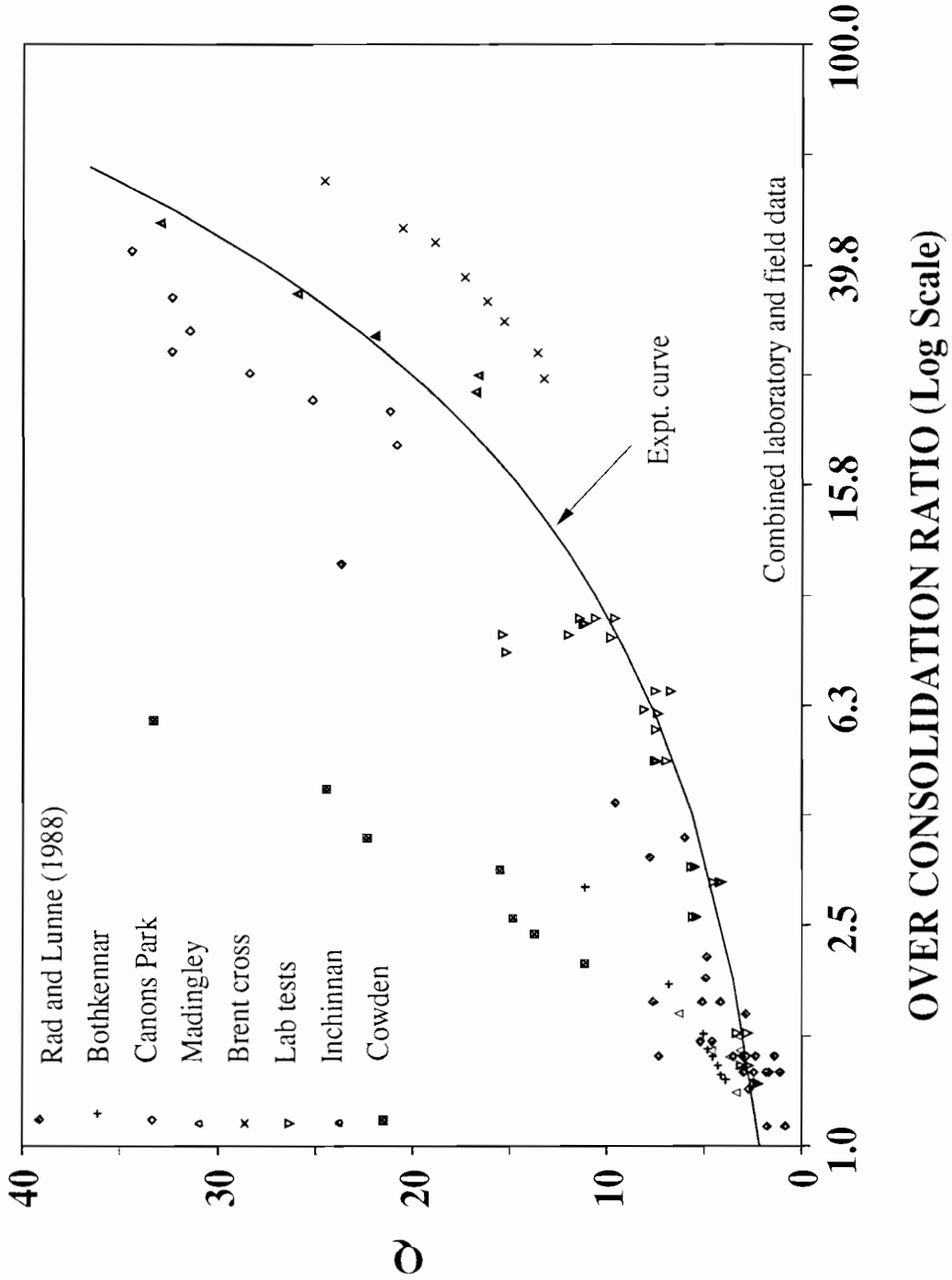

Figure 7.7 Comparison of the tip resistance factor Q between laboratory and field data.

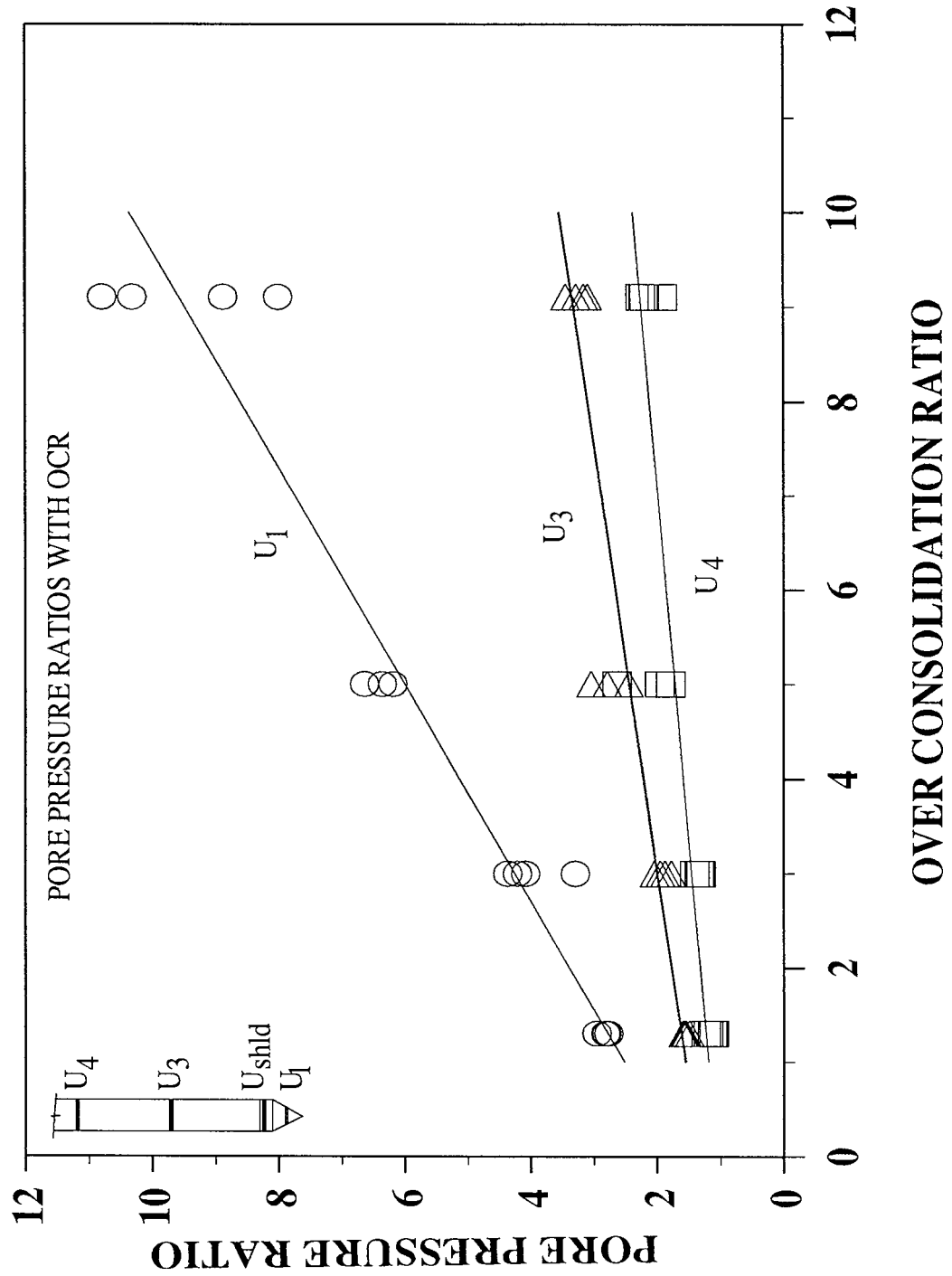

Figure 7.8 The variation of pore pressure ratios for $U_1, U_3,$ andU_4 with overconsolidation ratio.

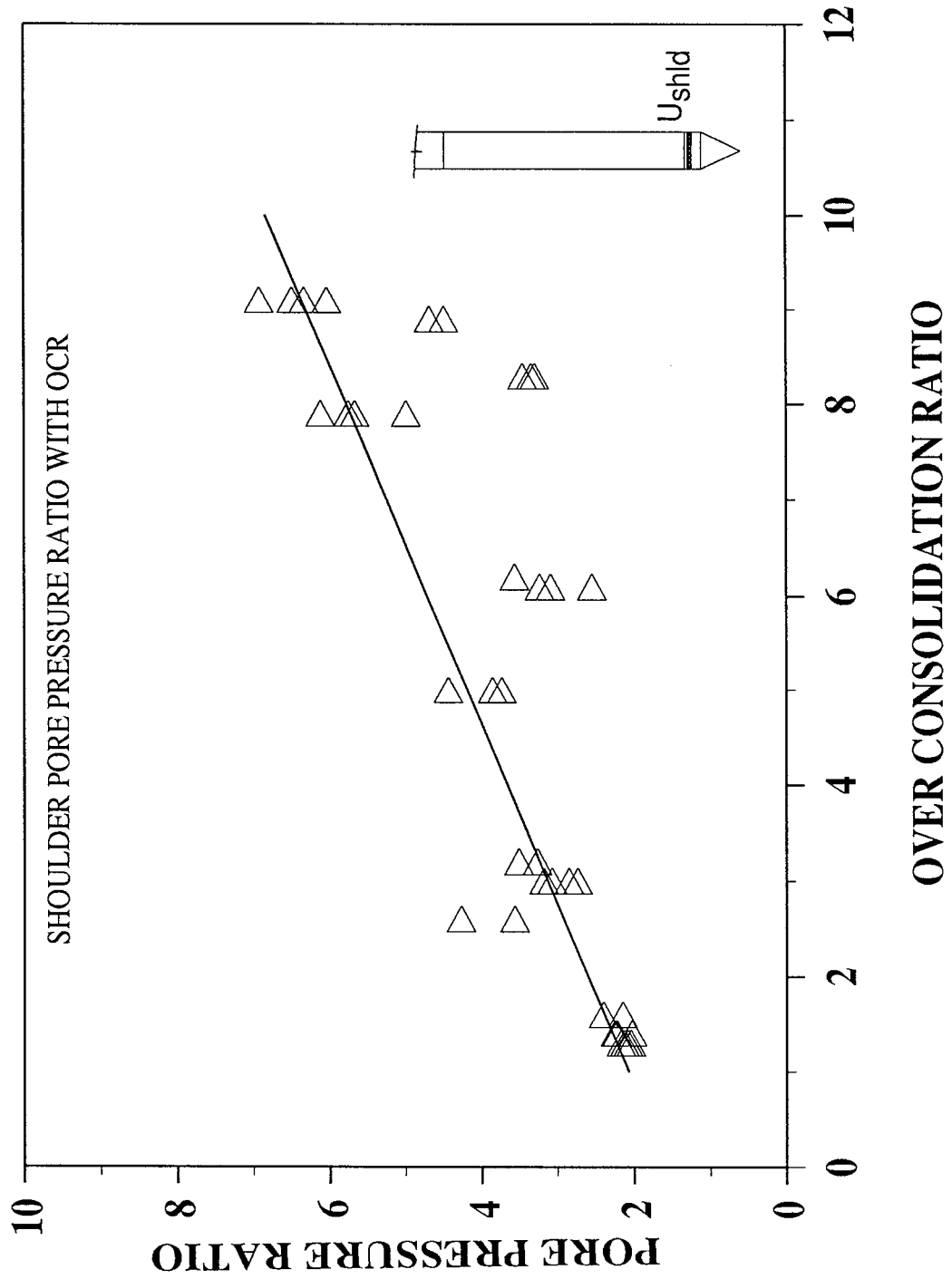

Figure 7.9 The variation of cone shoulder pore pressure ratio with over consolidation ratio.

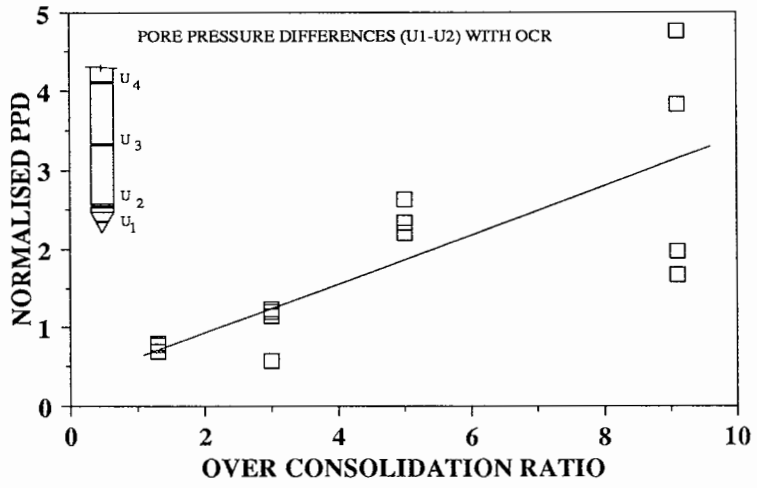

a)

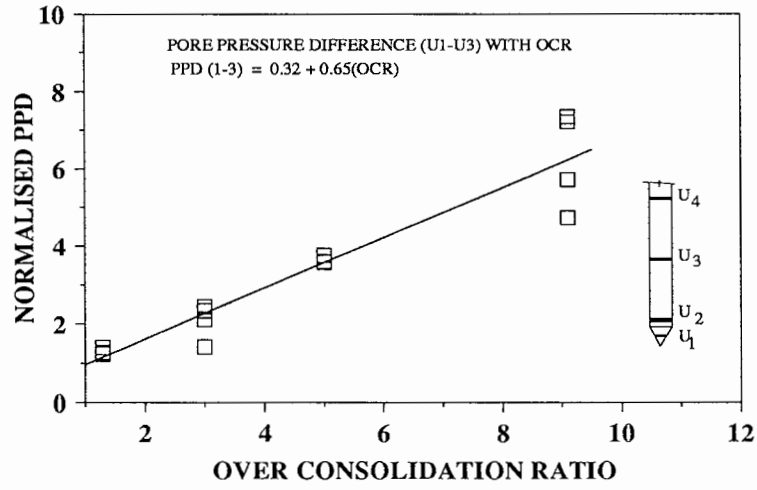

b)

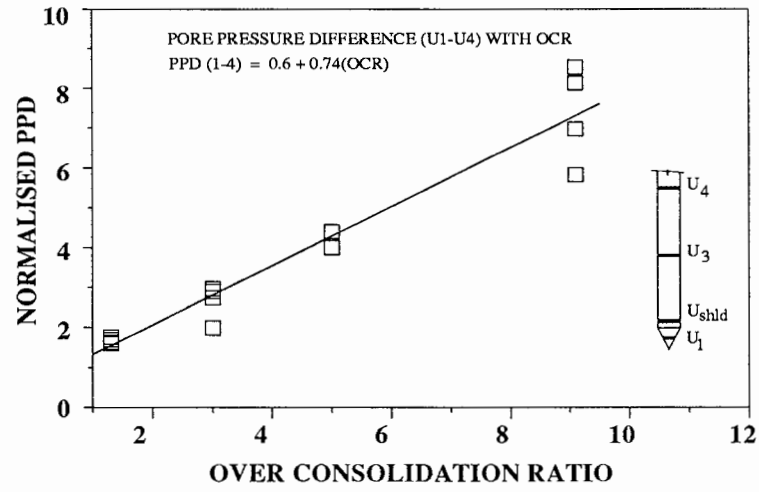

c)

Figure 7.10 The variation of dimensionless pore pressure differences with U_1 against over consolidation ratio.

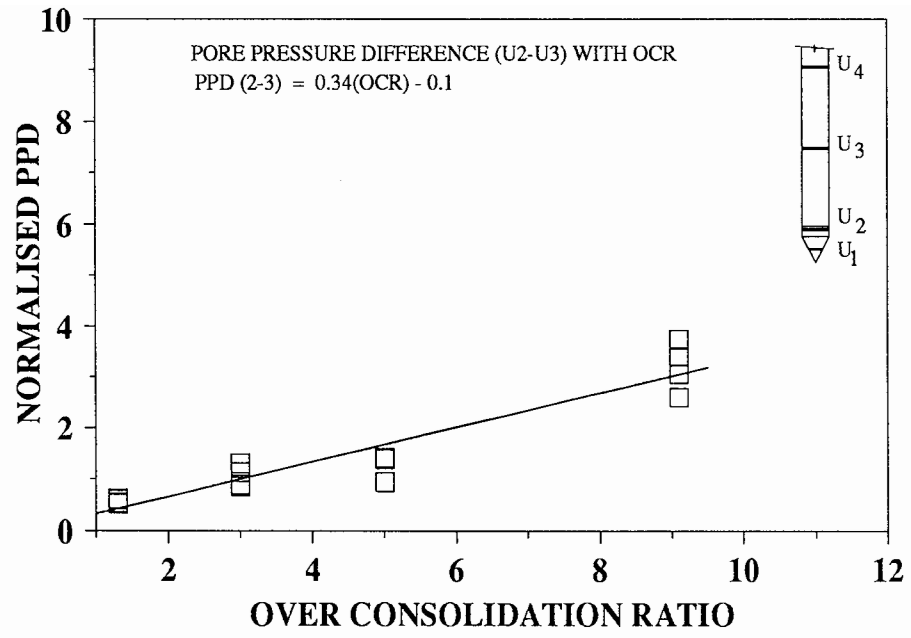

a)

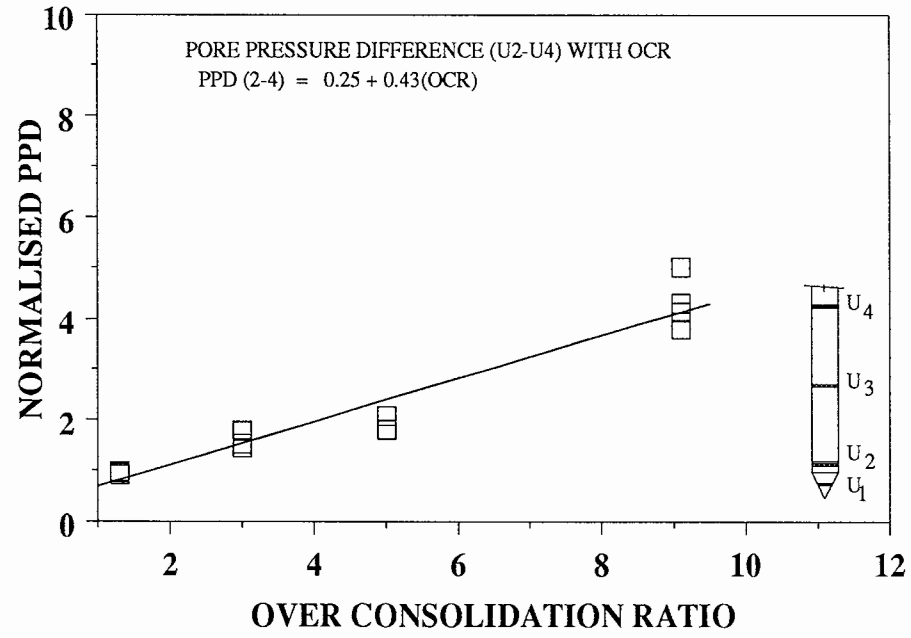

b)

Figure 7.11 The variation of dimensionless pore pressure differences with U_2 against over consolidation ratio.

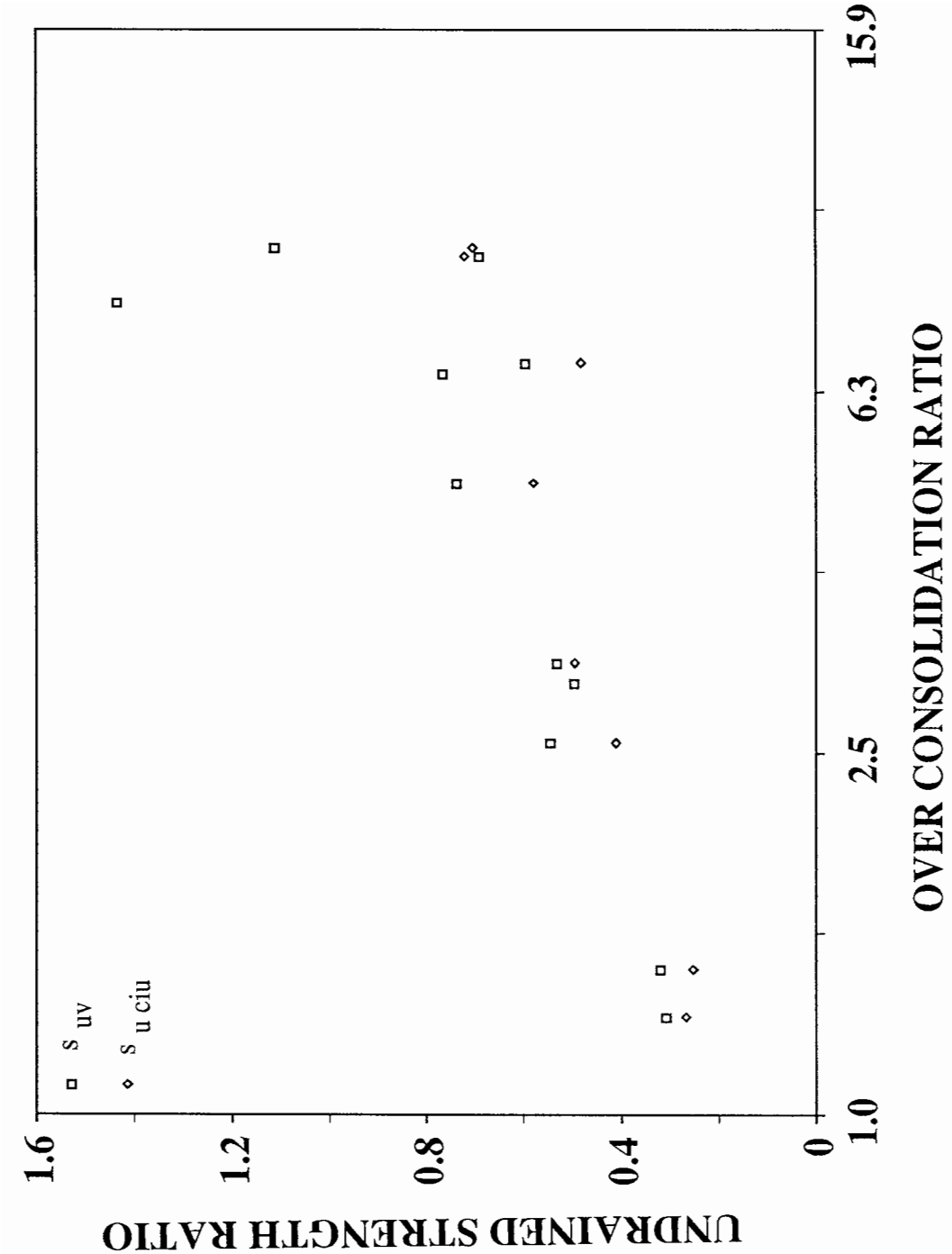

Figure 7.12 The variation of undrained strength ratios with over consolidation ratio.

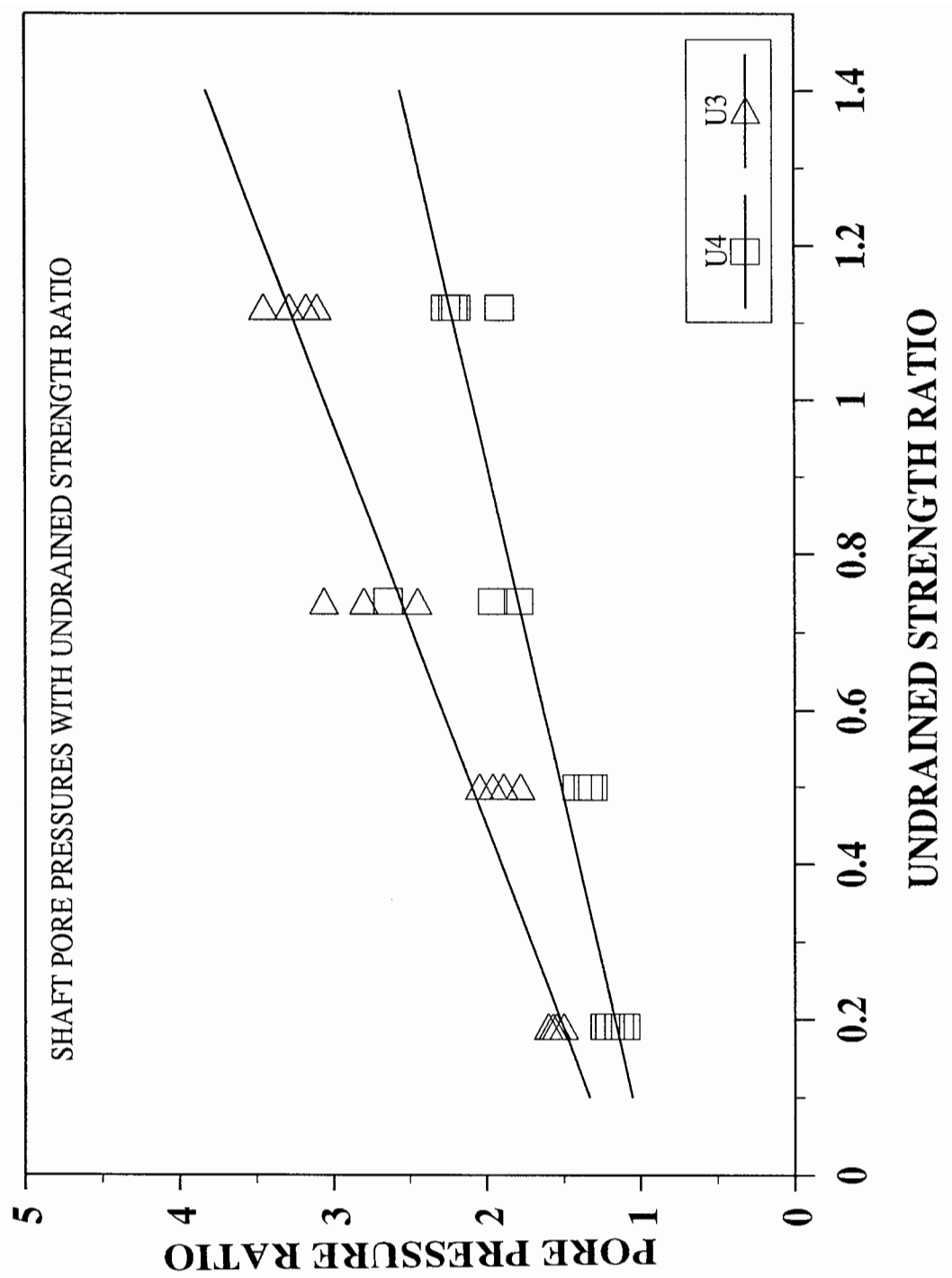

Figure 7.13 The variation of the excess pore pressure ratios on the piezocone shaft with over consolidation ratio.

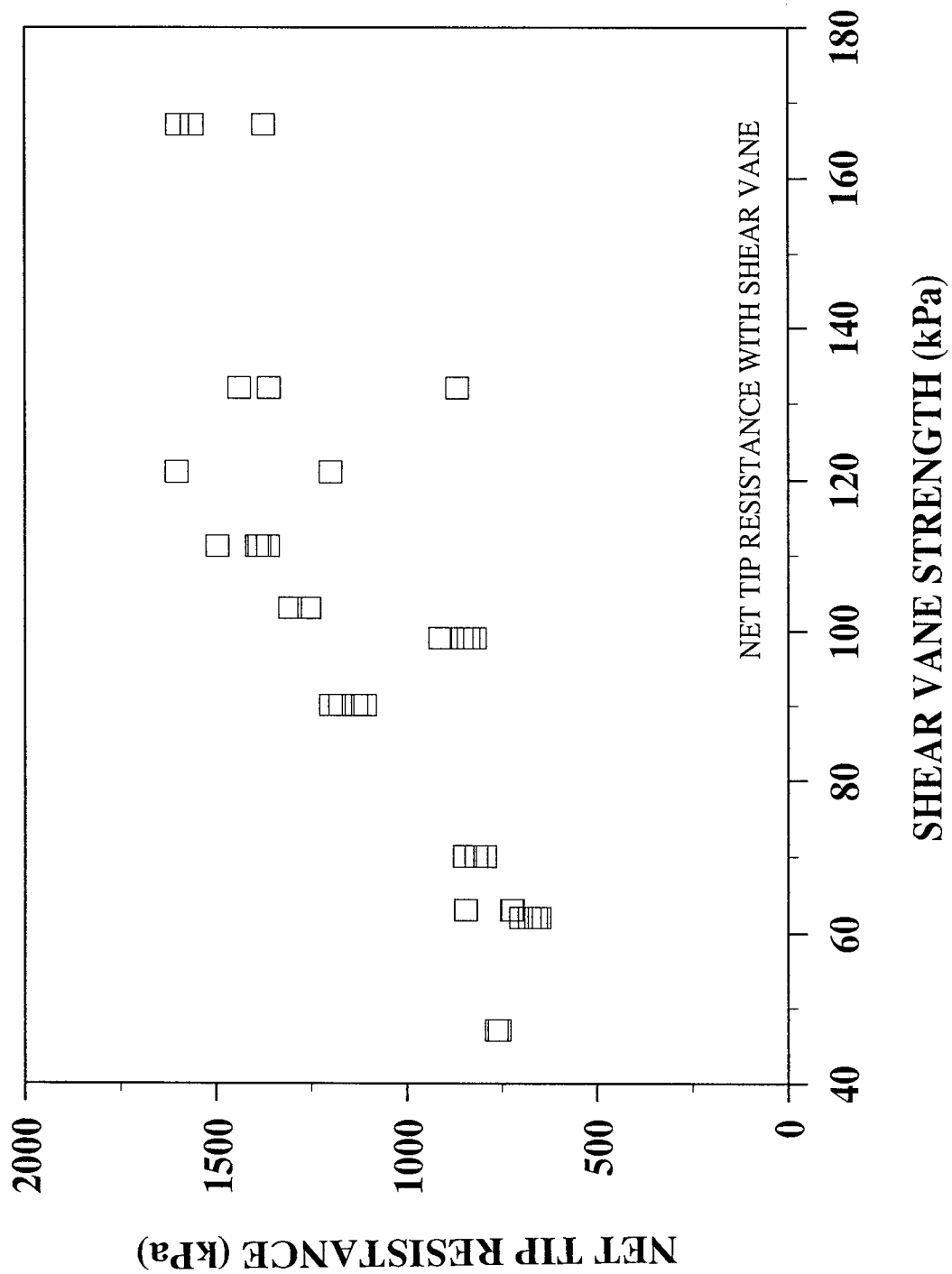

Figure 7.14 The variation of the net tip resistance with shear vane strength.

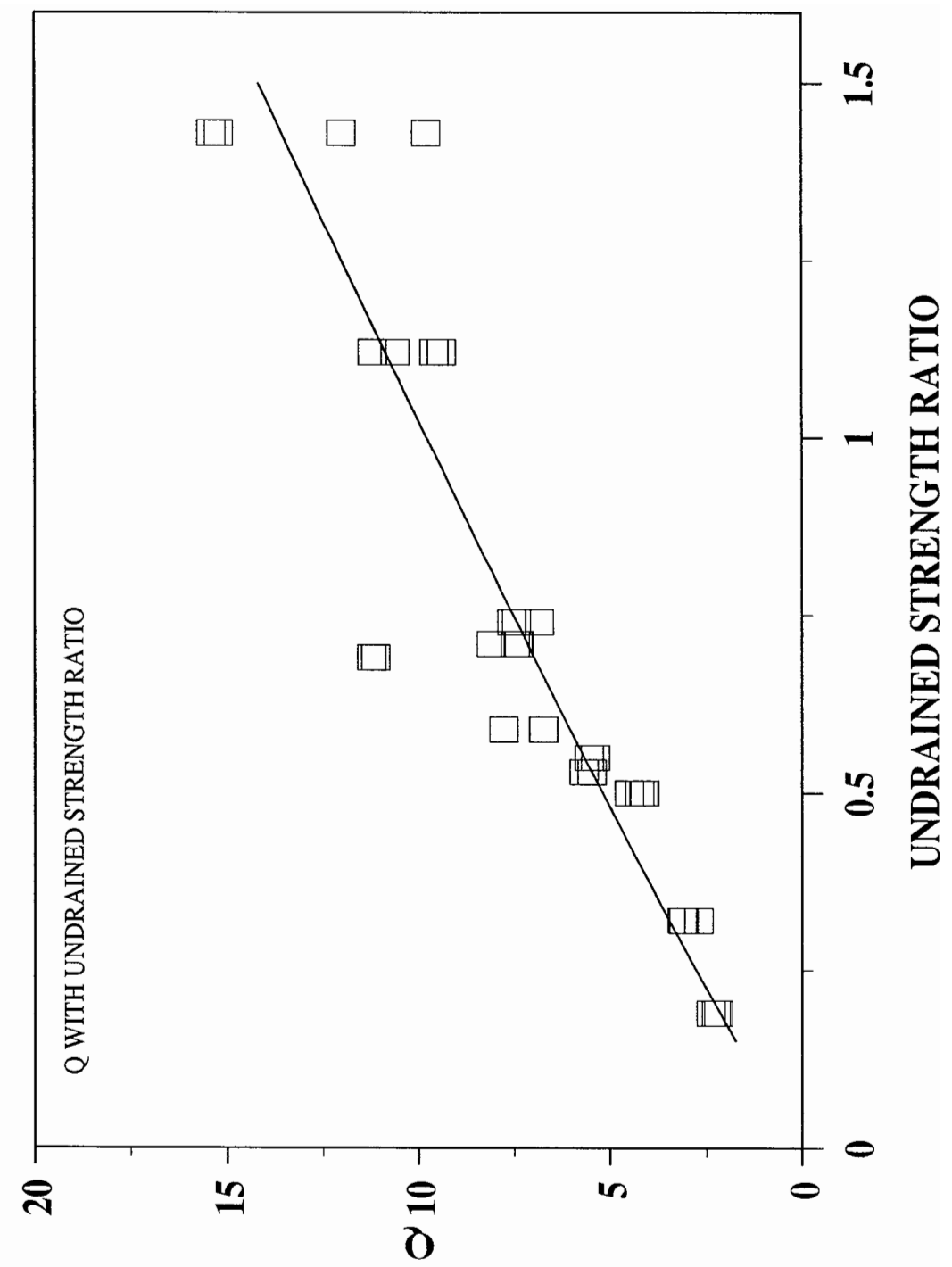

Figure 7.15 The variation of the tip resistance factor Q with the undrained strength ratio.

8 CONCLUDING REMARKS

This thesis has described the experimental programme which examined the behaviour of the piezocone in lightly over consolidated clay. Some important points arising from the programme will be outlined in this chapter in an itemised form. Recommendations for future studies will be stated at the end of the chapter. The relevant chapters or sections are given in square brackets.

8.1 Sample Preparation

The preparation of the kaolin sample was as important as the results which were obtained. Therefore, the following points were taken into account during sample preparation:

a) The consolidation chamber was prepared in advance to receive the kaolin slurry. This involved the calibration of all the transducers attached to the chamber and greasing the side walls and other ancillary parts. [See Chapter 4]

b) The sample was mixed thoroughly over a minimum time of two hours at a moisture content of around 120% to ensure that there were no macro fractures in the soil slurry. During mixing a vacuum was maintained to ensure the removal of any entrained air in the slurry. During the transportation of the slurry from the mixer to the consolidation chamber, care was taken not to get air into the thoroughly prepared slurry. [See Chapter 4]

During the consolidation and swelling of the sample, the following points were taken into account:

a) The pore pressure gradient across the sample was kept to a minimum to reduce the likelihood of crust formation at the drained ends of the sample, which would have lead to non uniform consolidation of the sample and probably increased the consolidation time. A flow restrictor, placed in the drainage line, away from the sample, ensured that the point of zero excess pore pressure was well removed from the filters on the consolidating sample. [See Chapter 4]

b) Where an over consolidated sample was required, care was taken to ensure that there was no risk of cavitation in the sample during unloading. This was done by either unloading in steps of 50 to 60 kPa and allowing excess pore pressure to equilibrate between steps or by a controlled slow unloading which did not allow a large build up of negative pore pressure. [See Chapter 4]

8.2 Testing Equipment

The calibre of the results from any testing equipment depends on how well it is prepared for the particular task and how much is known about the effect of individual components on the measurements made by the particular equipment. To this effect, the calibration of the piezocone, the shear vane, the transducers mentioned above, the flow pump apparatus and other measuring and recording instruments used, was of paramount importance during the test programme.

An important finding with the piezocone was that the α factor, also known as the (1-a) factor, which depends upon its geometry at the groove, seems also to depend upon its physical assembly and the state of repair of its components. The factor was determined during the calibration of the piezocone before each series of tests. [See Section 3.1.5]

The importance of the measurement of pore pressure at the position suitable for the determination of the α factor cannot be over emphasised. In the piezocones used in this study, as is the case with other piezocones, this is the cone shoulder position. [See Section 1.2]

8.3 Sample Quality

The tests for quality of the samples prepared for penetration testing were the variability of the shear vane strengths with depth and the distribution of moisture content in the sample. The

tests showed that the variability of shear strength and moisture content in the samples was insignificant. Therefore the samples prepared had uniform properties and were thereby suitable for the purposes of this penetration testing programme. [See Section 6.1]

8.4 Tip Resistance

Tip resistance results in each series were found to be repeatable from all the four testing positions. This implies that the boundary effects were equally felt at all the testing positions. [See Section 6.4]

The net tip resistance $(q_t - \sigma_{v0})$ made non dimensional by σ'_{v0} was found to be highly influenced by the vertical effective stress ratio (over consolidation ratio) and the coefficient of lateral stress at rest (K_0). The non dimensional net tip resistance is the tip resistance factor Q. The correlation equations are repeated below:

$$Q = 2.17(OCR)^{0.69} \qquad [8.1]$$

$$Q = 14.4K_0 - 7.9 \qquad [8.2]$$

With the results above, both the over consolidation ratio and the coefficient of lateral stress at rest may be estimated from piezocone data. There was no direct correlation between the net tip resistance and the vertical effective stress. [See Section 7.1]

8.5 Excess Pore Pressure

The generated excess pore pressure on the cone face and the piezocone shaft were found to correlate directly with the vertical effective stress ratio (OCR) and the coefficient of lateral earth pressure. [See Section 7.2]

The distribution of excess pore pressure along the shaft of the piezocone was found to depend upon the over consolidation ratio. [See Section 7.2.1]

During and after penetration, high localised pore pressure gradients were set up by the large excess pore pressure differences between the cone face and the other positions on the piezocone shaft. These appear to induce the migration of pore water up the shaft which caused increases in excess pore pressure. This increase was clearly seen in the early stages of dissipation of excess pore at positions well above the cone shoulder. [See Sections 6.5.1 and 6.9]

In the evaluation of the coefficient of consolidation c_h, from the dissipation of excess pore pressure at different pore pressure measurement locations, the solutions by Teh (1987) were found to yield values closer to those obtained from restricted flow consolidation and permeability tests. This result emphasises the influence of the rigidity index on dissipation solutions. [See Section 6.9.2]

8.6 Over Consolidation Ratio

Several methods of estimating over consolidation ratio from piezocone data were tested in the programme. These are summarised below:

a) The pore pressure factor B_q correlated, albeit poorly, with over consolidation ratios up to six, after which the factor seems to tend asymptotically to a value of approximately 0.4. [See Section 7.3.1]

b) The β factor correlates directly with over consolidation ratio. The constant of proportionality for its power function is small (-0.074) and negative. Since a small change

in β results in a large change in over consolidation ratio, the factor may not be expected to provide reliable predictions of OCR. [See Section 6.7]

c) The tip resistance factor Q has a direct correlation with over consolidation ratio. The power function which fitted laboratory results is given in Equation 7.10. Field data from more than 12 sites with different plasticity indices were found to agree with the laboratory data in the ranges of over consolidation ratios considered. [See Section 7.3.2]

d) The excess pore pressures at all the four measuring positions were found to correlate with over consolidation ratio through a factor (excess pore pressure ratio) called B_{mi}. At the cone face and cone shoulder, the factor was found to be more promising for estimation of over consolidation ratio. [See Section 7.3.3]

e) A parametric study of the re-defined pore pressure difference method reported by Sully et al (1988) showed workable correlations with over consolidation ratio using the pore pressure differences from any position on the piezocone. [See Section 7.3.4]

8.7 Shear Strength

An attempt to find direct correlations between shear strength and measured parameters on the piezocone yielded the following results:

a) The excess pore pressure on the piezocone shaft which is partly generated by the shear stresses in that area, was found to correlate directly with the undrained shear strength. [See Section 7.4.2]

b) The tip resistance factor Q was also found to have a direct correlation with the undrained shear strength. [See Section 7.4.3]

These direct correlations with over consolidation ratio, if confirmed by further research, would provide a quick estimation of undrained shear strength from piezocone data.

8.8 Recommendation for Future Research

The work described in this thesis has yielded interesting results which has led to an improved understanding of the interpretation of piezocone data in lightly over consolidated clay.

Although comparisons with field data have been made, it is important that the next stage of the work be continued in the field to verify the laboratory results. As a recommendation, the 5 cm^2 piezocone should be taken to:

a) Bothkennar. This is a normally consolidated site and the data from here would supplement that from Inchinnan (May 1987), which is of similar stress history.

b) Madingley. This is a highly over consolidated stiff clay site which would provide data at the upper end of the over consolidation ratio spectrum

c) a site not yet known which would provide the lightly over consolidated range of data.

Bothkennar and Madingley have been recommended here because they are test sites and the soil properties are well known.

9 REFERENCES

ALMEIDA M.S.S. and PARRY R.H.G. (1985). Small cone petrometer tests and piezocone tests in laboratory consolidated clays. *Geotechnical Testing Journal.* GTJODJ, Vol. 8, No. 1.

BALIGH M.M., LADD C.C. and VIVATRAT V. (1980). Cone penetration in profiling. *Jounal of the Geotechnical Engineering Division,* ASCE.

BALIGH M.M. and LEVADOUX J.N. (1980). Pore pressure dissipation after cone penetration. *MIT Research Report.* MITSG: 80-11.

BATTAGLIO M., JAMIOLKOWSKI M., LANCELLOTTA R. and MANISCALCO R. (1981). Piezometer probe in cohesive deposits. *Proc. of ASCE Special Conference on Cone Penetration Testing and Experience.* St Louis.

BECKER D.E., CROOKS J.H.A. and BEEN K. (1987). Interpretation of the vane test in terms of in-situ yield stresses. *Proc. of ASTM International Symposium on Laboratory and Field Vane Shear Strength Testing.* Tampa, Florida.

BEGEMANN H.K.S.Ph. (1963). The use of static soil penetrometer in Holland. *N.Z. Engineering.*

BISHOP A.W., KUMAPLEY N.K. and EL-RUWAYIH A. (1975). The influence of pore-water tension on the strength of clay. *Phil. Trans. Royal Society,* Vol. 278.

BOND A.J. (1988). Discussion on piezocone testing. *Proc. of the Geotechnology Conference on Penetration Testing in the U.K.* Birmingham.

BOND A.J. and JARDINE R.J. (1989). Instruments of measuring the effective stresses on a pile jacked into over consolidated clay. *Proc. of Conf. on Instrumentation in Geotechnical Engineering,* Nottingham.

BRENNER R.P. AND PANICHPATANANON S. (1982). Predictions of pile behaviour from Dutch cone soundings in Bangkok clay. *Proc. of ESOPT 2,* Vol 2. Amsterdam.

BRITISH STANDARD 1377 (1975). Methods of tests for soils for Civil Engineering purposes. *British Standards Institution,* London.

BROUG N.W.A. (1982). The analysis of the cone reistance, q_c and sleeve resistance, f_s as interactive stresses, resulting in a new pile bearing capacity design method. *Proc. of ESOPT 2,* Vol 2. Amsterdam.

BUSTAMANTE M and GIANESELLI L. (1982). Pile bearing capacity predictions by means of static penetrometer CPT. *Proc. of ESOPT 2.* Amsterdam, Vol. 2.

CAMPANELLA R.G., ROBERTSON P.K. and GILLESPIE D. (1981). In-situ testing in saturated silt. *Proc. 34th Canadian Geotechnical Conference.*

CAMPANELLA R.G., ROBERTSON P.K. and GILLESPIE D. (1983). Cone penetration testing in deltaic soils. *Canadian Geotechnical Journal.* Vol. 20.

CAMPANELLA R.G., SULLY J.P. and ROBERTSON P.K. (1988). Interpretation of piezocone soundings in clay - a case history. *Proc. of the Geotechnology Conference on Penetration Testing in the UK,* Birmingham.

CHEN P.K. and BASSETT R.H. (1988). The implications of observed deformations during cone penetration. *Proc. of the Geotechnology Conference on Penetration Testing in the U.K.* Birmingham.

COUTTS J.S. (1986). Correlation between piezocone results and laboratory data from six test locations. *MSc dissertation.* University of Surrey.

D'APPOLONIA D., POULOS H. and LADD C.C. (1971). Initial settlement of structures on clay. *Journal of Soil Mechanics and Foundations Division.* ASCE. Vol. 97. No. SM10.

DAVIES E.H. and POULOS H.G. (1970). An analysis of consolidation theories: A discussion. *Journal of Soil Mechanics and Foundations Division.* ASCE, Vol. 96.

DE BEER E.E., GOELEN E., HEYNEN W.J. and JOUSTRA K. (1988). Cone penetration test (CPT): International reference test procedure. *Proc. of ISOPT 1*, Orlando.

FANNIN J. (1986). Geodrid reinforcement of granular layers on soft clay - A study at model and full scale. *D.Phil. thesis,* Oxford University.

HEIJNEN W.J. (1974). Pentration testing in Netherlands. State of the art report. *Proc. of ESOPT 1*, Vol. 1.

HENDERSON T. (1987). Field measurements to examine the effects of scale and location of pore pressure in the piezocone. *Cooling Prize*, British Geotechnical Society.

HIGHT D.W., GENS A. and JARDINE R.J. (1985). Evaluation of geotechnical parameters from triaxial tests on offshore clay. *Offshore site investigation 1985, International Conference of the Society for Underwater Technology,* London.

HOULSBY G.T. (1986). Private communication.

HOULSBY G.T. and HITCHMAN R. (1988). Calibration chamber tests of a cone penetrometer in sand. *Geotechnique*, Vol. 38, No. 1.

HOULSBY G.T (1988). Introduction to papers on piezocone testing. *Proc. of the Geotechnology Conference on Penetration Testing in the U.K.* Birmingham.

ISSMFE (1977) *International Symposium for Soil Mechanics and Foundation Engineering*, Tokyo.

JAMIOLKOWSKI M., LADD C.C., GERMAINE J.T. and LANCELLOTTA R. (1985) New developments in field and laboratory testing of soils. *Proc. of 11th ICSMFE,* San Francisco.

JONES G.A. and RUST E. (1982). Piezometer penetration testing CUPT. *Proc. of ESOPT 2,* Amsterdam Vol 2.

KEAVENY J. and MITCHELL J.K. (1986). Strength of fine grained soils using the piezocone. *Proc. In-situ testing in Geotechnical Engineering.* ASCE Specialty publication No. 6. VPI Blacksburg V.A.

KIRKPATRICK W.M. and KAHN A.J. (1984). The influence of stress relief on the vane strength of clays. *Geotechnique*, Vol. 34, No. 3.

KIRKPATRICK W.M. and KAHN A.J. (1984). The reaction of clays to sampling stress relief. *Geotechnique*, Vol. 34, No. 1.

KONRAD J.M. and LAW K.T. (1987). Preconsolidation pressure from piezocone tests in marine clays. *Geotechnique* Vol 37 No. 2.

LOVE J.P. (1984). Model testing of geogrids. *D.Phil. thesis,* Oxford University.

LUNNE T., EIDSMOEN T., GILLESPIE D. and HOWLAND J.D. (1986). Laboratory and field evaluation of cone penetrometers. *Proc. of In Situ '86, GT Div., ASCE.* Blacksburg, Virginia.

LUTENEGGER A.J. and KABIR M.G. (1988). Interpretation of piezocone results in over consolidated clays. *Proc. of the Geotechnology Conference on Penetration Testing in the U.K.* Birmingham.

MacGREGOR M. and MacGREGOR A.G. (1978). *The midland valley of Scotland.* British regional geology, NERC, IGS, HMSO, Edinburgh

MAIR R.J. (1979). Centrifugal modelling of tunnel construction in soft clay. *Ph.D. thesis,* University of Cambridge.

MAY R.E. (1987). A study of the piezocone penetrometer in normally consolidated clay. *D.Phil Thesis.* Oxford University.

MAYNE P.W. (1986). CPT indexing of in-situ OCR in clays. *Proc. of In Situ '86, GT Div., ASCE.* Blacksburg, Virginia.

MAYNE P.W. (1988). Determining OCR in clays from laboratory strength. *Journal of Geotechnical Engineering.* Vol. 114, No. 1.

MAYNE P.W. and BACHUS R.C. (1988). Profiling OCR in clays by piezocone soundings. *Proc. of ISOPT 1.* Orlando.

MAYNE P.W. and KULHAWY F.H. (1982). K_0 - OCR relationships in soils. *Journal of Geotechnical Engineering.* ASCE.

MILLIGAN G. (1987). Private communication.

NAGESWARAN S. and HOULSBY G.T. (1982). Astudy of consolidation with radial drainage. *Oxford University Engineering Laboratory Soil Mechanics Note.* SM036/82.

NYIRENDA Z.M. and SILLS G.C. (1988). Discussion on piezocone testing. *Proc. of the Geotechnology Conference on Penetration Testing in the U.K.* Birmingham.

OLSEN R.E., NICHOLS R.W. and RICE T.L. (1985). Low gradient permeability measurements in a triaxial system. *Geotechnique,* Vol. 35, No. 2.

PAREZ L., BACHELIER M. and SECHET B. (1976). Pore pressure generated during penetration of the cone. *Proc. of 6th ICSMFE,* Vienna Vol 3.

POWELL J.J.M., QUARTERMAN R.S.T. and LUNNE T. (1988). Interpretation and use of the piezocone test in U.K. clays. *Proc. of the Geotechnology Conference on Penetration Testing in the U.K.* Birmingham.

POWELL J.J.M. (1988). Discussion on piezocone testing. *Proc. of the Geotechnology Conference on Penetration Testing in the U.K.* Birmingham.

POWELL J.J.M. (1989). Private communication.

RAD N.S and LUNNE T. (1988). Direct correlations between piezocone test results and undrained shear strength of clay. *Proc. of ISOPT 1*. Orlando.

RANDOLPH M.F., CARTER J.P. and WROTH C.P. (1979). Driven piles in clay - The effects of installation and subsequent consolidation. *Geotechnique*, Vol 29 No. 4.

RANDOLPH M.F. and WROTH C.P. (1979). An analytical solution for for the consolidation around a driven pile. *International Journal for Numerical and Analytical Methods in Geomechanics*, Vol 3.

RICHARDS A.F., OLEN K., KELLER G.H., and LAI J.Y. (1975). Differential piezometer probe for in situ measurement of sea-floor pore pressure. *Geotechnique* Vol 25 No. 2.

RIGDEN W.J., THORBURN S., MARSLAND A. and QUARTERMAN R.S.T. (1982). A dual load range cone penetrometer. *Proc. of ESOPT 2*. Amsterdam. Vol. 2.

ROBERTSON P.K., CAMPANELLA R.G., GILLESPIE D. and GREIG J. (1986). Use of piezometer cone data. *Proc. of In Situ '86, GT Div., ASCE*. Blacksburg, Virginia.

ROBERTSON P.K. (1988). Discussion on piezocone testing. *Proc. of the Geotechnology Conference on Penetration Testing in the U.K.* Birmingham.

ROBERTSON P.K. and CAMPANELLA R.G. (1984). Guidelines for the use and interpretation of the electronic cone penetration tests. *Soil Mechanics Series No.69, Department of Civil Engineering*. University of British Columbia.

SAGASETA C. (1984). From unpublished work done while on sabbatical leave at Oxford University.

SANGLERAT G. (1972). The penetrometer and soil exploration. *Developments in Geotechnical Engineering 1*. Elsevier Publishing Company.

SCHMERTMANN J.H. (1969). Dutch friction cone penetrometer exploration of the research area at field 5, Elgin Air Force Base, Florida. *Report S-69-4, U.S. Army Engineering Waterways Experimentation Station.* Vicksberg.

SCHMERTMANN J.H. (1974). General discussion. *Proc. of ESOPT1*, Vol 2.

SENNESET K., JANBU N. and SVANO G. (1982). Strength and deformation parameters from cone penetration tests. *Proc. of ESOPT 2*, Amsterdam.

SENNESET K. and JANBU N. (1984). Shear strength parameters obtained from static cone penetration tests. *A-84-1*, Institute of Geotechnics and Foundation Engineering, Norwegian Institute of Technology, Trondheim.

SILLS G.C., ALMEIDA M.S.S. and DANZIGER F.A.B. (1988a). Coefficient of consolidation from piezocone dissipation tests in very soft clays. *Proc. of ISOPT 1*. Orlando.

SILLS G.C., HOARE S.D.L. and BAKER N. (1986). An experimental assessment of the restricted flow consolidation test. *Consolidation of Soils: Testing and Evaluation, ASTM STP 892*. American Society for Testing and Materials, Philadelphia.

SILLS G.C., MAY R.E., HENDERSON T. and NYIRENDA Z.M. (1988b). Piezocone measurements with four pore pressure positions. *Proc. of the Geotechnology Conference on Penetration Testing in the U.K.* Birmingham.

SILLS G.C. (1975). Some conditions under which Biot's equations of consolidation reduce to Terzaghi's equation. *Geotechnique*, Vol 25, N0. 1.

SILLS G.C. (1987). Private communication.

SKEMPTON A.W. (1966). Summing up. *Proc. of Conference on Large Bored Piles.* London.

SMITS F.P. (1982). Penetration pore pressure measured with piezometer cones. *Proc. of ESOPT 2.* Amsterdam.

SUGAWARA N. (1988). On the estimation of in situ OCR using piezocone (CUPT). *Proc. of ISOPT 1.* Orlando.

SUGAWARA N. and CHIKARAISHI M. (1982). On estimation of ϕ for normally consolidated mine tailings by using the pore pressure cone penetrometer. *Proc. of ESOPT 2,* Amsterdam Vol 2.

SULLY J.P., CAMPANELLA R.G. and ROBERTSON P.K. (1988). Over consolidation ratio of clay from penetration pore pressures. *Journal of Geotechnical Engineering.* Vol. 114, No. 2.

TEH C.I. (1987). An analytical study of the cone penetration test. *D.Phil. thesis.* Oxford University.

TEH C.I. and HOULSBY G. (1988). Analysis of the piezocone in clay. *Proc. of ISOPT 1,* Orlando.

THOMAS S.D. (1986). Various techniques for the evaluation of the coefficient of consolidation. *Special Soil Mechanics Group Report,* Oxford University.

TOMLINSON. M.J. (1969). Foundation design and construction. Pitman, 3rd edition. London.

TORSTENSSON B.A. (1975). Pore pressure sounding instrument. *Proc. of the ASCE Conf. on In-situ Measurement of Soil Properties.* Raleigh.

TORSTENSSON B.A. (1978). The pore pressure probe. *Proc. of Geoteknkkdagn,* Tapir Forlag, Oslo.

TORSTENSSON B.A. (1982). A combined pore pressure and point resistance probe. *Proc. of ESOPT 2,* Amsterdam.

TUMAY M.T., BOGGESS R.L. and ACAR Y. (1981). Subsurface investigation with piezocone penetrometers. *Proc. of ASCE Conf. on Penetration Testing and Experience.* St Louis.

VIJAYVERGIYA V.N. and FOCHT J.A. (1972). A new way to predict capacity of piles. *Proc. of 4th Offshore Technology Conference,* Houston.

WISSA A.E.Z., MARTIN R.T. and GARLANGER J.E. (1975). The piezocone probe. *Proc. of the ASCE Conf. on In-situ Measurement of Soil Properties.* Raleigh.

WROTH C.P. (1984). The interpretation of in-situ tests. *Rankine lecture, Geotechnique.* Vol. 34.

WROTH C.P. (1988). Penetration testing - A more rigourous approach to interpretation. *Proc. of ISOPT 1*. Orlando.

WROTH C.P. and HOULSBY G.T. (1985). Soil mechanics, property characteristics and analysis. *Proc. of 11th ICSMFE*. Vol. 1. San Francisco.

ZUIDBERG H.M., SHARP L.H.J. and BERINGEN F.L. (1982). A penetrometer for simultaneous measuring of cone resistance, sleeve friction and dynamic pore pressure. *Proc. of ESOPT 2*. Amsterdam, Vol. 2.